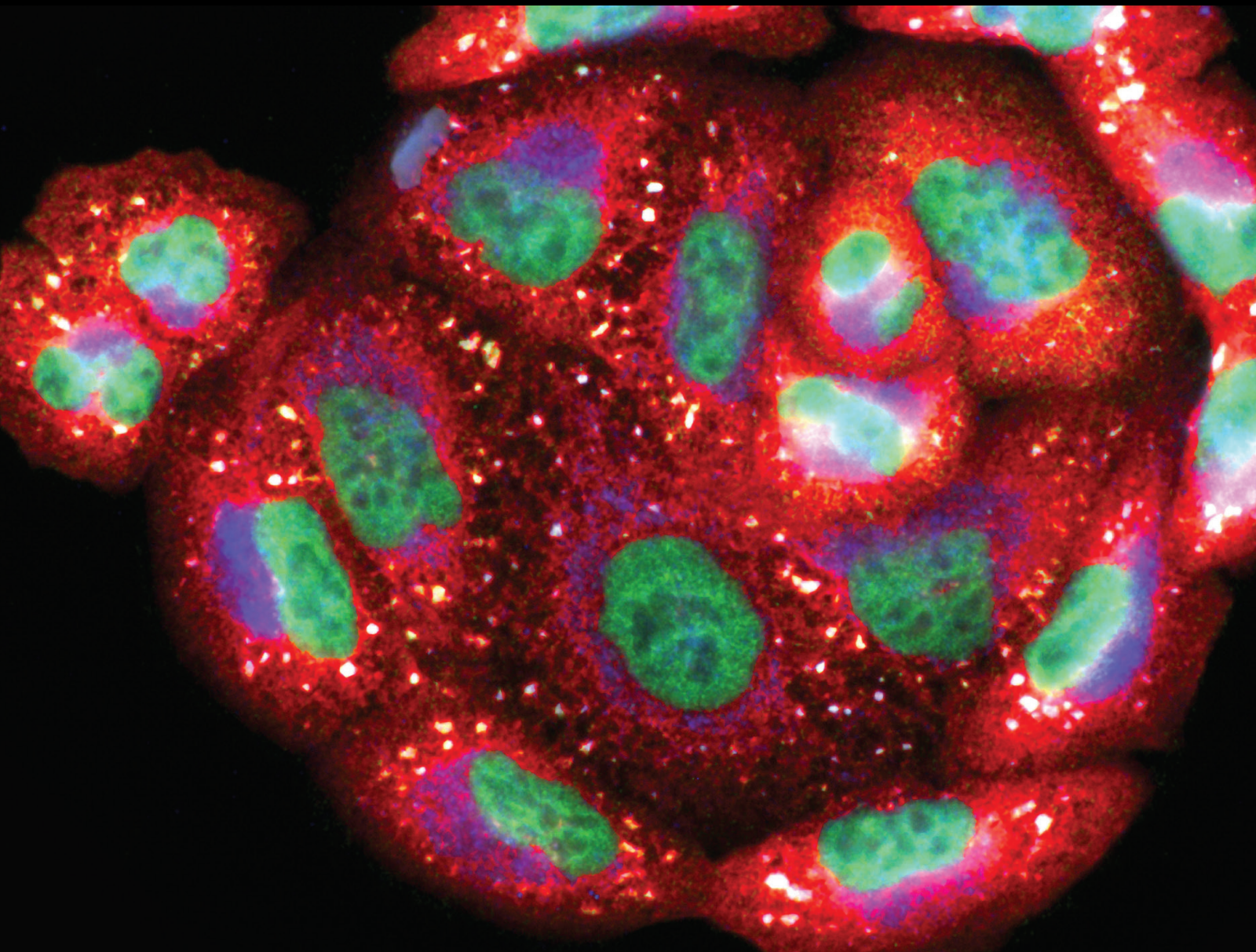# Therapeutic Management of the mTOR Pathway to Counteract Cancer and Aging

Lead Guest Editor: Marco Cordani
Guest Editors: Miguel Sánchez Álvarez, Raffaele Strippoli, Fidel Lolo, and Suresh Kumar

Therapeutic Management of the mTOR Pathway to Counteract Cancer and Aging

Therapeutic Management of the mTOR Pathway to Counteract Cancer and Aging

Lead Guest Editor: Marco Cordani
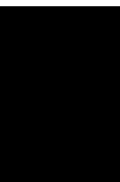Guest Editors: Miguel Sánchez Álvarez, Raffaele Strippoli, Fidel Lolo, and Suresh Kumar

Tim Hofer, Norway
John D. Horowitz, Australia
Silvana Hrelia, Italy
Dragan Hrncic, Serbia
Zebo Huang, China
Zhao Huang, China
Tarique Hussain, Pakistan
Stephan Immenschuh, Germany
Norsharina Ismail, Malaysia
Franco J. L, Brazil
Sedat Kacar, USA
Andleeb Khan, Saudi Arabia
Kum Kum Khanna, Australia
Neelam Khaper, Canada
Ramoji Kosuru, USA
Demetrios Kouretas, Greece
Andrey V. Kozlov, Austria
Chan-Yen Kuo, Taiwan
Gaocai Li, China
Guoping Li, USA
Jin-Long Li, China
Qiangqiang Li, China
Xin-Feng Li, China
Jialiang Liang, China
Adam Lightfoot, United Kingdom
Christopher Horst Lillig, Germany
Paloma B. Liton, USA
Ana Lloret, Spain
Lorenzo Loffredo, Italy
Camilo López-Alarcón, Chile
Daniel Lopez-Malo, Spain
Massimo Lucarini, Italy
Hai-Chun Ma, China
Nageswara Madamanchi, USA
Kenneth Maiese, USA
Marco Malaguti, Italy
Steven McAnulty, USA
Antonio Desmond McCarthy, Argentina
Sonia Medina-Escudero, Spain
Pedro Mena, Italy
Víctor M. Mendoza-Núñez, Mexico
Lidija Milkovic, Croatia
Alexandra Miller, USA
Sara Missaglia, Italy

Premysl Mladenka, Czech Republic
Sandra Moreno, Italy
Trevor A. Mori, Australia
Fabiana Morroni, Italy
Ange Mouithys-Mickalad, Belgium
Iordanis Mourouzis, Greece
Ryoji Nagai, Japan
Amit Kumar Nayak, India
Abderrahim Nemmar, United Arab Emirates
Xing Niu, China
Cristina Nocella, Italy
Susana Novella, Spain
Hassan Obied, Australia
Pál Pacher, USA
Pasquale Pagliaro, Italy
Dilipkumar Pal, India
Valentina Pallottini, Italy
Swapnil Pandey, USA
Mayur Parmar, USA
Vassilis Paschalis, Greece
Keshav Raj Paudel, Australia
Ilaria Peluso, Italy
Tiziana Persichini, Italy
Shazib Pervaiz, Singapore
Abdul Rehman Phull, Republic of Korea
Vincent Pialoux, France
Alessandro Poggi, Italy
Zsolt Radak, Hungary
Dario C. Ramirez, Argentina
Erika Ramos-Tovar, Mexico
Sid D. Ray, USA
Muneeb Rehman, Saudi Arabia
Hamid Reza Rezvani, France
Alessandra Ricelli, Italy
Francisco J. Romero, Spain
Joan Roselló-Catafau, Spain
Subhadeep Roy, India
Josep V. Rubert, The Netherlands
Sumbal Saba, Brazil
Kunihiro Sakuma, Japan
Gabriele Saretzki, United Kingdom
Luciano Saso, Italy
Nadja Schroder, Brazil

Anwen Shao ⓘD, China
Iman Sherif, Egypt
Salah A Sheweita, Saudi Arabia
Xiaolei Shi, China
Manjari Singh, India
Giulia Sita ⓘD, Italy
Ramachandran Srinivasan ⓘD, India
Adrian Sturza ⓘD, Romania
Kuo-hui Su ⓘD, United Kingdom
Eisa Tahmasbpour Marzouni ⓘD, Iran
Hailiang Tang, China
Carla Tatone ⓘD, Italy
Shane Thomas ⓘD, Australia
Carlo Gabriele Tocchetti ⓘD, Italy
Angela Trovato Salinaro, Italy
Rosa Tundis ⓘD, Italy
Kai Wang ⓘD, China
Min-qi Wang ⓘD, China
Natalie Ward ⓘD, Australia
Grzegorz Wegrzyn, Poland
Philip Wenzel ⓘD, Germany
Guangzhen Wu ⓘD, China
Jianbo Xiao ⓘD, Spain
Qiongming Xu ⓘD, China
Liang-Jun Yan ⓘD, USA
Guillermo Zalba ⓘD, Spain
Jia Zhang ⓘD, China
Junmin Zhang ⓘD, China
Junli Zhao ⓘD, USA
Chen-he Zhou ⓘD, China
Yong Zhou ⓘD, China
Mario Zoratti ⓘD, Italy

Contents

Research Article

Intercellular Transfer of Mitochondria between Senescent Cells through Cytoskeleton-Supported Intercellular Bridges Requires mTOR and CDC42 Signalling

Hannah E. Walters [ID][1,2] **and Lynne S. Cox** [ID][1]

[1]*Department of Biochemistry, University of Oxford, South Parks Road, Oxford OX1 3QU, UK*
[2]*Technische Universität Dresden, CRTD/Center for Regenerative Therapies Dresden, Dresden, Germany*

Correspondence should be addressed to Lynne S. Cox; lynne.cox@bioch.ox.ac.uk

Cellular senescence is a state of irreversible cell proliferation arrest induced by various stressors including telomere attrition, DNA damage, and oncogene induction. While beneficial as an acute response to stress, the accumulation of senescent cells with increasing age is thought to contribute adversely to the development of cancer and a number of other age-related diseases, including neurodegenerative diseases for which there are currently no effective disease-modifying therapies. Non-cell-autonomous effects of senescent cells have been suggested to arise through the SASP, a wide variety of proinflammatory cytokines, chemokines, and exosomes secreted by senescent cells. Here, we report an additional means of cell communication utilised by senescent cells via large numbers of membrane-bound intercellular bridges—or tunnelling nanotubes (TNTs)—containing the cytoskeletal components actin and tubulin, which form direct physical connections between cells. We observe the presence of mitochondria in these TNTs and show organelle transfer through the TNTs to adjacent cells. While transport of individual mitochondria along single TNTs appears by time-lapse studies to be unidirectional, we show by differentially labelled co-culture experiments that organelle transfer through TNTs can occur between different cells of equivalent cell age, but that senescent cells, rather than proliferating cells, appear to be predominant mitochondrial donors. Using small molecule inhibitors, we demonstrate that senescent cell TNTs are dependent on signalling through the mTOR pathway, which we further show is mediated at least in part through the downstream actin-cytoskeleton regulatory factor CDC42. These findings have significant implications for the development of senomodifying therapies, as they highlight the need to account for local direct cell-cell contacts as well as the SASP in order to treat cancer and diseases of ageing in which senescence is a key factor.

1. Introduction

Intercellular communication is crucial in regulating cellular function, for example, in response to environmental or intracellular stress. Such interplay has historically been thought to be coordinated through the secretion of soluble factors including chemokines, cytokines, growth factors, and hormones, and their recognition by cell surface receptors or through the secretion and internalisation of extracellular vesicles. However, recent evidence suggests that an alternative form of cell-cell communication can be mediated through intercellular membrane connections. Such connec-

tions, termed tunnelling nanotubes (TNTs) or intercellular bridges, have been characterised as long, fragile, open-ended and transient protrusions which mediate membrane continuity between connected cells. Since their initial description [1], nanotubes have been observed connecting cells of the same or different cell types, with a particular prevalence detected in immune cells including macrophages, monocytes and NK cells [2]. The cargo shuttled within nanotubes includes nutrients, sterols, plasma membrane components, signalling molecules, proteins, RNA species and ions that passively diffuse between connected cells, alongside larger cargos such as whole organelles or protein complexes that require transport by

myosin motors [3]. Nanotubes may play important physiological functions, for example, in osteoclast differentiation [4], and have been observed *in vivo*, both in murine myeloid cells in the cornea [5] and in human malignant pleural mesothelioma [6].

Intercellular bridges can form either by protrusion elongation, where one cell extends filopodia-like protrusions which subsequently connect with a second nearby cell, or by cell dislodgement, where two cells which are initially close move apart, leaving behind a long, thin membrane connection [2]. Both result in the formation of nanotubes with diameters ranging from 50 to 1500 nm, spanning tens to hundreds of microns between connected cells. Actin filaments (together with myosin) are present in "thin" TNTs, while "thick" TNTs additionally contain microtubules, raising the possibility that cytoskeletal composition could control TNT cargo transport through size exclusion [7]. Given the universal requirement for F-actin in bridge structures, it is unsurprising that regulators of actin cytoskeletal dynamics including Rac1, CDC42, and their respective downstream effectors WAVE and WASP are also implicated in bridge formation, as well as the myosin motor protein Myo10 [8]. CDC42 expression, which also regulates filopodia formation, appears important for both bridge elongation and intercellular cargo transport [9].

Intercellular communication through TNTs may represent a cellular response to stress, potentially allowing rescue through transfer of functional components from undamaged cells nearby. Consistent with this, both oxidative stress and DNA damage are associated with increased TNT formation [10], in a manner dependent on p53 [11]. Stressed cells appear to "reach out" to unstressed cells [11], and transfer of mitochondria from healthy neighbouring cells to stressed cells via TNTs has been speculated to serve as a rescue mechanism for stress tolerance. For example, intercellular mitochondrial transport allows survival of cancer cells experiencing loss of mitochondrial functionality [12]. As well as providing rescue from metabolic failure or mitochondrial dysfunction, mitochondrial transfer via TNTs has even been reported to result in cellular reprogramming [13]. Nanotube formation may also be involved in the induction of apoptosis, as the death signal Fas ligand has been noted to be shuttled via TNTs in T lymphocytes to induce cell death in target cells [14].

Stress is therefore associated with TNT formation, but cellular stress is also a known driver of cell senescence (reviewed by [15]). It is hence noteworthy that intercellular membrane connections have been observed to increase upon induction of cell senescence, with transfer of cytoplasmic proteins preferentially from senescent cells to natural killer (NK) cells in co-culture [16], resulting in increased NK cell activation and cytotoxicity. Proteomic analysis of the transferred cargo showed transfer of proteins implicated in actin reorganisation. In particular, CDC42 was reported to be substantially upregulated and highly active in senescent versus proliferating fibroblasts, while its inhibition substantially reduced protein transfer and NK cytotoxicity [16].

Here, we set out to investigate the composition and role of intercellular bridges in cell senescence and whether the bridges are capable of supporting transfer of organelles between cells. We report a high prevalence of membrane-bound TNTs formed by senescent cells, containing both actin and tubulin. We further show that mitochondria can be transferred through these bridges and that mTOR signalling and CDC42-mediated actin organisation pathways are critical for organelle transfer through tunnelling nanotubes in senescent cells. These findings highlight a potential target for new therapies directed against senescent cells.

2. Materials and Methods

2.1. Cell Culture.
HF043 neonatal foreskin fibroblasts (Dundee C l products) were verified to be primary diploid human fibroblasts, uncontaminated with any known lab cell line, by short tandem repeat analysis (Porton Down, UK). IMR90 ER:RAS fibroblasts (16-week female foetal lung fibroblasts) were a gift from Prof. Peter Adams (University of Glasgow, UK, and Sanford Burnham Prebys Medical Discovery Institute, La Jolla, USA). Cells were cultured in DMEM (D5796, Gibco) supplemented with 10% heat-inactivated FCS (Gibco) for HF043 or 1 mM sodium pyruvate (Gibco) and 20% FCS for IMR90 ER:RAS fibroblasts. (Media were not supplemented with antibiotics.) Cells were subcultured once they reached ~70% confluence as assessed using a digital EVOS microscope (Thermo Fisher), by washing in PBS (Sigma), 3-5 minute incubation with TrypLE Express trypsin (Thermo Fisher), and dilution and gentle trituration in complete media. Cell viability and number were assessed using a T4 Cellometer (Nexcelom), from which population doublings were subsequently calculated as $PD = (\log [\text{number harvested/number seeded}])/\log (2)$. Cells were seeded at 4-8 $\times 10^3$ cells/cm^2 in filter-capped flasks or multiwell plates (Greiner) and incubated with complete media in a humidified incubator at 37°C in 5% CO_2 and 20% O_2. Cells were regularly inspected by phase contrast microscopy for cell health and tested for mycoplasma contamination by PCR according to the method of Uphoff and Drexler [17, 18].

2.2. Drug Treatments.
All drugs used were reconstituted and stored as directed by the supplier (etoposide, 4-hydroxytamoxifen (4-OHT), mitomycin C, and CASIN—all from Sigma-Aldrich; AZD8055—Selleckchem). For routine drug treatment, cells were seeded in complete media and allowed to bed down overnight, before media were aspirated and replaced with drug-supplemented complete media. For drug treatment in co-culture assays, cells were seeded directly into drug-supplemented complete media. Optimum concentrations and dosing periods for induction of senescence without cell killing were selected according to previously published experiments [19–22].

2.3. Induction and Assessment of Senescence

2.3.1. Replicative Senescence (RS).
The primary human fibroblast line HF043 was grown in continuous culture until replicative exhaustion. Cells were determined to be replicatively senescent when populations fulfilled each of the following criteria: failure to increase the cell number within >2 weeks, a cumulative population doubling number of >85, and

positive SA-β-gal staining according to the manufacturer's instructions (Cell Signaling Technology #9860S). The secretion of IL-6, a canonical SASP factor, and upregulation of p21^{CDKN1} (see Supplementary Figures S1, S2, and S3) were assessed as additional readouts of senescence (see [23] for western blotting conditions and [20] for ELISA protocol).

2.3.2. DNA Damage-Induced Senescence (DDIS). Cells were treated for 7 days with 20 μM etoposide or 10 nM mitomycin C and verified as senescent by SA-β-gal staining and morphological assessment, as well as upregulation of p21^{CDKN1} (Supplementary Figures S2 and S3). Cells at low CPD (<50) were always used for DNA damage-induced senescence to avoid confounding effects of replicative senescence.

2.3.3. Oncogene-Induced Senescence (OIS). IMR90 ER:RAS cells were incubated with 1 μM 4-OHT for 7 days and assessed for senescence induction by SA-β-gal staining, morphological assessment (Supplementary Figure S2), and failure to re-proliferate.

2.4. Fluorescence Staining. For live imaging of mitochondria, cells were incubated for 30 minutes with MitoTracker Green FM or MitoTracker Red (1 : 1000 v/v dilution of 1 mM stock) according to the manufacturer's instructions (Invitrogen Molecular Probes), in complete media at 37°C in the dark. Media were replaced before imaging to avoid fluorescent flare. Alternatively, cells were incubated overnight with a GFP-BacMam probe for mitochondria (GFP fused to the leader sequence of E1 α pyruvate dehydrogenase) according to the manufacturer's instructions (CellLight, Invitrogen). For co-culture experiments, cells were stained with the appropriate label, washed 3x in PBS, and harvested by trypsin treatment (as above) before reseeding at 1 : 1 ratios. To assess potential confounding dye leakage, conditioned media were harvested at 24 h from stained cells and incubated for ≥24 h with control unstained cells.

For analysis of fixed samples, mitochondria were stained for mitochondrial-specific TFAM and analysed by immunofluorescence. Briefly, cells were washed in PBS, fixed in 3.7% formaldehyde (10 minutes, RT), washed twice in PBS, blocked in 5% donkey serum (Dako) in PBS, and incubated with the primary antibody (α-TFAM (mouse) Ab, Abnova B01P) diluted 1 : 200 in PBS containing 0.3% Triton X-100 v/v and 1% BSA w/v, at 4°C overnight in a humidified chamber. Cells were then washed twice in PBS and incubated with the secondary antibody (Alexa Fluor 488 α-mouse IgG (donkey), Invitrogen A-2102); 2 hours, RT in the dark, and 1 : 500 in a dilution buffer as for the primary antibody. Cells were washed twice in PBS and DNA-counterstained before imaging.

For F-actin staining, cells were washed in PBS, fixed in 3.7% v/v formaldehyde in PBS (10 minutes, RT) before washing in PBS, and then incubated for 40 minutes with FITC-phalloidin (6.6 nM in PBS, Molecular Probes, Thermo Fisher). Cells were then washed in PBS and imaged.

For tubulin staining, cells were incubated with Tubulin Tracker Green diluted in complete media according to the manufacturer's instructions (30 minutes, 37°C, Thermo Fisher), media were replaced, and cells were imaged live.

Plasma membranes were labelled by incubating cells with 1 : 250 wheat germ agglutinin (WGA, v/v) conjugated with the fluorophore FITC or rhodamine (Vector Labs), either live in complete media (immediately after staining to avoid WGA-induced cytotoxicity) or after 3.7% formaldehyde fixation in PBS (without permeabilisation). Our optimisation studies comparing live imaging with fixed cells suggested that while fixation improved the sharpness of cell staining, it did so without disrupting the intercellular bridge structures (data not shown).

DNA was stained using NucBlue Live (Hoechst 33342) according to the manufacturer's instructions (20 minutes, 1 drop/ml, and RT, Thermo Fisher) or using Hoechst 33342 within mounting dye (VECTASHIELD, Vector Labs) for fixed cells, with 1 drop of the mounting medium used for coverslip mounting.

2.5. Microscopy. Phase contrast microscopy was performed using a digital EVOS Core microscope (Thermo Fisher), with scale bars added to images using a graticule. Phase contrast microscopy was used for routine assessment of cells to determine % confluence before subculturing, as well as for morphological analysis. Fluorescence microscopy was performed using a ZOE fluorescent cell imager (Bio-Rad), with scale bars added automatically. For time-lapse imaging, the field of view was locked and images taken at 5-10 min intervals, timed according to a stopwatch. Within individual experiments, optical gain was fixed at the outset of image acquisition to ensure image-to-image comparability. Between experiments, brightness and (where stated) sharpness were normalised across different samples within PowerPoint. Where necessary, Fiji software was used to enhance colour discrimination.

2.6. Statistical Analysis. GraphPad Prism 9 statistical analysis package was used to perform statistical tests. For comparisons between >2 samples, ANOVAs (analysis of variance) were performed, with Tukey's tests to compare the means of each sample. All graphs show mean values with standard deviations (as error bars), calculated from $n \geq 3$ independent experiments or from technical triplicates from representative experiments of $n \geq 3$ unless otherwise stated.

3. Results

3.1. Intercellular Bridges Connect Senescent Cells. To examine whether intercellular bridges are associated with cell senescence, we induced replicative senescence (RS) in primary human skin fibroblasts (HF043) by longitudinal continuous cell culture (serial passaging) or induced DNA damage-induced senescence (DDIS) by treating cells with etoposide for 7 days (see Materials and Methods). In parallel, we treated IMR90 ER:RAS lung fibroblasts with tamoxifen (4-OHT) to trigger oncogene-induced senescence (OIS) and compared these with proliferating control cells. As expected, the proliferating cells showed characteristic spindle-like morphology, relatively small size and were mononuclear (Figure 1(a)), while the senescent cells by contrast were greatly enlarged, contained granular inclusions, and were
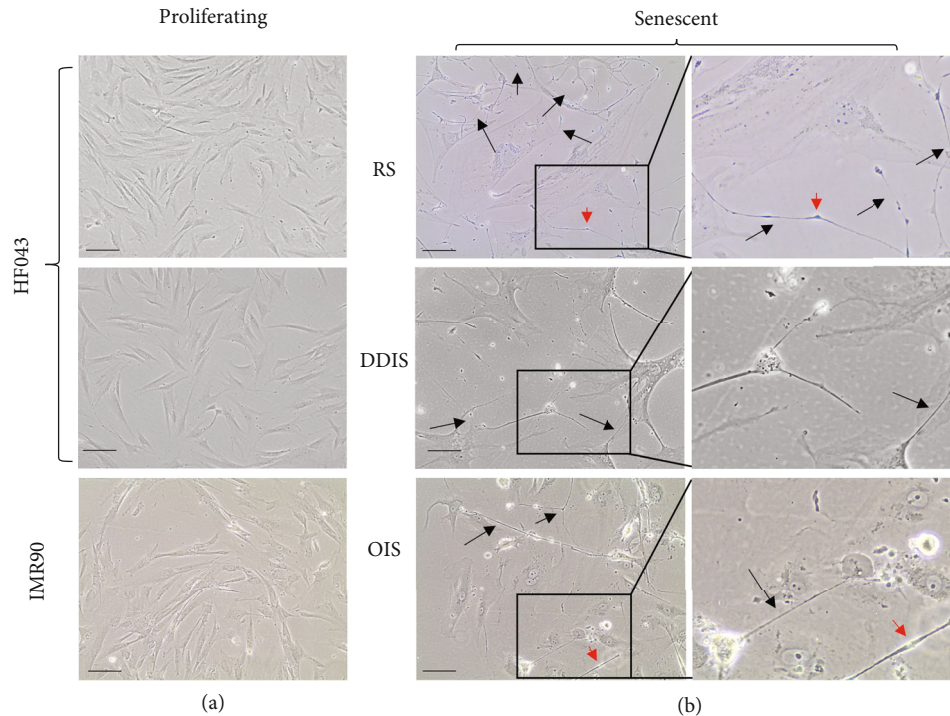
FIGURE 1: Senescent cells are connected by thin intercellular contacts *in vitro*. (a) Phase contrast images of proliferating HF043 fibroblasts at low cumulative population doubling (CPD < 40) and vehicle control proliferating IMR90 ER:RAS fibroblasts. (b) HF043 fibroblasts that have undergone replicative senescence (RS, CPD > 90) or DNA damage-induced senescence (DDIS, following 7-day 20 μM etoposide treatment), together with oncogene-induced senescent (OIS, 7-day 4-OHT) ER:RAS fibroblasts (right panels are enlarged inset regions from left panels). Black arrows indicate examples of intercellular bridges, and red arrowheads indicate bulky protrusions within the bridges. Representative data shown of $n > 3$ experiments. Scale bar 100 μm.

often multinucleated with prominent nucleoli, and cell margins were poorly defined under phase contrast optics (Figure 1(b)).

We observed by phase contrast microscopy a substantial number of long, thin structures of considerable length (tens to hundreds of microns) directly connecting nearby cells within senescent populations of both skin (HF043) and lung (IMR90) fibroblasts, irrespective of the mode of senescence induction (Figure 1(b), bridges indicated by black arrows). The bridge-like structures that we observe in the senescent cell populations were infrequent within proliferating control populations (Figure 1(a)), in agreement with previous data, suggesting that nanotube formation occurs in response to cellular stress [16], since senescence is a stress response. We further noted a number of swellings at various points along the nanotubes (red arrows, Figure 1(b)). These appear similar to protrusions previously described as "gondolas" within nanotubes, which are thought to be associated with the transport of large cargo [24] including organelles such as mitochondria.

3.2. Bridges Are Membrane-Bound and Contain Actin and Tubulin.

To determine whether the observed senescent cell bridges are membrane-bound, we stained cells with FITC-conjugated lectin wheat germ agglutinin (WGA) to assess the presence of the sugar O-GlcNAc, which is prevalent on mammalian membranes; DNA was counterstained with NucBlue Live. From Figure 2(a), multiple membrane-bound (WGA-positive) protrusions can be seen to extend between the senescent cells towards their neighbours, in such a way that the cells appear to form a "network" of interconnected cells rather than discrete cells. The diameter of such connections varied from ultrafine bridges (Figure 2(b)) reminiscent of "thin" TNTs to larger diameter bridges (Figure 2(c)) that appear consistent with previously described "thick" TNTs [7].

To determine whether these structures represent actin-stabilised tunnelling nanotubes (TNTs), formaldehyde-fixed cells were costained with rhodamine-WGA (for membranes) and FITC-phalloidin for actin and counterstained with Nuc-Blue Live for DNA (Figure 3(a)) or imaged live with Tubulin Tracker Green to identify polymerised tubulin (Figure 3(b)). Fluorescence microscopy demonstrated that the intercellular bridges contain actin (Figure 3(a)) and tubulin (Figure 3(b)); in both cases, the bridges stained positively with rhodamine-WGA, demonstrating the presence of O-GlcNAc, orthogonally confirming with a different dye our observations in Figure 2. These data suggest that senescent fibroblasts form intercellular nanotubes that contain actin and/or tubulin.

3.3. Mitochondria Are Present in Senescent Cell TNTs.

As signalling hubs and the major source of oxidative stress, mitochondria play an important role in senescence [25]. Senescent cells exhibit dramatic increases in mitochondrial
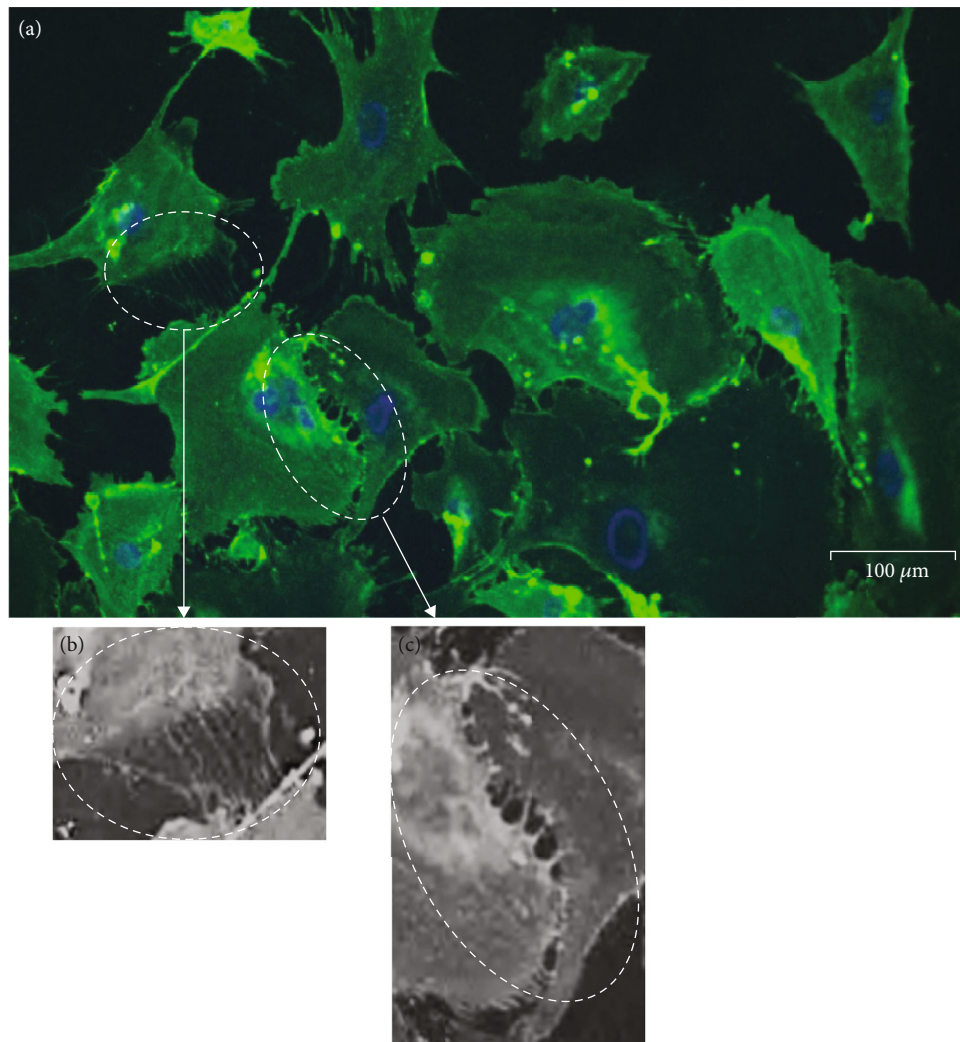
FIGURE 2: Intercellular bridges are membrane-bound and occur at a high frequency between senescent cells. (a) HF043 fibroblasts cultured to replicative senescence and imaged live with FITC-WGA (green) to highlight membrane-associated O-GlcNAc and NucBlue Live for DNA (blue). (b, c) Magnified images of thin bridges (b) and larger diameter bridges (c). Images in (b, c) have been recoloured in grayscale and sharpness-enhanced to show the bridges more clearly.

load [21], possibly to compensate for mitochondrial dysfunction, and the mitochondrial network becomes increasingly reticular through resistance to mitochondrial fission and mitophagy [26].

To ask whether the senescent cell TNTs are capable of transporting mitochondria, we labelled mitochondria in senescent fibroblasts (RS and DDIS in HF043 and OIS in IMR90, as above) with fluorescent dye. To avoid labelling bias, we compared a variety of mitochondrial dyes including the live stains MitoTracker Green, MitoTracker Red, and CellLight Mitochondria-GFP BacMam, where GFP is localised to mitochondria through fusion of GFP with the leader sequence from E1 alpha pyruvate dehydrogenase. We also examined staining patterns of the mitochondrial transcription factor TFAM in fixed samples. In all cases, cell membranes were stained with fluorescent WGA (dye colour indicated in labels of Figure 4).

As shown in Figure 4, we observed small foci (Figures 4(a) and 4(c)) or even reticular networks (Figures 4(b) and 4(d))

positive for mitochondrial staining in a substantial proportion of intercellular bridges, irrespective of the mitochondrial stain used, the mode of senescence induction, or whether cells were imaged live or fixed, showing the presence of mitochondria within TNTs of senescent cells.

3.4. Senescent Cell Tunnelling Nanotubes Support Intercellular Mitochondrial Transport. The mitochondria present in intercellular bridges may arise simply through a chance peripheral distribution at the time and subcellular location of bridge formation; alternatively, they could represent cargo being transported through the bridges, as previously suggested [12]. Hence, to assess whether the observed mitochondria were static or mobile within these intercellular bridges, time-lapse fluorescence microscopy of replicatively senescent HF043 fibroblasts stained with MitoTracker Red was conducted.

Mitochondrial motility was observed within minutes of staining, and mitochondria were seen to track along intercellular bridges, as seen in representative still images of time-lapse

(a)

(b)
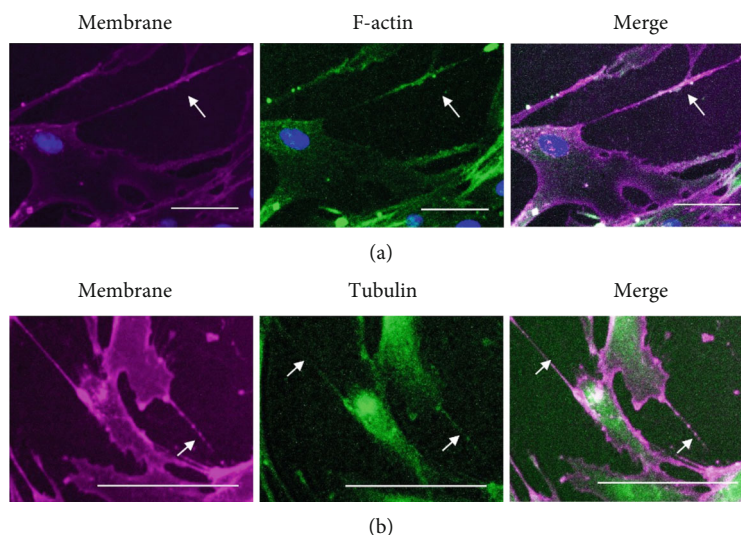
FIGURE 3: Intercellular contacts between senescent cells contain actin and tubulin. Replicatively senescent HF043 fibroblasts (CPD > 90) were (a) fixed and stained with rhodamine-WGA (membrane, purple), FITC-phalloidin (F-actin, green), and NucBlue Live (DNA, blue) or (b) imaged live with rhodamine-WGA (membrane, purple) and Tubulin Tracker Green (microtubules, green) prior to analysis by fluorescence microscopy. $n = 3$, representative images shown. Arrows indicate examples of intercellular bridges. Images have been false-coloured from the original red/green in Fiji to improve dye discrimination. Scale bar 100 μm.

microscopy (Figure 5; see also Supplementary Video (available here)). All movement detected for individual mitochondrial puncta was unidirectional, with an average speed of ~1 μm/minute within the observation period; the total distance travelled by the mitochondria in the example shown in Figure 5 was ~60 μm within 70 minutes.

These observations suggest that mitochondria are able to move within senescent intercellular bridges over the time-scale of minutes to hours. The observation of unidirectional movement suggests that mitochondrial motility may be regulated, rather than occurring by passive diffusion, possibly involving motor proteins acting on the underlying cytoskeletal framework of actin and/or tubulin.

3.5. Co-culture Demonstrates Transfer of Mitochondria between Cells.

To investigate whether this putative mitochondrial transport resulted in the transfer of mitochondria between cells, we next conducted a co-culture assay where separate populations of cells were stained with MitoTracker Green and MitoTracker Red, respectively, then thoroughly washed before harvesting and co-seeding at a 1 : 1 ratio (schematic shown in Figure 6(a), with images of co-seeded cells immediately after plating shown in Figure 6(b)).

To exclude the possibility of MitoTracker dye carry-over between different cell populations in co-culture experiments through dye leakage into the medium, conditioned medium (CM) controls were included in each experiment whereby media were harvested after 24 hours of exposure to stained cells (with either MitoTracker Green or MitoTracker Red, shown simply as "MitoTracker" in schematic Figure 6(c)), followed by incubation with unstained cells for 24 hours with inspection for any fluorescent signal by microscopy; no evidence of dye leakage was detected (Figure 6(d)).

Having optimised and verified labelling and co-culture conditions as shown in Figure 6, we then assessed whether

mitochondria were transferred between differentially labelled cell populations. One population of HF043 cells was labelled with MitoTracker Red (MT red) and another with Mito-Tracker Green (MT green), harvested, co-seeded at 1 : 1, and then imaged after 24 hours. Any transfer of mitochondria between cells of different populations might be visualised as discrete puncta of the opposite dye colour, as shown in the schematic (Figure 7(a)). Indeed, such puncta were detected in a number of co-cultured cells (white arrows, Figure 7(b)), irrespective of the MitoTracker dye used. In co-cultures of senescent cells, we also observed what appear to be mitochondrial reticular networks extending through TNTs between cells over considerable distances (>100 μm, white arrows Figure 7(c)), with large senescent "donor" cells also appearing to accept mitochondria from oppositely stained cell populations (yellow arrows, Figure 7(c)). We further observed instances where TNTs were stained with both red and green, suggesting formation by fusion of TNTs extruded from separate cells (blue arrow, Figure 7(c)). Mitochondria were also transferred through TNTs from labelled DDIS cells to unlabelled proliferating cells (Figures 7(d) and 7(e)).

3.6. Mitochondria Pass from Senescent Cells to Proliferating Cells and Vice Versa.

Intercellular mitochondrial transfer has been hypothesised as a rescue mechanism for stressed cells, including cancer cells that have lost mitochondrial functionality [12]. To determine whether, like stressed cancer cells, senescent cells can accept mitochondria from healthy proliferating cells, we conducted co-culture experiments between populations of proliferating and senescent cells, with "red"-stained proliferating cells co-cultured with "green"-stained proliferating cells (PRO-PRO), "red" senescent cells with "green" senescent cells (SEN-SEN), or proliferating and senescent (PRO-SEN) co-cultures (using both colour combinations to eliminate any effect of dye bias)—dye

HF043 (RS)　　　　　　　　IMR90 (OIS)

WGA mitoT DNA

(a)

WGA mitoT DNA

(d)

WGA mitoT DNA

(b)

HF043 (DDIS)

WGA TFAM DNA

(e)

WGA mitoGFP DNA

(c)

FIGURE 4: Mitochondria are present within senescent intercellular contacts. (a–c) Replicatively senescent HF043 fibroblasts were stained with (a) fluorescein-WGA and MitoTracker Red (mitoT), (b) rhodamine-WGA and MitoTracker Green (mitoT), and (c) rhodamine-WGA and CellLight Mitochondria-GFP BacMam (mitoGFP). (d) IMR90 ER:RAS cells induced to undergo oncogene-induced senescence (OIS) by 7 d treatment with 4-OHT were stained with fluorescein-WGA and MitoTracker Red (mitoT). Cells in (a–d) were imaged live. (e) HF043 fibroblasts treated for 7 d with mitomycin C to drive DNA damage-induced senescence (DDIS) were fixed and stained with anti-TFAM primary antibody, with Alexa Fluor 488 secondary antibody and rhodamine-WGA. Arrows indicate mitochondria within contacts. $n \geq 3$. DNA stained with NucBlue Live. Scale bar 100 μm.

colours are indicated in labels of Figure 8. Nuclei were counterstained using the live dye NucBlue Live prior to imaging.

After 24 hours of co-culture, we observed puncta of oppositely stained mitochondria within both proliferating and senescent fibroblasts, regardless of which population was stained with MitoTracker Green or MitoTracker Red (Figure 8(a)), as well as mitochondria-loaded bridges spanning alternately stained "red" and "green" cells, suggesting that mitochondria have been transferred between different cells, with proliferating and senescent cell populations able to act both as mitochondrial donors and acceptors. However, quantification of the extent of mitochondrial transfer shows that proliferating cells rarely act as mitochondrial donors, both in co-cultures with other proliferating cells and when co-cultured with senescent cells (Figure 8(b)). However,

mitochondrial transfer by senescent cells occurred at equivalent levels whether the acceptor cells were proliferating or senescent. We verified that mitochondrial transfer direction was not an artefact of the MitoTracker dye used (Supplementary Figure S4), supporting the conclusion that senescent cells are major mitochondrial donors.

Taken together, our results suggest that tubulin- and actin-based intercellular bridges may constitute an important mechanism of mitochondrial transfer and thus intercellular communication for senescent cells, and this transfer may occur from senescent to proliferating cells within a tissue.

3.7. Direct Intercellular Communication in Senescence Is Regulated by mTOR and CDC42 Signalling. Intercellular bridge structures between cancer cells have been reported
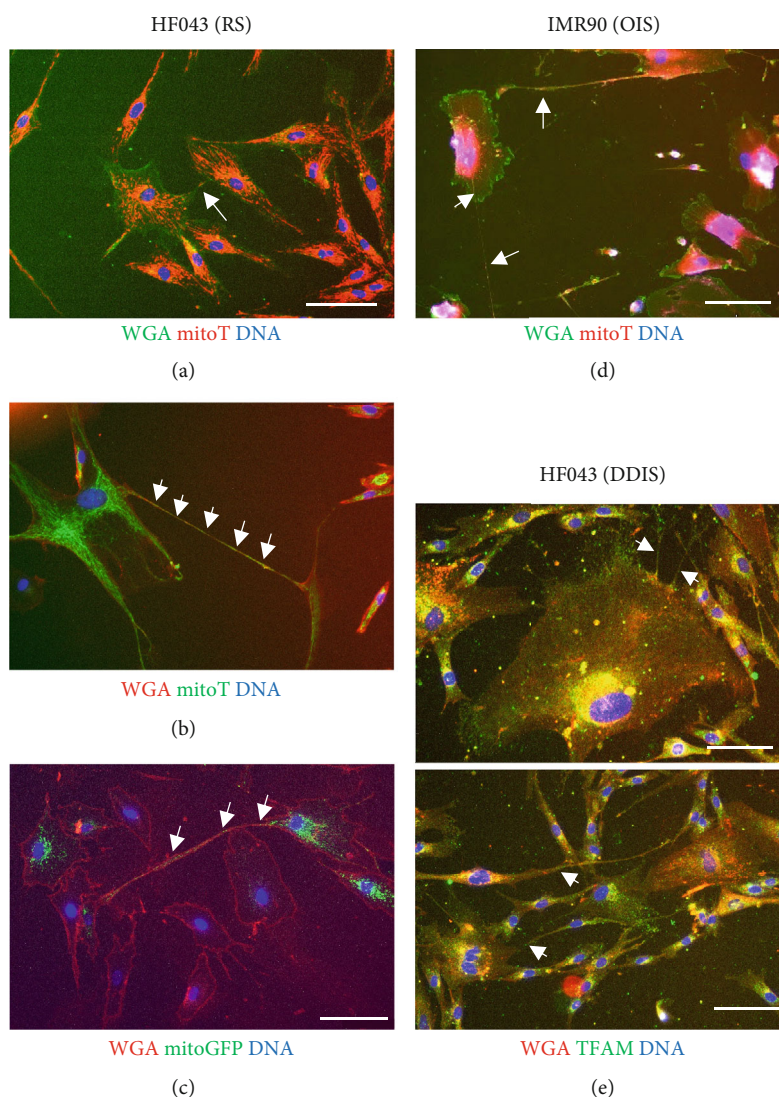
Time (minutes)

(a)   (b)
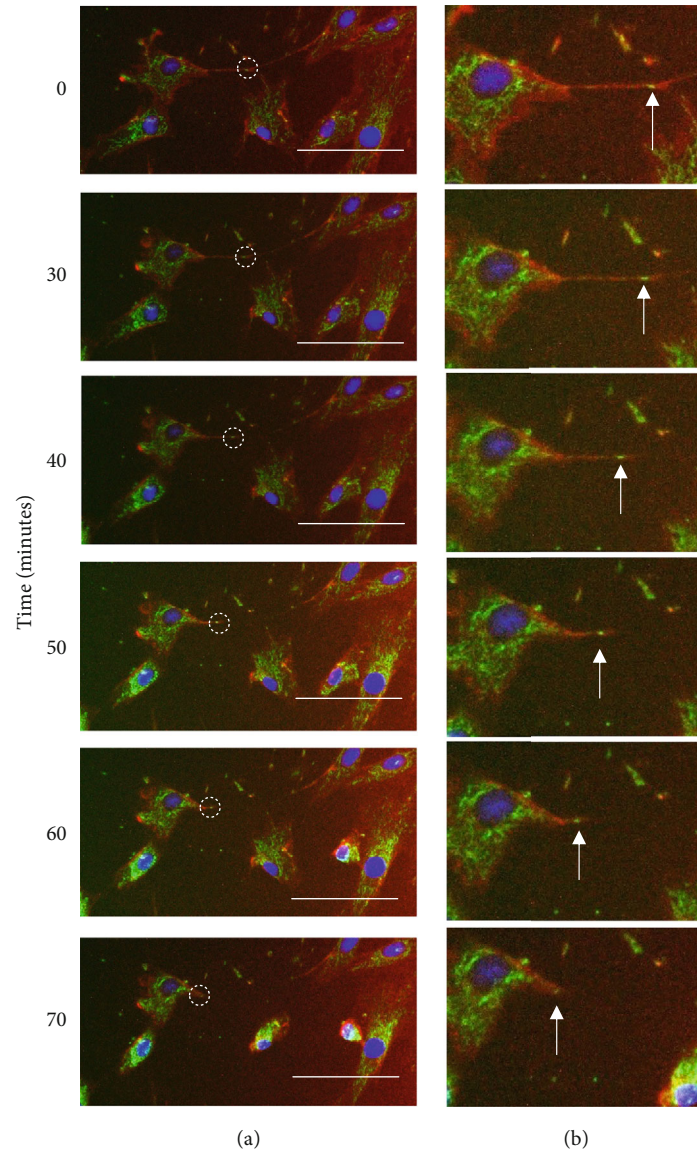
FIGURE 5: Mitochondria are motile within senescent intercellular bridges. (a) Replicatively senescent HF043 fibroblasts were stained with MitoTracker Green, rhodamine-WGA (red), and NucBlue Live (for DNA) and imaged live using time-lapse fluorescence microscopy, with time points following the start of the observation period indicated in minutes. The white dotted circle highlights a MitoTracker Green-positive punctum within a TNT. Representative images shown of $n = 3$ experiments. Scale bar 100 μm. (b) Magnification of TNT with position of moving MitoTracker-positive puncta indicated by arrows (see also Supplementary Video (available here)).

to be regulated by mTOR signalling [6], while actin regulatory factors have been implicated in senescent cell TNTs [16]. We therefore tested whether the intercellular bridges observed here are regulated by CDC42 or mTOR signalling, using the pharmacological inhibitors CASIN and AZD8055 to inhibit CDC42 and mTOR, respectively, in both the senescent and proliferating cell populations. As an ATP-competitive mTOR inhibitor, AZD8055 impacts not only pathways regulated by mTORC1 (such as translation and autophagy) but also those controlled by mTORC2, including actin polymerisation (e.g., [21]).

Populations of proliferating or senescent HF043 fibroblasts which had undergone either replicative senescence (RS) or DNA damage-induced senescence (DDIS) through

7-day treatment with 20 μM etoposide were exposed to the CDC42 inhibitor CASIN at 2 μM, pan-mTOR inhibitor AZD8055 [21] at 70 nM, or DMSO (vehicle control) for 24 hours prior to fixation with formaldehyde. Cells were then stained with fluorescein-WGA for cell membranes and NucBlue Live for nuclear DNA. The number of intercellular bridges connected at both ends was counted manually, and the number per cell was determined by normalising against nuclear number (Figure 9(a)).

We observed significantly more intercellular bridges within senescent (RS and DDIS) compared with proliferating control populations (PRO, Figure 9(a)), with an average of ~0.5 bridges per replicatively senescent (RS) cell. While a substantial proportion of cells exhibited several connections,

(a)

(b)

(c)

(d)
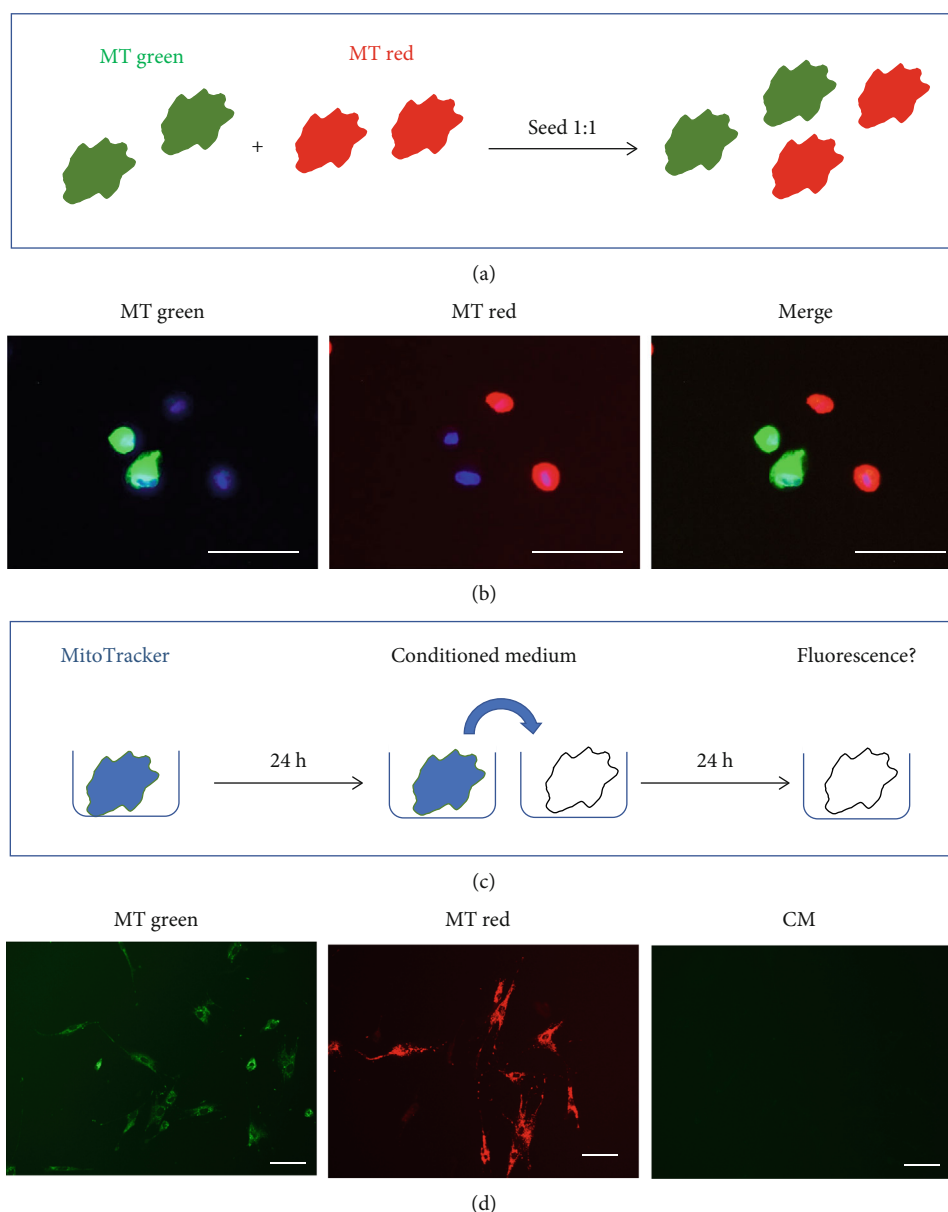
FIGURE 6: Co-culture assay for analysis of intercellular mitochondrial transfer. (a) Schematic of the co-culture setup. HF043 fibroblasts were stained with MitoTracker Green (MT green) or MitoTracker Red (MT red), washed thoroughly, and then seeded into co-culture at a 1 : 1 ratio. (b) Cells were imaged immediately after co-plating (proliferating cells shown). (c) Schematic of assay for dye leakage: cells were stained for 30 min with MitoTracker Green or Red, media replaced, and incubated for 24 h to generate conditioned medium (CM). This CM was then harvested and incubated with unstained cells for 24 h prior to fluorescence microscopy. (d) Representative images of proliferating cells stained with MitoTracker Green or MitoTracker Red or unstained cells incubated for 24 hours with conditioned media (CM) harvested from stained cells. $n \geq 3$. Scale bar 100 μm.

others had none. Notably, disruption of CDC42 signalling upon CASIN treatment, or inhibition of mTOR signalling with AZD8055, each significantly reduced the number of bridges between senescent cells, both in replicatively senescent populations and those induced by DNA damage (Figure 9(a)); representative fluorescence images of treated RS cells are shown in Figure 9(b). The very low frequency of bridges on treatment precluded analysis of the number of mitochondrial puncta transferred. The observed reduction in bridges was not due to toxicity at the drug doses used, as cell numbers were not diminished (as assessed by manual inspection). However, drug treatment did lead to lower apparent biochemical reducing capacity as measured by alamarBlue assays (Supplementary Figure S5), potentially because of decreased cell size following drug-induced structural rearrangements of the actin cytoskeleton (e.g., [21]). We further observed that the reduction in bridge number occurred in a dose-dependent manner (Supplementary Figure S6), strongly suggesting that mTOR and CDC42 are centrally important in TNT formation and/or stability.
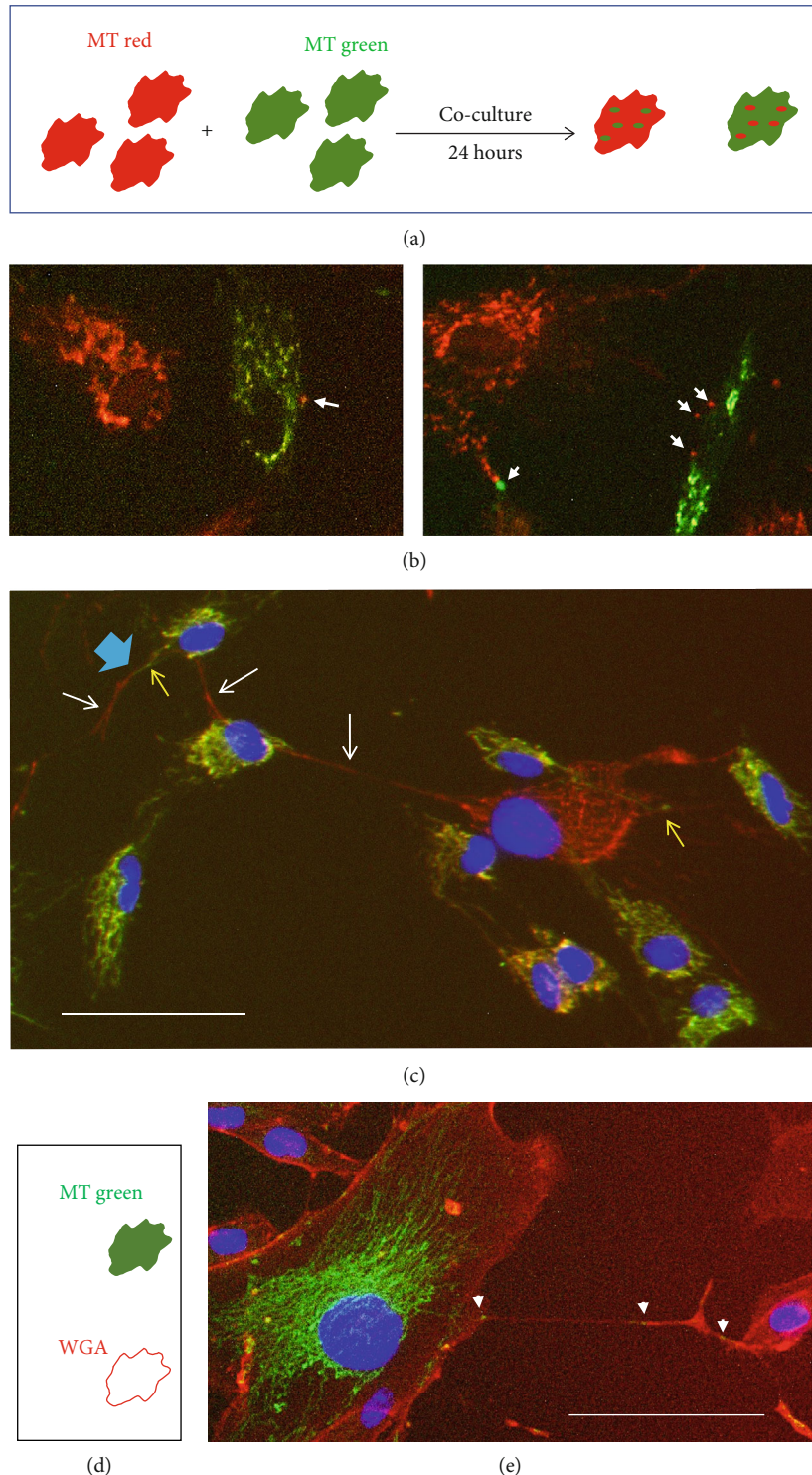
FIGURE 7: Mitochondrial transfer between co-cultured cells. (a) Schematic of co-culture experiment. One cell population is labelled by incubation with MitoTracker (MT) red and another with MT green for 30 min. Following washing and harvesting, the differently labelled cells are seeded at a 1:1 ratio and co-cultured for 24 h prior to fluorescence microscopy analysis. (b) Examples of mitochondrial puncta arising through the transfer between co-cultured cells (white arrows). (c) Example of TNTs that appear to contain reticular mitochondria. White arrows indicate TNTs arising from cells labelled with MitoTracker Red, and yellow arrows indicate those arising from cells labelled with MitoTracker Green. The blue arrow indicates a TNT that appears to be formed by the fusion of a bridge between two differently labelled cells. (d) Schematic showing co-culture between cells labelled with MitoTracker (MT) Green and unlabelled cells. (e) Representative image of co-culture with an MT green-labelled cell that has undergone mitomycin C-induced senescence (DDIS) and unlabelled proliferating cells (rhodamine-WGA was used subsequently to highlight cell membranes). White arrows indicate the presence of green mitochondrial puncta being transferred to a cell without mitochondrial labelling. Scale bar 100 μm.

(a)

(b)
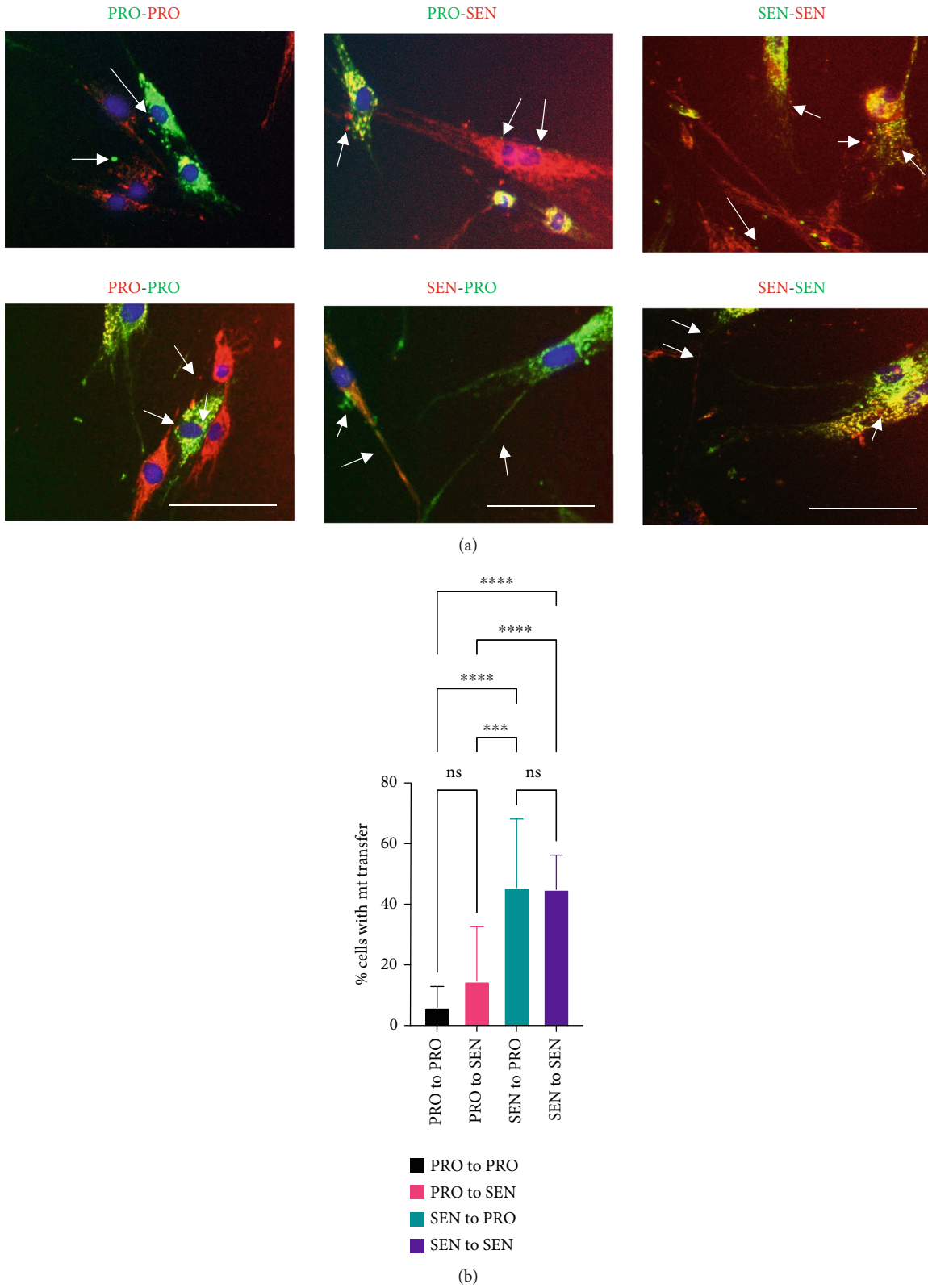
FIGURE 8: Intercellular mitochondrial transfer occurs between both proliferating and senescent cells. (a) Co-cultures of proliferating (PRO) or replicatively senescent (SEN) HF043 fibroblasts pre-stained with MitoTracker Green or Red were set up as in Figure 6(a) and imaged following 24 hours of co-incubation. Arrows indicate intercellular bridges or puncta of transferred mitochondria. DNA was stained with NucBlue Live immediately prior to analysis. Scale bar $100\,\mu$m. (b) Quantification of the mitochondrial transfer between proliferating (PRO) and senescent (SEN) cells. One-way ANOVA, ns = not significant. $^{***}p = 0.0002$, $^{****}p < 0.0001$ ($n = 16$ for PRO-PRO and SEN-SEN, $n = 9$ for each of PRO-SEN and SEN-PRO).

(a)

(b)
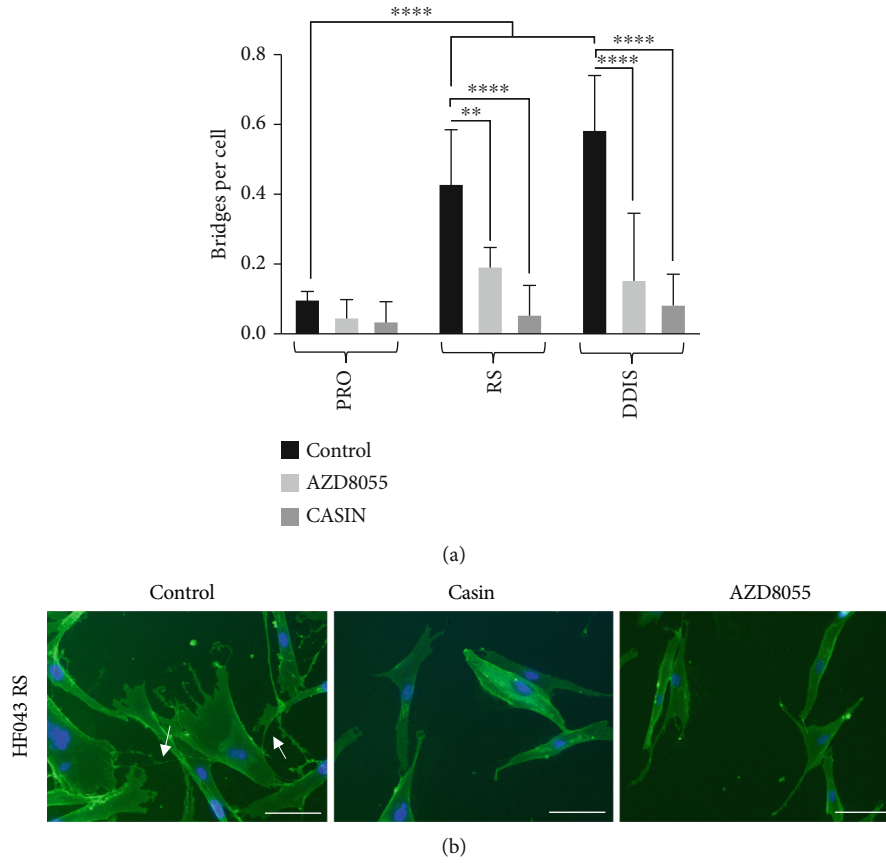
FIGURE 9: CDC42 and mTOR signalling are required for the formation of intercellular bridges in senescent cells. (a) HF043 fibroblasts that had undergone replicative senescence (RS, cumulative population doubling ≥ 90), DNA damage-induced senescence (DDIS, following 7-day treatment with 20 μM etoposide), and proliferating (PRO) control cell populations at low cumulative population doubling (CPD) were treated with the mTOR inhibitor AZD8055 (70 nM) or the CDC42 inhibitor CASIN (2 μM) for 24 hours before fixation and staining with fluorescein-WGA (green, for membranes) and NucBlue Live (for DNA). Intercellular bridges were manually quantified from >50 cells per replicate ($n = 3$). $^{**}p < 0.05$, $^{***}p < 0.001$. (b) Representative images of the control and drug-treated replicatively senescent fibroblasts. Arrows indicate intercellular bridges (TNTs). Scale bar = 100 μm.

4. Discussion

Entry into senescence is accompanied by development of a number of distinctive phenotypes including epigenetic alterations, lysosomal and mitochondrial dysfunction, proinflammatory secretion through the SASP, and morphological alterations including hypertrophy and changes to actin organisation networks. Furthermore, senescent cells are highly communicative, alerting immune cells to their presence for clearance [27] and regulating the proliferative capacity of surrounding healthy or cancerous cells positively and negatively [28, 29]. While this interplay has largely been attributed to secretion of exosomes and SASP factors, we show a high prevalence of intercellular bridges between senescent cells that may also be important in mediating these effects.

4.1. Supercellularity in Senescence? While intercellular nanotubes appear to constitute a highly localised form of communication, it is important to note that these bridges often do not just connect two cells but instead can form networks extending direct cell communication over larger distances. Indeed, we have observed cellular networks that appear

almost syncytial in nature, with multiple connections between multiple cells (e.g., Figure 2). Hence, by allowing the transport of cargo including whole organelles such as mitochondria between connected cells, intercellular nanotubes may create temporary syncytia or "supercellularity." Notably, syncytia are permanently created through cell-cell fusion, an essential event in a number of developmental and physiological processes, such as mammalian muscle and osteoclast function, and in the formation of the placental syncytiotrophoblast, a giant cell of ~12m^2 surface area [30]. Intriguingly, cell fusion events have been linked to cellular senescence: the placental syncytiotrophoblast itself shows a number of markers of senescence [30], while expression of fusogens such as endogenous retroviral ERVWE1 or measles virus induces cell fusion and induction of cell cycle arrest and senescence [31]. Through induction of senescence, fused cells co-ordinate a protection strategy to prevent division of multinucleated cells, while maintaining cell viability through resisting apoptosis, which may be important within the placental syncytiotrophoblast throughout pregnancy [31] and in other physiological contexts such as bone and muscle. It is interesting to speculate that through direct intercellular

nanotubes, senescent cells could also relay danger signals to neighbouring cells and co-ordinate induction of paracrine senescence, just as cell fusion may induce senescence in syncytia. It will be of interest to assess the degree of electrical continuity between such connected senescent cells, as direct cytoplasmic bridges large enough for passage of mitochondria negate the need for other junctional structures such as gap junctions. Membrane potentials have been reported to be very low in senescence [32], and this may have implications for the low propensity of senescent cells to undergo apoptosis. Direct cell-cell contacts leading to supercellularity are therefore of particular interest in senescence and in development of senomodifying therapies.

4.2. Pathological Relevance of Direct Intercellular Contacts.
While the data we present here suggest that a substantial proportion of senescent cells formed direct cell-cell bridges which can mediate intercellular mitochondrial transfer, it is important to note that these data were acquired in 2-dimensional *in vitro* cell culture of primary human skin and lung fibroblasts. While further work is undoubtedly required to probe the physiological relevance of these findings, previous *in vivo* work has shown that intercellular contacts can both rescue compromised cells and spread disease or infection, suggesting context-dependent function or exploitation by invading pathogens. Indeed, TNTs between tumour cells can play important roles in pathogenesis and invasion, for example, through intercellular transfer of the P-glycoprotein drug efflux pump to propagate multidrug resistance [33], together with intercellular mitochondrial transport for cellular rescue. TNTs have been implicated in the intercellular spread of pathogens such as HIV [34], influenza [35], and herpes viral particles as well as prions [36]. Importantly, in the context of age-related diseases, protein aggregates implicated in neurodegenerative diseases, including polyglutamine aggregates [37], α-synuclein [11, 38], and tau [39], have also been reported to be passed between cells through TNTs. The impact of intercellular tunnelling nanotubes is therefore likely to be determined by both the transferred cargo as well as the types and states of the connected cells.

4.3. Possible Roles of Mitochondrial Transfer through TNTs.
Mitochondria are important signalling hubs for oxidative stress, apoptosis, and senescence. While we note here transfer of mitochondria between cells, we did not address the functional status of the transferred mitochondria. Senescent cells are known to accumulate dysfunctional mitochondria, and previous reports suggest that healthy mitochondria may be preferentially transferred to stressed cells [12]. Measuring the O_2 consumption and activity of individual ETC components in senescent and proliferating cells following coculture would therefore be informative as to whether healthy or dysfunctional mitochondria are preferentially transferred. Another important line of enquiry is whether the nanotube structures that senescent cells make with NK cells [12] also participate in intercellular mitochondrial transfer, as well as analysing the impact of direct interaction between senescent and proliferating cells, e.g., through analysis of proliferation capacity in co-cultures with direct contact compared with barrier trans-well formats. Moreover, it will be important to investigate the role of these intercellular connections in a physiologically relevant model, for example, in 3D culture formats such as hydrogels of appropriate rigidity reflecting "young" and "old" tissue structures. Indeed, recently published data analysing TNT formation in mesenchymal stem cell (MSC) spheroids showed intercellular transfer of cytosolic dyes, and intriguingly, inclusion of low passage MSCs with high passage cells was seen to abrogate p16 expression in spheroids, dependent on TNT formation. Hence, in this context, TNTs appear to rescue the proliferation potential of high passage cells, potentially overcoming senescence induction [16].

4.4. Role of Cell-Cell Communication in Senescence.
While senescent cells are known to accumulate in tissues with chronological age and within tumours, they also play important roles in development, tissue regeneration, and wound healing. Furthermore, the profile of cytokines, chemokines, matrix remodelling enzymes and growth factors secreted in the SASP is highly heterogeneous between cell types and modes of senescence induction, perhaps underpinning the range of different paracrine responses to local induction of senescence. In these different physiological contexts, it is highly likely that senescent cells could exert a number of different impacts through direct intercellular bridges. Indeed, it is possible that within a tumour, intercellular bridges could participate in both rescuing cancer cells with dysfunctional mitochondria, but also in facilitating communication between the senescent and immune cells to promote immune surveillance [16]. It is also important to note that senescent cells have actually been shown to evade immune surveillance, for example, by HLA-E upregulation [40]; thus, TNTs may enable evasion of immune detection through shuttling of surface markers. Moreover, direct connections between senescent cells and proliferating neighbours may provide an additional means for spread of senescence—possibly even in the absence of secreted SASP factors that can induce bystander senescence. Therapies that focus on suppressing the SASP may therefore not be sufficient to ameliorate damaging aspects of senescent cell accumulation in cancer and ageing, and may additionally need to include approaches to disrupt direct cell-cell contacts through TNTs.

4.5. Targeting Intercellular Tunnelling Nanotubes in Human Disease.
Proteins that promote actin polymerisation and stabilisation play an important role in facilitating direct cell-cell contact via membrane-bound bridges [16]. Using co-culture assays and live cell imaging, we report here that not only do these bridges increase in frequency in senescence resulting from various stresses (replicative exhaustion, DNA damage, or oncogene activation), but that they are regulated by mTOR and CDC42 signalling, and facilitate direct intercellular mitochondrial transfer. Importantly, CDC42 may act downstream of constitutive mTOR activity in senescence.

While intercellular bridges may play important roles in physiological processes requiring cell-cell communication, such as aiding NK-mediated recognition of senescent cells

[31], the pathological effects of cell-cell bridges may be amenable to therapeutic intervention. CDC42 signalling, implicated in the actin organisation network, is reported to be elevated in senescent versus proliferating cells and to promote premature ageing [41] and, as we show here, is necessary for TNT formation and/or stability. Actin cytoskeletal rearrangements, regulated by mTOR- and CDC42-dependent pathways, are also likely to play a role in the enlarged, flattened morphology observed for senescent cells *in vitro* [21], as well as enlargement *in vivo* [42], and our results show that senescent cells have higher numbers of TNTs than proliferating cells.

The importance of CDC42 and mTOR in senescence may therefore extend beyond regulating the SASP [43, 44] and the biogenesis and secretion of exosomes [45], to promoting direct intercellular communication through the formation of direct cell-cell communication channels. Consequently, our findings highlight mTOR signalling as critical in directing the non-cell-autonomous roles of cellular senescence and further emphasise its validity as a therapeutic target for senomodifying therapies, building on reports of beneficial effects of mTOR inhibitors on senescence phenotypes *in vitro* [21] and longevity and health *in vivo* [46, 47]. It is tempting to speculate that the utility of mTOR inhibitors in a number of age-related diseases (reviewed in [48]) including Alzheimer's disease ([49]; reviewed in [50]) and immune senescence [51], as well as their ability to improve ageing human skin structure [52], may be at least in part through actin cytoskeletal modulation that impacts TNT formation.

Reducing TNT formation or stability through mTOR or CDC42 inhibition may be a useful therapeutic approach in cancer as well as in ageing, for example, through blocking the transfer of healthy mitochondria from bystander cells to rescue dysfunctional tumour cells, or through blocking the spread of drug resistance channels. Indeed, neutralising antibodies against the adhesion molecule ICAM-1 in T cell acute lymphoblastic leukaemia were shown to block the transfer of healthy mitochondria from MSCs, thereby causing an increase in chemotherapy-induced cancer cell death [53]. This approach may also be important in preventing the spread of pathogens such as HIV or protein aggregates implicated in neurodegeneration: inhibiting nanotube formation with latrunculin B was shown to prevent the spread of α-synuclein through healthy astrocytes in a model of Parkinson's disease propagation [54].

Alternatively, it may be possible to exploit the beneficial properties of nanotubes, for example, in treating diseases of organelle dysfunction or by using intercellular mitochondrial transfer as a rescue strategy for compromised cells during stroke, when ischaemic stress conditions may stimulate nanotube formation. In such circumstances, it may be possible to further promote nanotube formation by supplying a treatment that induces ROS, stabilizes microtubules or actin networks, or through inducing increased expression of trafficking adaptors in the mitochondria "donor" cells. It may even be possible to exploit intercellular nanotubes as a drug delivery pathway in cancer therapy, as nanoparticles have been shown to be loaded into and move through TNTs [55].

5. Conclusions

In conclusion, we have demonstrated here a high prevalence of intercellular bridges (also called tunnelling nanotubes (TNTs)) between senescent cells, which are membrane-bound and supported by a cytoskeleton containing actin and possibly also microtubules. Such bridges allow transfer of large cargo including mitochondria between cells. The dependence of such bridges on mTOR and CDC42 makes them amenable to small molecule intervention, providing additional therapeutic strategies to modulate senescent cell behaviour in both age-related diseases and cancer.

Data Availability

Data are available from the corresponding author upon reasonable email request.

Disclosure

The donors had no role in the design, conduct, or analysis of experiments, the preparation of the paper, or the decision to publish.

Conflicts of Interest

The authors declare no conflict of interest.

Acknowledgments

Supplementary Materials

Supplementary Video: time-lapse video microscopy of mitochondrial transfer via TNTs in replicatively senescent HF043 fibroblasts stained with MitoTracker Green, rhodamine-WGA, and NucBlue Live (for DNA). Scale bar 32 μm. Note: still images from this video are shown in Figure 5. Supplementary Figure S1: growth curve of primary skin fibroblasts. HF043 cells were continuously cultured until replicative senescence at cumulative population doubling (CPD) ≥ 86. Each point represents harvesting and reseeding of cells under continuous cultivation, when cell numbers are counted to calculate CPD. Supplementary Figure S2: markers of senescence. Proliferating and senescent cells were verified by both morphological analysis under phase contrast microscopy and staining for senescence-associated beta-galactosidase (SA-β-gal). For replicative senescence, proliferating HF043 cells at CPD < 40 and senescent cells at CPD ~ 87. For DNA damage-induced senescence, proliferating HF043 skin fibroblasts at low CPD were treated with etoposide (see Materials and Methods); for oncogene-induced senescence, proliferating IMR90 ER:RAS cells were treated with 4-hydroxytamoxifen (4-OHT) to induce

RAS expression. CTRL = control. Scale bar 50 μm. Supplementary Figure S3: markers of senescence. (A, B) IL-6 SASP factor secretion is elevated in senescent versus proliferating cells. (A) Standard curve for IL-6 ELISA using purified recombinant IL-6. (B) Measurement of IL-6 in proliferating (PRO) and replicatively senescent (SEN) cells by ELISA ($n = 3$, mean ± SD). (C) Upregulation of p21 in senescent cells. Representative western blotting of p21^{CDKN1} and loading control GAPDH in proliferating (PRO) cells with (+) or without (-) DNA damaging agent etoposide to induce DDIS, and replicatively senescent (SEN) cells without etoposide treatment. Supplementary Figure S4: senescent cells are the major donors for mitochondrial transfer. Cells were prelabelled with MitoTracker Green or MitoTracker Red as in the main text and co-cultured at a 1 : 1 ratio. (A) Enlarged areas from cells in Figures 4 and 7, showing transfer of both the red and green mitochondria between cells. Scale bar 50 μm. (B) Transfer of mitochondria quantified by MitoTracker dye colour of the donor and recipient; bars coloured by the MitoTracker label of recipient cells; the MitoTracker label of the donor and recipient is indicated by colour below each column (MitoTracker Green shown in green and MitoTracker Red shown in red). P = proliferating; S = replicatively senescent. One-way ANOVA. ns = not significant. $^{***}p = 0.0002$. (C) Violin plot of quantification of mitochondrial donation, according to the percentage of recipient cells stained with MitoTracker Red (R) showing donated MitoTracker Green (G) foci (%R cells with G mt) and the percentage of recipient cells stained with MitoTracker Green (G) showing donated MitoTracker Red (R) foci (i.e., %G cells with R mt). Two-way ANOVA. ns = not significant. $^{****}p < 0.0001$. Mean, 25th and 75th centiles, and individual data points are shown. mt = mitochondria. Supplementary Figure S5: dose-response curves for cells treated with (A) AZD8055 or (B) CASIN at concentrations from 0 to 10,000 nM. Cell reducing capacity, often used as a proxy for cell viability, was assessed by alamarBlue staining. Note: 0 nM not shown as data are plotted on a log scale; values are normalised to zero drug control, taken as 100%. Drug doses were tested on proliferating (PRO) cells as well as replicatively senescent (RS) and DDIS cells induced by etoposide treatment (ETOP). Mean and SD are shown from $n = 3$. Supplementary Figure S6: intercellular bridge formation is sensitive to CDC42 inhibition in a dose-dependent manner. HF043 fibroblasts at CPD 71 were incubated with 0, 1, 2, and 5 μm CASIN, an inhibitor of CDC42 for 24 h, and then stained with FITC-WGA (green), rhodamine-phalloidin (actin, red), and NucBlue Live for DNA (blue). Scale bar 100 μm. *(Supplementary Materials)*

References

[1] A. Rustom, R. Saffrich, I. Markovic, P. Walther, and H. H. Gerdes, "Nanotubular highways for intercellular organelle transport," *Science*, vol. 303, no. 5660, pp. 1007–1010, 2004.

[2] M. Dupont, S. Souriant, G. Lugo-Villarino, I. Maridonneau-Parini, and C. Verollet, "Tunneling nanotubes: intimate communication between myeloid cells," *Frontiers in Immunology*, vol. 9, p. 43, 2018.

[3] L. Marzo, K. Gousset, and C. Zurzolo, "Multifaceted roles of tunneling nanotubes in intercellular communication," *Frontiers in Physiology*, vol. 3, p. 72, 2012.

[4] A. Takahashi, A. Kukita, Y. J. Li et al., "Tunneling nanotube formation is essential for the regulation of osteoclastogenesis," *Journal of Cellular Biochemistry*, vol. 114, no. 6, pp. 1238–1247, 2013.

[5] H. R. Chinnery, E. Pearlman, and P. G. McMenamin, "Cutting edge: membrane nanotubes in vivo: a feature of MHC class II+ cells in the mouse cornea," *Journal of Immunology*, vol. 180, no. 9, pp. 5779–5783, 2008.

[6] E. Lou, S. Fujisawa, A. Morozov et al., "Tunneling nanotubes provide a unique conduit for intercellular transfer of cellular contents in human malignant pleural mesothelioma," *PLoS One*, vol. 7, no. 3, article e33093, 2012.

[7] B. Onfelt, S. Nedvetzki, R. K. Benninger et al., "Structurally distinct membrane nanotubes between human macrophages support long-distance vesicular traffic or surfing of bacteria," *Journal of Immunology*, vol. 177, no. 12, pp. 8476–8483, 2006.

[8] S. J. Hanna, K. McCoy-Simandle, V. Miskolci et al., "The role of Rho-GTPases and actin polymerization during macrophage tunneling nanotube biogenesis," *Scientific Reports*, vol. 7, no. 1, article 8547, 2017.

[9] H. Ohno, K. Hase, and S. Kimura, "M-Sec: emerging secrets of tunneling nanotube formation," *Communicative & Integrative Biology*, vol. 3, no. 3, pp. 231–233, 2010.

[10] S. Domhan, L. Ma, A. Tai et al., "Intercellular communication by exchange of cytoplasmic material via tunneling nano-tube like structures in primary human renal epithelial cells," *PLoS One*, vol. 6, no. 6, article e21283, 2011.

[11] Y. Wang, J. Cui, X. Sun, and Y. Zhang, "Tunneling-nanotube development in astrocytes depends on p53 activation," *Cell Death and Differentiation*, vol. 18, no. 4, pp. 732–742, 2011.

[12] X. Wang and H. H. Gerdes, "Transfer of mitochondria via tunneling nanotubes rescues apoptotic PC12 cells," *Cell Death and Differentiation*, vol. 22, no. 7, pp. 1181–1191, 2015.

[13] M. Koyanagi, R. P. Brandes, J. Haendeler, A. M. Zeiher, and S. Dimmeler, "Cell-to-cell connection of endothelial progenitor cells with cardiac myocytes by nanotubes: a novel mechanism for cell fate changes?," *Circulation Research*, vol. 96, no. 10, pp. 1039–1041, 2005.

[14] P. D. Arkwright, F. Luchetti, J. Tour et al., "Fas stimulation of T lymphocytes promotes rapid intercellular exchange of death signals via membrane nanotubes," *Cell Research*, vol. 20, no. 1, pp. 72–88, 2010.

[15] J. P. de Magalhães and J. F. Passos, "Stress, cell senescence and organismal ageing," *Mechanisms of Ageing and Development*, vol. 170, pp. 2–9, 2018.

[16] A. Biran, M. Perelmutter, H. Gal et al., "Senescent cells communicate via intercellular protein transfer," *Genes & Development*, vol. 29, no. 8, pp. 791–802, 2015.

[17] C. C. Uphoff and H. G. Drexler, "Comparative PCR analysis for detection of mycoplasma infections in continuous cell lines," *In Vitro Cell Dev Biol Anim*, vol. 38, no. 2, pp. 79–85, 2002.

[18] C. C. Uphoff and H. G. Drexler, "Detecting mycoplasma contamination in cell cultures by polymerase chain reaction," *Methods in Molecular Medicine*, vol. 88, pp. 319–326, 2004.

[19] L. Alili, J. Diekmann, M. Giesen, O. Holtkötter, and P. Brenneisen, "A drug-induced accelerated senescence (DIAS) is a possibility to study aging in time lapse," *Age*, vol. 36, no. 3, article 9658, 2014.

[20] A. Rolt, A. Nair, and L. S. Cox, "Optimisation of a screening platform for determining IL-6 inflammatory signalling in the

senescence-associated secretory phenotype (SASP)," *Biogerontology*, vol. 20, no. 3, pp. 359–371, 2019.

[21] H. E. Walters, S. Deneka-Hannemann, and L. S. Cox, "Reversal of phenotypes of cellular senescence by pan-mTOR inhibition," *Aging*, vol. 8, no. 2, pp. 231–244, 2016.

[22] R. Yosef, N. Pilpel, N. Papismadov et al., "p21 maintains senescent cell viability under persistent DNA damage response by restraining JNK and caspase signaling," *The EMBO Journal*, vol. 36, no. 15, pp. 2280–2295, 2017.

[23] H. E. Walters and L. S. Cox, "Generation of a novel model of primary human cell senescence through Tenovin-6 mediated inhibition of sirtuins," *Biogerontology*, vol. 20, no. 3, pp. 303–319, 2019.

[24] P. Veranic, M. Lokar, G. J. Schutz et al., "Different types of cell-to-cell connections mediated by nanotubular structures," *Biophysical Journal*, vol. 95, no. 9, pp. 4416–4425, 2008.

[25] C. Correia-Melo, F. D. Marques, R. Anderson et al., "Mitochondria are required for pro-ageing features of the senescent phenotype," *The EMBO Journal*, vol. 35, no. 7, pp. 724–742, 2016.

[26] V. I. Korolchuk, S. Miwa, B. Carroll, and T. von Zglinicki, "Mitochondria in cell senescence: is mitophagy the weakest link?," *eBioMedicine*, vol. 21, pp. 7–13, 2017.

[27] Y. Ovadya, T. Landsberger, H. Leins et al., "Impaired immune surveillance accelerates accumulation of senescent cells and aging," *Nature Communications*, vol. 9, no. 1, article 5435, 2018.

[28] J. M. Gonzalez-Meljem, J. R. Apps, H. C. Fraser, and J. P. Martinez-Barbera, "Paracrine roles of cellular senescence in promoting tumourigenesis," *British Journal of Cancer*, vol. 118, no. 10, pp. 1283–1288, 2018.

[29] G. Nelson, J. Wordsworth, C. Wang et al., "A senescent cell bystander effect: senescence-induced senescence," *Aging Cell*, vol. 11, no. 2, pp. 345–349, 2012.

[30] L. S. Cox and C. Redman, "The role of cellular senescence in ageing of the placenta," *Placenta*, vol. 52, pp. 139–145, 2017.

[31] A. Chuprin, H. Gal, T. Biron-Shental et al., "Cell fusion induced by ERVWE1 or measles virus causes cellular senescence," *Genes & Development*, vol. 27, no. 21, pp. 2356–2366, 2013.

[32] B. Carroll, G. Nelson, Y. Rabanal-Ruiz et al., "Persistent mTORC1 signaling in cell senescence results from defects in amino acid and growth factor sensing," *The Journal of Cell Biology*, vol. 216, no. 7, pp. 1949–1957, 2017.

[33] J. Pasquier, L. Galas, C. Boulange-Lecomte et al., "Different modalities of intercellular membrane exchanges mediate cell-to-cell p-glycoprotein transfers in MCF-7 breast cancer cells," *The Journal of Biological Chemistry*, vol. 287, no. 10, pp. 7374–7387, 2012.

[34] S. Sowinski, C. Jolly, O. Berninghausen et al., "Membrane nanotubes physically connect T cells over long distances presenting a novel route for HIV-1 transmission," *Nature Cell Biology*, vol. 10, no. 2, pp. 211–219, 2008.

[35] A. Kumar, J. H. Kim, P. Ranjan et al., "Influenza virus exploits tunneling nanotubes for cell-to-cell spread," *Scientific Reports*, vol. 7, article 40360, 2017.

[36] K. Gousset, E. Schiff, C. Langevin et al., "Prions hijack tunnelling nanotubes for intercellular spread," *Nature Cell Biology*, vol. 11, no. 3, pp. 328–336, 2009.

[37] M. Costanzo, S. Abounit, L. Marzo et al., "Transfer of polyglutamine aggregates in neuronal cells occurs in tunneling nanotubes," *Journal of Cell Science*, vol. 126, pp. 3678–3685, 2013.

[38] S. Abounit, L. Bousset, F. Loria et al., "Tunneling nanotubes spread fibrillar α-synuclein by intercellular trafficking of lysosomes," *The EMBO Journal*, vol. 35, no. 19, pp. 2120–2138, 2016.

[39] S. Abounit, J. W. Wu, K. Duff, G. S. Victoria, and C. Zurzolo, "Tunneling nanotubes: a possible highway in the spreading of tau and other prion-like proteins in neurodegenerative diseases," *Prion*, vol. 10, no. 5, pp. 344–351, 2016.

[40] B. I. Pereira, O. P. Devine, M. Vukmanovic-Stejic et al., "Senescent cells evade immune clearance via HLA-E-mediated NK and CD8(+) T cell inhibition," *Nature Communications*, vol. 10, no. 1, article 2387, 2019.

[41] L. Wang, L. Yang, M. Debidda, D. Witte, and Y. Zheng, "Cdc42 GTPase-activating protein deficiency promotes genomic instability and premature aging-like phenotypes," *Proceedings of the National Academy of Sciences of the United States of America*, vol. 104, no. 4, article 1248, 2007.

[42] A. Biran, L. Zada, P. Abou Karam et al., "Quantitative identification of senescent cells in aging and disease," *Aging Cell*, vol. 16, no. 4, pp. 661–671, 2017.

[43] N. Herranz, S. Gallage, M. Mellone et al., "mTOR regulates MAPKAPK2 translation to control the senescence-associated secretory phenotype," *Nature Cell Biology*, vol. 17, no. 9, pp. 1205–1217, 2015.

[44] R. M. Laberge, Y. Sun, A. V. Orjalo et al., "MTOR regulates the pro-tumorigenic senescence-associated secretory phenotype by promoting IL1A translation," *Nature Cell Biology*, vol. 17, no. 8, pp. 1049–1061, 2015.

[45] W. Zou, M. Lai, Y. Zhang et al., "Exosome release is regulated by mTORC1," *Advanced Science*, vol. 6, no. 3, article 1801313, 2019.

[46] D. E. Harrison, R. Strong, Z. D. Sharp et al., "Rapamycin fed late in life extends lifespan in genetically heterogeneous mice," *Nature*, vol. 460, no. 7253, pp. 392–395, 2009.

[47] S. R. Urfer, T. L. Kaeberlein, S. Mailheau et al., "A randomized controlled trial to establish effects of short-term rapamycin treatment in 24 middle-aged companion dogs," *GeroScience*, vol. 39, no. 2, pp. 117–127, 2017.

[48] H. E. Walters and L. S. Cox, "mTORC inhibitors as broad-spectrum therapeutics for age-related diseases," *International Journal of Molecular Sciences*, vol. 19, no. 8, article 2325, 2018.

[49] P. Spilman, N. Podlutskaya, M. J. Hart et al., "Inhibition of mTOR by rapamycin abolishes cognitive deficits and reduces amyloid-beta levels in a mouse model of Alzheimer's disease," *PLoS One*, vol. 5, no. 4, article e9979, 2010.

[50] R. Selvarani, S. Mohammed, and A. Richardson, "Effect of rapamycin on aging and age-related diseases-past and future," *Geroscience*, vol. 43, no. 3, pp. 1135–1158, 2021.

[51] J. B. Mannick, M. Morris, H. P. Hockey et al., "TORC1 inhibition enhances immune function and reduces infections in the elderly," *Science Translational Medicine*, vol. 10, no. 449, article eaaq1564, 2018.

[52] C. L. Chung, I. Lawrence, M. Hoffman et al., "Topical rapamycin reduces markers of senescence and aging in human skin: an exploratory, prospective, randomized trial," *GeroScience*, vol. 41, no. 6, pp. 861–869, 2019.

[53] J. Wang, X. Liu, Y. Qiu et al., "Cell adhesion-mediated mitochondria transfer contributes to mesenchymal stem cell-induced chemoresistance on T cell acute lymphoblastic leukemia cells," *Journal of Hematology & Oncology*, vol. 11, no. 1, p. 11, 2018.

[54] J. Rostami, S. Holmqvist, V. Lindstrom et al., "Human astrocytes transfer aggregated alpha-synuclein via tunneling nanotubes," *The Journal of Neuroscience*, vol. 37, no. 49, pp. 11835–11853, 2017.

[55] J. Kristl, K. T. Plajnsek, M. E. Kreft, B. Jankovic, and P. Kocbek, "Intracellular trafficking of solid lipid nanoparticles and their distribution between cells through tunneling nanotubes," *European Journal of Pharmaceutical Sciences*, vol. 50, no. 1, pp. 139–148, 2013.

Research Article

Ginsenoside Rg5 Inhibits Human Osteosarcoma Cell Proliferation and Induces Cell Apoptosis through PI3K/Akt/mTORC1-Related LC3 Autophagy Pathway

Ming-Yang Liu,[1,2] Fei Liu,[3] Yan-Jiao Li,[4] Jia-Ning Yin,[5] Yan-Li Gao,[5] Xin-Yue Wang,[6] Chen Yang,[2] Jian-Guo Liu,[2] and Hai-Jun Li [1]

[1]Department of Immunity, Institute of Translational Medicine, The First Hospital of Jilin University, China
[2]Departments of Orthopaedics, The First Hospital of Jilin University, China
[3]Department of Obstetrics, The First Hospital of Jilin University, China
[4]Department of Pharmacy, The First Hospital of Jilin University, China
[5]Department of Pediatrics, The First Hospital of Jilin University, China
[6]Department of Scientific Research, College of Basic Medicine, Jilin University, China

Correspondence should be addressed to Hai-Jun Li; hjli2012@jlu.edu.cn

The function and mechanism underlying the suppression of human osteosarcoma cells by ginsenoside-Rg5 (Rg5) was investigated in the present study. MG-63, HOS, and U2OS cell proliferation was determined by MTT assay after Rg5 treatment for 24 h. Rg5 inhibited human osteosarcoma cell proliferation effectively in a dose-dependent manner. The range of effective inhibitory concentrations was 160-1280 nM. Annexin V-FITC and PI double-staining assay revealed that Rg5 induced human osteosarcoma cell apoptosis. Western blotting, qRT-PCR, and FACS experiments revealed that Rg5 inhibited human osteosarcoma cells via caspase-3 activity which was related to the LC3-mediated autophagy pathway. Rg5 decreased the phosphorylation of PI3K, Akt, and mTORC1 activation. In contrast, LC3-mediated autophagy and caspase-3 activity increased significantly. A PI3K/AKT stimulator, IGF-1, reversed Rg5-induced cell autophagy and apoptosis in MG-63 cells. Collectively, the current study demonstrated that Rg5 induced human osteosarcoma cell apoptosis through the LC3-mediated autophagy pathway. Under physiological conditions, activation of PI3K/AKT/mTORC1 inhibits LC3 activity and caspase-3-related cell apoptosis. However, Rg5 activated LC3 activity by inhibiting the activation of PI3K/AKT/mTORC1. The present study indicated that Rg5 could be a promising candidate as a chemotherapeutic agent against human osteosarcoma.

1. Introduction

Osteosarcoma (OS) causes a 2.4% death rate in child cancers, which is a fatal malignancy in pediatric patients [1]. The 5-year survival rate is no more than 70% because there are limited effective therapies except for surgical treatment [2]. OS is believed to be derived from malignant mesenchymal stem cells of the long bones [3–6]. Chemotherapy is still suitable for patients who are not suitable for surgery. However, side effects and drug resistance limited the use of chemotherapy drugs [7]. Herbal medicines and natural prod-

ucts have drawn increasing attention to novel anticancer agents because of the outstanding effectiveness and safety [8–10].

Ginseng has been used for over 2,000 years in various countries in East Asia, including Korea, China, Japan, and Vietnam [11]. Ginsenosides are the most effective components in ginseng. Rg5 is a minor ginsenoside but exhibits a superior pharmaceutical effect comparing with other major ginsenosides [12–14]. Rg5 promoted breast cancer cell apoptosis and inhibited cell proliferation by activating the AMPK pathway [15–17]. Through inducing G2/M phase cell cycle arrest and ROS-mediated MAPK activity, Rg5 inhibit

human gastric cancer cell proliferation [18]. Rg5 also suppressed proliferation and promoted the apoptosis of human esophageal cancer cells and human hepatoma HepG2 cells [19, 20]. Additionally, inhibiting the AKT signaling pathway and downregulating BCL2 expression is the main mechanism of Rg5 on inhibition of retinoblastoma cells [21]. Therefore, Rg5 may serve as a chemosensitizer for reversing multidrug resistance [22].

Autophagy is considered to be an important cellular metabolic process [23, 24]. The function of autophagy regulates cell fate via different mechanisms [25, 26]. There is no study on the function of Rg5 on human osteosarcoma cells and the related mechanisms from now on. The current study investigated whether ginsenoside Rg5 induce the osteosarcoma cell apoptosis and the potential mechanisms. These findings may contribute to further understand the inhibitory effect of Rg5 against human osteosarcoma cell proliferation, as well as highlight the possibility of Rg5 as therapeutic agents for human osteosarcoma.

2. Material and Methods

2.1. Reagents. Rg5 was purchased from the Yuanye Pharmaceutical Company (#P186763-78-0, Shanghai, China). Rg5 was dissolved in dimethylsulfoxide (DMSO, #D8370, Solarbio, Beijing, China) at 100 mM and stored at -20°C. MTT (#M2003) and RNase (#R4875) were purchased from Sigma (Shanghai, China). Annexin V/PI kit was purchased from BD company (#556547, Franklin Lakes, NJ, USA). LC3 siRNA reagent kit (#6215), the primary and second antibodies used in western blotting, was purchased from CST (Boston, MA, USA). DMEM cell culture medium (#12491-023), FBS (#10099141), antibiotic for cell culture (#10378016), and trypsin (#25300054) were from GIBCO (Grand Island, NY, USA).

2.2. Cell Proliferation Assay. HOS, MG-63, and U2OS were purchased from ATCC in Shanghai of China. 5×10^4 cells were seeded in a 96-well plate for 24 h, then treated with Rg5 (0, 10, 20, 40, 80, 160, 320, 640, and 1280 nM) for another 24 h for MTT assay. MTT (1.0 mg/mL) was added to each well, and the cells were incubated for 4 h. The MTT solution was then aspirated, and 100 μL DMSO was then added. The 96-well plates were read using a microplate spectrophotometer (Synergy H1, BioTek, USA) at 540 nm. The inhibition percentage was calculated as (1 − the value in experimental group/the value in the control group) × 100%.

2.3. FCM Experiment. Annexin V-FITC and PI double staining flow cytometry analyses were employed to assess cell apoptosis. MG-63, HOS, and U2OS cells were collected on the experimental endpoint. Cell apoptosis was analyzed using a flow cytometer (FACScan; BD Biosciences, Franklin Lakes, NJ, USA) with FlowJo 7.6 FACS analysis software (FlowJo LLC, Ashland, OR, USA). For LC3 staining, cells were stained with FITC-conjugated mouse anti-human LC3 (#bs-8878R, BIOSS). All antibodies were 100-fold dilutions and incubated in 4°C for 15 mins.

2.4. Western Blotting. Cell total protein was extracted, and the protein concentration was determined according to the manufacturer's protocol. A total of 5-40 μg cell total protein was separated by 10% SDS-PAGE and then electrophoretically transferred to polyvinylidene fluoride membranes (0.45 μm; EMD Millipore, Billerica, MA, USA) and blocked at 37°C for 1 h with 5% skim milk in Tris-buffered saline (TBS) with Tween-20 (0.1%). Caspase-3 (#9662), cleaved caspase-3 (#9661), LC3 (#4108), PI3K (#4225), p-PI3K (#13857), AKT (#4691), p-AKT (#4060), mTOR (#2972), Raptor (#2280), and β-actin ($^{\#}$4970) expression levels were determined semiquantitatively by densitometric analysis with the Quantity One software (V4.62, Bio-Rad Laboratories, Inc., Hercules, CA, USA).

2.5. qPCR Experiment. Total cellular RNA was isolated by TRIzol (Invitrogen, Carlsbad, USA). Total RNA was transcribed to cDNA by a reverse transcription kit (TransGen, Beijing, China). qRT-PCR was conducted using the Fast Start Universal SYBR Green Master (ROX) kit (Roche, Shanghai, China). Reactions were performed using 3 μL of cDNA in a 20 μL reaction volume and the following thermal cycle profile: 10 seconds for predenaturation at 94°C, 5 seconds for denaturation at 94°C, and 30 seconds for extension at 60°C, for 40 cycles. The primer sequences are shown as follows: LC3 sense, 5′-GACCATCTGGTTCAGGTTCC-3′, and antisense, 5′-ACATTCCCG AAACTCAGTCG-3′; caspase-3 sense, 5′-CCTCTGACTTCCAGGTGGTCT-3′, and antisense, 5′-TTCGTTGTGTTGCTGTAGCCAAA-3′; and GAPDH sense, 5′-CCAGGTGGTCTCCTCTGACTT-3′, and antisense, 5′-GTTGCTGTAGCCAAATTCGTTGT-3′. All primers were synthesized by Shanghai Sangon in China. The length of caspase-3 is 159 bp, and the PCR products were analyzed by agarose gel electrophoresis.

2.6. RNA Interference Experiment. The sequence of LC3-specific small interfering RNA (siRNA) reagent and the scramble control (GenePharma, Shanghai, China) is as follows: LC3 siRNA sense, 5′-GUGCAUCAGAUUUC ATT-3′, and antisense, 5′-UGAAAAGC UCUGCACTT-3′; scramble sense, 5′-GCUCAUCATTGUGCAGA-3′, and antisense, 5′-UGAGCCACUUGAAAUCT-3. The MG-63 cell line was planted in a 12-well plate at a 5×10^4/mL density and was transfected with 50 pmol of LC3 siRNA or scramble control using Lipofectamine 2000 (Life Technologies, Gaithersburg, MD, USA) and then incubated for 6 h. LC3 expressions were detected using a western blotting experiment.

2.7. Statistical Analysis. All data are shown as Mean ± Standard Deviation (M ± SD) and analyzed using the D'Agostino and Pearson omnibus normality test with at least three independent repetitions. Mean values were compared using either a paired t-test (two groups) or ANOVA (more than two groups). $p < 0.05$ were considered to be significant.
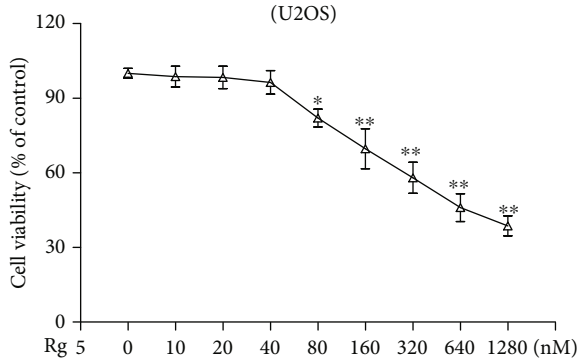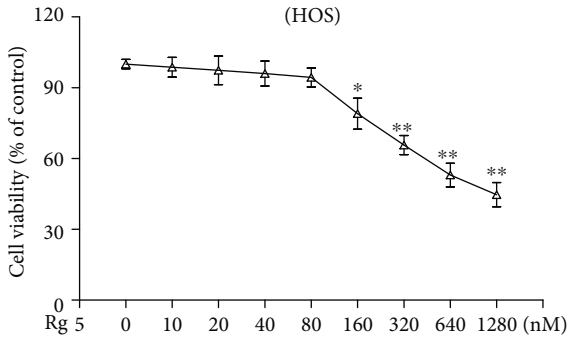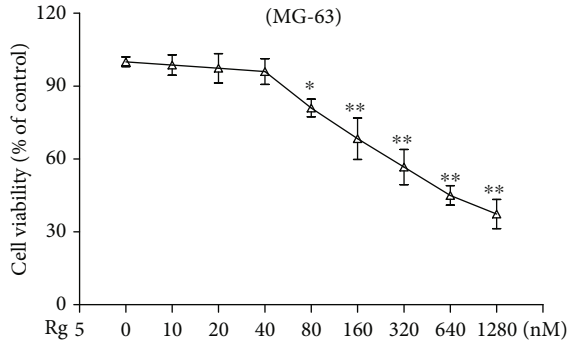
(a)
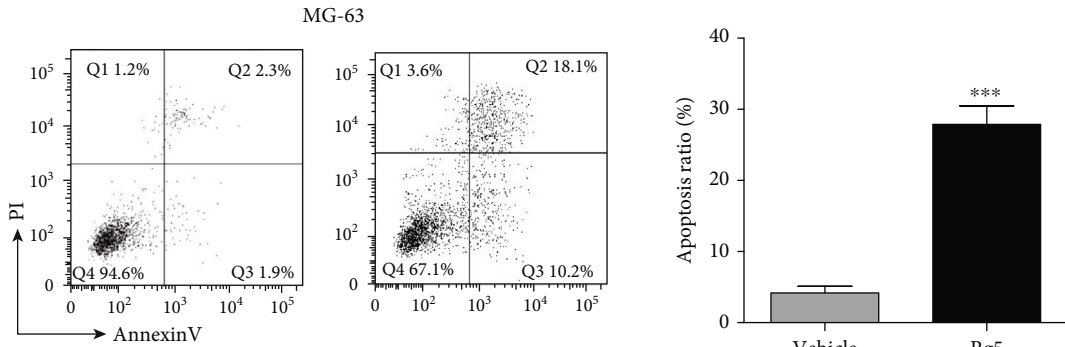
(b)

Figure 1: Continued.
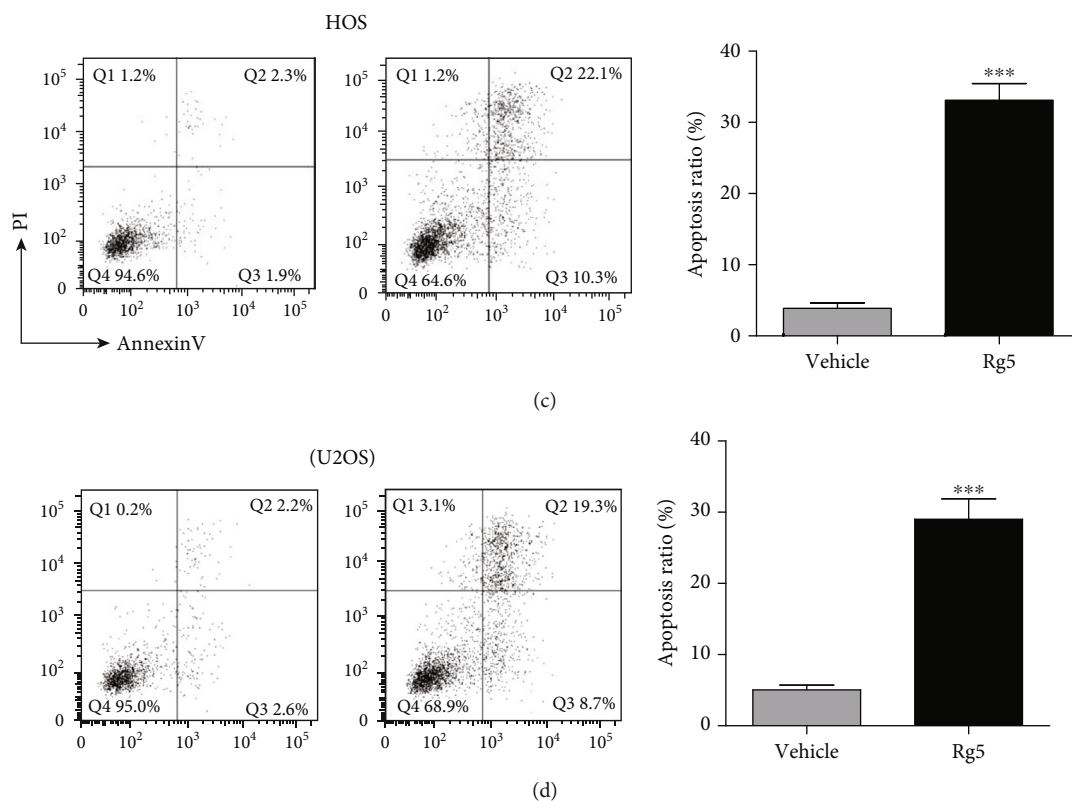
FIGURE 1: Rg5 inhibited human osteosarcoma cell growth and induced apoptosis. (a) MG-63 cells, HOS cells, and U2OS cell vitality were tested by MTT after 24 h treatment of Rg5 with various doses. The concentration for flow cytometric experiment is 160 nM. Representative figures and statistical analysis of the percentage of apoptotic cells in MG-63 (b), HOS (c), and U2OS (d) cells. The data are shown as M ± SD ($n = 3$, $^*p < 0.05$, $^{**}p < 0.01$, and $^{***}p < 0.001$ vs. control).

3. Results

3.1. Rg5 Inhibited Cell Growth and Induced Human Osteosarcoma Cell Apoptosis.

MG-63, HOS, and U2OS cells were treated with Rg5 (0, 10, 20, 40, 80, 160, 320, 640, and 1280 nM) for 24 h; cell proliferation was determined by MTT assay (Figure 1(a)). Rg5 significantly inhibited the growth of MG-63 cells at doses of 80-1280 nM ($p < 0.01$). The susceptibility of HOS cells to Rg5 was slightly weaker than MG-63 cells. The range of effective inhibitory concentrations was 160-1280 nM ($p < 0.01$). The susceptibility of U2OS is similar with MG-63 cells, and the range of effective inhibitory concentrations was 80-1280 nM ($p < 0.001$). Based on the MTT results, we chose 160 nM of Rg5 as the working concentration for apoptosis detection after 24 h treatment. The numbers of apoptotic cells ranged from 4.5 ± 0.8% to 29.9 ± 3.1% in MG-63 cells (Figure 1(b), $p < 0.001$), 3.4 ± 0.9% to 32.3 ± 3.9% in HOS cells (Figure 1(c), $p < 0.001$), and 4.6 ± 1.1% to 27.2 ± 3.5 % in U2OS cells (Figure 1(d), $p < 0.001$).

3.2. Rg5 Inhibited Human Osteosarcoma Cells via Caspase-3 Activity Related to the LC3 Autophagy Pathway.

MG-63 cells, as a representative cell of osteosarcoma, were chose for the mechanism study. MG-63 cells were treated with Rg5 (160 nM) for 12 h. Caspase-3 and LC3 autophagy-related protein was detected by western blotting, qRT-PCR, or FACS. The ratio of LC3-II/LC3-I increased approximately 3-fold after Rg5 treatment (Figures 2(a) and 2(b), $p < 0.01$), accompanied by cleaved caspase-3 activity (Figures 2(a) and 2(c), $p < 0.01$). Caspase-3 gene expression was also confirmed by qRT-PCR experiments (Figure 2(d), $p < 0.01$). Fluorescence-labeled flow cytometry for LC3 expression showed that Rg5 significantly increased the mean fluorescence intensity (MFI) of LC3 in MG-63 cells (Figures 2(e) and 2(f), 960 ± 50 vs. 450 ± 30, $p < 0.01$).

3.3. Inhibition of Autophagy Reduced Rg5-Induced Caspase-3 Activity and Cell Apoptosis.

3-MA acts as an inhibitor of autophagy. 5 mM 3-MA alone or combining with 160 nM Rg5 was used to treat MG-63 cells for 12 h and for caspase-3 and LC3 autophagy-related protein detection by western blotting, qRT-PCR, or FACS. The ratio of LC3-II and LC3-I was reduced when 3-MA was added to the Rg5 treatment system (Figures 3(a) and 3(b), $p < 0.01$). The inhibition effect of 3-MA on LC3-mediated autophagy was also confirmed by fluorescence-labeled flow cytometry (Figures 3(e) and 3(f), $p < 0.01$). Interestingly, when LC3 activity was blocked by 3-MA, caspase-3 activity was also reduced at the protein level (Figure 3(c), $p < 0.01$) compared with Rg5 alone. Furthermore, cell apoptosis staining assays showed that 3-MA decreased Rg5-induced MG-63 cell apoptosis (Figures 3(e) and 3(f), $p < 0.01$).

(a)

(b)

(c)

(d)

(e)

(f)
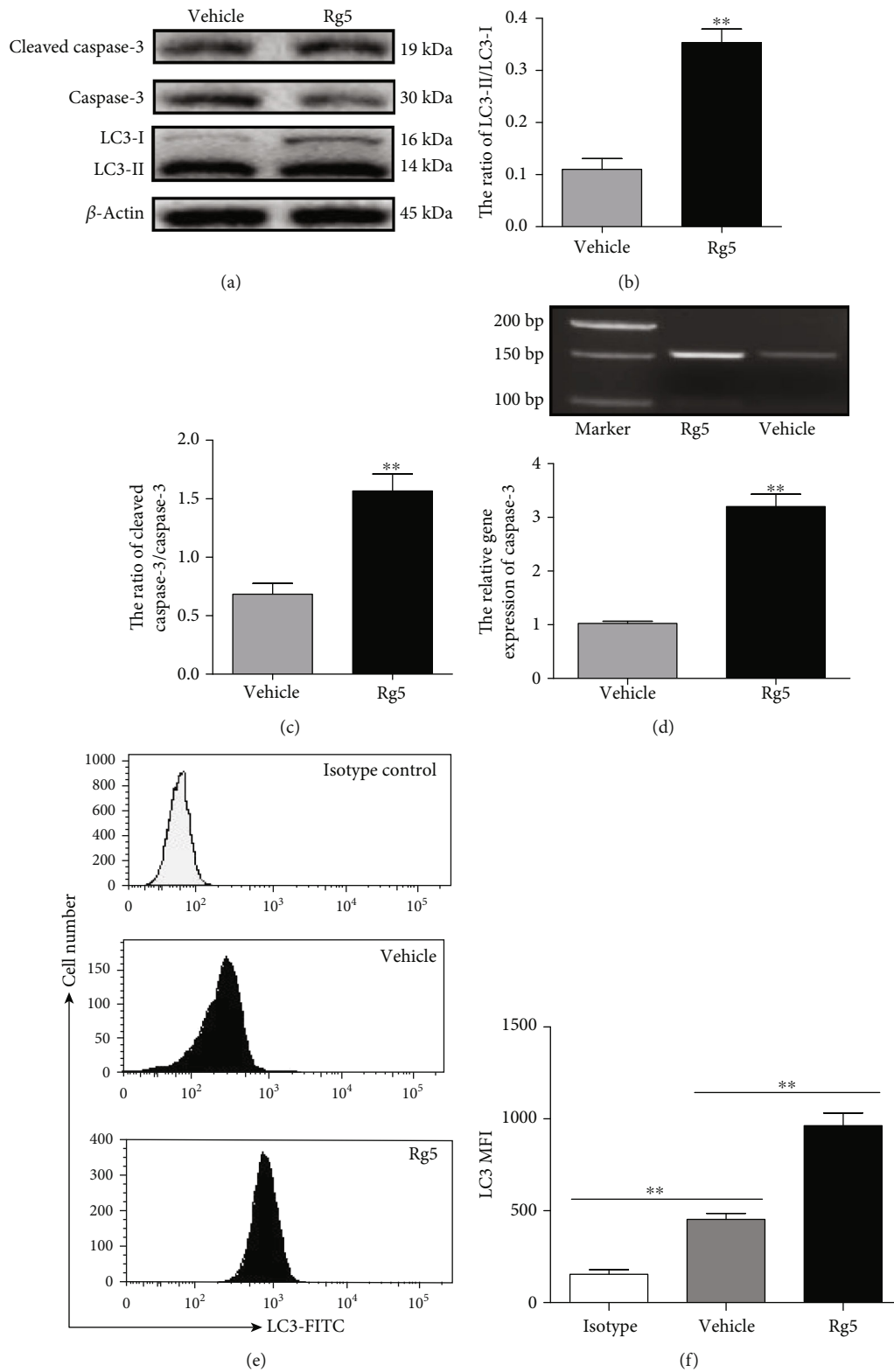
FIGURE 2: Rg5 inhibited MG-63 cells via caspase-3 activity that was related to the LC3-mediated autophagy pathway. MG-63 cells were treated with 160 nM of Rg5, and total proteins were extracted. The expression levels related proteins were detected by western blotting, qRT-PCR, or FACS. (a) Representative image of proteins detected by western blotting. The ratio of LC3-II/LC3-I (b) and cleaved caspase-3/caspase-3 (c) in MG-63 cell. (d) The relative gene expression of caspase-3. (e, f) The MFI of LC3 detected by FACS. The data are shown as M ± SD ($n = 3$, **$p < 0.01$ vs. control).

(a)

(b)

(c)

(d)

(e)

(f)
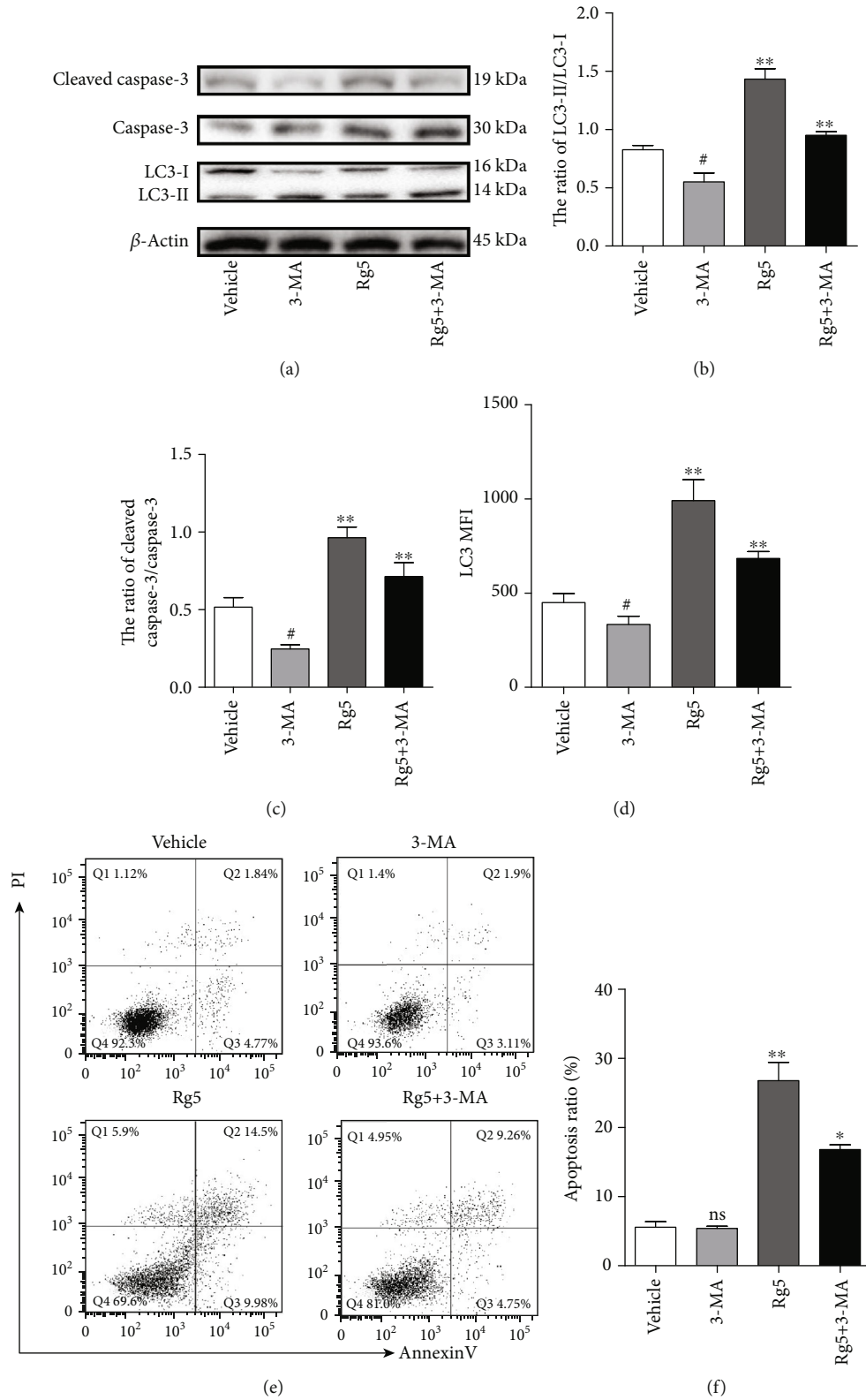
FIGURE 3: Inhibition of autophagy reduced Rg5-induced caspase-3 activity and cell apoptosis. 5 mM 3-MA combining or alone with 160 nM Rg5 was used to treat MG-63 cells for 12 h and for caspase-3 and LC3 autophagy-related protein detection by western blotting or FACS. (a) Representative image of proteins detected by western blotting. (b) The ratio of LC3-II/LC3-I in MG-63 cells. (c) The ratio of cleaved caspase-3/caspase-3 in MG-63 cells. (d) The MFI of LC3 in MG-63 cells detected by FACS. (e, f) MG-63 cell apoptosis detected by FACS. The data are shown as M ± SD ($n = 3$, $^{ns}p > 0.05$, $^{#}p < 0.05$, 3-MA treatment comparing with control; $^{*}p < 0.05$, $^{**}p < 0.01$ vs. control).

(a)

(b)

(c)

(d)

(e)

(f)
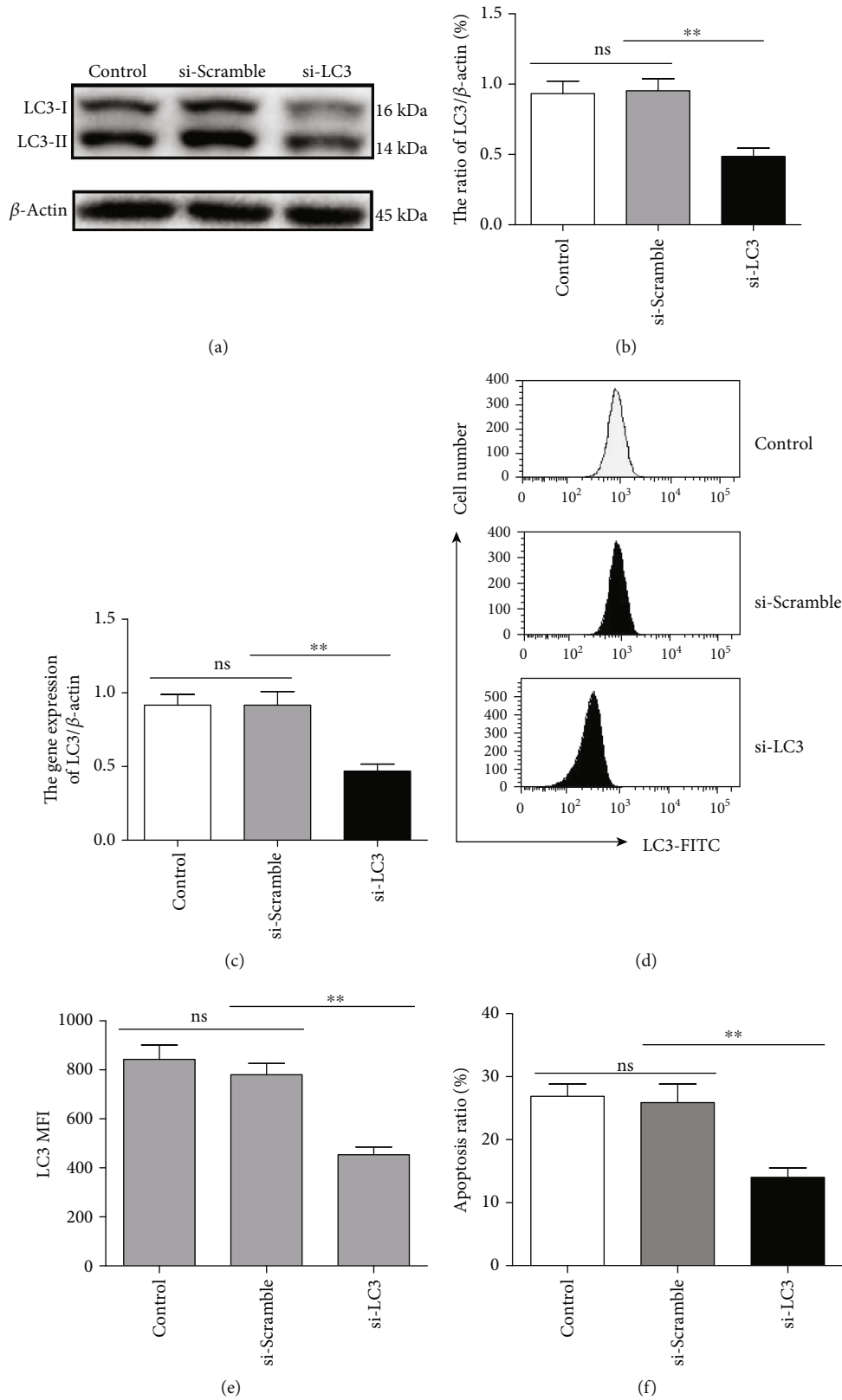
FIGURE 4: Silencing LC3 affects Rg5-induced tumor cell apoptosis. LC3 protein and gene expression were detected by western blot (a, b) and qRT-PCR experiments (c) when the LC3 expression was silenced by RNAi in MG-63 cells. (d, e) The MFI of LC3 in MG-63 cells detected by FACS. (f) MG-63 cell apoptosis detected by FACS. The data are shown as M ± SD ($n = 3$, $^{ns}p > 0.05$, $^{**}p < 0.01$ vs. control).

(a)

(b)

(c)

(d)

(e)

(f)

FIGURE 5: Continued.

(g)

(h)
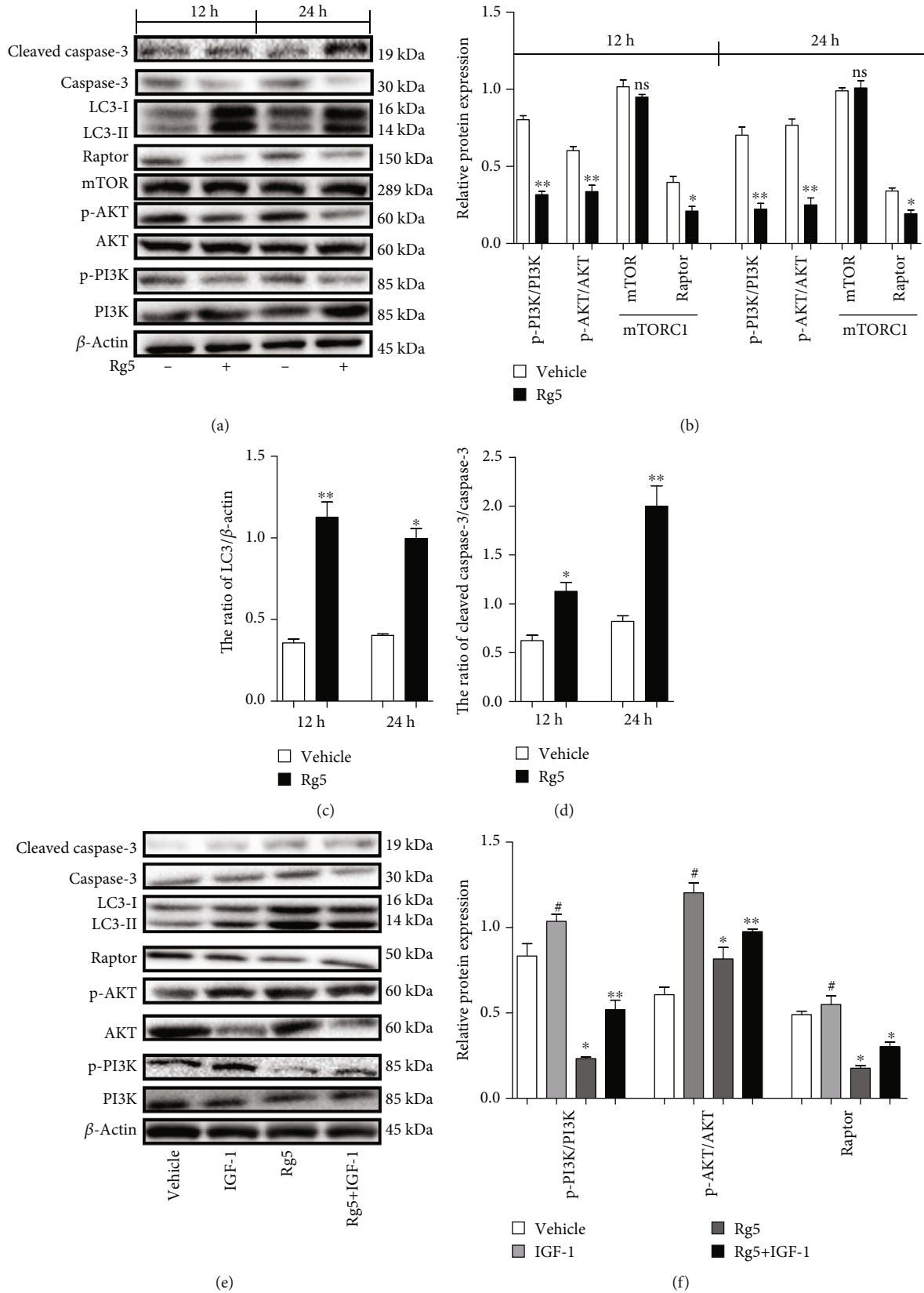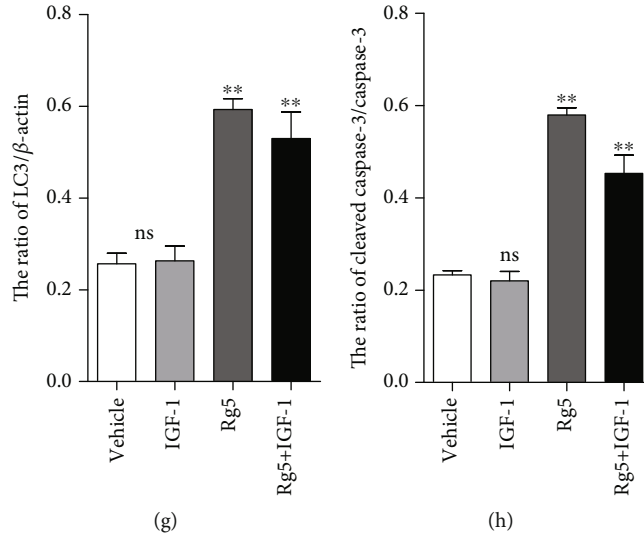
FIGURE 5: The PI3K/AKT/mTORC1 pathway is involved in Rg5-induced human osteosarcoma cell autophagy activation. (a) Representative image of proteins detected by western blotting at 12 h and 24 h after the treatment. (b) Phosphorylated PI3K, Akt, and TORC1 in MG-63 cells. (c) The ratio of LC3/β-actin in MG-63 cells. (d) The ratio of cleaved caspase-3/caspase-3 in MG-63 cells. (e, f) Phosphorylated PI3K, Akt, and TORC1 in MG-63 treated with IGF-1 were detected by WB at 24 h after the treatment. (g) The ratio of LC3/β-actin in MG-63 cells. (h) The ratio of cleaved caspase-3/caspase-3 in MG-63 cells. The data are shown as M ± SD ($n = 3$, #$p < 0.05$ IGF treatment comparing with control; ns$p > 0.05$, *$p < 0.05$, **$p < 0.01$ vs. control).

(a)

(b)
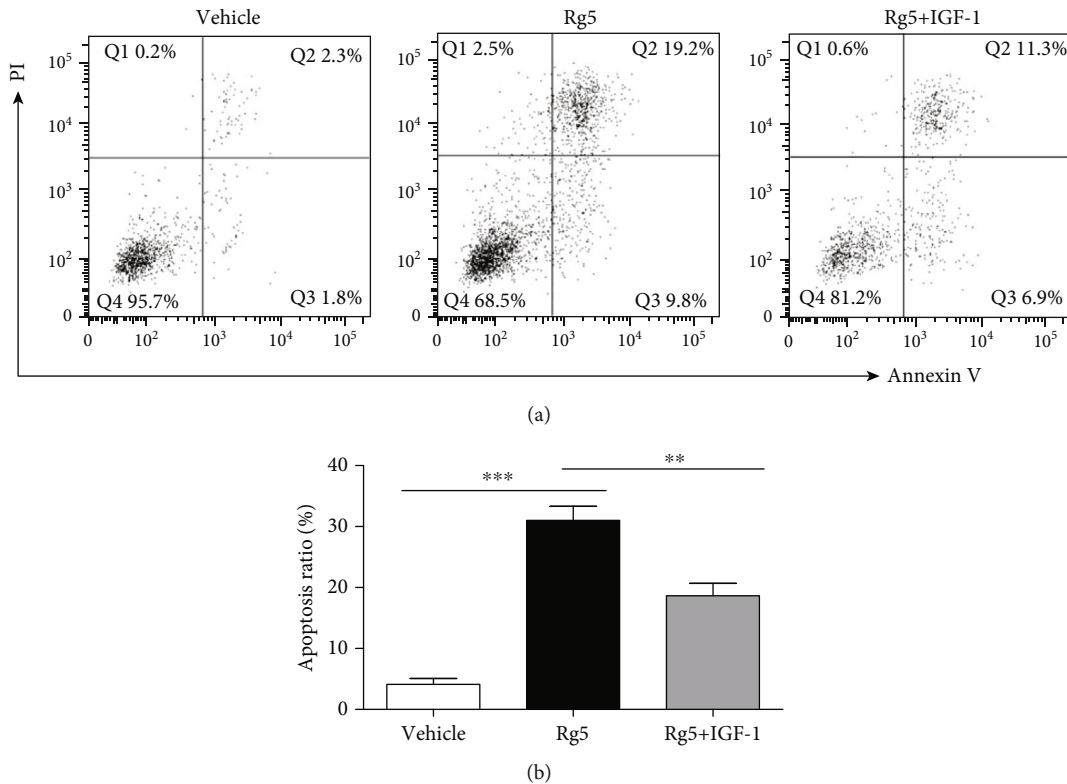
FIGURE 6: The PI3K/AKT/mTORC1 pathway is involved in Rg5-induced human MG-63 cell apoptosis. (a, b) Cell apoptosis of MG-63 cells treated with Rg5 alone or together with IGF-1 was examined by FACS. The data are shown as M ± SD ($n = 3$, ns$p > 0.05$, IGF treatment comparing with control, **$p < 0.01$, ***$p < 0.001$ vs. control).
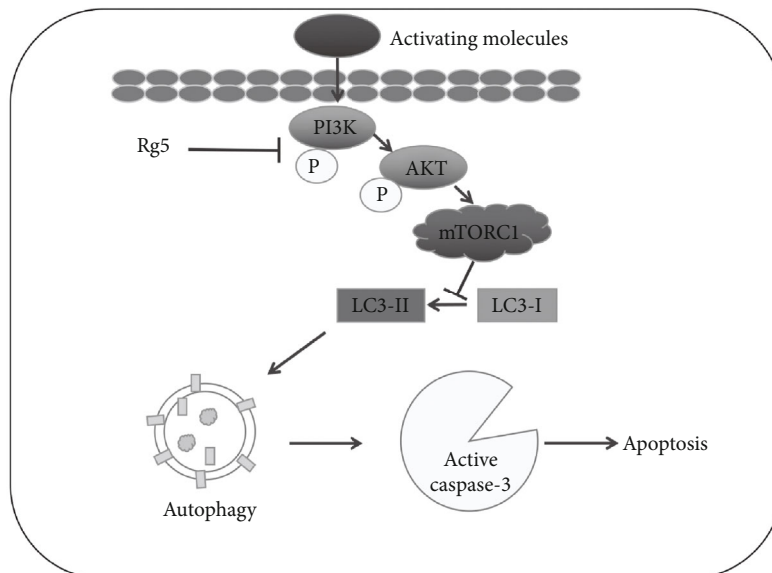
FIGURE 7: Schematic outline of ginsenoside Rg5 inhibits the human osteosarcoma cell through LC3 autophagy-related apoptosis. Under physiological conditions, the activation of PI3K/AKT/mTORC1 could inhibit the LC3 activity and caspase-3-related cell apoptosis. But Rg5 activated LC3 activity through inhibiting the phosphorylation of PI3K/AKT/mTORC1 to inhibit the human osteosarcoma cell proliferation and induce cell apoptosis.

3.4. Silencing LC3 Affects Rg5-Induced Tumor Cell Apoptosis. LC3 protein and gene expression were decreased significantly by western blot (Figures 4(a) and 4(b), $p < 0.01$) and qRT-PCR experiments (Figure 4(c), $p < 0.01$) when the LC3 expression was silenced by RNAi in MG-63 cells. The MFI level of LC3 also decreased significantly (Figures 4(d) and 4(e), $p < 0.01$). The numbers of apoptotic cells decreased significantly in LC3-silenced MG-63 cells compared to those of the control cells (Figure 4(f), $p < 0.01$). These results proved that the LC3 autophagy pathway is a key factor in MG-63 cell apoptosis initiated by Rg5.

3.5. The PI3K/AKT/mTORC1 Pathway Is Involved in Rg5-Induced Human Osteosarcoma Cell Autophagy Activation and Apoptosis. mTORC1 is a complex consisting of four proteins, including mTOR, Raptor, GβL, and DEPTOR [27]. Downregulation of phosphorylated PI3K ($p < 0.05$) and phosphorylated Akt ($p < 0.05$) and upexpression of Raptor ($p < 0.01$), meaning of mTORC1 activation, unless the stable expression of mTOR, were observed by western blot assay on MG-63 cell treatment with Rg5 for 12 h and 24 h in Figures 5(a) and 5(b). In contrast, LC3-mediated autophagy (Figures 5(a) and 5(c), $p < 0.01$) and caspase-3 activity (Figures 5(a) and 5(d), $p < 0.01$) increased significantly when MG-63 cells were treated with Rg5. To further confirm that Rg5 induced LC3-mediated autophagy and caspase-3 activity by inhibiting PI3K/AKT/mTOR phosphorylation, we used the PI3K activator IGF-1 combined with Rg5 treatment in MG-63 cells. Not surprisingly, IGF-1 reversed the Rg5-induced reduction in PI3K, Akt, and Raptor activation (Figures 5(e) and 5(f), $p < 0.01$). Moreover, the LC3 and caspase-3 activity decreased when IGF-1 was added compared with that of Rg5 treatment alone (Figures 5(g) and 5(h), $p < 0.01$). Cell apoptosis was evaluated by Annexin V-

FITC and PI double-staining. As shown in Figures 6(a) and 6(b), the numbers of apoptotic cells decreased significantly when IGF-1 was used together with Rg5 ($p < 0.01$). These results indicated that Rg5 inhibited the PI3K/AKT/mTORC1 pathway and then induced human osteosarcoma cell autophagy activation and cell apoptosis.

4. Discussion and Conclusion

Osteosarcoma (OS) causes a 2.4% death rate in child cancers worldwide. At present, there remain a number of side effects of chemotherapeutic drugs in human osteosarcoma treatment [28]. Natural medicines have some advantage in the cancer treatment to overcome the associated side effects [8]. So the increasing interest has drawn more and more attention for novel anticancer agents from natural products [9].

The present study investigated the antiproliferative and apoptosis-inducing effects of ginsenoside Rg5 on human osteosarcoma cells. MG-63, HOS, and U2OS were chose as target cells. Rg5 inhibited MG-63, HOS, and U2OS cell proliferation at concentrations ranging from 80 to 1280 nM. The susceptibility of HOS cells to Rg5 was slightly weaker than that of MG-63 and U2OS cells. Cell apoptosis was closely related to cell proliferation inhibition [29, 30]. FACS experiment revealed that Rg5 significantly induced human osteosarcoma cell apoptosis. To observe the mechanism of Rg5 on osteosarcoma cell apoptosis, the caspase-3 gene was detected. As expected, Rg5 significantly increased the activation of caspase-3. Autophagy is considered to be an important cellular metabolic process [24]. The function of autophagy can regulate cell fate via different mechanisms [25, 31]. The present study revealed that the ratio of LC3-II/LC3-I increased approximately 3-fold after Rg5 treatment,

accompanied by cleaved caspase-3 activity. These results suggest that autophagy may be associated with caspase-3-related cell apoptosis. 3-MA, an LC3-mediated autophagy inhibitor, was used to treat MG-63 cells combining with Rg5. As expected, cleaved caspase-3 activity and cell apoptosis were significantly reduced when LC3-mediated autophagy was inhibited by 3-MA. This mechanism was also confirmed in LC3 RNA-silenced MG-63 cells.

More and more novel anticancer agents from natural products have been used in osteosarcoma treatment. Sapio et al. demonstrate that CGA acts as an anticancer molecule affecting the cell cycle and provoking cell growth inhibition mainly by apoptosis induction by ERK1/2 activation [32]. They also reported AdipoR affected osteosarcoma cell cycle and cell death in the mTORC1 pathway [33]. Akt signaling pathways are responsible for antiproliferative actions in some cells [34]. Although there is no study on Rg5 on the Akt signaling pathway, a previous study revealed that Rg3 attenuates lipopolysaccharide-induced acute lung injury via activation of the PI3K/AKT/mTOR pathway [35]. To further verify which signaling molecules are related to MG-63 cell autophagy and apoptosis, the current study examined the expression of MAPK components and AKT using western blotting. Downregulation of phosphorylated PI3K, phosphorylated Akt, and phosphorylated TORC1 was observed using western blotting after 12 h and 24 h treatment of MG-63 cells with Rg5. In contrast, LC3 autophagy and caspase-3 activity increased significantly. To further confirm that Rg5 induced LC3-mediated autophagy and caspase-3 activity by inhibiting PI3K/AKT/mTOR phosphorylation, we used the PI3K activator IGF-1 combined with Rg5 treatment in MG-63 cells. LC3 and caspase-3 activity decreased when IGF-1 was added compared with that of Rg5 treatment alone. Cell apoptosis, cell migration ability, and invasion ability decreased significantly when IGF-1 was used together with Rg5. These results revealed that Rg5 inhibited the PI3K/AKT/mTORC1 pathway, induced human osteosarcoma cell autophagy activation, and induced cell apoptosis.

In conclusion, these data demonstrated that Rg5 inhibited proliferation and induced apoptosis through the LC3 autophagy pathway. Under physiological conditions, the activation of PI3K/AKT/mTORC1 could inhibit the LC3 activity and caspase-3-related cell apoptosis. But Rg5 activated LC3 activity through inhibiting the phosphorylation of PI3K/AKT/mTORC1 (Figure 7). The present study indicated that Rg5 could be a promising candidate as a chemotherapeutic agent against human osteosarcoma.

Abbreviations

Rg5: Ginsenoside-Rg5
MTT: Methylthiazolyldiphenyl-tetrazolium bromide
qRT-PCR: Real-time quantitative PCR
FACS: Fluorescence activated cell sorter
OS: Osteosarcoma
ROS: Reactive oxygen species
FBS: Fetal bovine serum
PI: Propidium iodide
MFI: Mean fluorescence intensity.

Data Availability

The data used to support the findings of this study are available from the corresponding author upon request (Dr. Haijun Li, hjli2012@jlu.edu.cn).

Conflicts of Interest

The authors declare that they have no competing interests.

Authors' Contributions

Ming-Yang Liu, Fei Liu, Jia-Ning Yin, and Yan-Li Gao contribute equally to this work.

Acknowledgments

References

[1] C. Rothermundt, B. M. Seddon, P. Dileo et al., "Follow-up practices for high-grade extremity osteosarcoma," *BMC Cancer*, vol. 16, no. 1, p. 301, 2016.

[2] R. Kumar, M. Kumar, K. Malhotra, and S. Patel, "Primary osteosarcoma in the elderly revisited: current concepts in diagnosis and treatment," *Current Oncology Reports*, vol. 20, no. 2, p. 13, 2018.

[3] J. L. Ferguson and S. P. Turner, "Bone cancer: diagnosis and treatment principles," *American Family Physician*, vol. 98, no. 4, pp. 205–213, 2018.

[4] S. Toki, E. Kobayashi, A. Yoshida et al., "A clinical comparison between dedifferentiated low-grade osteosarcoma and conventional osteosarcoma," *Bone Joint J.*, vol. 101-B, no. 6, pp. 745–752, 2019.

[5] Z. Wang, Z. Wang, B. Li, S. Wang, T. Chen, and Z. Ye, "Innate immune cells: a potential and promising cell population for treating osteosarcoma," *Frontiers in Immunology*, vol. 10, p. 1114, 2019.

[6] D. Z. Wang, S. F. Jing, S. B. Hao, X. Y. Huang, Q. T. Miao, and J. F. Gao, "miR-218 promotes apoptosis of U2OS osteosarcoma cells through targeting BIRC5," *European Review for Medical and Pharmacological Sciences*, vol. 22, no. 20, pp. 6650–6657, 2018.

[7] T. Makovec, "Cisplatin and beyond: molecular mechanisms of action and drug resistance development in cancer chemotherapy," *Radiology and Oncology*, vol. 53, no. 2, pp. 148–158, 2019.

[8] S. A. M. Khalifa, N. Elias, M. A. Farag et al., "Marine natural products: a source of novel anticancer drugs," *Marine Drugs*, vol. 17, no. 9, p. 491, 2019.

[9] F. Khan, F. Ahmed, P. N. Pushparaj et al., "Ajwa Date (Phoenix dactylifera L.) Extract inhibits human breast adenocarcinoma (MCF7) cells in vitro by inducing apoptosis and cell cycle arrest," *PLoS One*, vol. 11, no. 7, article e0158963, 2016.

[10] L. C. Sayles, M. R. Breese, A. L. Koehne et al., "Genome-informed targeted therapy for osteosarcoma," *Cancer Discovery*, vol. 9, no. 1, pp. 46–63, 2019.

[11] M. Zheng, Y. Xin, Y. Li et al., "Ginsenosides: a potential neuroprotective agent," *BioMed Research International*, vol. 2018, Article ID 8174345, 11 pages, 2018.

[12] L. D. Liang, T. He, T. Du, Y. G. Fan, D. S. Chen, and Y. Wang, "Ginsenoside-Rg5 induces apoptosis and DNA damage in human cervical cancer cells," *Molecular Medicine Reports*, vol. 11, no. 2, pp. 940–946, 2015.

[13] W. Huang, L. Sun, B. Wang et al., "Ginsenosides, potent inhibitors of sialyltransferase," *Zeitschrift für Naturforschung C*, vol. 75, no. 1-2, pp. 41–49, 2020.

[14] Y. Liu and D. Fan, "The preparation of ginsenoside Rg5, its antitumor activity against breast cancer cells and its targeting of PI3K," *Nutrients*, vol. 12, no. 1, p. 246, 2020.

[15] S. J. Kim and A. K. Kim, "Anti-breast cancer activity of fine black ginseng (Panax ginseng Meyer) and ginsenoside Rg5," *Journal of Ginseng Research*, vol. 39, no. 2, pp. 125–134, 2015.

[16] Y. Zou and P. Liu, "Ginsenoside-Rg5 inhibits proliferation of the breast carcinoma cells through promotion of the proteins involved in AMP kinase pathway," *International Journal of Clinical and Experimental Medicine*, vol. 9, pp. 17664–17669, 2016.

[17] Y. Liu and D. Fan, "Ginsenoside Rg5 induces apoptosis and autophagy via the inhibition of the PI3K/Akt pathway against breast cancer in a mouse model," *Food & Function*, vol. 9, no. 11, pp. 5513–5527, 2018.

[18] Y. Liu and D. Fan, "Ginsenoside Rg5 induces G2/M phase arrest, apoptosis and autophagy via regulating ROS-mediated MAPK pathways against human gastric cancer," *Biochemical Pharmacology*, vol. 168, pp. 285–304, 2019.

[19] D. Zhang, A. Wang, J. Feng, Q. Zhang, L. Liu, and H. Ren, "Ginsenoside Rg5 induces apoptosis in human esophageal cancer cells through the phosphoinositide-3 kinase/protein kinase B signaling pathway," *Molecular Medicine Reports*, vol. 19, no. 5, pp. 4019–4026, 2019.

[20] Y. S. Wang, H. Li, Y. Li, H. Zhu, and Y. H. Jin, "Identification of natural compounds targeting annexin A2 with an anticancer effect," *Protein & Cell*, vol. 9, no. 6, pp. 568–579, 2018.

[21] Y. Cui, Y. Su, L. Deng, and W. Wang, "Ginsenoside-Rg5 inhibits retinoblastoma proliferation and induces apoptosis through suppressing BCL2 expression," *Chemotherapy*, vol. 63, no. 5, pp. 293–300, 2018.

[22] S. L. Feng, H. B. Luo, L. Cai et al., "Ginsenoside Rg5 overcomes chemotherapeutic multidrug resistance mediated by ABCB1 transporter: *in vitro* and *in vivo* study," *Journal of Ginseng Research*, vol. 44, no. 2, pp. 247–257, 2020.

[23] Z. Xu, X. Han, D. Ou et al., "Targeting PI3K/AKT/mTOR-mediated autophagy for tumor therapy," *Applied Microbiology and Biotechnology*, vol. 104, no. 2, pp. 575–587, 2020.

[24] L. Galluzzi and D. R. Green, "Autophagy-independent functions of the autophagy machinery," *Cell*, vol. 177, no. 7, pp. 1682–1699, 2019.

[25] N. M. Kocaturk, Y. Akkoc, C. Kig, O. Bayraktar, D. Gozuacik, and O. Kutlu, "Autophagy as a molecular target for cancer treatment," *European Journal of Pharmaceutical Sciences*, vol. 134, pp. 116–137, 2019.

[26] M. Russo and G. L. Russo, "Autophagy inducers in cancer," *Biochemical Pharmacology*, vol. 153, pp. 51–61, 2018.

[27] T. R. Peterson, M. Laplante, C. C. Thoreen et al., "DEPTOR is an mTOR inhibitor frequently overexpressed in multiple myeloma cells and required for their survival," *Cell*, vol. 137, no. 5, pp. 873–886, 2009.

[28] J. D. Robertson and S. Orrenius, "Role of mitochondria in toxic cell death," *Toxicology*, vol. 181-182, pp. 491–496, 2002.

[29] L. Pan, T. Zhang, H. Sun, and G. Liu, "Ginsenoside Rg3 (Shenyi capsule) combined with chemotherapy for digestive system cancer in China: a meta-analysis and systematic review," *Evidence-Based Complementary and Alternative Medicine*, vol. 2019, Article ID 2417418, 19 pages, 2019.

[30] J. Li, Q. Wang, Z. Wang et al., "Tetrandrine inhibits colon carcinoma HT-29 cells growth via the Bcl-2/caspase 3/PARP pathway and G1/S phase," *Bioscience Reports*, vol. 39, no. 5, article BSR20182109, 2019.

[31] J. Xu, H. Wang, Y. Hu et al., "Inhibition of CaMKIIα activity enhances antitumor effect of fullerene C60 nanocrystals by suppression of autophagic degradation," *Advanced Science*, vol. 6, no. 8, p. 1801233, 2019.

[32] L. Sapio, A. Salzillo, M. Illiano et al., "Chlorogenic acid activates ERK1/2 and inhibits proliferation of osteosarcoma cells," *Journal of Cellular Physiology*, vol. 235, no. 4, pp. 3741–3752, 2020.

[33] L. Sapio, E. Nigro, A. Ragone et al., "AdipoRon affects cell cycle progression and inhibits proliferation in human osteosarcoma cells," *Journal of Oncology*, vol. 2020, Article ID 7262479, 12 pages, 2020.

[34] Z. Ren, X. Chen, L. Hong et al., "Nanoparticle conjugation of ginsenoside Rg3 inhibits hepatocellular carcinoma development and metastasis," *Small*, vol. 16, no. 2, article e1905233, 2020.

[35] J. Yang, S. Y. Li, L. Y. Wang et al., "Ginsenoside Rg3 attenuates lipopolysaccharide-induced acute lung injury via MerTK-dependent activation of the PI3K/AKT/mTOR pathway," *Frontiers in Pharmacology*, vol. 9, p. 850, 2018.

Research Article

The Combination Treatment of Curcumin and Probucol Protects Chondrocytes from TNF-*α* Induced Inflammation by Enhancing Autophagy and Reducing Apoptosis via the PI3K-Akt-mTOR Pathway

Guangtao Han, Yubiao Zhang, and Haohuan Li ⓘD

Department of Orthopedics, Renmin Hospital of Wuhan University, Wuhan, Hubei 430060, China

Correspondence should be addressed to Haohuan Li; lihaohuan@whu.edu.cn

Guangtao Han and Yubiao Zhang contributed equally to this work.

Osteoarthritis (OA) is a chronic joint disease characterized by cholesterol accumulation in chondrocytes, cartilage degeneration, as well as extracellular matrix (ECM) destruction, and joint dysfunction. Curcumin, a chemical that can reduce cholesterol levels in OA patients, also can inhibit the progression of OA. However, a high concentration of curcumin may also trigger apoptosis in normal chondrocytes. Besides curcumin, probucol that is found can also effectively decrease the cholesterol level in OA patients. Considering that high cholesterol is a risk factor of OA, it is speculated that the combination treatment of curcumin and probucol may be effective in the prevention of OA. To investigate the possible effects of such two chemicals on OA pathophysiology, chondrocyte apoptosis and autophagy behavior under inflammatory cytokine stress were studied, and specifically, the PI3K-Akt-mTOR signaling pathway was studied. *Methods*. Cell proliferation, colony formation, and EdU assay were performed to identify the cytotoxicity of curcumin and probucol on chondrocytes. Transwell assay was conducted to evaluate chondrocyte migration under TNF-*α* inflammation stress. Immunofluorescence, JC-1, flow cytometry, RT-PCR, and western blot were used to investigate the signal variations related to autophagy and apoptosis in chondrocytes and cartilage. A histological study was carried out on OA cartilage. Glycosaminoglycan (GAG) release was determined to evaluate the ECM degradation under stress. *Results*. Compared with a single intervention with curcumin or probucol, a combined treatment of these two chemicals is more effective in terms of protecting chondrocytes from stress injury induced by inflammatory cytokines. The promoted protection may be attributed to the inhibition of apoptosis and the blockage of the autophagy-related PI3K/Akt/mTOR pathway. Such results were also verified in vitro by immunofluorescence staining of OA chondrocytes and in vivo by immunohistochemistry staining of cartilage. Besides, in vivo studies also showed that when applied in combination, curcumin and probucol could block the PI3K-AKT-mTOR signaling pathway; promote COL-II expression; suppress P62, MMP-3, and MMP-13 expression; and inhibit TNF-*α*-stimulated cartilage degradation. Moreover, the combined medication could help reduce the release of ECM GAGs in OA cartilage and alleviate the severity of OA. *Conclusion*. A combined treatment of curcumin and probucol could be used to protect chondrocytes from inflammatory cytokine stress via inhibition of the autophagy-related PI3K/Akt/mTOR pathway both in vitro and in vivo, which might be of potential pharmaceutical value for OA prevention and therapy.

1. Introduction

OA is a chronic inflammatory disease closely related to cartilage degeneration. Researchers have found that a high level of total cholesterol is related to the OA process. Specifically, in a prospective cohort study, total cholesterol and triglycerides are verified to be associated with new bone marrow lesion formation in asymptomatic middle-aged women [1] and result in cartilage defect and OA eventually. Another possible explanation could be lipid embolism caused by serum cholesterol, which may cause osteonecrosis leading to OA.

Hypertension, obesity, abnormal blood lipids, and high cholesterol, such conditions known as "metabolic syndrome" [2] are common among OA patients. The interrelationship between high cholesterol levels and increased risk of OA has been studied extensively in recent years [3, 4], and previous reports have shown that inhibition of de novo cholesterol synthesis may provide better OA remiment outcome [5, 6]. In this context, OA should be considered as a syndrome rather than merely a joint disease.

Autophagy is an important self-maintenance mechanism by which a cell protects itself when facing harmful stress [7]. Active autophagy is related to cholesterol effluent, and it can delay disease progress to a certain alleviated extent. Specifically, nitro-oleic acid, a ligand of CD36, reduces cholesterol accumulation by modulating fluidized LDL uptake and cholesterol efflux in RAW264.7 macrophages, and FGF21 induces autophagy-mediated cholesterol efflux to inhibit atherogenesis via the upregulation of RACK1 [8].

However, autophagy activity tends to drop in several cells and tissues with age. In OA chondrocytes, autophagy markers decrease significantly [9], accompanying with dysfunctional autophagy, enhanced apoptosis, and less migration [10]. Therefore, chemicals that can regulate autophagy in chondrocytes and stabilize the cholesterol level may be of potential medication value for OA prevention and therapy.

Curcumin, a diferuloylmethane, is extracted from the root of *Curcuma longa* [11]. In China and India, *Curcuma longa* has been used as a medicinal herb with a long history. Recent research indicated that curcumin can function to reduce cholesterol levels [12]. Additionally, previous authors have verified that curcumin can promote autophagy and reduce apoptosis in several cells [13]. Moreover, probucol, another cholesterol regulator, can also activate autophagy and inhibit apoptosis in nerve cells by blocking PI3K/Akt/mTOR signals [14]. Since autophagy takes an important role in chondrocyte physiology, and the PI3K/Akt/mTOR pathway is essential in regulating autophagy in OA patients [15], we speculated that curcumin and probucol may be of potential value for OA prevention. In the present study, these two chemicals were applied together to investigate their effects on chondrocytes in vitro and on cartilage in vivo.

2. Materials and Methods

2.1. Animals.
Healthy male Sprague Dawley rats from the Animal Experimental Center of Wuhan University (Wuhan, China) were involved in this study. The rats were fed under specific pathogen-free conditions at a constant room temperature (24°C) and relative humidity (45%–55%). All rats had free access to sterile food and water and lived under a light/dark cycle of 12 h. The present study was approved by the Laboratory Animal Welfare & Ethics Committee, Renmin Hospital of Wuhan University. Efforts were made to minimize animal suffering in the study.

2.2. Reagents.
The reagents included DMEM/F12 high glucose (Hyclone, Utah, USA), penicillin (Hyclone, Utah, USA), streptomycin (Hyclone, Utah, USA), curcumin (Bellancom, Beijing, China), trypsin (Google Biotechnology, Wuhan, China), collagenase-II, bovine serum albumin (BSA), probucol (Sigma-Aldrich, St. Louis, MO, USA), Key-Fluor488 Click-iT EdU kits, DAPI, (KeyGEN BioTECH, Nanjing, China), AnnexV-PI kits (BD, USA), Counting Kit-8 (CCK-8) reagents, goat serum (Beyotime Institute of Biotechnology, Shanghai, China), TNF-α (Peprotech, Inc., Suzhou, China), Caspase-3, Bcl-2, Lc3, Bax, PI3K, p-PI3K, Akt, p-Akt, mTOR, p-mTOR, GADPH, Berclin-1, COL-II, P62, FITC, Cy3, MMP-3, JC-1 assay kits (Abcam, USA), TRIzol reagents (Invitrogen, Thermo Fisher Scientific, Inc. USA), a RevertAid First Strand cDNA Synthesis kit (Fermentas; Thermo Fisher Scientific, Inc. USA), MMP detection kits (Solarbio Science & Technology, Beijing, China), and chemiluminescent luminol reagent (Santa Cruz Biotechnology, Texas, USA).

2.3. Chondrocyte Culture and Identification.
Briefly, cartilage was extracted from the knee joints of 35 male Sprague-Dawley rats (4 weeks, weighing 140 ± 10 g). Cartilage samples were minced into thin slices (1 mm^3) and digested with 3 ml of 0.25% trypsin for 40 min followed by further treatments with type II collagenase for another 6 h. Chondrocytes were then been centrifuged and collected. Subsequently, the isolated chondrocytes were cultured in 5 ml of DMEM/F12 with 20% fetal bovine serum and incubated at 37°C in 5% CO_2.

2.4. CCK-8 Assay.
To determine the appropriate study concentration of probucol and curcumin for further investigation in the subsequent experiments, cell viability was detected by the CCK-8 test. The chondrocytes were first cultured in a 96-well plate, and CCK-8 reagents were added, which was incubated at 37°C for another 2 h. The chondrocyte viability was detected by OD 450 nm with an automatic microplate reader. All studies were conducted in triplicate.

2.5. Cell Groups.
Based on the above CCK-8 results, cells were randomly divided into five groups ($n = 3$): control, TNF-α, TNF-α + curcumin (50 μM), TNF-α + probucol (100 μM), and TNF-α + probucol (50 μM) + curcumin (25 μM). After excluding other cytokines or growth factors, TNF-α aqueous solution (20 ng/ml) was mixed with normal chondrocytes to mimic the inflammatory cytokine environment in OA [16]. 36 h later, curcumin, probucol, or both of them were added, and the chondrocytes were further incubated for another 24 h.

2.6. Flow Cytometry of Annexin V-FITC-PI Staining.
The apoptosis rates of chondrocytes were measured with an AnnixV-PI apoptosis detection kit. In short, the chondrocytes were held at 25°C for 15 min and treated with PI

(a)

(b)

(c)

Control   OA   OA+curcumin

OA+probucol   OA+curcumin+probucol

(d)
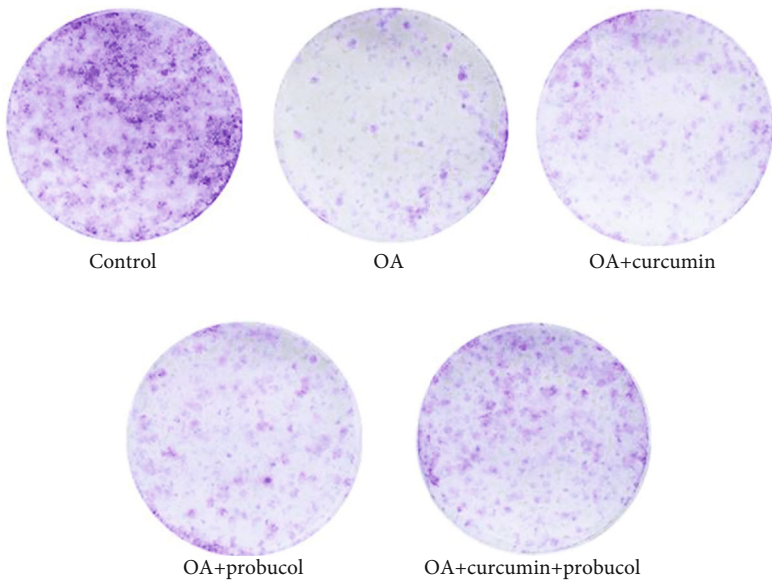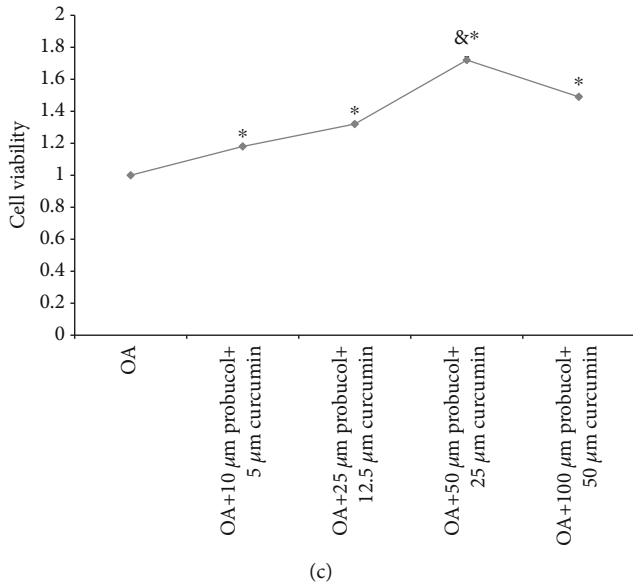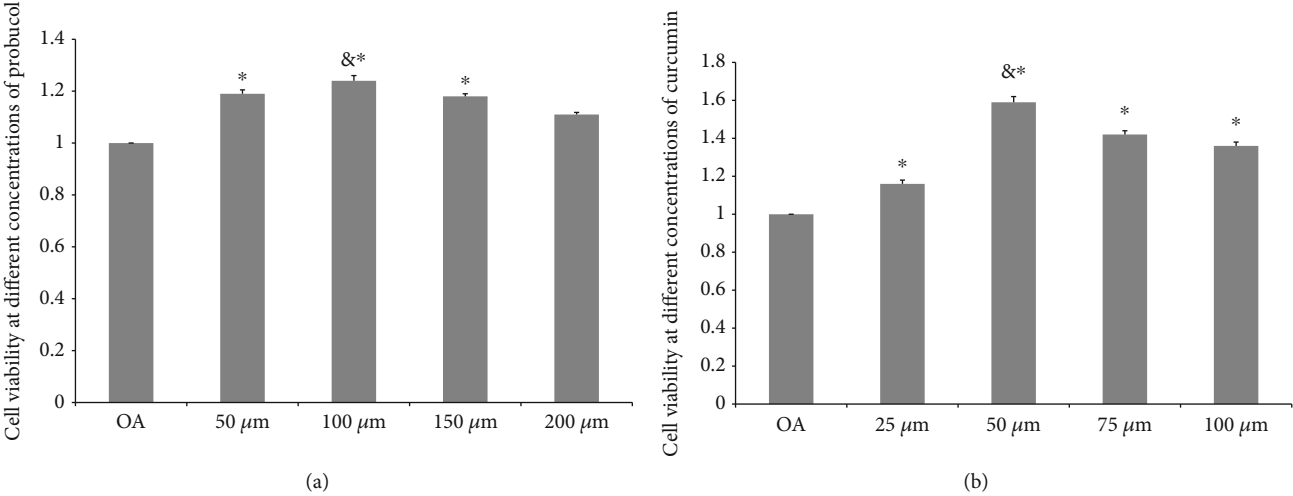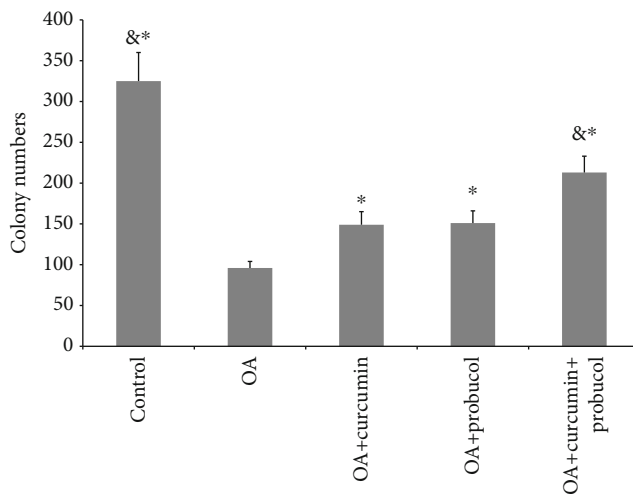
FIGURE 1: Continued.

(e)
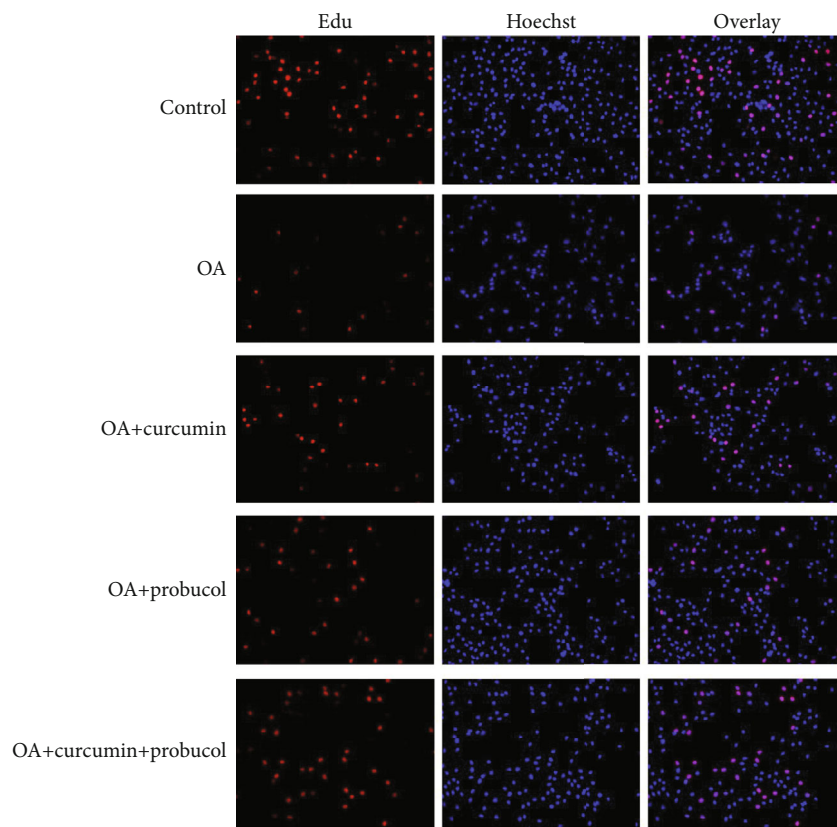
(f)

Figure 1: Continued.

(g)
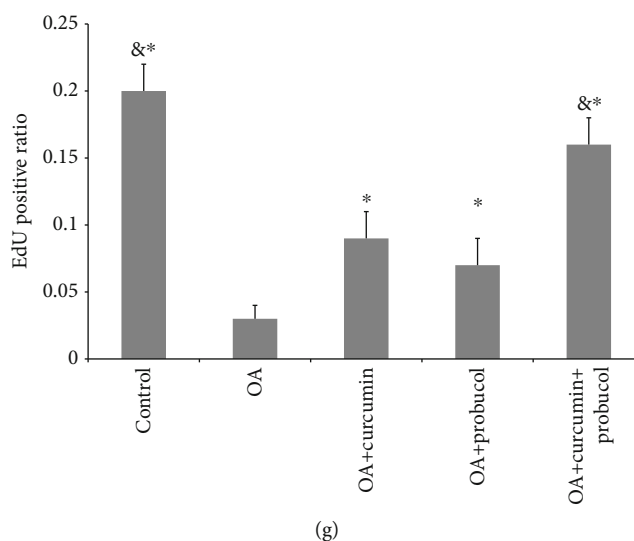
FIGURE 1: Probucol and curcumin enhance chondrocyte proliferation. (a) Cell viability at different probucol concentrations. (b) Cell viability at different curcumin concentrations. (c) Cell viability at different curcumin-probucol concentrations. (d) After incubated in 96-well plates, the cells were subsequently treated with curcumin and probucol. Cell proliferation in the control, OA, OA + curcumin, OA + probucol, and OA + curcumin + probucol groups was measured by colony formation assays. (e) Statistical analysis of the number of chondrocyte colonies. (f) Compared with the OA group, more EdU-labeled cells exhibited red fluorescence in the curcumin and probucol groups. Therefore, when applied together, curcumin and probucol would significantly reduce the number of EdU-labeled cells compared with either the curcumin or probucol groups. All cell nuclei displayed blue fluorescence with Hoechst33342 staining (magnification ×200). (g) The relative ratio of EdU-positive cells in the curcumin + probucol group was significantly higher than the other four groups at 24 h. The data are shown as the means ± SD. & and ∗ indicate $P \leq 0.01$ and 0.05 vs. OA, respectively. All experiments were carried out three times.

solution (5 μl) and FITC-labeled annexin V (5 μl) for 10 min in the dark. The apoptosis rates were evaluated with a flow cytometer (BD Biosciences, USA).

2.7. Colony Formation Assay.
The chondrocytes were placed on a six-well plate and mixed with curcumin and probucol at predescribed concentrations. After that, the cells were incubated for another two weeks without curcumin and probucol. Subsequently, the colonies were fixed with methanol, stained with Wright-Giemsa solution, and counted for their numbers [17].

2.8. Transwell Migration Assay.
Transwell assays were used to evaluate cell migration. First, the transwell chambers were washed with serum-free medium, and chondrocytes were cultured in DMEM medium with 10% FBS as the chemical attractant. After incubation for 48 h, cells attached to the membrane were discarded, and those entering the lower membrane were fixed with methanol and stained with 0.2% crystal violet. Under a microscope (×200), the cells invaded by the matrix gel in 5 random fields of view were photographed.

2.9. JC-1 for Mitochondrial Membrane Permeability (MMP) Assessment.
An MMP detection kit was used to evaluate the MMP in chondrocytes. After the chondrocytes were washed with PBS, 800 μl of JC-1 working fluid was mixed with the chondrocytes and stained at 37°C for 25 minutes. Subsequently, 2 ml of medium containing serum was added to the working fluid after staining. The red-green fluorescence ratio was measured by a FACS Caliber flow cytometer

(Becton, Dickinson, and Company) and an Olympus fluorescence microscope (Olympus Corporation, Japan).

2.10. EdU Incorporation Assay.
Chondrocyte proliferation was assessed by a keyFluor488 Click-iT-EdU kit. First, the chondrocytes were placed in a six-well plate, and 100 μl of EdU was added into the plate, followed by incubation at 37°C for 2 h. Second, the cells were fixed with 4% paraformaldehyde at room temperature, washed with BSA containing 3% glycine, and incubated with 0.5% TritonX-100 and 1× click-it reaction solution in the dark at room temperature. Last, Hoechst 33342 was added to the six-well plate, and the whole plate was placed in a dark environment for 20 minutes and then washed three times with PBS. The stained cells were observed with a fluorescence microscope.

2.11. Reverse Transcription Quantitative Polymerase Chain Reaction (RT-PCR).
TRIzol reagents were used to isolate the total RNA from chondrocytes. To determine the expression levels of inflammation-related genes, first-strand complementary cDNA chains were synthesized using the RevertAid First Strand cDNA Synthesis kit (Fermentas; Thermo Fisher Scientific, Inc.). Quantitative PCR was performed for 40 cycles in a StepOnePlus device (Applied Biosystems; Thermo Fisher Scientific, Inc.), and each cycle contained temperature at 95°C for 10 secs, followed by 5 seconds at 95°C and 20 seconds at 60°C. The additional primers were as follows: COL2, 5′-CTTAGGACAGAGAGAGAAGG-3′; Rev, 5′-ACTCTGGGTGGCAGAGTTTC-3′; MMP-3, 5′-TTTGGCCGTCTCTTCCATCC-3′; Rev, 5′-GGAGGC
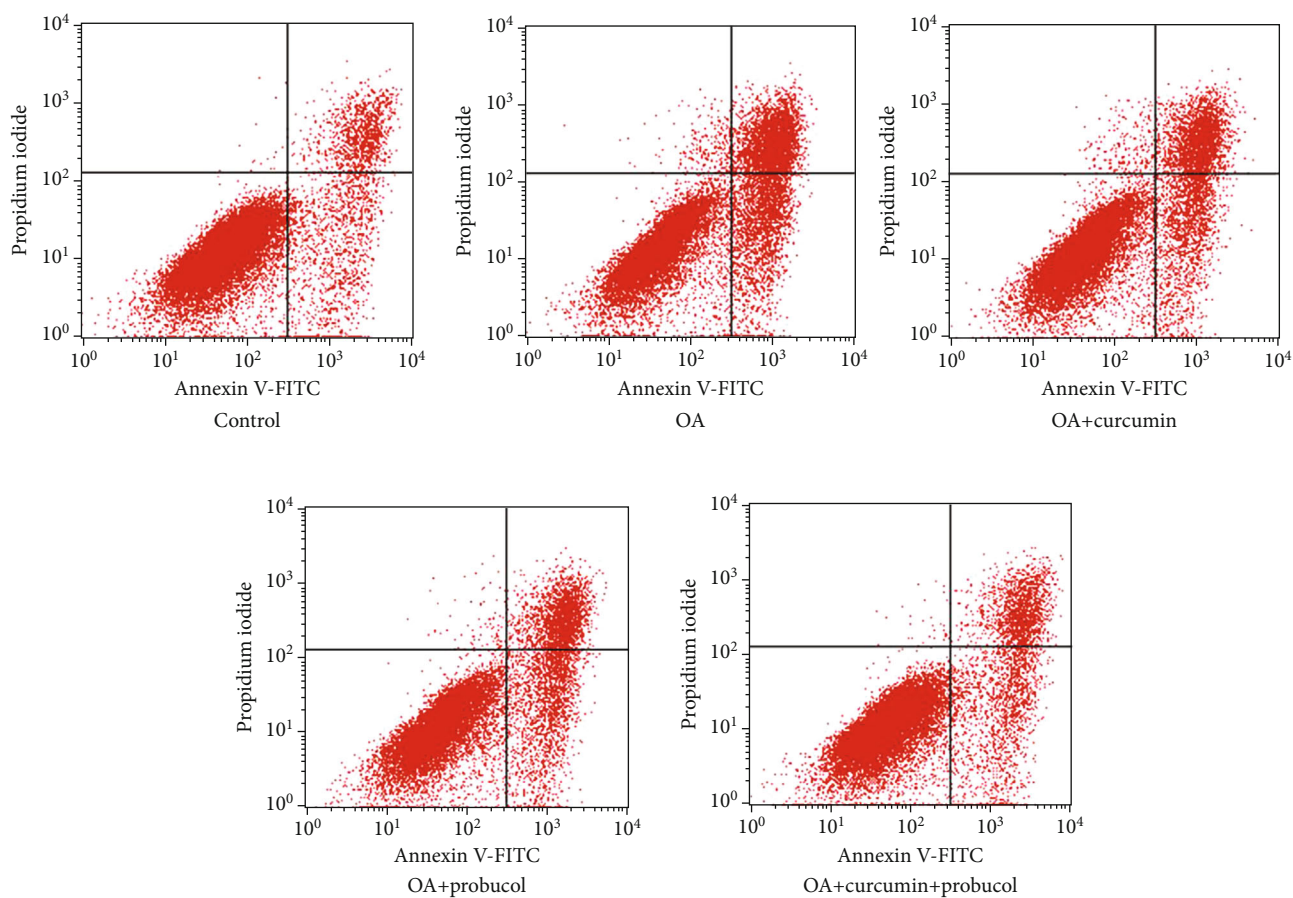
(a)
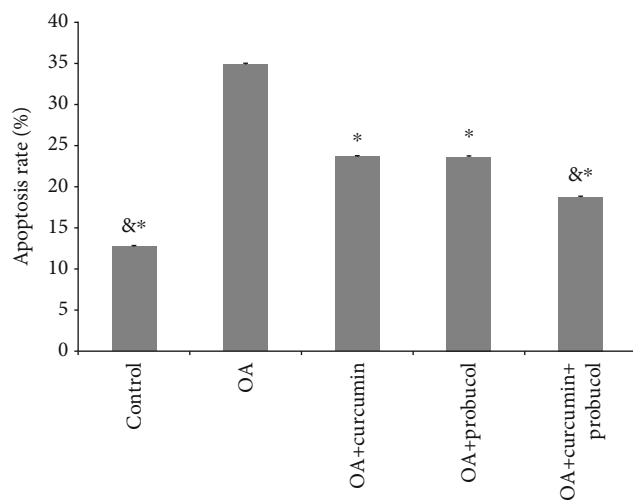
(b)
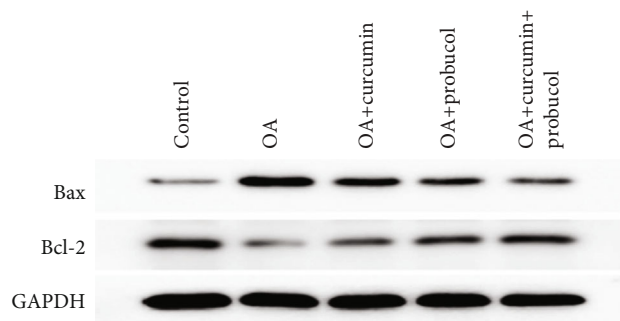
(c)

Figure 2: Continued.

(d)

(e)
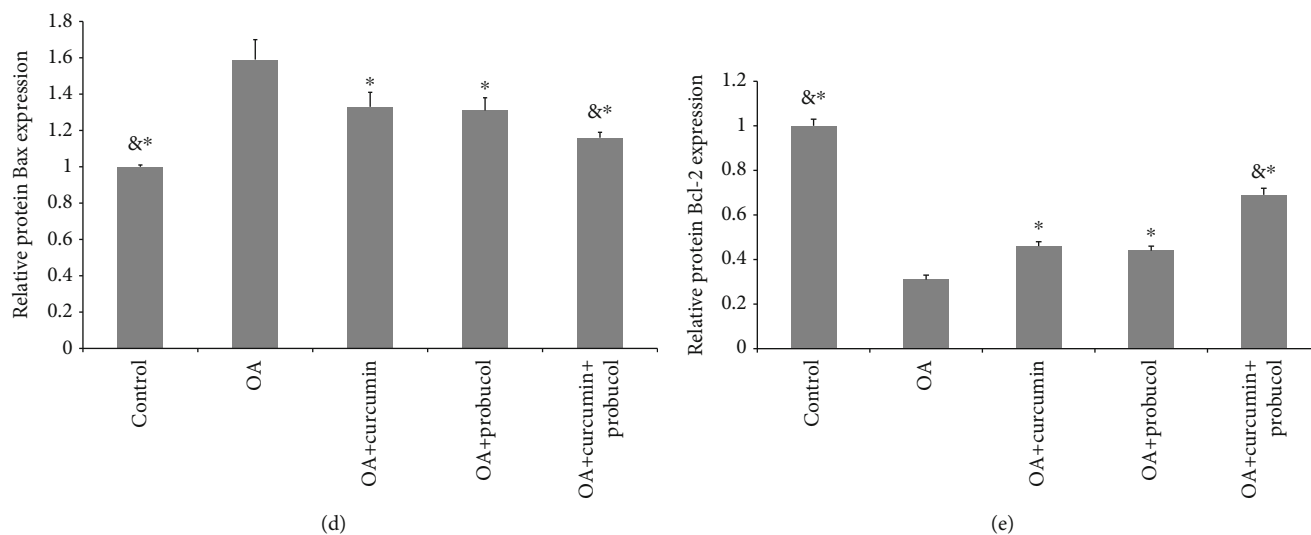
Figure 2: Probucol and curcumin can reduce chondrocyte apoptosis. (a) Probucol and curcumin inhibit apoptosis in chondrocytes. (b) The cell apoptosis rate significantly decreased after a treatment of curcumin + probucol for 24 h. (c) Bcl-2 and Bax protein concentration in chondrocytes (from Western blot assays). (d) Analysis of Bax expression based on the Western blot results. (e) Analysis of Bcl-2 expression based on the Western blot results. The data are shown as the means ± SD. & and ∗ indicate $P \leq 0.01$ and 0.05 vs. OA, respectively. All experiments were carried out three times.

(a)

(b)
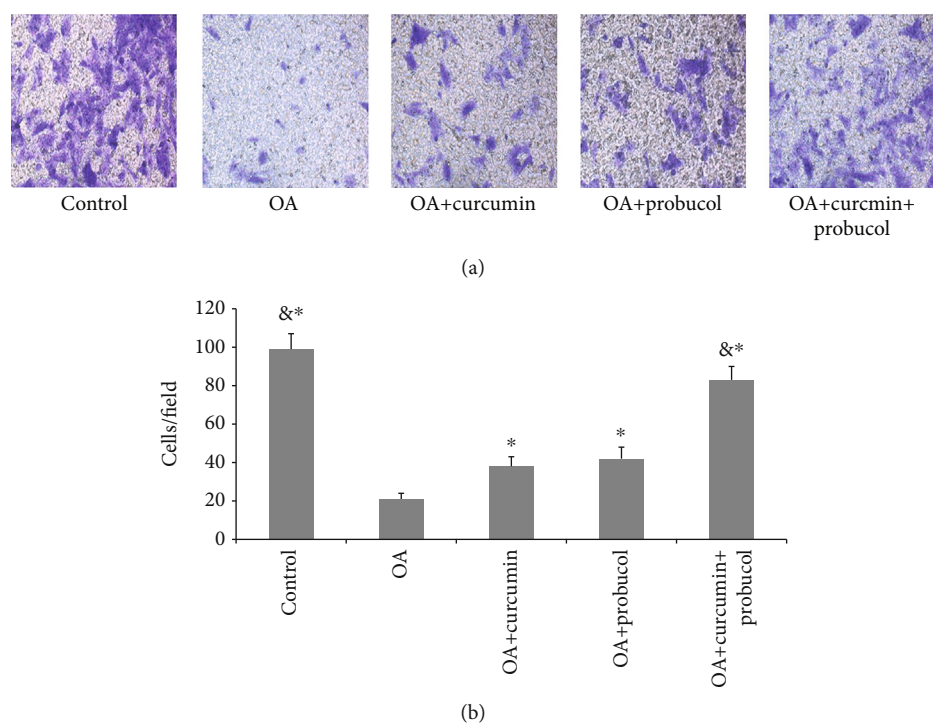
Figure 3: Probucol and curcumin enhance chondrocyte invasion. (a) Photographs of chondrocytes taken under a microscope (magnification ×200). (b) The migration rates were calculated based on the number of chondrocytes. The data are shown as means ± SD. & and ∗ indicate $P \leq 0.01$ and 0.05 vs. OA, respectively. All experiments were carried out three times.

CCAGAGTGTGAATG-3′; MMP-13, 5′-GG AGCATG GCGACTTCTAC-3′; Rev, 5′-GAGTGCTCCAGGGTCC TT; GADPH, 5′-CTCAACTACATGGTCTACATGTTC CA-3′; and Rev, 5′-CTTCCCATTCTCAGCCTTGACT-3′. GADPH was used as an internal reference. Moreover, the 2-ΔΔCq method was employed to calculate the relative levels of mRNA expression.

2.12. Western Blot. To extract the total proteins from the chondrocytes, organophosphorus inhibitors, protease inhibitors, and RIPA lysates were mixed at a ratio of 1:1:50. The proteins were separated by electrophoresis and transferred to polyvinylidene fluoride membranes, which were sealed for one hour. After that, a primary antibody was added to the membranes, which were then washed three times with
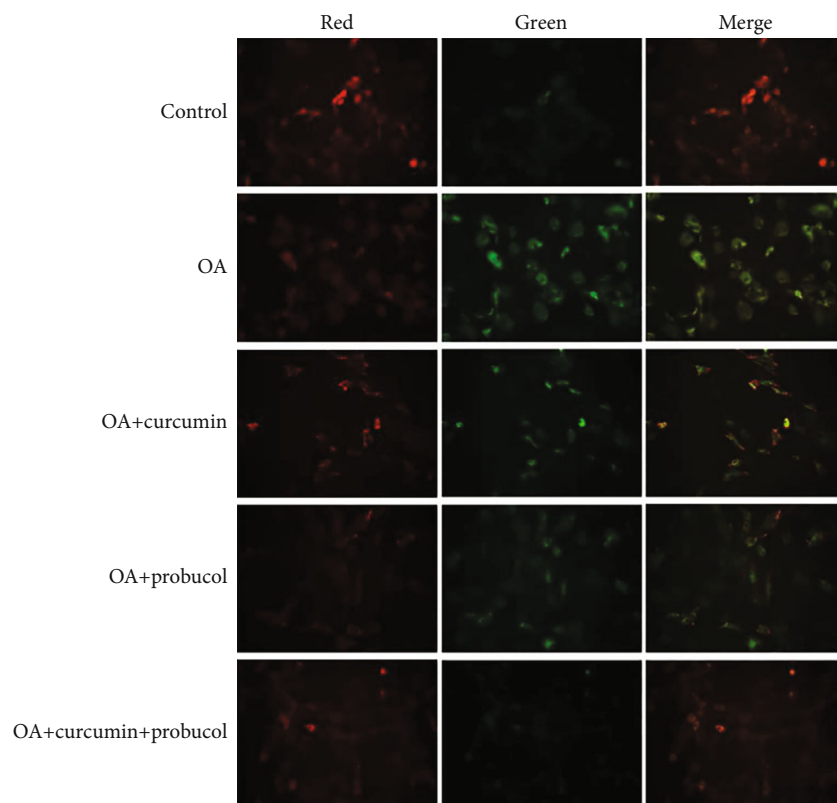
(a)
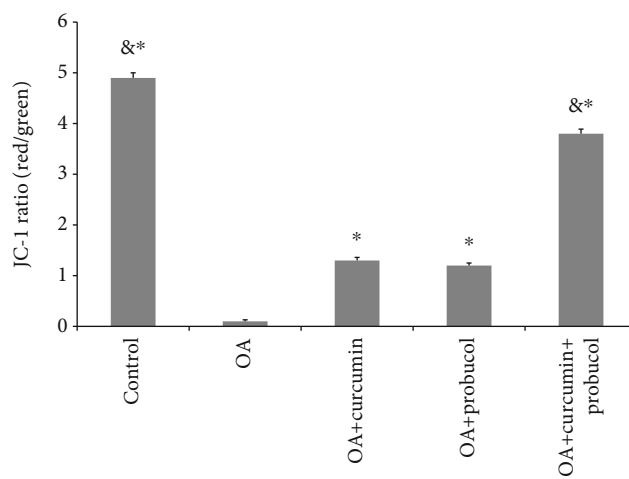
(b)

Figure 4: Continued.

(c)

(d)
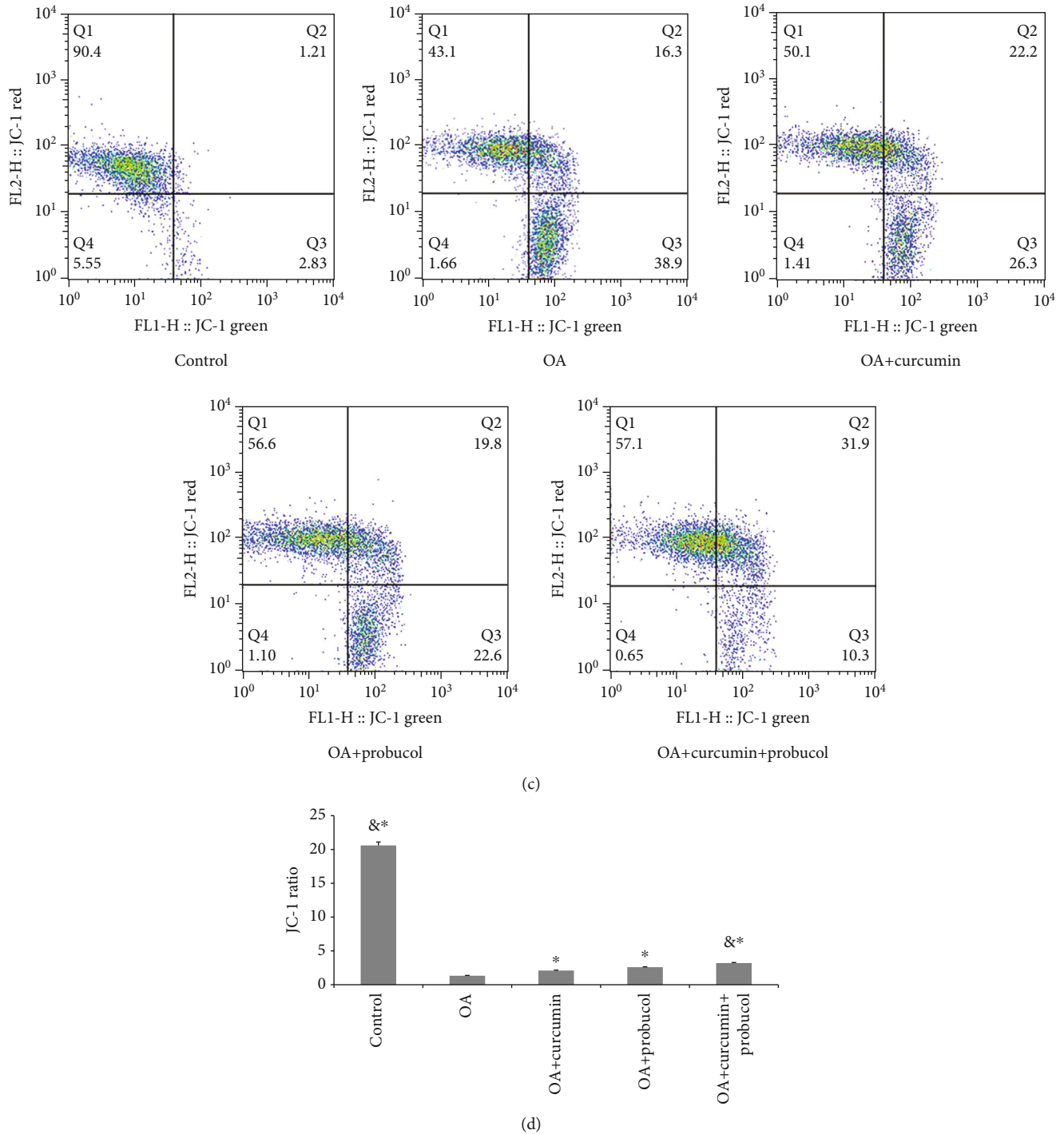
FIGURE 4: Probucol and curcumin increase the mitochondrial membrane potential of chondrocytes. (a) Changes in the chondrocyte MMP were observed by fluorescence microscopy (magnification ×200). Red fluorescence suggested normal MMP and green fluorescence indicated MMP decrease or loss. (b) The JC-1 ratios were calculated based on the number of chondrocytes. (c and d) Quantitative PNS analysis on $\Delta\psi$ m of chondrocytes. The data are shown as the means ± SD. & and ∗ indicate $P \leq 0.01$ and 0.05 vs. OA, respectively. All experiments were carried out three times.

TBST and incubated with horseradish peroxidase-labeled anti-rabbit goat IgG for 1 hour. Subsequently, the membranes were washed with TBST again, and the protein bands were observed with chemiluminescent luminol reagent (Santa Cruz Biotechnology, Inc.) and an Image Lab quanti-

tative analysis system (Bio-Rad Laboratories Inc.). The relative protein levels were compared by normalizing to GADPH. The primary antibodies were as follows: Bcl-2, Bax, Beclin-1, LC3, mTOR, PI3K, Akt, p-Akt, p-PI3K, p-mTOR, and GAPDH.

(a)

(b)

(c)

(d)

Figure 5: Continued.

(e)

(f)
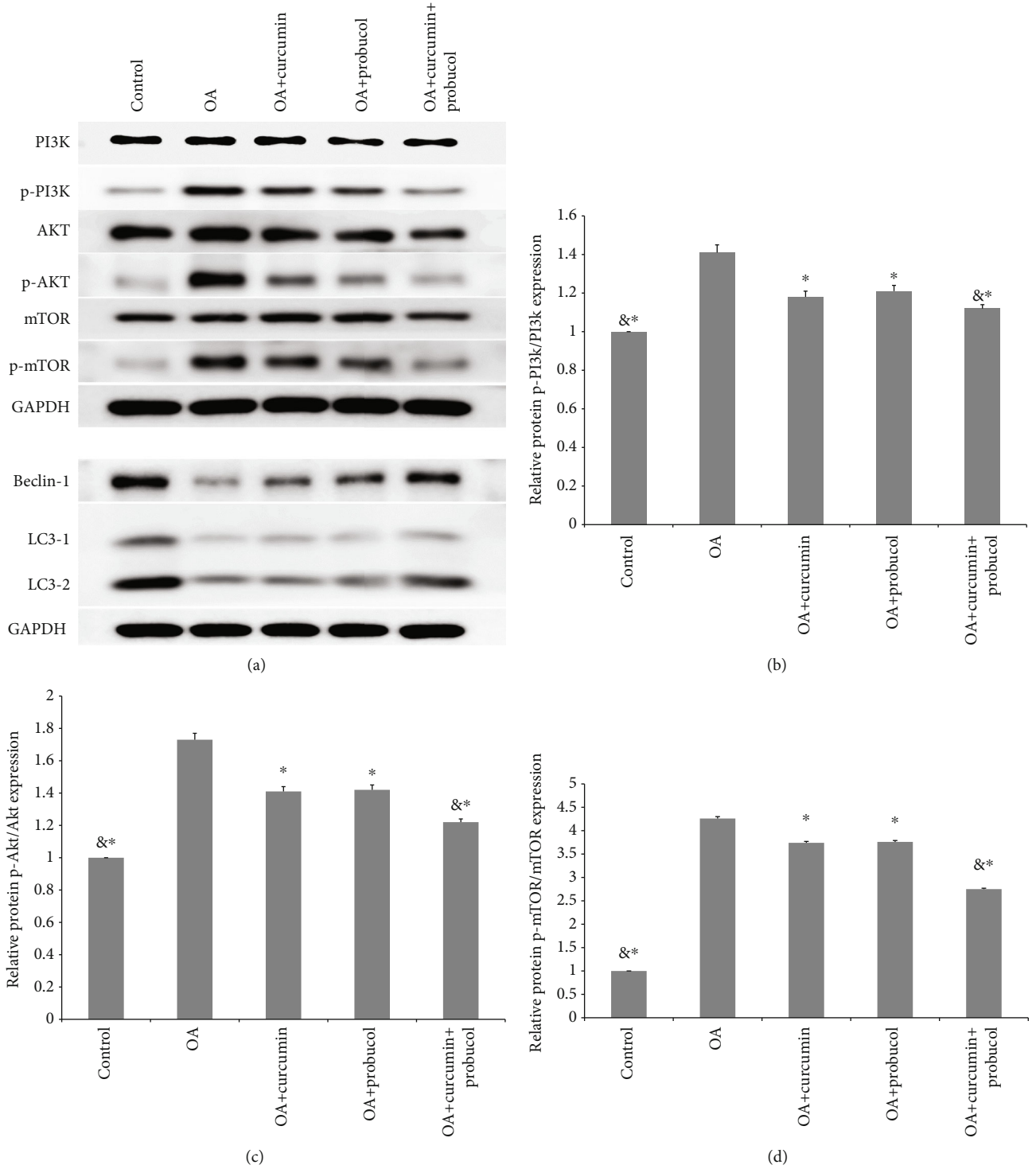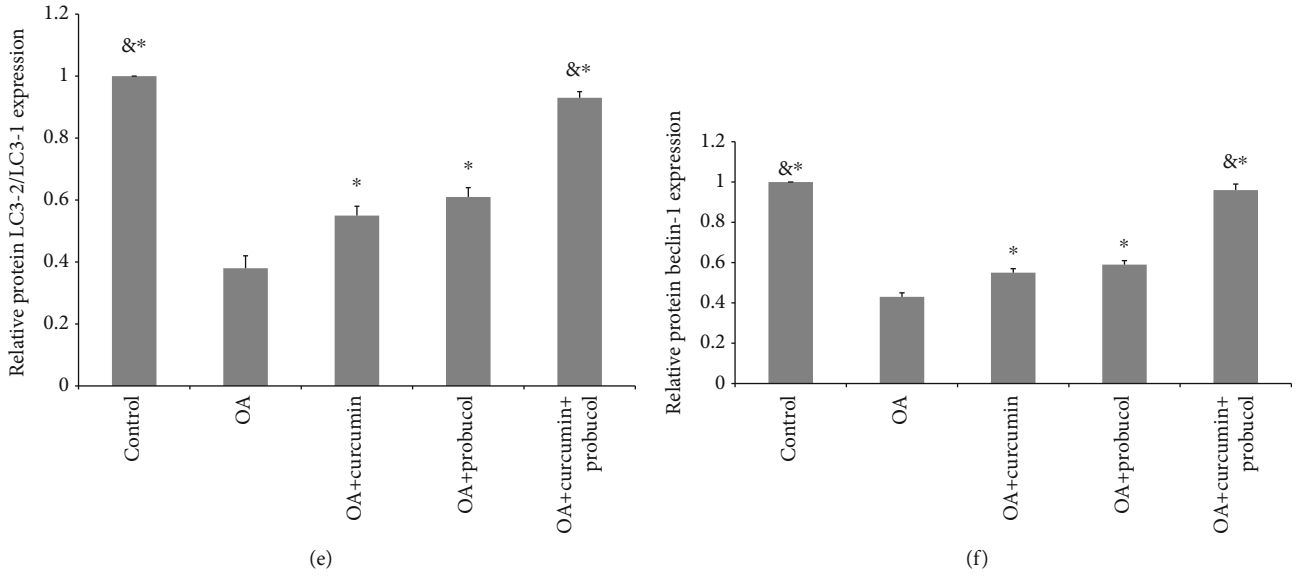
FIGURE 5: Probucol and curcumin inhibited OA by targeting the PI3K/Akt/mTOR pathway in chondrocytes. (a–f) Western blot results for quantitative analysis of PI3K, p-PI3K, Akt, p-Akt, mTOR, and p-mTOR protein expression in chondrocytes. The data are shown as the means ± SD. & and ∗ indicate $P \leq 0.01$ and 0.05 vs. OA, respectively. All experiments were carried out three times.

(a)

(b)
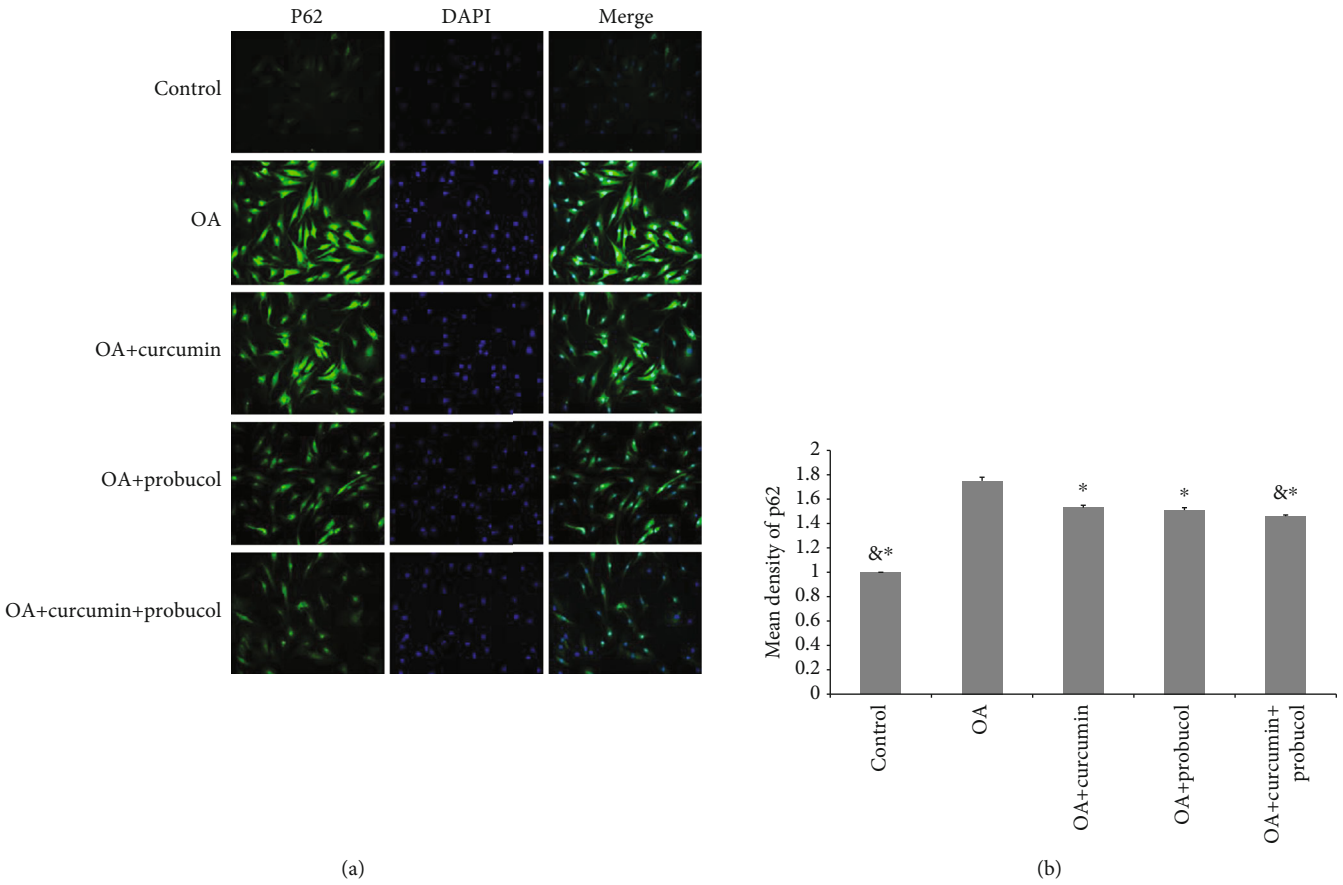
FIGURE 6: (a and b) Immunofluorescence staining revealed the amount of P62 protein in the chondrocytes. The data are shown as the means ± SD. & and ∗ indicate $P \leq 0.01$ and 0.05 vs. OA, respectively. All experiments were carried out three times.
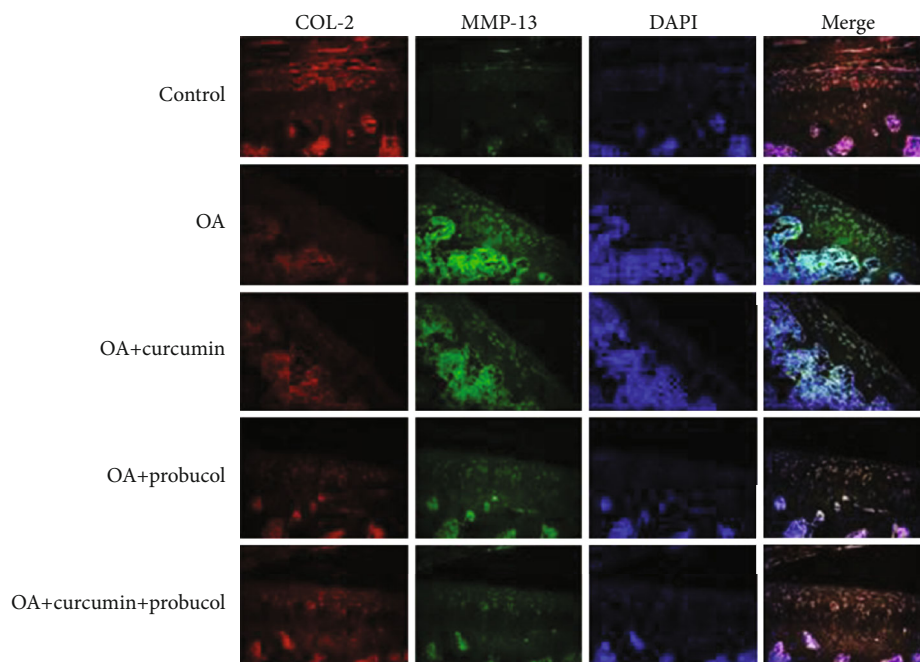
(a)
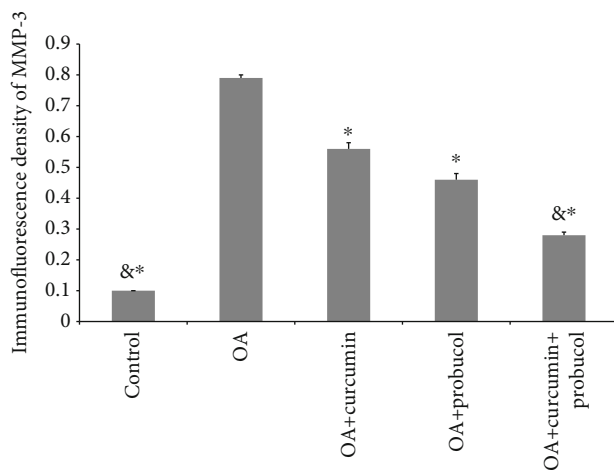
(b)
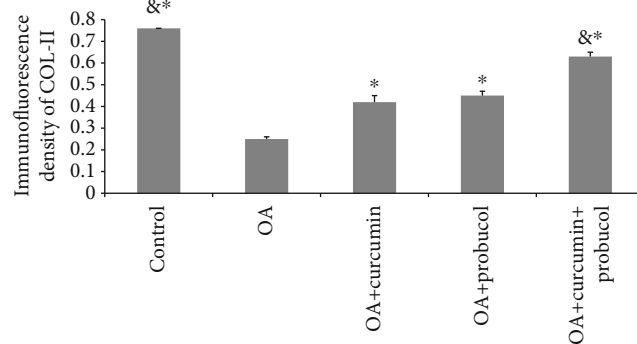
(c)
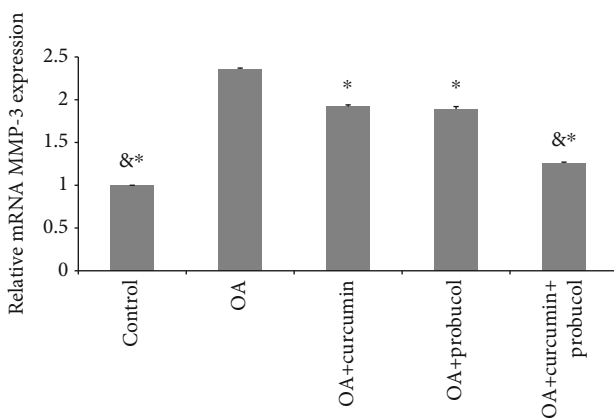
(d)
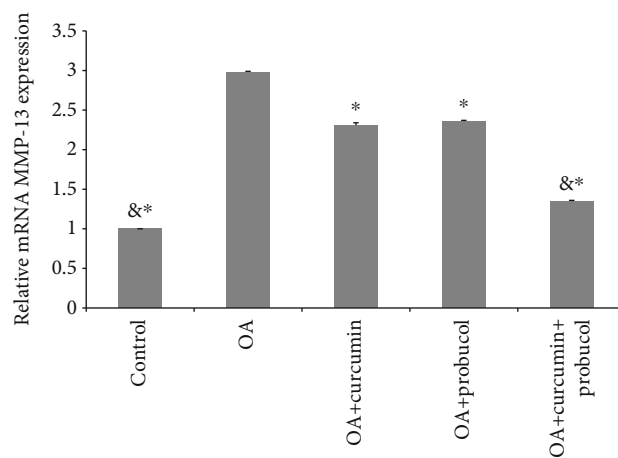
(e)

Figure 7: Continued.

(f)
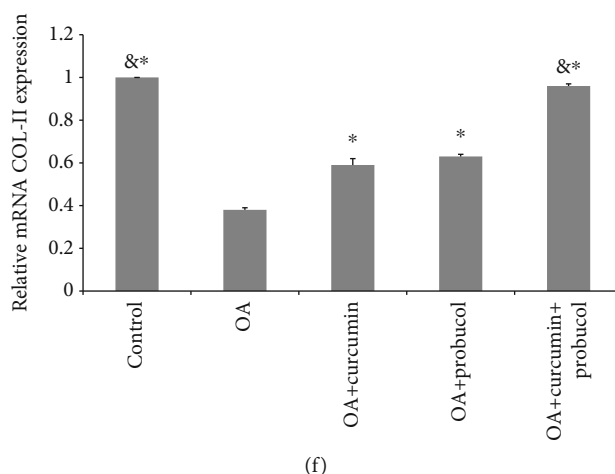
FIGURE 7: Probucol and curcumin treat OA in vitro and in vivo. (a–c) Quantification results of COL-II and MMP-3 proteins are shown by immunohistochemistry staining (magnification ×200). (d–f) The RT-PCR results for COL-II, MMP-3, and MMP-13. & and ∗ indicate $P \leq 0.01$ and 0.05 vs. OA, respectively. All experiments were carried out three times.

2.13. OA Animal Model In Vivo Study. SD rats (8 weeks old, weighing 250-280 g) were randomly divided into five groups, which are denoted as control ($n = 12$), OA ($n = 12$), OA +50 mg/kg curcumin ($n = 12$), OA+100 mg/kg probucol ($n = 12$), and OA+75 mg/kg curcumin-probucol ($n = 12$). The specific dosages were determined according to the earlier literature [18]. A rat OA model was created by excising the medial meniscus and the anterior cruciate ligament of the rats' right knee. Four weeks later, the groups with medications were treated with curcumin and probucol intramuscular injections once every three days for a total of 8 weeks, while the OA and the control groups were injected with normal saline. All rats were sacrificed after 3 months.

2.14. Immunofluorescence and Immunohistochemistry. After washed with PBS, the cartilage tissues and chondrocytes were fixed with paraformaldehyde for 12 h at 4°C and then dehydrated in 30% sucrose solution. Next, the tissues were sliced into pieces of 10 μM and incubated with P62 and COL-II at room temperature for 1 h. Subsequently, the section slices were then immunostained with FITC or Cy3-labeled secondary antibodies for 1 h, and DAPI was applied to counterstain the nuclei for 5 min. The sections were then incubated overnight with the primary antibodies for MMP-3 or MMP-13 at 4°C, and they were then incubated with biotinylated secondary antibodies. All sections were observed under an Olympus fluorescence microscope mentioned above. The proportions of stain-positive cells in the samples were analyzed by Image Pro Plus 6.0 (Media Cybernetics, Inc., USA).

2.15. Glycosaminoglycan Release Assay. Papain-digested cartilage explants and their defrosted supernatants were examined in 96-well plates using the dimethyl methylene blue (DMMB) method [16]. Briefly, each sample was diluted in distilled water to a total volume of 40 μl per well in triplicate. Shark chondroitin sulfate (Sigma-Aldrich) was used as a standard (0-70 ng). DMMB solution (200 μl) was added to each well, and the whole plate was immediately transferred to a Multiskan Ascent Scanner (Thermo Labsystems,

Basingstoke, UK) with Ascent Software (version 2.6, Thermo Labsystems, Finland). Total GAG release was observed from a spectrophotometric reading of the digested cartilage and its supernatants at 540 nm. For each well, the percentage of GAG release was calculated by dividing the GAG readings from the supernatants by the total GAG release.

2.16. Statistical Analysis. For each group, the data are expressed as means ± SD. Intragroup differences were assessed with Student's t-test and one-way analysis of variance by SPSS 16.0 (SPSS, Inc., USA) followed by a Bonferroni posthoc correction for multiple testing with GraphPad Prism (version 7.04; GraphPad Software, Inc., USA). Specifically, differences with $P < 0.05$ were considered statistically significant.

3. Results

3.1. Effects of Probucol and Curcumin on Chondrocyte Proliferation. CCK-8 was used to detect chondrocyte activity. The most appropriate concentrations of probucol and curcumin to counteract inflammatory cytokine stress were found to be 100 μM and 50 μM, respectively (Figures 1(a) and 1(b)). It is noteworthy that both these substances could promote chondrocyte proliferation in a dose-dependent manner. Here, we chose these substances at optimal concentrations of 12.5%, 25%, 50%, and 100% to the most appropriate concentration for combinations [10]. Considering the possible reported side effects of such substances [19], a combination of curcumin 25 μM + probucol 50 μM was used in this study, and the results suggest that such a combination can promote chondrocyte proliferation (Figures 1(c)). Colony formation assays further confirmed that they play a promotive role in chondrocyte proliferation (Figures 1(d) and 1(e)), and such effect is in a synergistic way by the two chemicals. In the EdU assays with TNF-α treatment, the chondrocytes showed a low proliferation ratio. However, after treating with 50 μM curcumin or 100 μM probucol, the proliferation ratio got increased; and with the combined treatment, such increasement became more significant (Figures 1(f) and 1(g)).

(a)

(b)

(c)

(d)

(e)

(f)

FIGURE 8: Continued.

Beclin-1

LC3-1

LC3-2

GADPH

TNF-α	−	+	+	+
Curcumin-probucol	−	−	−	+
3BDO	−	−	+	+

(g)

(h)
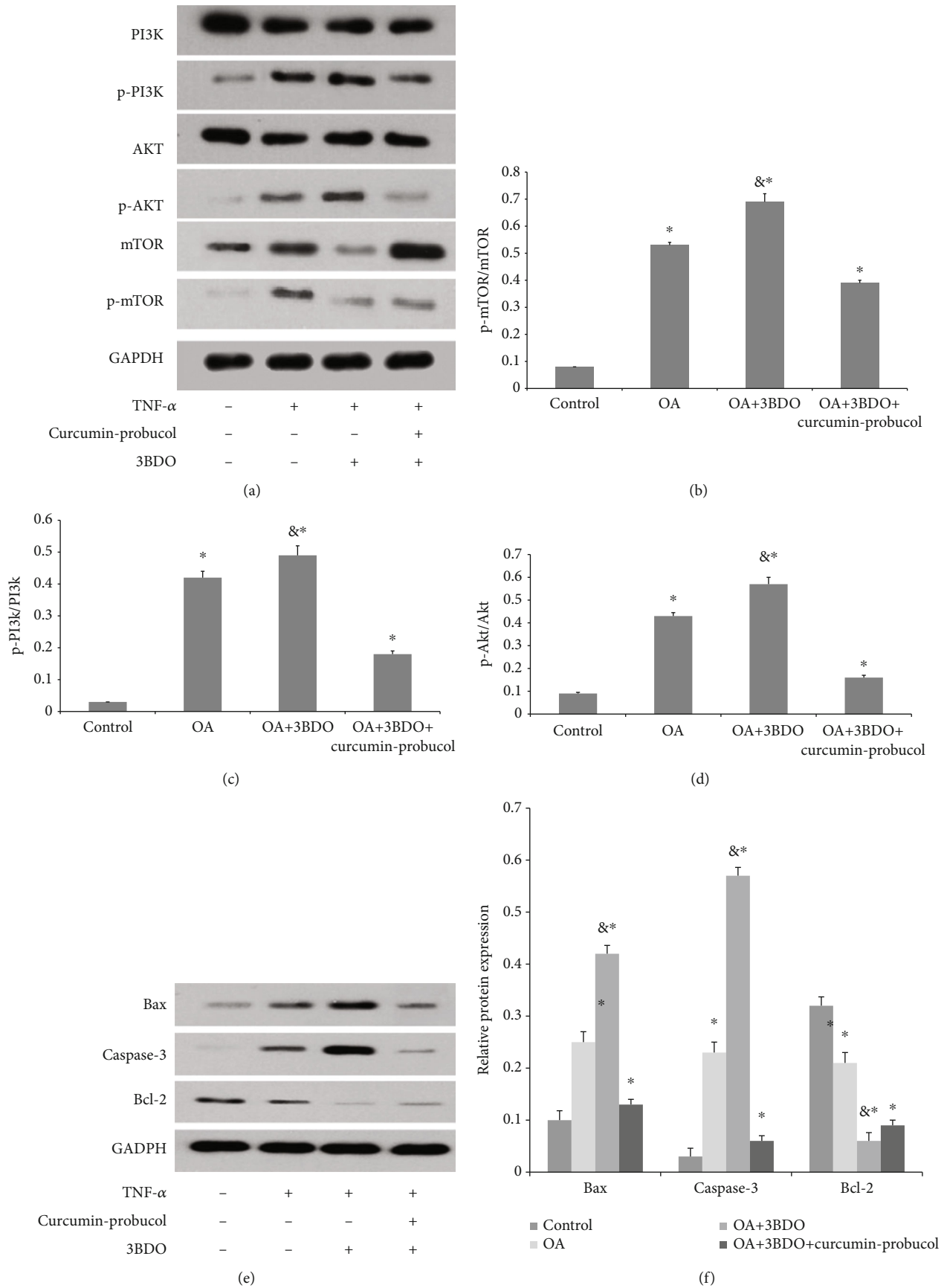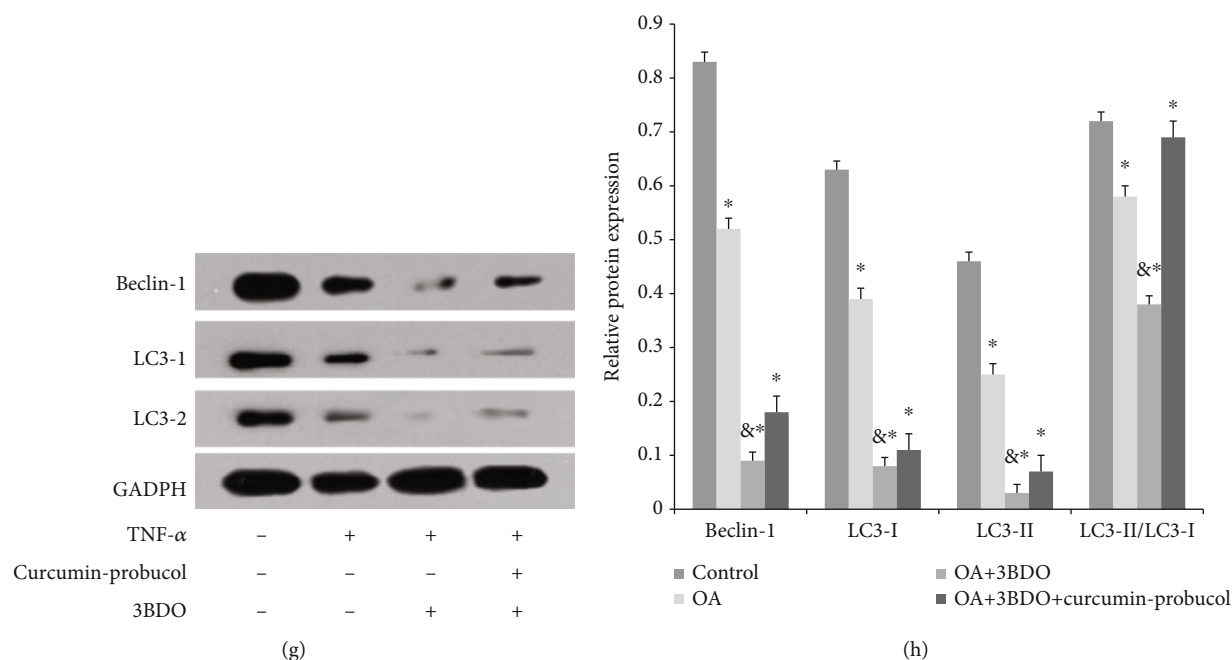
FIGURE 8: Probucol and curcumin treat OA cartilage by targeting the PI3K-Akt-mTOR pathway. (a–d) Western blot and quantification results of PI3K, p-PI3K, AKT, p-AKT, mTOR, and p-mTOR proteins in rat articular cartilage. (e and f) Quantification results of apoptosis-related proteins (Caspase-3 and Bax) and antidegradation proteins. (g and h) Quantitative results of autophagy-related protein expression (beclin-1 and LC3). & and ∗ indicate $P \leq 0.01$ and 0.05 vs. control, respectively. All experiments were carried out three times.

3.2. Effects of Probucol and Curcumin on Apoptosis and Apoptosis-Related Genes in Chondrocytes. AnnexV/PI was used to detect chondrocyte apoptosis. It was found that TNF-α induced chondrocyte apoptosis (34.92% ± 0.75%). However, with 50 μM curcumin or 100 μM probucol addition, the TNF-α-induced apoptosis percentages dropped to 23.58% ± 0.6% and 23.49% ± 0.55%, respectively. Moreover, the apoptosis ratio of chondrocytes decreased significantly to 17.45% ± 0.45% in the curcumin + probucol group (Figures 2(a) and 2(b)).

Besides the apoptosis-inducing effects, TNF-α can also downregulate the expression of the Bax gene while upregulating Bcl-2 expression. Compared with the OA group, both the curcumin and probucol groups showed lower Bax expression, and the expression of Bcl-2 in these two groups was higher than that in the TNF-α group. Furthermore, the expression of apoptosis-related proteins was significantly lower in the curcumin + probucol group compared with the TNF-α group (Figures 2(c)–2(e)). All experiments were carried out three times.

3.3. Effects of Probucol and Curcumin on Chondrocyte Migration. Transwell assays were used to observe cell migration, and TNF-α has been verified to reduce the mobility of chondrocytes. Compared with the TNF-α group, the curcumin and probucol groups were found to promote chondrocyte migration, and such promotive effect became more significant in the curcumin + probucol group. Eventually, chondrocyte mobility in the curcumin + probucol group was similar to that of normal chondrocytes (Figures 3(a) and 3(b)).

3.4. Effects of Probucol and Curcumin on the Mitochondria in Chondrocytes. Mitochondria play an important role in energy production, cell signal transduction, cell differentiation, and apoptosis. The mitochondrial membrane potential ($\Delta \psi$ m) is an important parameter of mitochondrial function, which is used as an indicator of cell viability and usually changes when apoptosis occurs. The effects of probucol and curcumin on OA chondrocytes were influenced by apoptosis, which depends on mitochondria. JC-1 assays were performed to measure $\Delta \psi$ m. In a JC-1 assay, dyes would stay in the cytoplasm and emit green fluorescence in apoptotic cells; while in normal cells, dyes would gather in the mitochondria and emit red fluorescence. The results showed that the green fluorescence was brighter in the TNF-α group, suggesting that TNF-α can reduce $\Delta \psi$ m of chondrocytes and induce apoptosis. However, curcumin and probucol can increase $\Delta \psi$ m, and such increases in the two substances were found to be synergistic by flow cytometry (Figures 4(a)–4(d)). All experiments were carried out three times.

3.5. Effects of Probucol and Curcumin on the Activity of Autophagy-Related Proteins and the Autophagy-Related PI3K/Akt/mTOR Pathway. PI3K/Akt/mTOR is an important pathway in autophagy. To study the effects of curcumin and probucol on the expression of autophagy-related proteins, chondrocytes were cultured for 24 hours, then TNF-α, TNF-α +50 μM curcumin, TNF-α +100 μM probucol, and TNF-α +50 μM probucol +25 μM curcumin were mixed with the chondrocytes and incubated for 24 hours. Western blot assays were used to evaluate the expression of PI3K, p-
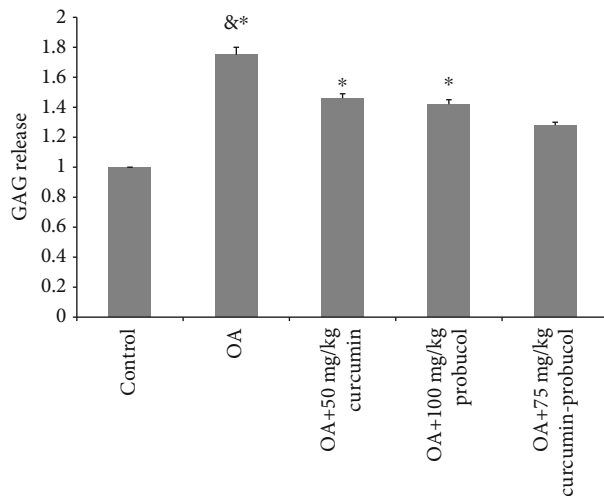
Figure 9: The percentage of cartilage GAG released into the medium at various curcumin and probucol concentrations. & and ∗ indicate $P \leq 0.01$ and 0.05 vs. control, respectively. All experiments were carried out three times.

PI3K, Akt, mTOR, p-Akt, p-mTOR, and autophagy-related proteins, such as LC3 and beclin-1. Besides, the autophagy-related factor P62 was detected by immunofluorescence. Compared with the OA group, probucol and curcumin could significantly reduce the phosphorylation degrees of p-PI3K, p-Akt, and p-mTOR, while significantly increasing the amount of autophagy-related proteins (Figures 5(a)–5(f)). Such effects became stronger when the two substances were applied together. Immunofluorescence showed that the expression of P62 decreased significantly. Therefore, the results suggested that probucol and curcumin regulate the mTOR signaling pathway through the PI3K-Akt pathway to promote autophagy and inhibit apoptosis of chondrocytes (Figures 6(a) and 6(b)).

3.6. Effects of Probucol and Curcumin on the Metabolism of Cartilage ECM. Subsequently, the effects of probucol and curcumin on inflammatory factors in experimental animals were investigated. The immunohistochemistry assays and RT-PCR verified the expression of ECM-related genes, namely, COL-II, MMP-13, and MMP-3. RT-PCR confirmed that the expression of MMP-13 and MMP-3 was induced by TNF-α, but the expression of COL-II was inhibited. However, both probucol and curcumin could significantly inhibit the degradation of COL-II while suppressing the expression of MMP-3 and MMP-13, and the combined administration of the two chemicals can inhibit the expression of inflammatory genes in OA chondrocytes (Figures 7(a)–7(f)). Moreover, 3BDO was used to verify the therapeutic effects of probucol and curcumin as potential antagonists for mTOR signaling. As is seen in the figures below, 3BDO, an agonist of the PI3K-Akt-mTOR pathway, could enhance the expression of p-PI3K/PI3K, p-AKT/AKT, and p-mTOR/mTOR, but curcumin-probucol acted as antagonists against 3BDO (Figures 8(a)–8(h)).

3.7. Effects of Curcumin and Probucol on GAG Release. Lastly, compared to control, GAG release was reported to show a significant increase in OA chondrocytes. The results from this study suggested that probucol or curcumin could reduce OA-stimulated GAG release when applied alone. However, the combined administration of such two substances via intramuscular injection could significantly ($P < 0.001$) reduce the percentage of OA-stimulated GAG release to a level similar to control (Figure 9). As a result, it is fair to infer that the combined medication of curcumin and probucol could inhibit OA by reducing GAG Release.

4. Discussion

One reason why only modest benefit can be obtained from early antiproinflammation cytokine therapy for OA treatment is because of the "one size-fits–fits-all" approach [20, 21]. Actually, from a clinical point of view, OA exhibits great etiological heterogeneity, which was not addressed in those early studies [22]. However, increasing evidence suggests that new OA therapies require a paradigm shift that considers OA as a complex and heterogeneous disease involving interactions among multiple organ systems, not merely a joint disease.

Hypercholesterolemia can lead to severe metabolic diseases; such mellitus characteristics increase the risk of OA [20]. The possible mechanisms behind such phenomenon may be explained as follows [22]: (1) as cholesterol is the primary component of cell membrane, its variations can alter the membrane fluidity and compromise its function. Specifically, the ABCA1 gene, which is involved in cholesterol reverse transport [23], mediates lipid efflux from cells, and changes in this gene may be relevant to OA; (2) hypercholesterolemia may impair mitochondrial function and increase oxidative stress, leading to the progress of OA [24]. Regulation of cholesterol levels in chondrocytes can help maintain normal mitochondrial functions; (3) in hypercholesterolemia, the accumulation of LDL-based lipoproteins in the cartilage ECM also can trigger inflammation. Again, the ABCA1 gene is involved in this process.

The catabolic environment in OA is favored for chondrocyte apoptosis, and it restricts autophagy, which plays a physiologically protective role from harmful stress. The activation of the PI3K/Akt/mTOR pathway not only promotes the expression of P62, an autophagy-related factor, but also affects the expression of apoptosis factors (Bcl-2 and Bax). Besides, this pathway is also involved in the activation of inflammation. Such effects eventually lead to higher MMP-3 and MMP-13 expression in chondrocytes and cartilage. Moreover, the expression of COL-II, a synthetic factor of ECM, is inhibited by the activation of the PI3K-Akt-mTOR pathway, promoting the development of OA [17]. Therefore, inhibiting this pathway is of particular importance for OA therapy [25].

At present, some cholesterol regulatory drugs can inhibit the synthesis of cholesterol, thus, being of potential therapeutic significance for OA [26]. Curcumin and probucol were both reported as cholesterol regulators [27, 28]. Specifically, curcumin can inhibit cholesterol metabolism, while probucol can be used to treat atherosclerosis by inhibiting TNF-α-

induced cholesterol metabolism [29]. Moreover, the two substances have both been reported to inhibit the PI3K/Akt/mTOR pathway [30, 31], and the PI3K pathway is involved in the regulation of mitochondrial activity and ROS production [32]. Specifically, curcumin can regulate several signal transcription pathways and function primarily by inhibiting the activity of NF-ƙB, a transcription factor associated with inflammation [33]. And probucol can inhibit atherosclerosis in mice by promoting ECM production [34]. In addition, curcumin treats OA by maintaining the levels of ECM-related factors, mainly COL-II and Sox-9 [35]. Based on these previously published findings, the two chemicals were investigated as potential candidates for OA therapy in the present study, and TNF-α was selected as the inflammatory stress cytokine of the chondrocytes.

In the present study, reduced autophagy and increased apoptosis in chondrocytes were observed after TNF-α stimulation, which is inconsistent with the results from Shakeri's report [36]. With combined administration of curcumin and probucol, autophagy was promoted and apoptosis was suppressed, indicating their protective effects on chondrocytes. However, aside from proliferation and apoptosis, cell migration also plays an important role in biological processes, and chondrocyte migration is especially necessary for cartilage repair [37, 38]. Previous researches have shown that chondrocytes migrate in vitro in response to chemoattractant factors, such as cytokines, growth factors, and ECM components. The dysfunctional migration of chondrocytes leads to their aggregation in OA and changes in ECM components [39]. However, in this study, curcumin and probucol were verified to promote chondrocyte migration, further suggesting their therapeutic potential for OA.

To explore the signaling pathways involved in curcumin-probucol treatment, further studies with 3BDO, a PI3K/AKT/mTOR signaling pathway agonist, were conducted. The results confirmed that curcumin and probucol antagonize 3BDO and thereby inhibiting the PI3K/AKT/mTOR signaling pathway, alleviating cartilage destruction in OA. Besides, morphological studies on cartilage were also performed to evaluate cartilage degeneration in vivo, and the results further verified the protective effects of such two substances on the cartilage matrix. Moreover, when applied alone, both curcumin and probucol can promote the expression of COL-II in ECM while inhibiting the expression of MMP-3 and MMP-13. A combined administration of such two chemicals would produce synergistic protective effects, and such findings were verified both in vitro and in vivo.

Curcuma longa, from which curcumin is extracted, has a history of thousands of years in Asian countries as a dietary spice and a therapeutic agent [40]. However, it was not until the mid-20th century that the biological properties of curcumin were scientifically identified [41]. Recent researches suggested that curcumin might take function in OA therapy [42–46]. Moreover, Henrotin et al. stated that even curcumin has not been considered as a recommended intervention for OA treatments, yet it still should be investigated for its safety and efficacy [22]. Some recent publications verified that different cell types have its specific permeability characteris-

tics towards curcumin intake, and different intracellular curcumin concentrations might control its performance in vivo [23, 24]. In vitro experiments verified that $20\,\mu M$ curcumin would not bring toxicity to human articular cartilage [45]. However, at a concentration of $50\,\mu M$, it will lead to a decrease in the survival rate of chondrocytes [46, 47].In our study, the optimal curcumin concentration to treat OA was determined to be $50\,\mu M$, but due to the potential considerable toxicity to normal chondrocytes at such concentration [48], caution still must be taken when applying curcumin for clinical treatment of OA.

Furthermore, lower aggrecan loss in IL-1β-stimulated articular cartilage explants has been reported to occur at a curcumin concentration no lower than $100\,\mu M$ [49]. Additionally, it was reported that probucol would also bring side effects, such as ventricular arrhythmia, torsades de pointes, and syncope [50]. Probucol can induce long-term QT syndrome by blocking the ethera-go-go-related genes [36]. Moreover, the bioavailability of curcumin is also very low because of its rapid metabolism, poor solubility and stability in aqueous solutions, and extensive binding to plasma proteins. A pharmacokinetic study suggested that curcumin is not absorbed adequately from the gastrointestinal tract. The peak serum concentration of curcumin was found to be only $1.77\,\mu M$ even with the highest dose of 8000 mg/day [51], which means its serum concentration in people who take in only 2 grams of curcumin is nearly undetectable [40]. In this study, the dosages of both chemicals were carefully designed to avoid possible side effects; meanwhile, we intended to verify whether the substances would still bring protective effects on chondrocytes and cartilage at such low concentrations. In this study, curcumin dosages that are close to its actual concentration in the human body were applied even though they are not enough to protect the cartilage in terms of total maintenance of proteoglycans. However, the results still suggested that a combined administration of the two chemicals can enhance the autophagy of chondrocytes, promote their proliferation, inhibit their apoptosis, increase their migration, and maintain their mitochondrial functions and the stability of the cartilage ECM by inhibiting the PI3K/Akt/mTOR pathway, and these findings had been confirmed in our in vivo animal studies.

Cholesterol regulatory drugs have various functions related to immune regulation and cartilage protection [52], and they may be promising candidates to alleviate cartilage degeneration. However, there are still several questions to be resolved, and the most important one is to what extent should cholesterol levels be lowered so that they can be always maintained at the level required for the stability of the internal cartilage environment. Besides, OA patients should be further categorized into different phenotypes based on their cholesterol metabolism situation.

In summary, OA patients are frequently accompanied with metabolic disorders, so it is necessary to regard the pathological mechanisms of OA as a metabolic disorder syndrome. Apart from their effects in regulating cholesterol levels, curcumin and probucol can also maintain chondrocyte stability by balancing cell autophagy and apoptosis. Moreover, lowering cholesterol levels by medication or

changing food intake and lifestyle is one of the fundamentals to prevent the onset and progression of OA, and a combined administration of curcumin and probucol is promising for OA prevention and treatment.

Data Availability

The data used to support the findings of this study are available from the corresponding author upon request.

Conflicts of Interest

The authors declare that they have no competing interests.

Authors' Contributions

Guangtao Han and Yubiao Zhang contributed equally to this work. They are co-first authors.

Acknowledgments

References

[1] M. L. Davies-Tuck, F. Hanna, S. R. Davis et al., "Total cholesterol and triglycerides are associated with the development of new bone marrow lesions in asymptomatic middle-aged women - a prospective cohort study," *Arthritis Research & Therapy*, vol. 11, no. 6, p. R181, 2009.

[2] T. P. Andriacchi, T. M. Griffin, R. F. Loeser et al., "Bridging disciplines as a pathway to finding new solutions for osteoarthritis, a collaborative program presented at the 2019 Orthopaedic Research Society and the Osteoarthritis Research Society International - ScienceDirect," *Osteoarthritis and Cartilage Open*, vol. 2, no. 1, article 100026, 2020.

[3] J. Niu, M. Clancy, P. Aliabadi, R. Vasan, and D. T. Felson, "Metabolic syndrome, its components, and knee osteoarthritis: the Framingham Osteoarthritis Study," *Arthritis & Rhematology*, vol. 69, no. 6, pp. 1194–1203, 2017.

[4] S. Farnaghi, R. Crawford, Y. Xiao, and I. Prasadam, "Cholesterol metabolism in pathogenesis of osteoarthritis disease," *International Journal of Rheumatic Diseases*, vol. 20, no. 2, pp. 131–140, 2017.

[5] A. Tsezou, D. Iliopoulos, K. N. Malizos, and T. Simopoulou, "Impaired expression of genes regulating cholesterol efflux in human osteoarthritic chondrocytes," *Journal of Orthopaedic Research*, vol. 28, no. 8, pp. 1033–1039, 2010.

[6] W.-S. Choi, G. Lee, W.-H. Song et al., "The CH25H-CYP7B1-RORα axis of cholesterol metabolism regulates osteoarthritis," *Nature*, vol. 566, no. 7743, pp. 254–258, 2019.

[7] G. Kroemer, G. Mariño, and B. Levine, "Autophagy and the Integrated Stress Response," *Molecular Cell*, vol. 40, no. 2, pp. 280–293, 2010.

[8] L. Xiaolong, G. Dongmin, M. Liu et al., "FGF21 induces autophagy-mediated cholesterol efflux to inhibit atherogenesis via RACK1 up-regulation," *Journal of Cellular and Molecular Medicine*, vol. 24, no. 9, pp. 4992–5006, 2020.

[9] R. F. Loeser, "Aging and osteoarthritis," *Current Opinion in Rheumatology*, vol. 23, no. 5, pp. 492–496, 2011.

[10] S. Wang, Y. Zheng, Z. Hu, Z. Wang, Y. Zhang, and L. Wei, "Downregulated miR-302d-3p promotes chondrocyte proliferation and migration by regulation of Unc-51-like kinase 1," *International Journal of Molecular Medicine*, vol. 44, no. 3, pp. 1039–1047, 2019.

[11] S. Shishir, S. Gautam, and B. B. Aggarwal, "Curcumin: getting back to the roots," *Annals of the New York Academy of Sciences*, vol. 1056, no. 1, pp. 206–217, 2005.

[12] L. Zhang, X. Tao, Q. Fu et al., "Curcumin inhibits cell proliferation and migration in NSCLC through a synergistic effect on the TLR4/MyD88 and EGFR pathways," *Oncology Reports*, vol. 42, no. 5, pp. 1843–1855, 2019.

[13] H. Fu, C. Wang, D. Yang et al., "Curcumin regulates proliferation, autophagy, and apoptosis in gastric cancer cells by affecting PI3K and P53 signaling," *Journal of Cellular Physiology*, vol. 233, no. 6, pp. 4634–4642, 2018.

[14] X. Li, K. Feng, J. Li, D. Yu, Q. Fan, T. Tang, X. Yao, and X. Wang, Eds., "Curcumin inhibits apoptosis of chondrocytes through activation ERK1/2 signaling pathways Induced autophagy," *Nutrients*, vol. 9, no. 4, p. 414, 2017.

[15] Z. Zhou, S. Chen, H. Zhao et al., "Probucol inhibits neural cell apoptosis via inhibition of mTOR signaling pathway after spinal cord injury," *Neuroscience*, vol. 329, pp. 193–200, 2016.

[16] C. Cai, S. Min, B. Yan et al., "MiR-27a promotes the autophagy and apoptosis of IL-1β treated articular chondrocytes in osteoarthritis through PI3K/AKT/mTOR signaling," *Aging*, vol. 11, no. 16, pp. 6371–6384, 2019.

[17] Y. Zhang, W. Cai, G. Han et al., "Panax notoginseng saponins prevent senescence and inhibit apoptosis by regulating the PI3K-AKT-mTOR pathway in osteoarthritic chondrocytes," *International Journal of Molecular Medicine*, vol. 45, no. 4, pp. 1225–1236, 2020.

[18] R. W. Farndale, D. J. Buttle, and A. J. Barrett, "Improved quantitation and discrimination of sulphated glycosaminoglycans by use of dimethylmethylene blue," *Biochimica et Biophysica Acta*, vol. 883, no. 2, pp. 173–177, 1986.

[19] T. Nicoliche, D. C. Maldonado, J. Faber, and M. C. P. . Silva, "Evaluation of the articular cartilage in the knees of rats with induced arthritis treated with curcumin," *PLoS One*, vol. 15, no. 3, article e0230228, 2020.

[20] X. Chevalier, P. Ravaud, E. Maheu et al., "Adalimumab in patients with hand osteoarthritis refractory to analgesics and NSAIDs: a randomised, multicentre, double-blind, placebo-controlled trial," *Annals of the Rheumatic Diseases*, vol. 74, no. 9, pp. 1697–1705, 2015.

[21] M. S. M. Persson, A. Sarmanova, M. Doherty, and W. Zhang, "Conventional and biologic disease-modifying anti-rheumatic drugs for osteoarthritis: a meta-analysis of randomized controlled trials," *Rheumatology*, vol. 57, no. 10, pp. 1830–1837, 2018.

[22] Y. Henrotin, F. Priem, and A. Mobasheri, "Curcumin: a new paradigm and therapeutic opportunity for the treatment of osteoarthritis: curcumin for osteoarthritis management," *SpringerPlus*, vol. 2, no. 1, p. 56, 2013.

[23] G. J. Zhao, S. L. Tang, Y. C. Lv et al., "Antagonism of betulinic acid on LPS-mediated inhibition of ABCA1 and cholesterol efflux through inhibiting nuclear factor-kappaB signaling

pathway and miR-33 expression," *PLoS One*, vol. 8, no. 9, article e74782, 2013.

[24] J. S. Teodoro, S. Nunes, A. P. Rolo, F. Reis, and C. M. Palmeira, "Therapeutic options targeting oxidative stress, mitochondrial dysfunction and inflammation to hinder the progression of vascular complications of diabetes," *Frontiers in Physiology*, vol. 9, p. 1857, 2018.

[25] F. Guo, Z. Yong, and Y. Zheng, "Moracin M inhibits lipopolysaccharide-induced inflammatory responses in nucleus pulposus cells via regulating PI3K/Akt/mTOR phosphorylation," *International Immunopharmacology*, vol. 58, pp. 80–86, 2018.

[26] B. G. Seol, J. H. Kim, M. Woo et al., "Skate cartilage extracts containing chondroitin sulfate ameliorates hyperlipidemia-induced inflammation and oxidative stress in high cholesterol diet-fed LDL receptor knockout mice in comparison with shark chondroitin sulfate," *Nutrition Research and Practice*, vol. 14, no. 3, pp. 175–187, 2020.

[27] J.-L. Huang, C. Yu, M. Su et al., "Probucol, a "non-statin" cholesterol-lowering drug, ameliorates D-galactose induced cognitive deficits by alleviating oxidative stress via Keap1/Nrf2 signaling pathway in mice," *Aging*, vol. 11, no. 19, pp. 8542–8555, 2019.

[28] J. J. A. Ferguson, E. Stojanovski, L. MacDonald-Wicks, and M. L. Garg, "Curcumin potentiates cholesterol-lowering effects of phytosterols in hypercholesterolaemic individuals. A randomised controlled trial," *Metabolism*, vol. 82, pp. 22–35, 2018.

[29] Y. Li, L. Tian, D. Sun, and D. Yin, "Curcumin ameliorates atherosclerosis through upregulation of miR-126," *Journal of Cellular Physiology*, vol. 234, no. 11, pp. 21049–21059, 2019.

[30] Y.-y. Wang, H. Li, X.-h. Wang, M. Yuan, and G.-p. Li, "Combination of rosuvastatin and probucol inhibits MMP-9 expression via upregulation of miR-497 in cultured HUVECs and apoE knockout mice," *Journal of Thrombosis and Thrombolysis*, vol. 41, no. 4, pp. 592–605, 2016.

[31] J.-H. Kim, T. G. Choi, S. Park et al., "Mitochondrial ROS-derived PTEN oxidation activates PI3K pathway for mTOR-induced myogenic autophagy," *Cell Death & Differentiation*, vol. 25, no. 11, pp. 1921–1937, 2018.

[32] C. Csaki, A. Mobasheri, and M. Shakibaei, "Synergistic chondroprotective effects of curcumin and resveratrol in human articular chondrocytes: inhibition of IL-1beta-induced NF-kappaB-mediated inflammation and apoptosis," *Arthritis Research & Therapy*, vol. 11, no. 6, article R165, 2009.

[33] K. Choy, K. Beck, F. Y. Png et al., "Processes involved in the site-specific effect of probucol on atherosclerosis in apolipoprotein E gene knockout mice," *Arteriosclerosis, Thrombosis, and Vascular Biology*, vol. 25, no. 8, pp. 1684–1690, 2005.

[34] C. Kang, E. Jung, H. Hyeon, S. Seon, and D. Lee, "Acid-activatable polymeric curcumin nanoparticles as therapeutic agents for osteoarthritis," *Nanomedicine: Nanotechnology, Biology and Medicine*, vol. 23, article 102104, 2020.

[35] E. H. Frank, A. J. Grodzinsky, T. J. Koob, and D. R. Eyre, "Streaming potentials: a sensitive index of enzymatic degradation in articular cartilage," *Journal of Orthopaedic Research*, vol. 5, no. 4, pp. 497–508, 1987.

[36] A. Shakeri, A. F. G. Cicero, Y. Panahi, M. Mohajeri, and A. Sahebkar, "Curcumin: a naturally occurring autophagy modulator," *Journal of Cellular Physiology*, vol. 234, no. 5, pp. 5643–5654, 2019.

[37] O. Sarah, "PBMCs stimulate chondrocyte migration and cartilage repair," *Nature Reviews Rheumatology*, vol. 11, no. 10, pp. 563–564, 2015.

[38] D. Ye, W. Jian, J. Feng, and X. Liao, "Role of long noncoding RNA ZFAS1 in proliferation, apoptosis and migration of chondrocytes in osteoarthritis," *Biomedicine & Pharmacotherapy*, vol. 104, pp. 825–831, 2018.

[39] T. Pufe, G. Groth, M. B. Goldring, B. Tillmann, and R. Mentlein, "Effects of pleiotrophin, a heparin-binding growth factor, on human primary and immortalized chondrocytes," *Osteoarthritis and Cartilage*, vol. 15, no. 2, pp. 155–162, 2007.

[40] S. C. Gupta, S. Patchva, W. Koh, and B. B. Aggarwal, "Discovery of curcumin, a component of golden spice, and its miraculous biological activities," *Clinical and Experimental Pharmacology & Physiology*, vol. 39, no. 3, pp. 283–299, 2012.

[41] B. Joe, M. Vijaykumar, and B. R. Lokesh, "Biological properties of curcumin-cellular and molecular mechanisms of action," *Critical Reviews in Food Science and Nutrition*, vol. 44, no. 2, pp. 97–111, 2004.

[42] V. Kuptniratsaikul, P. Dajpratham, W. Taechaarpornkul et al., "Efficacy and safety of Curcuma domestica extracts compared with ibuprofen in patients with knee osteoarthritis: a multicenter study," *Clinical Interventions in Aging*, vol. 9, pp. 451–458, 2014.

[43] V. Kuptniratsaikul, S. Thanakhumtorn, P. Chinswangwatanakul, L. Wattanamongkonsil, and V. Thamlikitkul, "Efficacy and safety of Curcuma domestica extracts in patients with knee osteoarthritis," *Journal of Alternative and Complementary Medicine*, vol. 15, no. 8, pp. 891–897, 2009.

[44] S. Lev-Ari, L. Strier, D. Kazanov et al., "Curcumin synergistically potentiates the growth inhibitory and proapoptotic effects of celecoxib in osteoarthritis synovial adherent cells," *Rheumatology*, vol. 45, no. 2, pp. 171–177, 2006.

[45] C. C. Yeh, Y. H. Su, Y. J. Lin et al., "Evaluation of the protective effects of curcuminoid (curcumin and bisdemethoxycurcumin)-loaded liposomes on bone turnover in a cell-based model of osteoarthritis," *Drug Design, Development and Therapy*, vol. 4, no. 9, pp. 2285–2300, 2015.

[46] Y. Nakagawa, S. Mukai, S. Yamada et al., "Short-term effects of highly-bioavailable curcumin for treating knee osteoarthritis: a randomized, double-blind, placebo-controlled prospective study," *Journal of Orthopaedic Science*, vol. 19, no. 6, pp. 933–939, 2014.

[47] M. Mathy-Hartert, I. Jacquemond-Collet, F. Priem, C. Sanchez, C. Lambert, and Y. Henrotin, "Curcumin inhibits proinflammatory mediators and metalloproteinase-3 production by chondrocytes," *Inflammation Research*, vol. 58, no. 12, pp. 899–908, 2009.

[48] S. Toegel, S. Q. Wu, C. Piana et al., "Comparison between chondroprotective effects of glucosamine, curcumin, and diacerein in IL-1β-stimulated C-28/I2 chondrocytes," *Osteoarthritis and Cartilage*, vol. 16, no. 10, pp. 1205–1212, 2008.

[49] A. L. Clutterbuck, A. Mobasheri, M. Shakibaei, D. Allaway, and P. Harris, "Interleukin-1β-Induced extracellular matrix degradation and glycosaminoglycan release Is inhibited by curcumin in an explant model of cartilage inflammation," *Annals of the New York Academy of Sciences*, vol. 1171, no. 1, pp. 428–435, 2009.

[50] D. C. John and T. W. Simmons, "Polymorphic ventricular tachycardia (torsade de pointes) associated with the use of

probucol," *The New England Journal of Medicine*, vol. 326, no. 21, pp. 1435-1436, 1992.

[51] A. L. Cheng, C. H. Hsu, J. K. Lin et al., "Phase I clinical trial of curcumin, a chemopreventive agent, in patients with high-risk or pre-malignant lesions," *Anticancer Research*, vol. 21, no. 2895, article e2900, 2001.

[52] P. Liczbiński, J. Michałowicz, and B. Bukowska, "Molecular mechanism of curcumin action in signaling pathways: review of the latest research," *Phytotherapy Research*, vol. 34, no. 8, pp. 1992–2005, 2020.

Research Article

Genomic and Transcriptome Analysis to Identify the Role of the mTOR Pathway in Kidney Renal Clear Cell Carcinoma and Its Potential Therapeutic Significance

Xiangyu Che [ID],[1] **Xiaochen Qi,**[1] **Yingkun Xu** [ID],[2] **Qifei Wang** [ID],[1] **and Guangzhen Wu** [ID][1]

[1]*Department of Urology, The First Affiliated Hospital of Dalian Medical University, Dalian, Liaoning 116011, China*
[2]*Department of Urology, Shandong Provincial Hospital, Cheeloo College of Medicine, Shandong University, Jinan, Shandong 250021, China*

Correspondence should be addressed to Qifei Wang; wangqifei6008@hotmail.com
and Guangzhen Wu; wuguang0613@hotmail.com

The mTOR pathway, a major signaling pathway, regulates cell growth and protein synthesis by activating itself in response to upstream signals. Overactivation of the mTOR pathway may affect the occurrence and development of cancer, but no specific treatment has been proposed for targeting the mTOR pathway. In this study, we explored the expression of mTOR pathway genes in a variety of cancers and the potential compounds that target the mTOR pathway and focused on an abnormal type of cancer, kidney renal clear cell carcinoma (KIRC). Based on the mRNA expression of the mTOR pathway gene, we divided KIRC patient samples into three clusters. We explored possible therapeutic targets of the mTOR pathway in KIRC. We predicted the IC50 of some classical targeted drugs to analyze their correlation with the mTOR pathway. Subsequently, we investigated the correlation of the mTOR pathway with histone modification and immune infiltration, as well as the response to anti-PD-1 and anti-CTLA-4 therapy. Finally, we used a LASSO regression analysis to construct a model to predict the survival of patients with KIRC. This study shows that mTOR scores can be used as tools to study various treatments targeting the mTOR pathway and that we can predict the recovery of KIRC patients through the expression of mTOR pathway genes. These research results can provide a reference for future research on KIRC patient treatment strategies.

1. Introduction

Renal cell carcinoma (RCC) is the eighth most common malignant tumor in the United States [1]. The estimated incidence of kidney cancer in 2020 was 74,000. The typical symptoms of kidney cancer patients, such as pain, lumps, and hematuria, account for only 10% of cases [2]. Due to the kidney's ability to compensate when there is damage, it is usually impossible to detect the loss of kidney function early. Therefore, RCC is clinically insidious in terms of the development of the disease. Approximately one-third of patients have metastatic disease at the time of diagnosis, and patients with locally advanced kidney cancer have a 40% risk of recurrence after tumor resection [3, 4]. The development of targeted therapy and immunotherapy in the past decade has filled the gap in the treatment of advanced kidney cancer. Although the tumor response rate to these drugs is relatively high, most patients eventually experience cancer progression. For current treatments, the emergence of drug resistance is a major challenge, forcing us to reconsider the treatment of RCC [5].

Current studies have shown that the emergence of drug resistance is related to the existence of tumor stem cells and the activation of other pathways [6]. The mechanisms include the activation of the WNT-β-catenin, TP53, c-Met, and VEGF/angiogenesis signaling pathways [7–9]. In addition, although the current tumor research has made unprecedented progress in cancer genetics, we have not yet reached a unified view of genetics, for example, combining gene mutations, copy number variations, driving pathways, and

other aspects to overcome tumors [10]. Here, we analyzed gene mutations, copy number changes, gene expression, and gene prognosis correlation results of 33 tumors from The Cancer Genome Atlas (TCGA). We combined this analysis with functional research to dissect the components that identify specific temporal events that reflect the complexity of the mTOR signaling pathway.

The mTOR pathway senses and integrates multiple intracellular and environmental signals through two protein complexes with different structures and functions: mTOR complex 1 (mTORC1) and mTOR complex 2 (mTORC2) [11, 12]. mTOR signaling is usually involved in regulating cell survival, cell growth, cell metabolism, protein synthesis, autophagy, and homeostasis [13]. In addition, mTOR negatively regulates autophagy in different ways. The pathological relevance of mTOR signal dysregulation has been explained in many human diseases, especially in various human cancers. The mTOR signaling pathway has been reported to be overactivated in more than 70% of cancers [14]. It has been widely demonstrated in animal models and clinical cancer patients in the past few years [15, 16]. The regulation of the mTOR pathway is also affected by the positive and negative regulators that cross-talk with it, such as phosphoinositide 3-kinase (PI3K)/AKT, mitogen-activated protein kinase (MAPK), vascular endothelial growth factor (VEGF), nuclear factor κB (NFκB) and p53, which form a more complex signal cascade [17].

Therefore, this study used the mutation, expression, and clinical data from the TCGA database to analyze the CNV, SNV, and gene expression status of mTOR signaling pathway genes in 33 tumors and the relationship between each tumor and patient prognosis. Surprisingly, most of the genes in the mTOR pathway in clear cell renal cell carcinoma are protective for patient prognosis. To further explain this phenomenon, we used bioinformatics methods to analyze the mTOR pathway-related genes in kidney renal clear cell carcinoma (KIRC). This study is aimed at systematically evaluating mTOR pathway-related genes and the KIRC prognoses associated with them. Through the expression pattern of mTOR pathway-related genes in KIRC, the prognostic value and impact on immune correlation can improve prognostic risk stratification and promote treatment decisions in KIRC patients.

2. Materials and Methods

2.1. Acquisition of Gene Data and Patient Clinical Information Data.
The mTOR pathway genes were identified using the REACTOME dataset in the gene set enrichment analysis (GSEA) website. We obtained 32 types of cancer and 40 mTOR pathway genes. The CNV, SNV, and gene expression data were downloaded from The Cancer Genome Atlas (https://portal.gdc.cancer.gov) database [18, 19]. We used the Perl language to analyze the data and TBtools to visualize the results. The RNA-seq KIRC cohort included 72 normal samples and 539 cancer samples.

2.2. Connectivity Map Analysis (CMap) and Mechanism of Action (MoA).
To determine which target drugs are useful for mTOR pathway therapy, we used the Broad Institute's Connectivity Map Build02 (CM), which allows users to predict compounds that can activate or inhibit tumors based on the gene expression characteristics of different tumors [20]. To further study the mechanism of action (MoA) and drug targets related to the mTOR pathway, we conducted a specific analysis using the Connectivity Map tool [10, 21]. We obtained 16 differential expression characteristics of mRNA by performing differential expression analyses on mTOR pathway gene expression samples. CMap is a method similar to GSEA; it is based on the Kolmogorov-Smirnov test's pattern-matching strategy, which is used to find similarities between differentially expressed genes (DEGs). Then, we compared the DEG rankings to determine the positive or negative regulatory relationship of the genes, thereby generating an enrichment score (ES) from -1 to 1, and finally sorted the above scores based on all of the case data in the database. For each cancer type, we obtained two tables that applied the connection diagram findings to the expression characteristics of the mTOR pathway. A p value < 0.05 was used as an inclusion criterion to determine the average meaningful compound of each tumor type. These compounds may inhibit or activate the mTOR pathway in tumors. We use the "GEOquery" package in R to get data from the Gene Expression Omnibus (GEO) database, the "xlsx," "tidyverse," "plyr," and "circlize" packages to process and analyze the data, and the "pheatmap" package to plot the heat map.

2.3. Cluster Analysis Based on mTOR Scores.
Because the gene expression profile in the previously obtained data set had a large variation, we constructed an mTOR-score model based on mRNA expression to show the differential expression between the samples. According to the expression of mRNA in normal tissues, the expression statuses of the mRNA in the tumor tissues were classified into three categories: mTOR active (cluster1), normal (cluster2), and mTOR inactive (cluster3). To further illustrate the relationship between gene expression levels among these three clusters, a violin plot was used to depict the enrichment score levels of the three clusters. Statistical significance was set at $p < 0.05$. The "gplots" package was used in RStudio for cluster analysis. We used the "survival" package in RStudio to plot the survival curve of the three clusters. A heat map was drawn by "pheatmap" in RStudio to describe the relationship between the three groups of clusters and the clinicopathological characteristics of the KIRC patients. Statistical significance was set at $p < 0.05$.

2.4. GDSC Database and pRRophetic Algorithm.
The Genomics of Drug Sensitivity in Cancer (GDSC) is the largest public pharmacogenomics database (https://www.cancerrxgene.org/). We used the GDSC database to predict the chemotherapeutic response. We selected several classic and novel targeted drugs to treat KIRC. We used the "pRRophetic" package in R to perform the prediction process; a ridge regression was used to estimate the half-maximal inhibitory concentration (IC50) of the sample [22, 23]. We also used a 10-fold cross-validation based on the GDSC training set to estimate the precision of the prediction. Except for "combat"

and "allSoldTumours" tissue types, we set all parameters to default. The repetitive expression of genes was summarized as an average value. Statistical significance was set at $p < 0.05$.

2.5. Classical Cancer-Related Genes and Histone Modification. For the mTOR pathway, the differential expression of known classical oncogenes and histone modification-related genes leads to activation or inhibition of the mTOR pathway. To explore the potential regulatory mechanism of the mTOR pathway in KIRC, we examined the expression levels of various oncogenes in three groups of clusters in the form of a heat map to explore the influence of differentially expressed oncogenes on the mTOR pathway. Using the same approach, we also demonstrated the relationship between the three clusters of mTOR pathways and two gene types, SIRT and HDAC, which are involved in histone modification. Statistical significance was set at $p < 0.05$.

2.6. Immune Cell Infiltration and Immunotherapy. We used a single-sample gene set enrichment analysis combined with the expression of related genes in the TCGA database to quantify immune cells [24]. Then, a heat map expressing the correlation between the two was drawn using the "ggplot2" and "dplyr" packages in R. An ssGSEA analysis can be applied to gene signals expressed by immune cell populations in a single sample. Twenty-nine types of immune cells and regulators used in this study involved innate and adaptive immunity. Based on the results of ssGSEA, we showed the correlation between mTOR scores and the immune substances in Figure 1(e), where the area of a sphere represents the degree of correlation. The color represents the p value. R software packages "data.table," "dplyr," "tidyr," "ggplot2," and "ggstatsplot" were used to analyze and plot the figure. We then selected six classical immune regulators: inflammation, promotion, parainflammation, T cell costimulation, Tfh, and TIL. We used the "ggscatterstats" package to draw the scatter diagram to represent their specific correlations to the mTOR scores separately. PD-1 and CTLA-4 are two types of immune regulatory factors related to T cell-killing tumor cells [25–27]. The correlation between CTLA-4, PD-1, and mTOR scores was demonstrated through a visual correlation matrix analysis. The three graphs in the upper right of Figure 1(k) correspond to correlation coefficients, while the three graphs in the lower left show a specific correlation. Based on the correlation between PD-1, CTLA-4, and mTOR scores, we hypothesized that immunotherapy based on PD-1 and CTLA-4 would respond to the mTOR pathway. TIDE and subclass mapping are two algorithms used to predict a single sample's response possibility or a subtype of immunotherapy [26–28]. Their source sites are http://tide.dfci.harvard.edu/ and https://cloud.genepattern.org/gp. TIDE was used to predict single-sample immune checkpoint inhibitor response, and a submap was used to predict the immunotherapy responses of the subtypes. We used a Bonferroni correction to correct the p value of the test level. Finally, the heat map was plotted using the "pheatmap" package. Statistical significance was set at $p < 0.05$.

2.7. Construction of the Prediction Model with a LASSO Regression Analysis. We used "pheatmap" to describe the expression levels of mTOR pathway genes in normal and KIRC tissues. We used "corrplot" to describe the coexpression relationship between any two of the mTOR pathway genes. A hazard ratio analysis was performed to analyze the relationship between the pathway and progression of KIRC. A LASSO regression curve using the "glmnet" package was used to establish a risk model. Risk score = $\sum ni = 1$ (Expi * Coei); N, Coei, and Expi represent the gene number, the regression correlation coefficient obtained by the LASSO regression analysis, and the gene expression level, respectively. We determined the cut-off value of each risk score in the tumor group using the "survminer" package. We divided the samples into high-risk and low-risk groups based on the best cut-off values. We acquired the survival curve of the two groups with the "survival" package in RStudio. Then, we used the "survival-ROC" package to plot the ROC curve and get the AUC value. We used a heat map to show the correlation of clinicopathological features between the low-risk and high-risk groups. Statistical significance was set at $p < 0.05$.

2.8. Validation of the Prediction Model and Nomogram. We use the Sankey diagram plotted by the "ggalluvial" package to show the multiple attributes of protective and risky genes with statistical significance in an HR analysis. We obtained protein-related information from the HPA website (https://www.proteinatlas.org/) [29]. Univariate and multivariate Cox regression analyses were used to show the correlations between age, stage, grade, T (tumor), M (metastasis), and risk score in the model. N (node) was not included in the analysis because the sample quantity was not large enough to support the study. All statistical analyses were performed using RStudio. The nomogram was drawn by the "rms" package in R. Finally, in order to make our conclusion more convincing, we used KIRC clinical specimens to conduct immunohistochemical experiments on the two key molecules involved in the model, PRKAA2 and EIF4EBP1. A p value < 0.05 was considered statistically significant.

3. Results

3.1. Widespread Genetic Mutations of mTOR Pathway Genes in 32 Types of Cancer. Through the TCGA Pan-cancer Project, copy number variation (CNV), single-nucleotide variation (SNV), and gene expression levels (Figure 2) of 40 types of mTOR pathway-related genes and in 32 cancer types were studied. We downloaded the data from The Cancer Genome Atlas (TCGA) database and analyzed them using R [30]. We found that only a few types of cancer, such as THCA, THYM, and PRAD, had almost no CNV gains or CNV losses in mTOR pathway genes (Table S1, S2). In addition, CNV of mTOR pathway genes are present in most cancers. We also found that changes in SNV, the mTOR pathway gene, were also predominant in most cancers (Table S3). A large frequency of SNVs occurred in UCEC, SKCM, and COAD. To further study the expression of mTOR pathway genes in different cancers, we used log2(FC) of the gene expression level between normal and
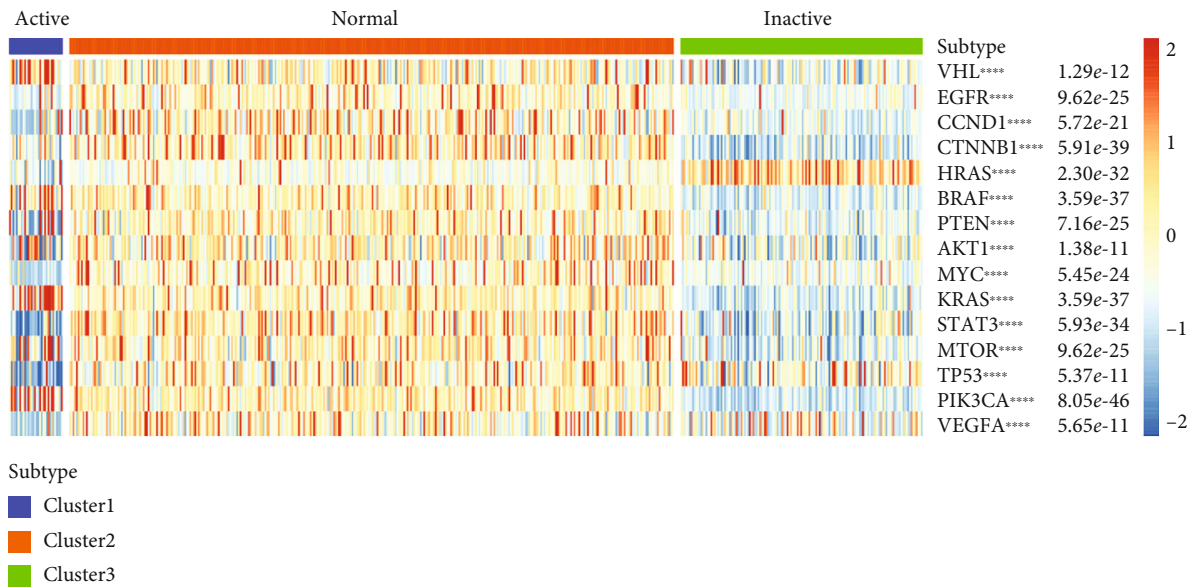
(a)
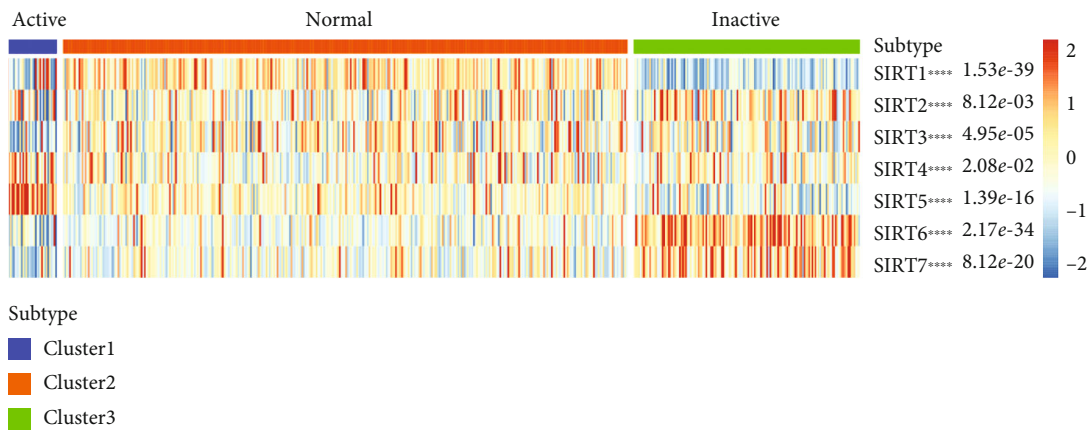
(b)
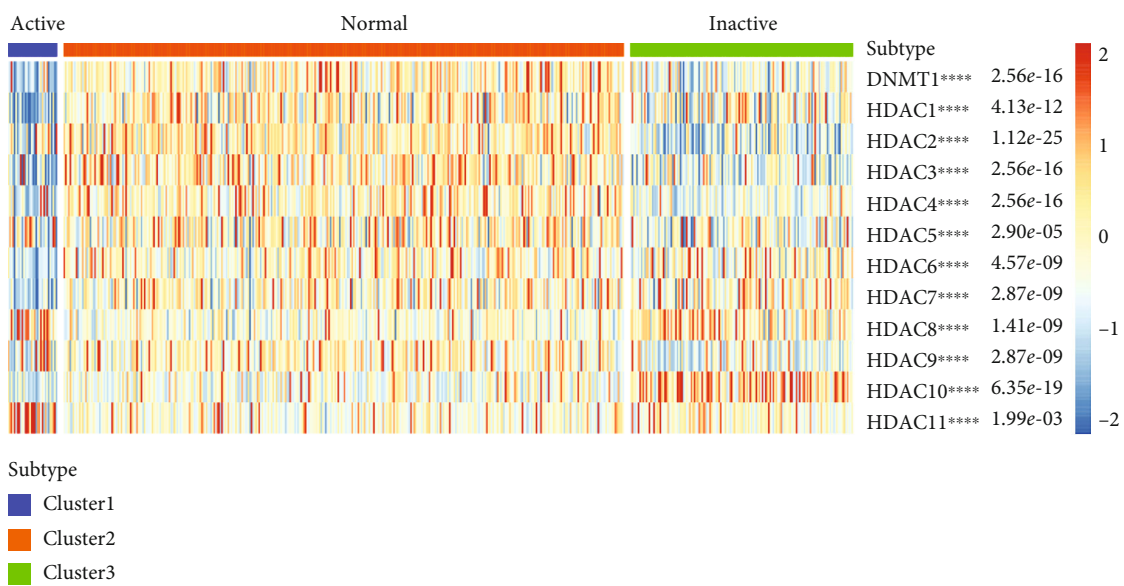
(c)

Figure 1: Continued.

(d)

(e)

Figure 1: Continued.

Inflammation.promoting

$t_{\text{Student}}(537) = -8.77$, $p = 2.31\text{e-}17$, $\hat{r}_{\text{Pearson}} = -0.35$, $\text{CI}_{95\%}$ [-0.43, -0.28], $n_{\text{paris}} = 539$

$\text{Log}_e(\text{BF}_{01}) = -33.06$, $\hat{p}_{\text{median}}^{\text{posterior}} = -0.35$, $\text{CI}_{95\%}^{\text{HDI}}$ [-0.43, -0.28], $r_{\text{Caucity}}^{\text{JZS}} = 0.71$

(f)

Parainflammation

$t_{\text{Student}}(537) = -9.54$, $p = 4.83\text{e-}20$, $\hat{r}_{\text{Pearson}} = -0.38$, $\text{CI}_{95\%}$ [-0.45, -0.31], $n_{\text{paris}} = 539$

$\text{Log}_e(\text{BF}_{01}) = -33.06$, $\hat{p}_{\text{median}}^{\text{posterior}} = -0.38$, $\text{CI}_{95\%}^{\text{HDI}}$ [-0.44, -0.30], $r_{\text{Caucity}}^{\text{JZS}} = 0.71$

(g)

T_cell_co.stimulation

$t_{\text{Student}}(537) = -10.53$, $p = 1.1\text{e-}23$, $\hat{r}_{\text{Pearson}} = -0.41$, $\text{CI}_{95\%}$ [-0.48, -0.34], $n_{\text{paris}} = 539$

$\text{Log}_e(\text{BF}_{01}) = -47.39$, $\hat{p}_{\text{median}}^{\text{posterior}} = -0.41$, $\text{CI}_{95\%}^{\text{HDI}}$ [-0.48, -0.34], $r_{\text{Caucity}}^{\text{JZS}} = 0.71$

(h)

Tfh

$t_{\text{Student}}(537) = -9.14$, $p = 1.31\text{e-}18$, $\hat{r}_{\text{Pearson}} = -0.37$, $\text{CI}_{95\%}$ [-0.44, -0.29], $n_{\text{paris}} = 539$

$\text{Log}_e(\text{BF}_{01}) = -35.88$, $\hat{p}_{\text{median}}^{\text{posterior}} = -0.36$, $\text{CI}_{95\%}^{\text{HDI}}$ [-0.43, -0.29], $r_{\text{Caucity}}^{\text{JZS}} = 0.71$

(i)

TIL

$t_{\text{Student}}(537) = -8.85$, $p = 1.29\text{e-}17$, $\hat{r}_{\text{Pearson}} = -0.36$, $\text{CI}_{95\%}$ [-0.43, -0.28], $n_{\text{paris}} = 539$

$\text{Log}_e(\text{BF}_{01}) = -33.63$, $\hat{p}_{\text{median}}^{\text{posterior}} = -0.35$, $\text{CI}_{95\%}^{\text{HDI}}$ [-0.43, -0.28], $r_{\text{Caucity}}^{\text{JZS}} = 0.71$

(j)

(k)

Figure 1: Continued.

(l)

FIGURE 1: (a–c) Heat map showing that mTOR scores were associated with other signaling pathways in KIRC. (a) The correlation with potentially targetable classical genes. (b) The correlation with sirtuin family genes. (c) The correlation with HDAC family genes. (d) Heat map showing the correlation between mTOR pathway genes and substances related to immune filtering. Purple means positive and yellow means negative. $^*p < 0.05$ and $^{**}p < 0.01$. (e) Plot showing the degree of correlation; the area of the sphere represents the abs(correlation), and the color indicates the p value. (f–j) Scatter diagram showing the specific relationship between the five immune-infiltration-related substances and the mTOR scores. It can be seen from the diagram that they are all negatively correlated. (k) The plot shows the correlation analysis between PD-1, CTLA-4, and the mTOR scores. In the figure, a scatter plot and color block are, respectively, used to represent their specific correlation and correlation coefficients. (l) Submap analysis indicating that the mTOR-inactive cluster could be more sensitive to PD-1 (the programmed cell death protein 1) inhibitors (nominal p value = 0.029).

cancer tissues. We found that most of the mTOR pathway-related genes had a high expression level in most cancers, except for a few genes such as CAB39L and PRKAA2, which had a lower expression in most cancers compared to normal tissues. This was also consistent with the conclusion that mTOR is an oncogene-activated pathway (Table S4) [31, 32]. We also examined gene mutations in KIRC, as shown by the heat map. No large CNV or SNV values were noted; the CNV frequency was lower than 0.4, and most of the CNVs fluctuated around 0.2. For SNVs, the frequencies of all other genes were lower than 0.02, except for mTOR, which reached 0.06–0.08.

3.2. Connectivity Map (CMap) Analysis Identifying Potential Compounds/Inhibitors That Can Target the mTOR Pathway.

We used Connectivity Map (CMap) [33], a systematic approach that is driven by data, to discover links between genes, chemicals, and biological situations to search for compounds and inhibitors that might target mTOR-related pathways (Figure 3(a)). According to the results and the actual situation, most of these candidate compounds have been reported to be used against cancer. Some of the candidate compounds have been reported to directly or indirectly affect the mTOR pathway. bergenin has been reported to have anticancer effects in cervical cancer and bladder cancer [34, 35] and to have a relationship with the mTOR pathway [36]. There have also been reports indicating that mepacrine has anticancer effects [37] and that it is correlated with the mTOR pathway [38].

The CMap mode-of-action (MoA) analysis of the 11 compounds revealed their action mechanisms (Figure 3(b)).

It is convenient to explore their common internal mechanisms. Interestingly, each of these 11 compounds has a separate anticancer mechanism of action: indoprofen (cyclooxygenase inhibitor and prostanoid receptor antagonist); mepacrine (cytokine production inhibitor, NFκB pathway inhibitor, and TP53 activator), molindone (dopamine receptor antagonist), depudecin (HDAC inhibitor), lovastatin (HMGCR inhibitor), bergenin (interleukin inhibitor), zardaverine (phosphodiesterase inhibitor), rifabutin (protein synthesis inhibitor), TTNPB (retinoid receptor agonist), fasudil (Rho-associated kinase inhibitor), and buspirone (serotonin receptor agonist). The corresponding action mechanisms are shown in parentheses.

3.3. The Role of mTOR Genes in Cancer.

The mammalian or mechanistic target of rapamycin (mTOR) pathway plays a vital role in cancer and regulates cell survival, metabolism, growth, and protein synthesis [16]. The mTOR signaling pathway has been reported to be overactivated in most human cancers [39]. It has been reported that excessive activation of the mTOR pathway and abnormal cell metabolism jointly lead to cancer occurrence [40]. We determined whether the genes involved exists as risky genes or as protective genes based on the relationship between patient survival rates and the mTOR pathway gene expression levels reported in the TCGA database. A high expression of a gene that led to an increased survival rate indicated that it was a protective gene, while a high expression of a gene that caused a decreased survival rate led it to be judged as a risky gene. We used this method to analyze the survival landscape of the mTOR pathway genes. As shown in the resulting figure,
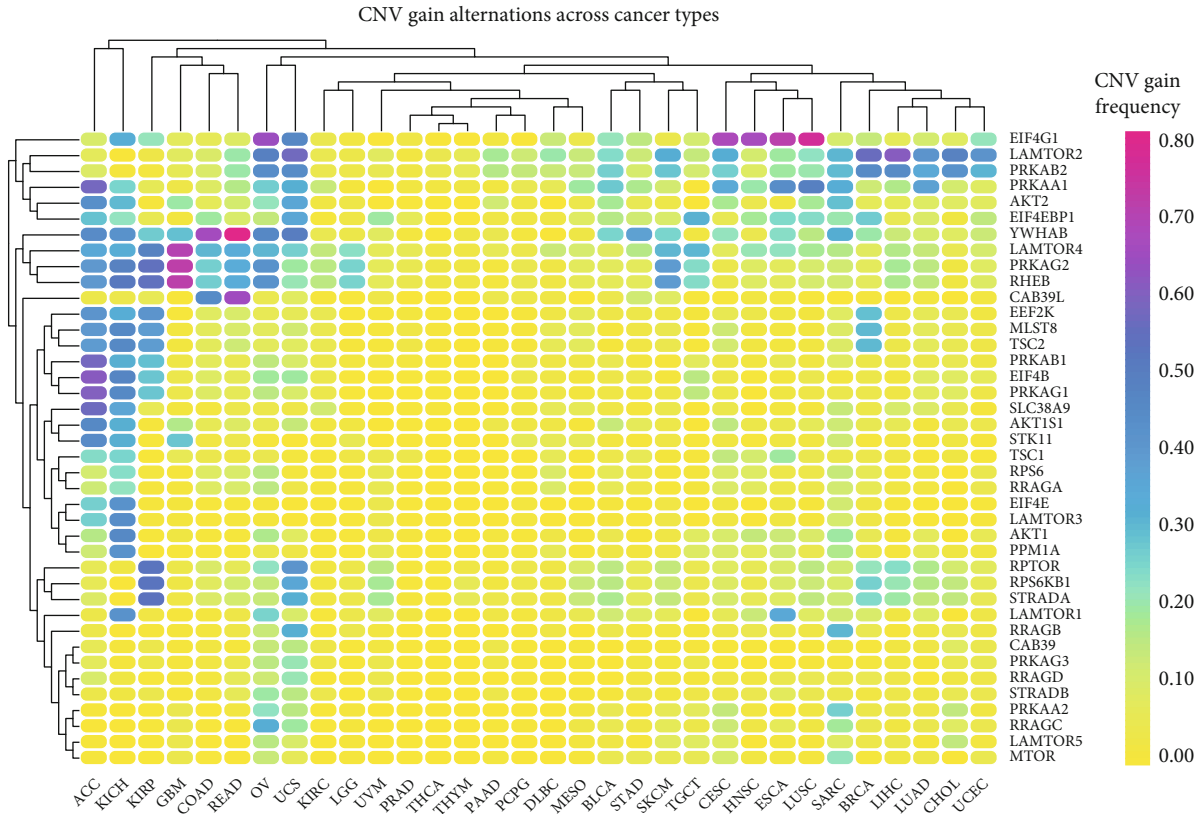
(a)
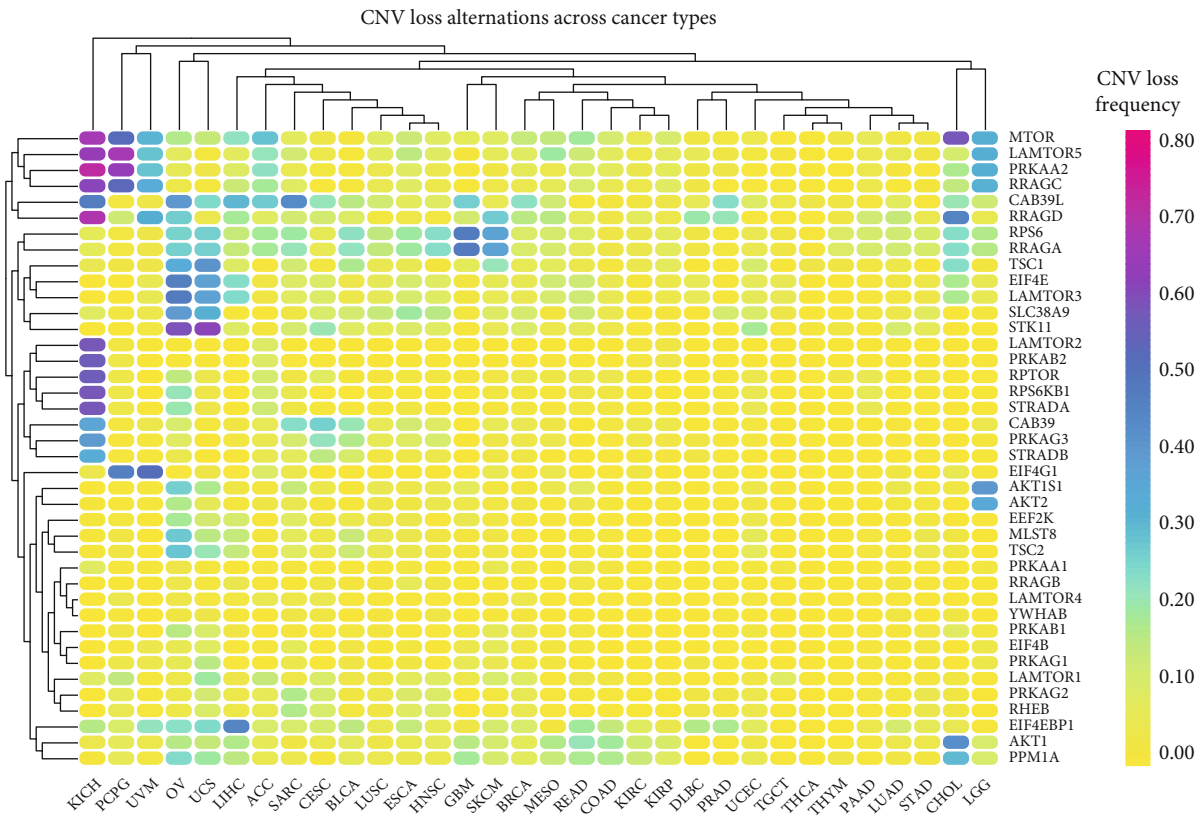
(b)
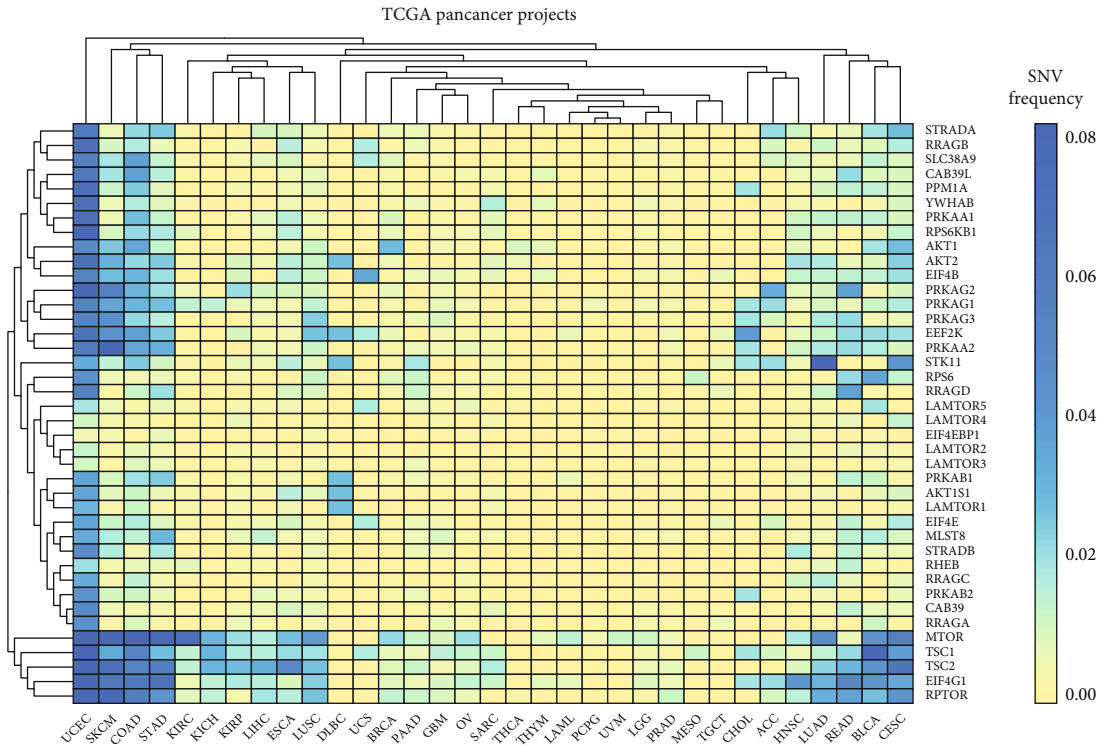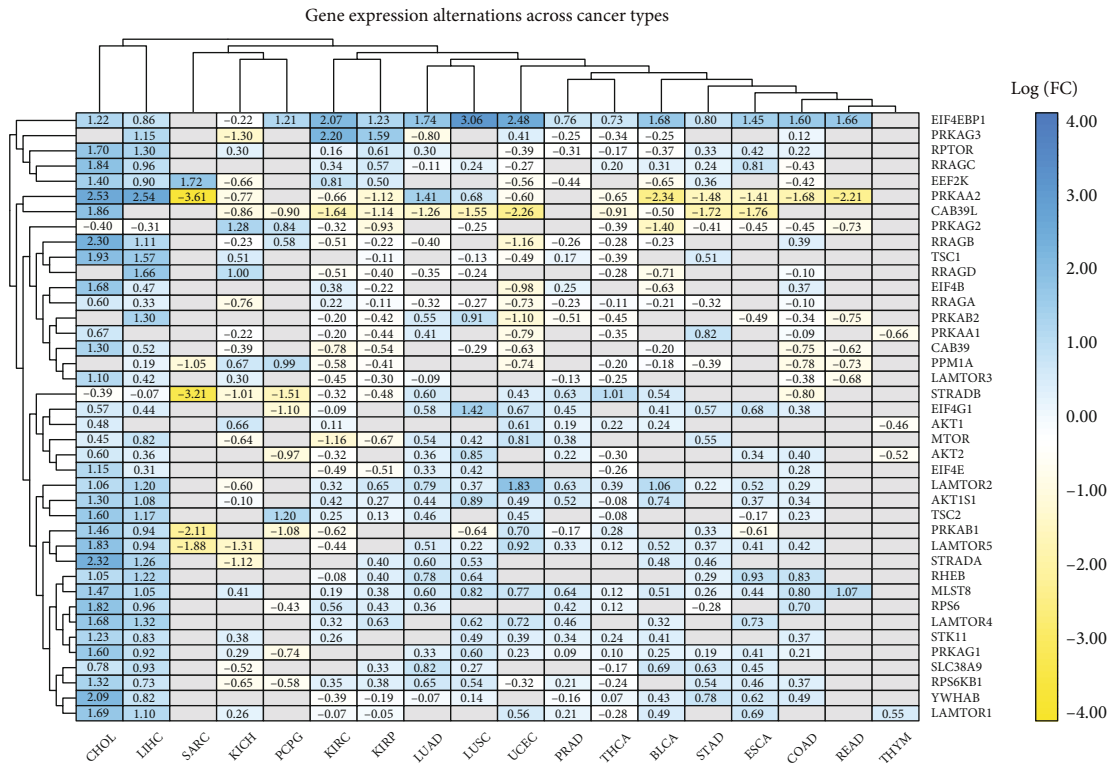
FIGURE 2: Continued.

FIGURE 2: (a, b) The CNV frequencies of the 40 mTOR pathway genes are shown for the 32 tumor types. The color code bar refers to differential gain or loss of copy numbers on the right side; purple indicates a CNV gain and yellow indicates a CNV loss. (c) The SNV frequencies of the 40 mTOR pathway genes are shown for the 32 tumor types. The color code bar refers to the degree of SNV on the right side, with blue representing a high frequency and yellow representing a low frequency. (d) There were changes in the expression of 40 mTOR pathway genes among the 32 different types of cancer. The color code bar shows the corresponding value of log2(FC) on the right side.
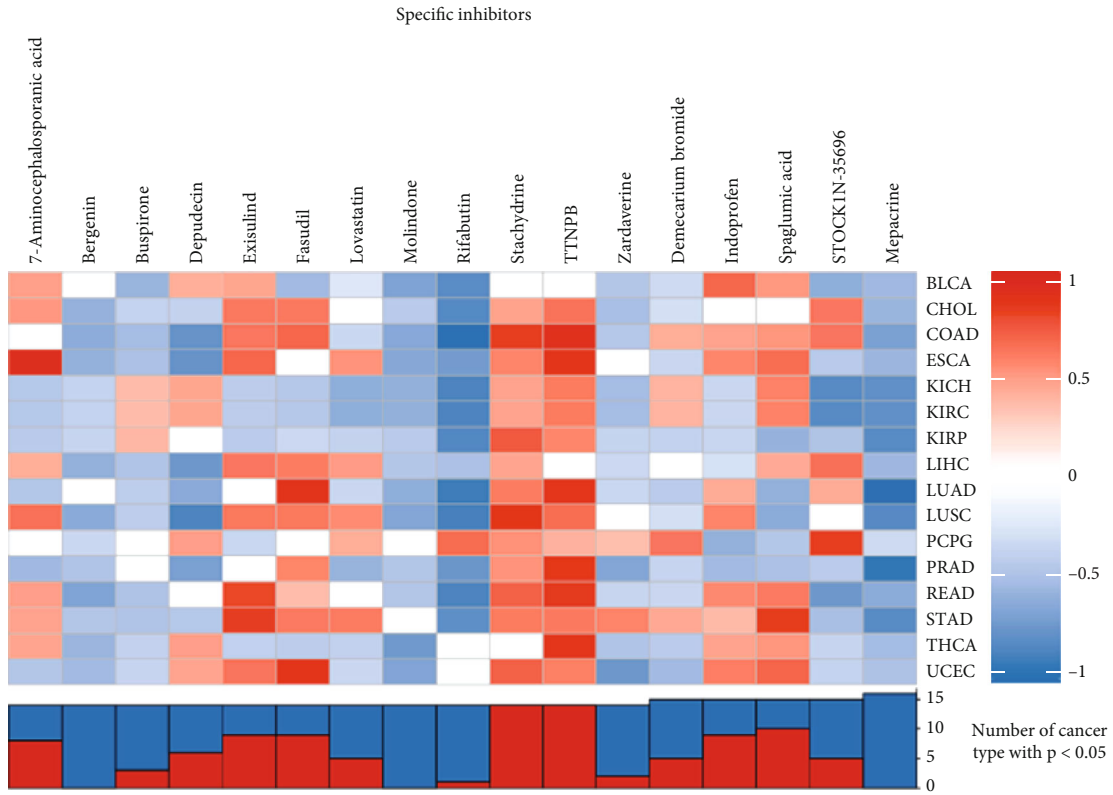
(a)
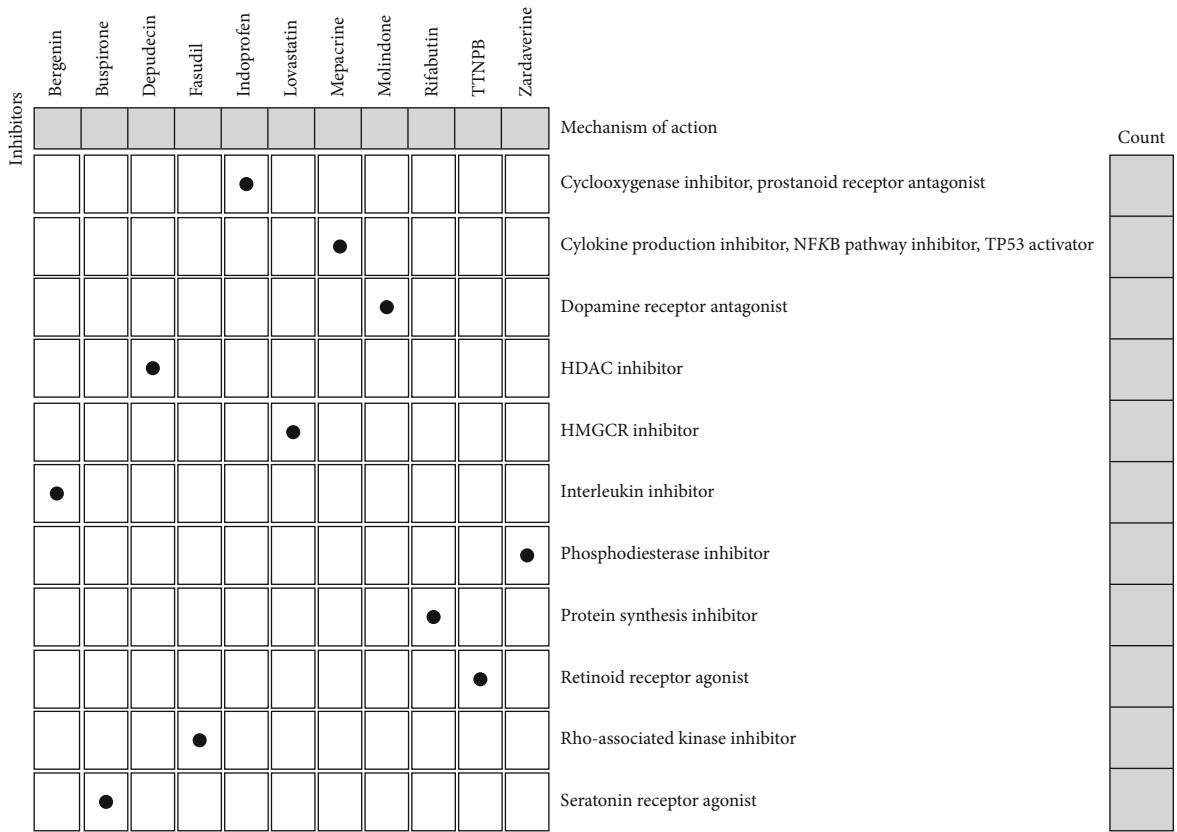
(b)

Figure 3: Continued.
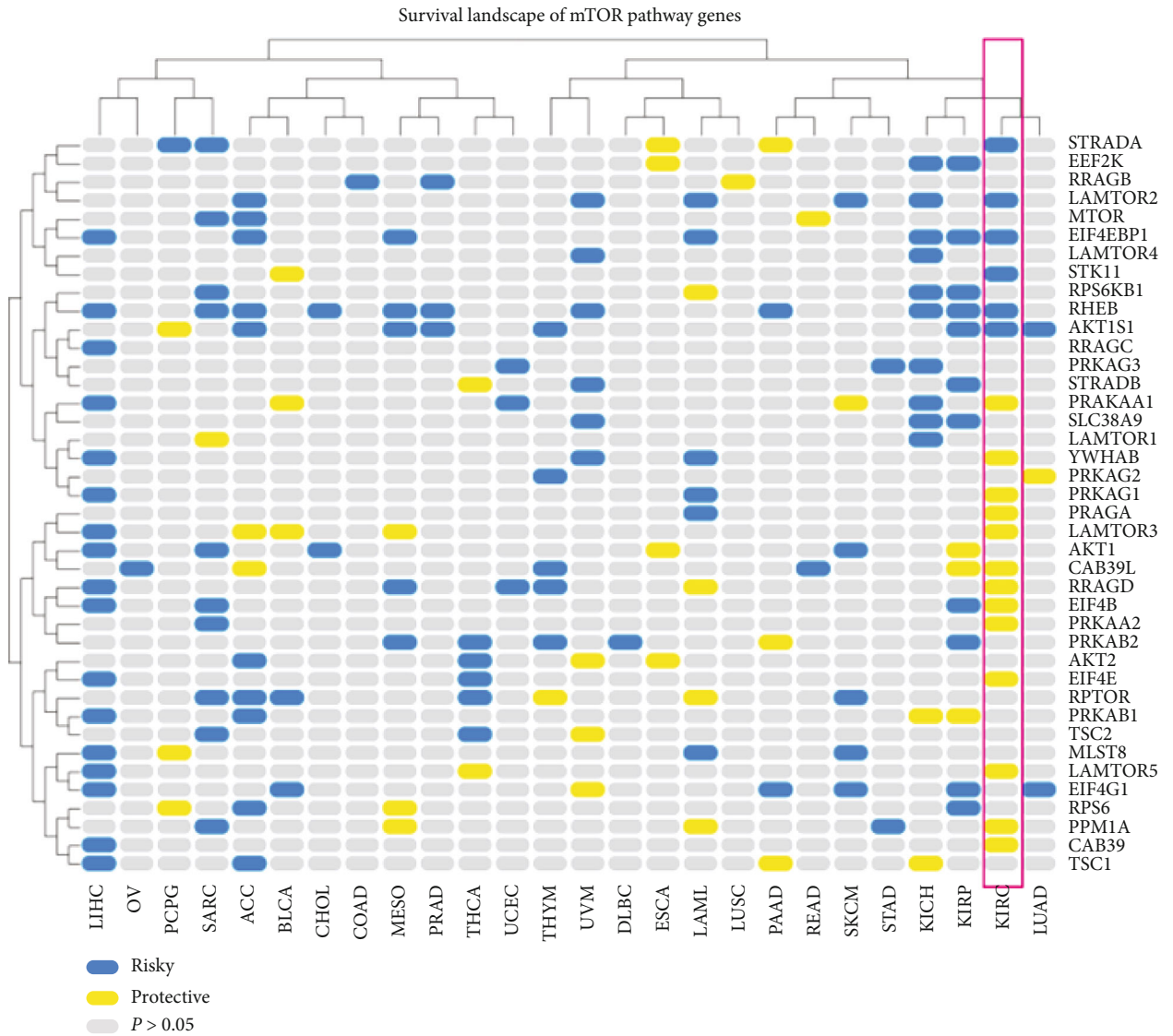
(c)

FIGURE 3: Continued.

(d)
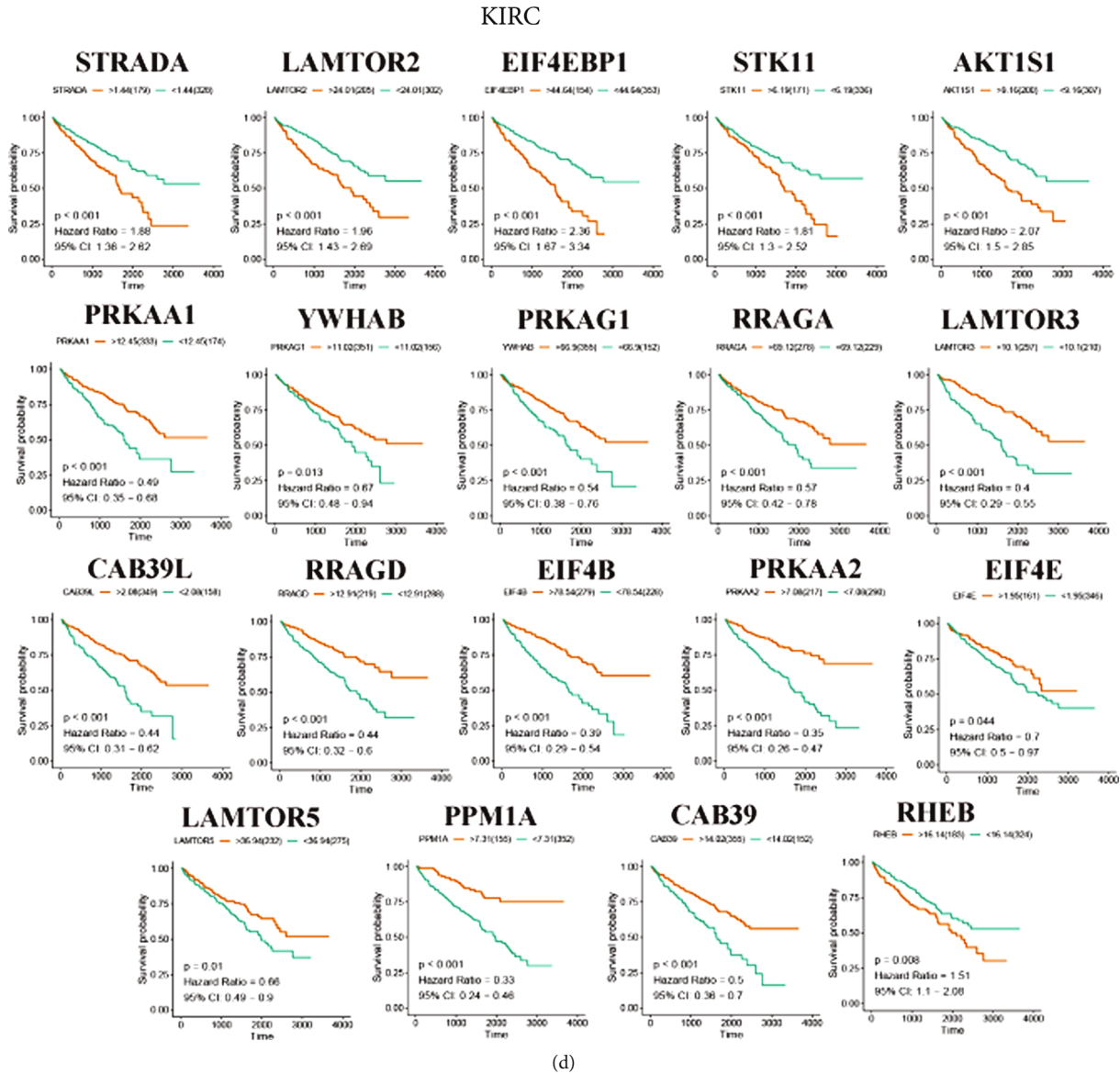
Figure 3: (a) Heat map shows each compound's enrichment score for each cancer type from the CMap. These are ordered from right to left in descending order of significant enrichment based on cancer type. The color bar refers to different enrichment scores: blue means positive and red means negative. (b) Heat map showing the mechanisms (column) shared by each compound (row) from the CMap. (c) Heat map showing the survival landscape of the mTOR pathway genes, with blue representing risky genes and yellow representing protective genes. The grey bar represents no statistical significance. (d) The survival curve of the statistically significant mTOR pathway genes in KIRC.

since the mTOR pathway itself is a cancer pathway, related genes are present as risky genes in most cancers (Figure 3(c)). However, we found an interesting result indicating that most mTOR-related genes exist as protective genes in KIRC, which contradicts previous studies' results. Therefore, we focused on the relationship between mTOR-related pathway genes and the survival rate of patients with KIRC. We plotted the Kaplan-Meier curve (K-M curve) for each of the statistically significant gene pathways based on patient survival data, according to $p < 0.05$. The results obtained are consistent with the conclusion of the survival landscape of mTOR pathway genes (Figure 3(d)). This suggests that there are still some underexplained roles of the mTOR pathway in KIRC.

3.4. Cluster Analysis Based on mTOR Scores. To explore the specific relationship between mTOR and KIRC patients, we constructed an mTOR-score model based on the mRNA expression of the 40 genes. According to the final mTOR-score results, the patient samples were divided into three clusters. cluster1: mTOR-active cluster; cluster2: normal cluster; cluster3: mTOR-inactive cluster (Figure 4(a), Table S6). We can also see the gene enrichment scores of the three clusters through the violin plot: cluster1>cluster2>cluster3 (Figure 4(b)). It is worth mentioning that the quantity of samples in cluster1 was relatively small compared to the other two groups, which will influence the subsequent experiments. After plotting the survival curves of the three clusters, we found that the mTOR-inactive cluster had the

(a)

(b)
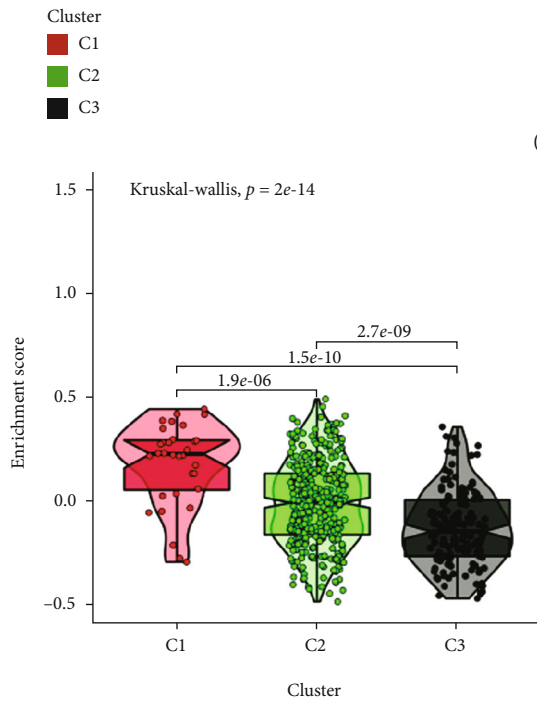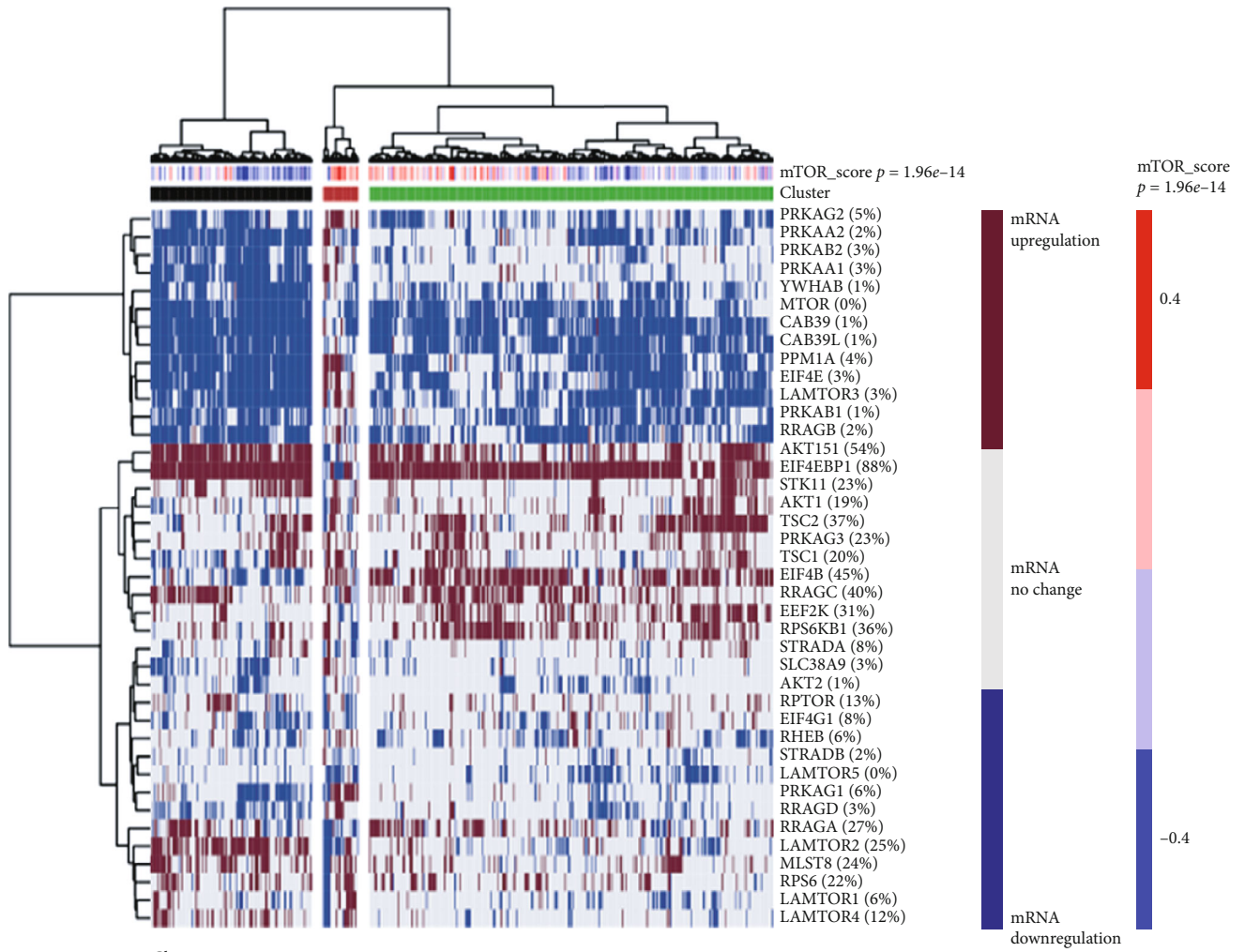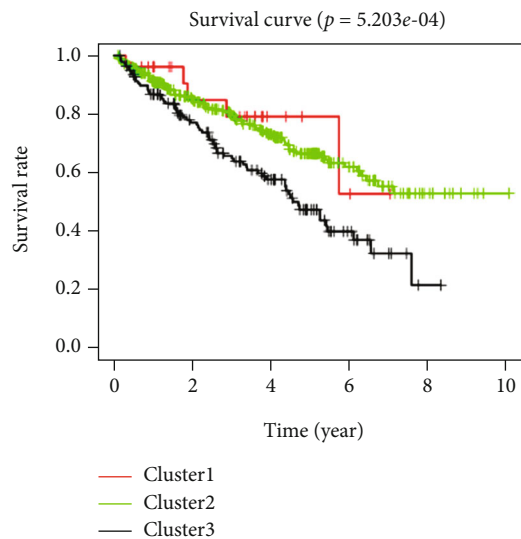
(c)

FIGURE 4: Continued.
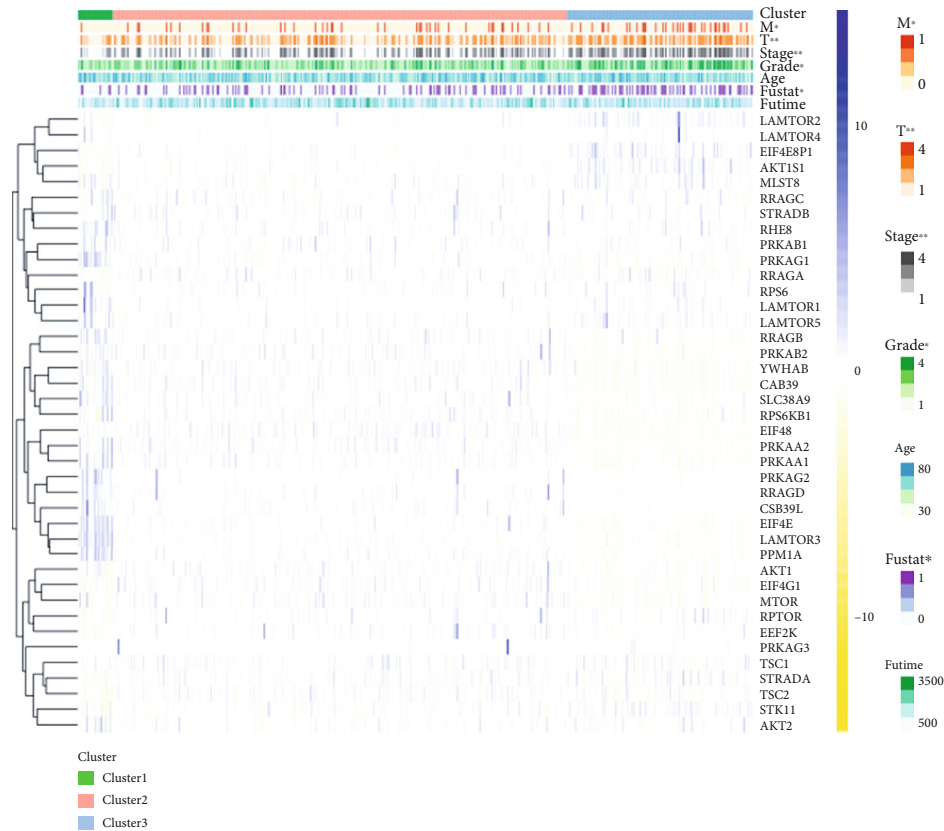
(d)

FIGURE 4: (a) Clustering of gene data from the TCGA database reveals three clusters. Upregulation of mTOR pathway genes was demonstrated in cluster1, and downregulation of mTOR pathway genes was demonstrated in cluster3. In cluster2, mTOR pathway genes were affected the least. The percentage of patients whose genes were altered is provided, showing the high frequency of changes in mTOR pathway genes. (b) The Violin plot shows the enrichment score of the three clusters. The plot shows the enrichment scores of the three clusters, from high to low, as cluster1, then cluster2, followed by cluster3. (c) The survival curves of the three clusters are shown in the plot. Survival in cluster1 is higher than that in cluster2, and survival in cluster2 is higher than that in cluster3. (d) Heat map showing the correlation between mTOR scores and the clinicopathological characteristics of KIRC patients. $^*p < 0.05$, $^{**}p < 0.01$, and $^{***}p < 0.001$.

lowest survival rate, the second cluster was the normal group, and the mTOR-active cluster had the highest survival rate (Figure 4(c)). This result supports the previously discovered abnormal phenomenon that mTOR pathway-related genes are mostly protective genes in KIRC. We then analyzed the relationship between these three clusters and the clinicopathological characteristics of KIRC patients, and the results showed that T (tumor), M (metastasis), stage, grade, and fustat, were related to the mTOR pathway (Figure 4(d)). The mTOR pathway scores were generally protective. The higher the mTOR score, the lower the grade and stage, and the better the prognosis.

3.5. The Relationship between Classic Anticancer Drugs and mTOR. To further explore the drug sensitivity between mTOR clusters, we also conducted a GDSC drug sensitivity analysis. Our research is mainly focused on drugs to treat tumors, especially drugs for targeted therapy of kidney cancer and classical drugs for tumor research, such as metformin. There have been reports that cancer can be targeted with inhibitors of the mTOR pathway [41, 42]. At present, there are many kinds of targeted anticancer drugs, but their

mechanisms of action are quite different. Pazopanib, sorafenib, and sunitinib are three drugs that are multitarget kinase inhibitors [43]. Gefitinib inhibits epidermal growth factor receptor (EGFR) [44], bosutinib is a tyrosine kinase inhibitor (TKI) [45], and axitinib inhibits the VEGF pathway [46]. Studies have also found a connection between the mTOR pathway and temsirolimus and metformin [47, 48]. Metformin, an antidiabetic drug, can also be used to prevent cancer alone and in combination with other drugs, mainly by reducing glycemia to cut-off the PI3K/MAPK pathway, which is involved in cell growth, or by activating the AMPK pathway, targeting tumor metabolism angiogenesis, cancer stem cells, and other pathways [49]. Therefore, it is necessary to explore the correlation and mechanism between these targeted drugs and the mTOR pathway.

We constructed a ridge regression model to predict the IC50 of drugs (contained in the GDSC) against cancer cells through the cell expression profile of the Genomics of Drug Sensitivity in Cancer (GDSC) database; three clusters were obtained through a cluster analysis. Using this method, we can infer the relationship between these drugs and the mTOR pathway genes (Figure 5). Considering $p < 0.05$ to indicate
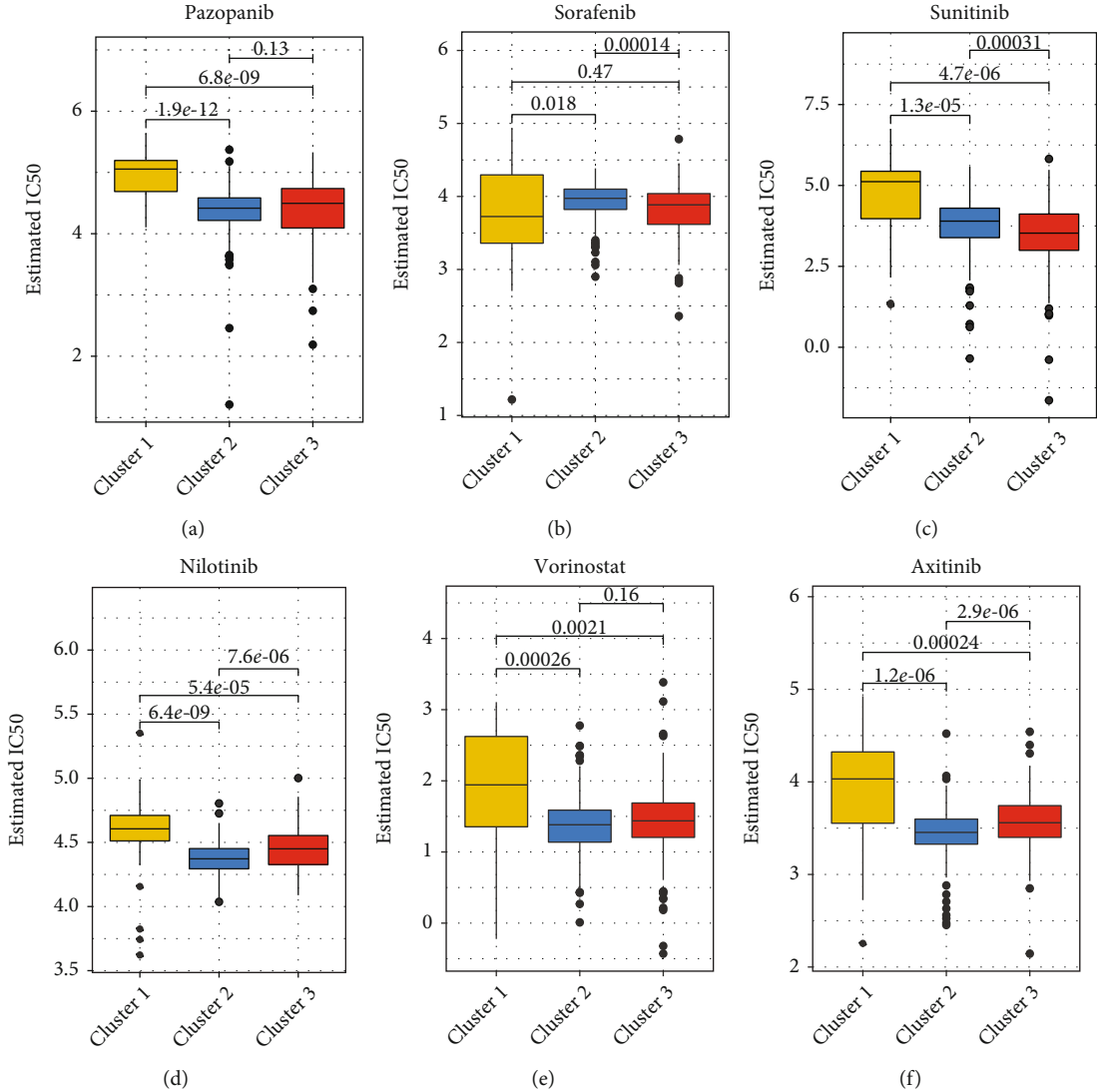
Figure 5: Continued.
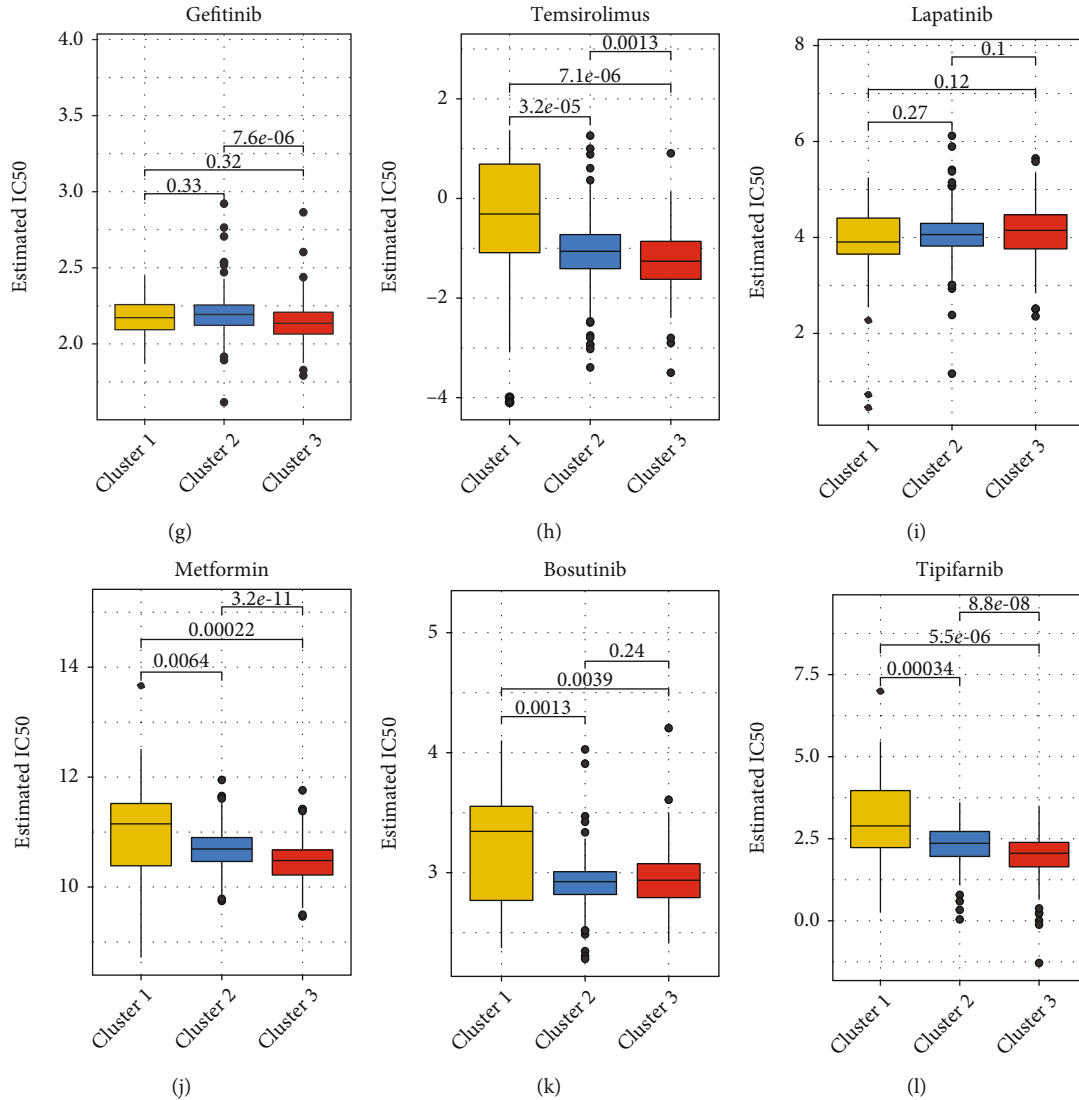
FIGURE 5: (a–l) The estimated IC50 for 12 types of common chemotherapeutic agents are shown in the plot for cluster1, cluster2, and cluster3. The 12 types of chemotherapeutic agents are pazopanib, sorafenib, sunitinib, nilotinib, vorinostat, axitinib, gefitinib, temsirolimus, lapatinib, metformin, bosutinib, and tipifarnib.

statistical significance, the cluster-wise significance for each drug was as follows: pazopanib—C1>C3; sorafenib—C2>C3; sunitinib: C1>C3; nilotinib—C1>C3>C2; vorinostat—C1>C3>C2; axitinib—C1>C3>C2; gefitinib—C2>C3; temsirolimus—C1>C2>C3; lapatinib—no significance; metformin—C1>C2>C3; bosutinib—C1>C3; tipipifarnib—C1>C2>C3. C1, C2, and C3 represent cluster1, cluster2, and cluster3. The lower the IC50, the better the drug efficacy. We can understand the therapeutic effects of the drugs in the three clusters through this analysis method to assist in the development of precise cancer treatments in the future.

3.6. The mTOR Pathway's Destruction Is Related to the Dysregulation of Several Potential Target Oncogenes and Tumor Suppressor Genes. To further explore the potential regulatory mechanism of the mTOR pathway in KIRC, we studied the relationship between various well-known oncogenes in KIRC and tumor suppressor genes in the three

mTOR pathway clusters. We found that the expression of the HRAS, MYC, and VEGFA oncogenes in the inactive group was significantly higher than that in the active group. In comparison, the expression of tumor suppressor genes VHL and PTEN in the inactive group was significantly lower than that in the active group. The above results indicate that the poor prognosis of the inactive group may be related to the abnormal expression of these genes. The expression of oncogenes BRAF, AKT1, KRASM, TOR, and PIK3CA in the active group was significantly higher than that in the inactive group.

In comparison, the expression of the tumor suppressor gene TP53 in the active group was significantly lower than that in the inactive group, indicating that the activation of the mTOR pathway may be closely related to the participation of these genes. Interestingly, we found that the expression of EGFR, MYC, CCND1, CTNNB1, and STAT3 in the normal group was significantly higher than that in the

inactive and active groups (Figure 1(a)). This special phenomenon once again illustrates that mTOR plays different roles in different stages of tumor development through the degree of activation. Proper activation of the mTOR pathway increases the expression of oncogenes, and pathway inhibition may cause downregulation of certain oncogenes' expression levels, and at the same time activate other oncogenes through the cross-talk pathway to cause tumor progression. Although the biological mechanisms of these associations may be complicated, the oncogenes mentioned above or tumor suppressor genes may be potential targets for mTOR signaling interruption in KIRC.

Recently, an increasing number of studies have found that sirtuins are involved in various biological processes related to tumorigenesis, such as changes in cancer-related metabolic pathways, uncontrolled proliferation, genome instability, and tumor microenvironment. In human cancers, sirtuins are thought to play complex roles. Depending on the type of cancer and the experimental conditions, they act as both oncogenes and tumor suppressors [50, 51]. The analysis of the transcriptomes of TCGA KIRC patients showed that there is a strong correlation between abnormal sirtuin and HDAC expression levels and the mTOR pathway. A recent study found that the ethanol extract of *Patrinia scabiosaefolia* induces the death of human renal cell carcinoma 786-O cells via SIRT1 and mTOR signaling-mediated metabolic disruptions [52]. SIRT5-mediated SDHA desuccinylation promotes clear cell renal cell carcinoma tumorigenesis [53]. In addition, the SIRT family shows a differentially expressed organization in RCC. Among the seven SIRTs, SIRT1, SIRT3, and SIRT6 can be used as tumor suppressors in KIRC [54]. In our study, the expression of SIRT2, SIRT3, SIRT6, and SIRT7 in the inactive group was significantly higher than that in the active group. In comparison, the expression of SIRT1, SIRT4, and SIRT5 in the inactive group was significantly lower than that in the active group (Figure 1(b)). In summary, these results indicate that sirtuins and mTOR signaling pathways may act synergistically to promote or inhibit multiple processes in the progression of KIRC. Histone deacetylases (HDACs) catalyze the removal of acetyl groups from lysine residues on histones and nonhistone proteins and play a vital role in regulating gene transcription [55]. Deacetylation of histone tails induces chromatin condensation and allows DNA to bind more tightly to the histone core, preventing the transcription mechanism from reaching the promoter region, thereby inhibiting transcription [56]. In this study, we found that the expression of HDAC8, HDAC9, and HDAC11 in the active group was significantly higher than that in the inactive group. In comparison, the expression of HDAC1, HDAC6, HDAC7, and HDAC10 in the active group was significantly lower than that in the inactive group (Figure 1(c)). At present, SIRT and HDAC inhibitors provide new prospects for tumor treatment, and our research results can further offer new directions for future tumor precision treatment. For example, HDAC10 was almost not expressed in the active group, but was abnormally high in the inactive group. Therefore, the use of HDAC10 inhibitors may be more beneficial to patients with inactivation of the mTOR pathway (Figure 1(c)).

3.7. mTOR Pathway Implication in Immune Cell Infiltration and in Immune Checkpoints Targeting Cancer Therapy. The tumor microenvironment (TME) is a mixture of fluid, stromal cells, immune cells, extracellular matrix molecules, and various cytokines and chemokines. The cells and molecules in the TME are dynamic in promoting tumor immune escape, tumor growth, and metastasis [57, 58]. As a major regulator of metabolism, mTOR signaling controls immune cell biology in a cell type-specific manner. In addition, mTOR activity needs to be adjusted to maintain proper immune function [59]. To further study the relationship between the mTOR pathway in KIRC and patient immunity, we first performed a correlation analysis between the mTOR pathway and immune cell infiltration. We found that many genes related to the mTOR signaling pathway are associated with the infiltration of multiple immune cells, especially RRAGC, LAmTOR2, EIF4EBP1, PRKAB1, PRKAB2, and other genes, among which RRAGC, LAmTOR2, and EIF4EBP1 were positively correlated with immune cell infiltration.

In contrast, PRKAB1 and PRKAB2 were negatively correlated with immune cell infiltration (Figure 1(d)). We further used the "ggstatsplot package" in R to analyze the relationship between the mTOR pathway score and immune cell infiltration. The results showed that the mTOR score was negatively correlated with various immune cell infiltrations, such as T cell costimulation, parainflammation, Tfh, TIL, and inflammation promotion (Figures 1(e)–1(j)). Immune checkpoint blocking antibodies, including anti-CTLA-4 and anti-PD-1, can induce tumor responses in a variety of tumor types, including melanoma, non-small-cell lung cancer (NSCLC), and kidney renal clear cell carcinoma (KIRC) [60]. In addition, the therapeutic effect of immune checkpoints may be related to the expression of CTLA-4 and PD-1. In the correlation analysis, we found that the mTOR pathway score is negatively correlated with CTLA-4 and PD-1 (Figure 1(k)), so it is potentially inferred that patients with mTOR pathway inactivation may have higher expression of CTLA-4 and PD-1 than patients with mTOR pathway activation. In addition to the TIDE prediction, we also used subclass mapping to compare the expression profiles of the two subtypes (cluster1+cluster2 and cluster3) that responded to immunotherapies [23]. We were delighted to see that the mTOR-inactive cluster was more responsive to anti-PD-1 therapy (Figure 1(l)). Unfortunately, following a Bonferroni correction of the results, the difference between the two groups was not statistically significant (Figure 1(l)).

3.8. LASSO Regression to Establish the Prediction Model. We found that 36 of 40 mTOR pathway genes were differentially expressed by analyzing gene expression in 72 normal tissue samples and 539 KIRC cancer tissues (Figure 6(a), Table S7). We performed a hazard ratio analysis to show the relationship between these gene pathways and the progression of KIRC (Figure 6(b), Table S5). A coexpression analysis was used to analyze the relationship between gene pathways, and the results showed that there were coexpression relationships among these genes (Figure 6(c)). To explore the possibility of using the mTOR pathway genes to build a model to predict KIRC patient

(a)

	p value	Hazard ratio
PRKAB1	0.057	0.975 (0.951-1.001)
YWHAB	0.004	0.987 (0.979-0.996)
CAB39	0.010	0.959 (0.929-0.990)
STK11	0.013	1.133 (1.027-1.250)
STRADA	< 0.001	1.745 (1.375-2.215)
EIF4E	0.015	0.686 (0.506-0.929)
PRKAG2	0.127	0.964 (0.920-1.010)
RPTOR	0.184	1.056 (0.975-1.143)
AKT1S1	< 0.001	1.105 (1.053-1.159)
PRKAA2	< 0.001	0.848 (0.805-0.893)
PRKAG3	0.913	1.083 (0.259-4.524)
LAMTOR1	0.458	0.994 (0.979-1.010)
STRADB	0.104	1.024 (0.995-1.054)
MLST8	0.139	1.036 (0.989-1.085)
EIF4G1	0.821	1.002 (0.988-1.016)
RPS6	0.379	1.000 (0.999-1.000)
TSC1	0.293	0.963 (0.899-1.033)
EEF2K	0.228	0.951 (0.877-1.032)
LAMTOR3	< 0.001	0.848 (0.800-0.900)
RRAGB	0.888	1.006 (0.923-1.097)
PPM1A	< 0.001	0.842 (0.782-0.906)
LAMTOR5	0.044	0.987 (0.974-1.000)
EIF4EBP1	< 0.001	1.003 (1.001-1.005)
PRKAB2	0.097	0.941 (0.875-1.011)
SLC38A9	0.991	0.998 (0.699-1.424)
AKT2	0.065	1.080 (0.995-1.173)
MTOR	0.071	0.894 (0.792-1.010)
PRKAG1	0.012	0.928 (0.875-0.984)
AKT1	0.734	0.989 (0.927-1.055)
RHEB	0.001	1.028 (1.011-1.046)
LAMTOR2	0.001	1.012 (1.005-1.019)
PRKAA1	< 0.001	0.937 (0.905-0.970)
RPS6KB1	0.338	1.065 (0.936-1.212)
LAMTOR4	0.822	0.999 (0.994-1.005)
RRAGA	0.008	0.990 (0.982-0.997)
RRAGD	0.006	0.971 (0.952-0.992)
CAB39L	< 0.001	0.756 (0.653-0.875)
RRAGC	0.384	0.955 (0.861-1.059)
EIF4B	< 0.001	0.989 (0.984-0.994)
TSC2	0.160	1.061 (0.977-1.152)

Hazard ratio

(b)

Figure 6: Continued.

(c)

FIGURE 6: Continued.

(d)

(e)

(f)

(g)

(h)

(i)
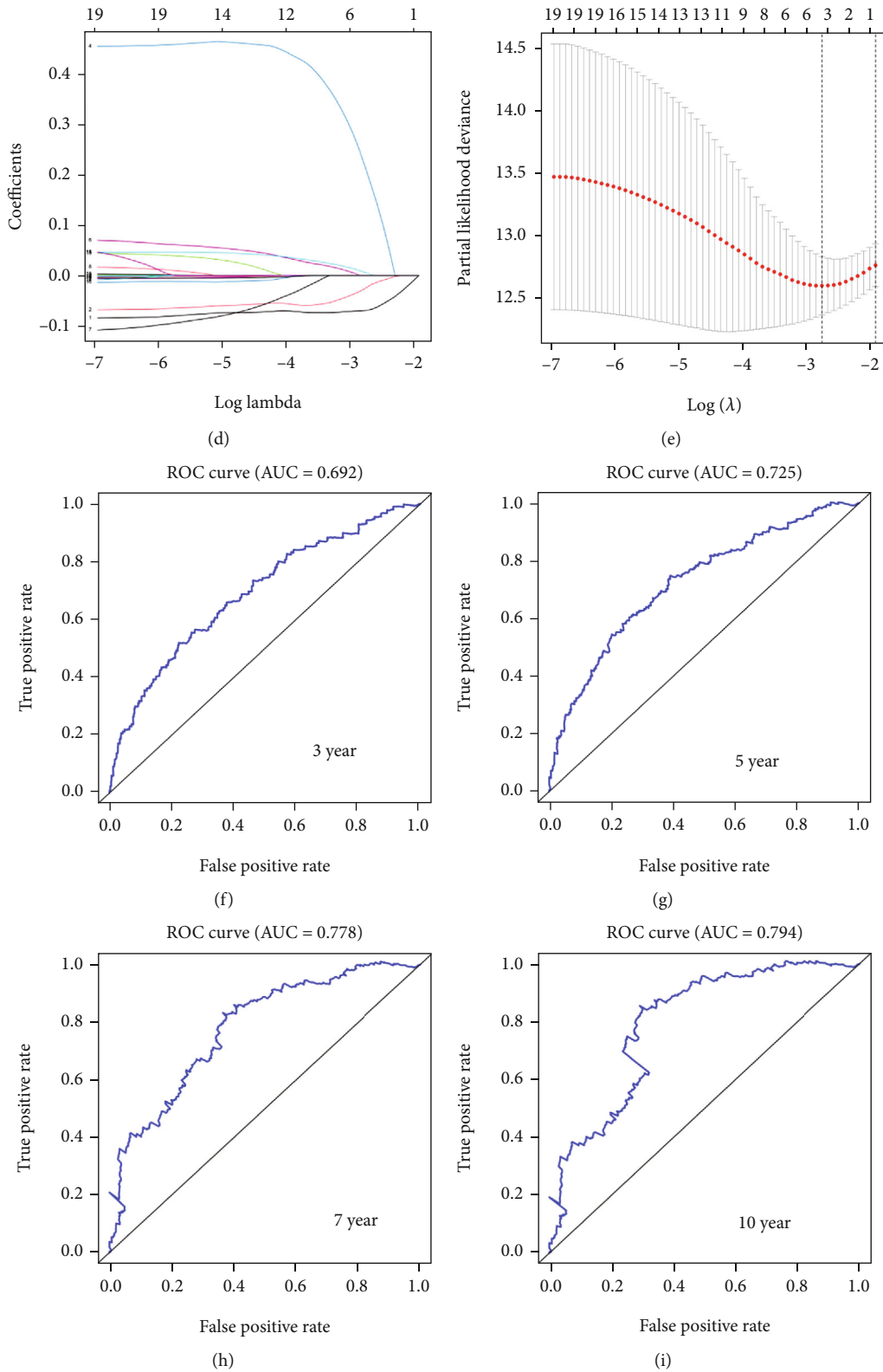
FIGURE 6: Continued.
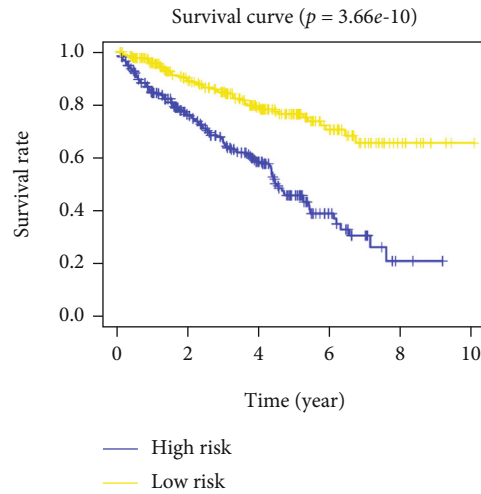
(j)
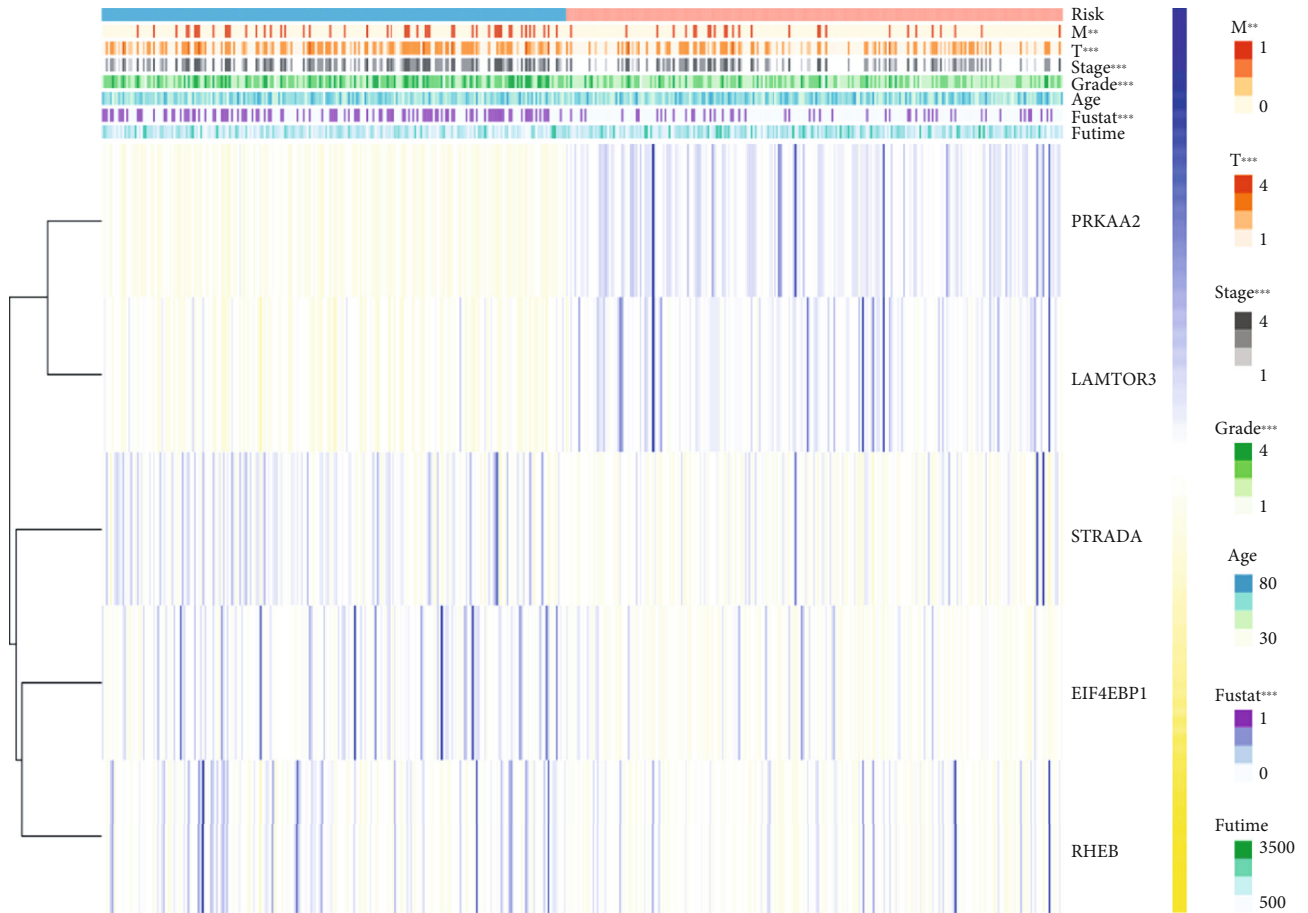
(k)

FIGURE 6: (a) The expression of 40 mTOR pathway genes in KIRC patients. In the color bar on the right side, blue represents upregulation and yellow represents downregulation. N (green) is the normal sample, T (red) is the tumor sample. $^*p < 0.05$, $^{**}p < 0.01$, $^{***}p < 0.001$. (b) The plot shows the hazard ratio (HR) analysis with 95% confidence intervals (CI) and p values for the mTOR pathway genes. (c) The plot shows the result of the coexpression analysis of 40 mTOR pathway genes. Many of them were correlated in KIRC tissues. (d) The LASSO coefficient profiles of mTOR pathway genes in KIRC. (e) Five genes were selected by LASSO Cox regression analysis. (j) The survival curve was obtained based on this model. Blue and yellow correspond, respectively, to the high-risk group and the low-risk group. (f–i) ROC curves of 3, 5, 7, and 10 years; the AUCs of the curves are 0.692, 0.725, 0.778, and 0.794, respectively. (k) The correlation of five selected genes and the clinicopathological characteristics in two groups. The color bar shows the expression of the genes. Blue represents upregulation, and yellow represents downregulation. $^*p < 0.05$, $^{**}p < 0.01$, $^{***}p < 0.001$.

(a)

(b)

Figure 7: Continued.

(c)

(d)

(e)
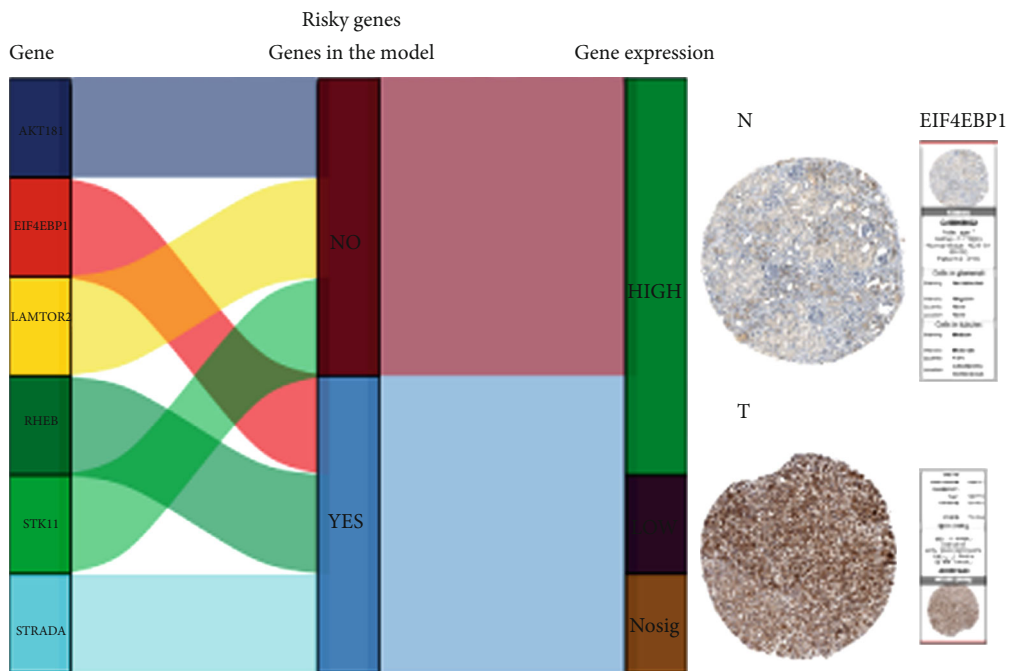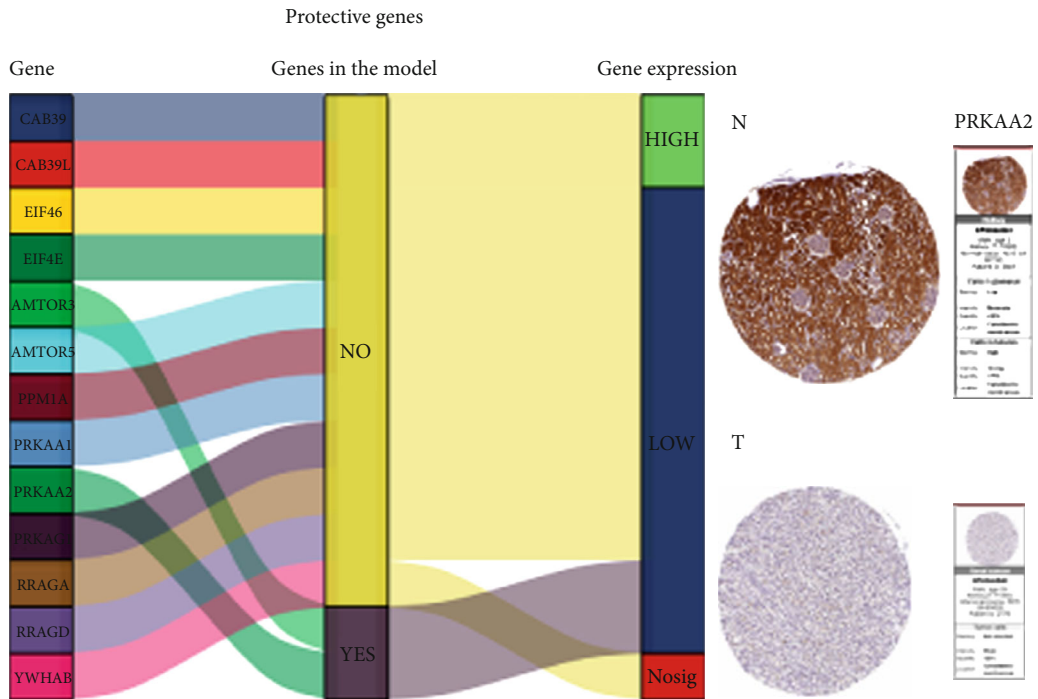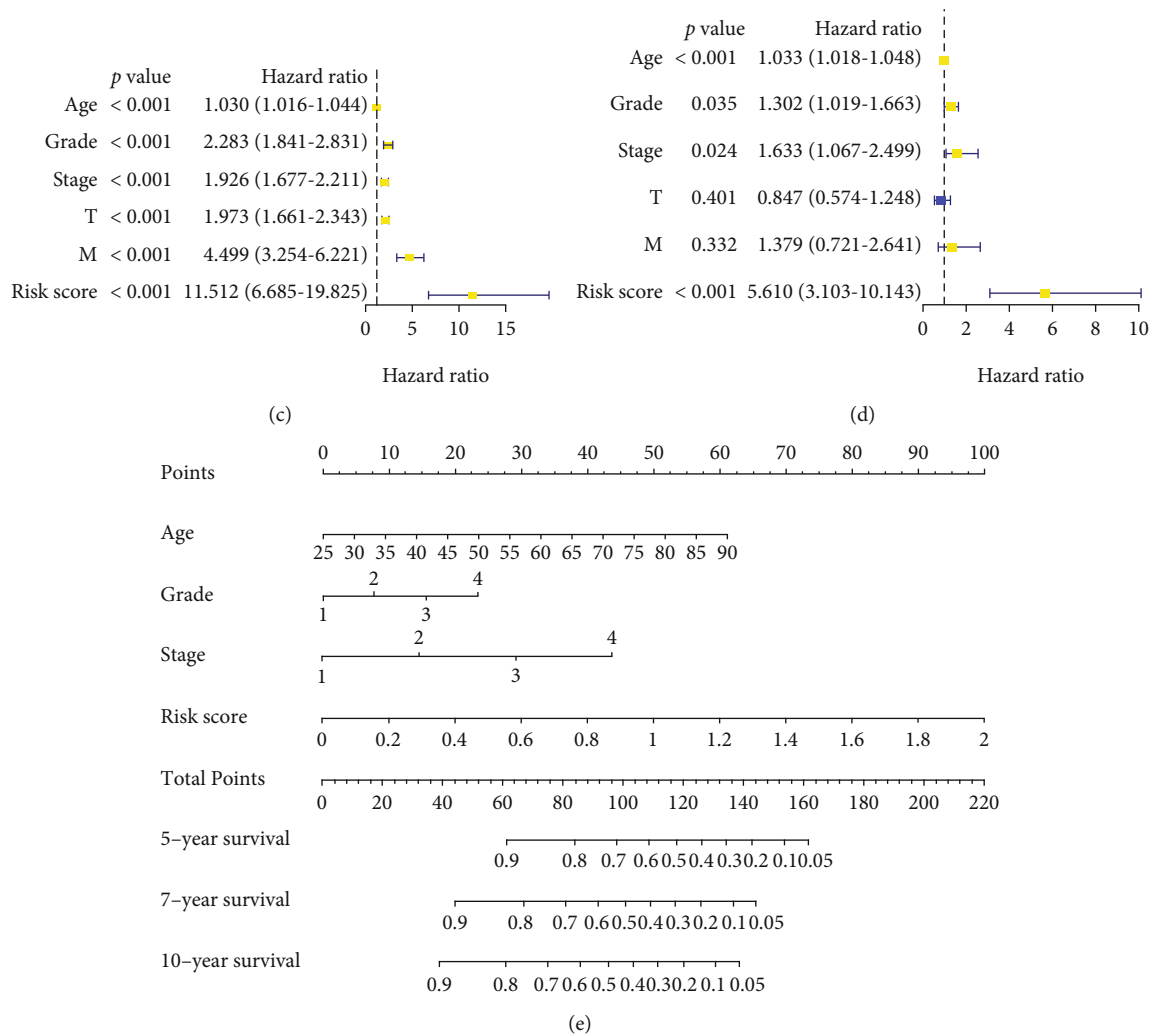
FIGURE 7: (a, b) Sankey diagrams were plotted for two types of genes, risky and protective. Immunohistochemical images were obtained from the HPA website for PRKAA2 and EIF4EBP1, which are representative of the two gene groups. (c) Univariate Cox analysis. (d) Multivariate Cox analysis. (e) Nomogram of the model.

prognosis, we conducted a LASSO regression analysis (Figures 6(d) and 6(e)) to establish the model. We selected five genes as risk factors: PRKAA2, AmTOR3, STRADA, EIF4EBP1, and RHEB. We used this model to divide the sample into two groups: high-risk and low-risk groups based on the best cut-off values of the risk scores. We plotted the survival curves of the two groups, which showed that the low-risk group predicted better survival than the high-risk group (Figure 6(j)). A receiver operating characteristic (ROC) curve analysis was then performed to analyze the predictive prognostic performance of the new survival model in KIRC patients. The 3-year survival had an area under the curve (AUC) of 0.692; 5-year survival, AUC = 0.725; 7-year survival, AUC = 0.778; and 10-year survival, AUC = 0.794 (Figures 6(f)–6(i)). Generally, an AUC value greater than 0.7 is considered predictive. We then used heat maps to demonstrate the correlation between the model and the pathological features of renal cell carcinoma. The results show that M, T, stage, grade, and fustat were related to the model we established (Figure 6(k)).

3.9. Validation of the Model and Representation Using a Nomogram. We selected genes that were statistically significant in the previous HR analyses. They were divided into two groups according to risky genes and protective genes. After the mulberry diagram was drawn to classify them, we found that both AmTOR3 and PRKAA2, which are protective genes, were in the model and showed low expression levels in KIRC tissues, while EIF4EBP1, a risky gene, was highly expressed in KIRC tissues. In addition, we obtained the immunohistochemical information of PRKAA2 and EIF4EBP1 from the human protein atlas (HPA) website [61] and verified the results of their gene expression at the protein level (Figures 7(a) and 7(b)). In addition, the results of immunohistochemistry experiments on the two molecules PRKAA2 and EIF4EBP1 on our KIRC clinical specimens are also consistent with the above results, and the corresponding results are shown in Supplementary Materials Figure S1. We then performed univariate and multivariate Cox regression analyses and found that the risk model was a risk factor in both regression analyses and was prominent in the

multivariate Cox regression model (Table S8 and Table S9) (Figures 7(c) and 7(d)). Finally, we used a nomogram to predict the risk and prognosis of patients with KIRC. The nomogram generated a total of nine rows (Figure 7(e)). The second to the ninth rows were age, grade, stage, risk score, total points, 5-year survival, 7-year survival, and 10-year survival. From the second to the fifth lines, the patient scores were found and added together to obtain the total scores, corresponding to 5-, 7-, and 10-year survival.

4. Discussion

Rapamycin was first identified by Sehgel in 1964 [62], and its two important target genes TOR1 and TOR2 were identified in 1991 [63]. The mTOR protein was identified three years later as a direct target of the rapamycin complex [64]. In recent years, the mechanism of the mTOR pathway in the human body has been gradually explored. It regulates various cellular processes, including protein synthesis, growth, metabolism, senescence, regeneration, and autophagy. At present, the mTOR gene has been found to play a role in a variety of diseases [65], such as neurological diseases [66–70], tumors [39, 71–74], and diabetes [75, 76].

mTOR contains two complexes, mTORC1 and mTORC2. mTORC1 promotes protein synthesis by phosphorylation of two key effectors, S6K1 and 4EBP, and inhibits protein decomposition by blocking AMPK activation of ULK1, thereby controlling cell growth and division. The most important role of mTORC2 may be to activate AKT to promote cell survival [39]. Both play important roles in the occurrence and development of cancer. mTORC1 regulates mutations in many oncogenic pathways, such as the PI3K/AKT pathway and the Ras/Raf/Mek/Erk (MAPK) pathway. Simultaneously, mTORC2 also affects cancer by activating AKT, which promotes proliferation and suppresses apoptosis [15]. Drugs targeting mTOR have been developed based on the above mechanism. First-generation rapamycin and rapalog mainly downregulate the activation of mTORC1 to S6K1 by inhibiting mTORC1 to reduce the growth and proliferation of cancer cells. However, mTORC1 achieves a carcinogenic effect by inhibiting 4EBP, so the effects from rapalogs are not ideal. Following this, second-generation mTOR kinase inhibitors that simultaneously act on mTORC1 and mTORC2 have also been developed. These can compete with mTOR catalytic sites for ATP and selectively inhibit mTORC1 and mTORC2 [16, 39]. At present, there have been third-generation mTOR inhibitors targeting more mTOR molecule binding sites, aiming at reducing tumor resistance through stronger binding with mTOR molecules [77].

In cancer, the mechanism of the mTOR pathway is more complicated. The conclusions are as follows: (1) The upstream signaling pathway overactivates the mTOR pathway [78]. (2) The expression of the mTOR gene is modified or regulated by miRNAs [79]. (3) The mTOR pathway gene regulates the human immune system and causes the immune escape of tumor cells [80, 81]. Based on the current research results, we first chose to study the expression level of mTOR pathway genes in cancer and their differential expression

levels. We then focused on some potential compounds that may target the mTOR pathway, laying a foundation for future studies. We then compared the mTOR pathway genes in normal and cancer tissues to determine whether they exist as risky or protective genes. In our results, we found an interesting phenomenon: compared with other cancer types, the mTOR pathway gene in KIRC mostly exists as a protective gene, which is inconsistent with previous research results that mTOR pathway overexpression can lead to the occurrence of cancer. Therefore, we turned our attention to KIRC.

KIRC samples were divided into three clusters according to their mTOR scores, which were based on their mRNA expression levels. The three clusters represented three different gene expression states in the mTOR pathway for the convenience of subsequent experiments. After plotting the survival curves for the three clusters, we found that the mTOR pathway gene expresses inactive clustering survival rates, confirming our previous findings that mTOR is protective in KIRC. In fact, we also found relevant research reports pertaining to this abnormal mTOR action. Zhong et al. reported in the literature in October 2020 that mTOR pathway-related genes were enriched in their low-risk group of KIRC samples [82]. However, the reason for this phenomenon remains unclear. Based on the mechanism of mTOR and previous studies on the mechanism of mTOR in KIRC [83], we found that the activation of the mTOR pathway in KIRC is still the cause of cancer development; however, our results contradict the conclusion that mutations in the mTOR pathway promote cancer progression. We studied the mTOR pathway gene survival landscape in patients with KIRC and found that more than half of the statistically significant mTOR pathway genes have a protective effect in KIRC.

There is a well-established system for targeted therapies for KIRCs. The efficacy of targeted mTOR pathway therapies for cancer is currently well established. The first of the aforementioned three generations of mTOR inhibitors, everolimus, is still widely used in the treatment of patients with advanced renal cell carcinoma after the failure of sunitinib or sorafenib. Therefore, we used CMap to look for potential drugs to treat KIRC and performed a GDSC analysis to confirm the effects of some of the most common targeted mTOR pathway gene drugs in KIRC therapy. We hope that these analyses will help in the clinical treatment of KIRC. The results showed that most targeted drug therapies for KIRC are related to the impact of mTOR pathway gene expression levels. These results could provide new insights into the development of targeted drugs to treat KIRC in the future, especially those that target the mTOR pathway.

Currently, research on immunotherapy for cancer is very popular. The treatment of histone acetylation [84, 85] and the enhancement of T cell-killing effects are relatively accepted concrete means. By observing the expression of some classical protooncogenes, tumor suppressor genes (KRAS, VHL, and so on), and immune-related genes, especially histone acetylation, in the three clusters, we found the effects of these genes in the mTOR pathway, and most of the genes were positively or negatively correlated with the mTOR pathway. However, the expression of some genes in cluster1 (mTOR active) and cluster3 (mTOR inactive) was

consistent and contrary to that in cluster2 (normal). Among them, we found an interesting phenomenon: for example, mTOR pathway upregulation or downregulation were both related to low expression levels of MYC and EGFR. Meanwhile, HDAC8 exhibited the opposite: mTOR pathway upregulation or downregulation were both related to its high expression. For this nonlinear relationship, we speculate that there are still undiscovered intermediate pathways between the expression of the mTOR pathway and the expression of such genes, which need to be further elucidated.

We observed a correlation between many immune-infiltration-related factors and mTOR pathway genes. The results showed that almost all immune-infiltration-related factors were negatively correlated with mTOR. This indicates that the activation of the mTOR pathway suppresses immune infiltration of the body. Therefore, from the perspective of immunity, the mTOR pathway is still a cancer pathway, which cannot support the previous conclusions obtained by studying the mTOR-score-related survival curve in KIRC. These results indicate that the mechanism of the mTOR pathway is not fully understood.

Immunotherapy for T cells has been the main treatment method for KIRC, with PD-1 and CTLA-4 as the research focus [25]. Inhibition of PD-1 and CTLA-4 increases T cell killing. In our study of three mTOR-score clusters' responsiveness to PD-1 and CTLA-4 inhibitor targets, we combined cluster1 and cluster2 as mTOR-active clusters because of the small size of cluster1, and we defined cluster3 as an mTOR-inactive cluster. We were delighted to see that the mTOR-inactive cluster was more likely to be responsive to anti-PD-1 therapy. Unfortunately, following a Bonferroni correction, the results were not statistically significant.

We then analyzed the differential expression of these 40 mTOR pathway genes in cancer and normal tissues and performed an HR analysis and coexpression analysis of these genes. Subsequently, five genes in the mTOR pathway genes were screened using a LASSO regression to construct a model to predict the survival rate of KIRC patients. We hope that this prediction model will provide some help for future clinical studies.

Abbreviations

mTOR:	Mammalian target of rapamycin
KIRC:	Kidney renal clear cell carcinoma
RCC:	Renal cell carcinoma
THCA:	Thyroid carcinoma
THYM:	Thymoma
PRAD:	Prostate adenocarcinoma
UCEC:	Uterine corpus endometrial carcinoma
SKCM:	Skin cutaneous melanoma
COAD:	Colon adenocarcinoma
TCGA:	The Cancer Genome Atlas
GDSC:	Genomics of Drug Sensitivity in Cancer
HPA:	The Human Protein Atlas
LASSO:	Least absolute shrinkage and selection operator
GSEA:	Gene set enrichment analysis
CMap:	Connectivity map
CNV:	Copy number variation
SNV:	Single-nucleotide variation
WNT-β-catenin:	Wingless/integrated-β-catenin
TP53:	Tumor protein 53
VEGF:	Vascular endothelial growth factor
CAB39L:	Calcium-binding protein 39-like
PRKAA2:	AMPK alpha 2 subunit alpha 2
PRKAB1:	AMPK alpha 2 subunit beta 1
PRKAB2:	AMPK alpha 2 subunit beta 2
TME:	The tumor microenvironment
LAmTOR2:	Late endosomal and lysosomal adaptor and MAPK (mitogen-activated protein kinase) and mTOR (mechanistic target of rapamycin) activator complex
EIF4EBP1:	4E binding protein 1
CTLA-4:	Cytotoxic T-lymphocyte-associated protein 4
PD-1:	Programmed cell death protein 1
HMGCR:	Recombinant 3-hydroxy-3-methylglutaryl coenzyme a reductase
TTNPB:	4-[(1E)-2-(5,5,8,8-Tetramethyl-5,6,7,8-tetrahydro-2-naphthalenyl)-1-propen-1-yl] benzoic acid
HRAS:	HRas protooncogene
MYC:	Myelocytomatosis oncogene
VEGFA:	Vascular endothelial growth factor A
VHL:	Von Hippel-Lindau
PTEN:	Phosphatase and tensin homolog
BRAF:	Mutant serine/threonine protein kinase B-Raf
KRASM:	KRAS-mutant
TOR:	Target of rapamycin
EGFR:	Epidermal growth factor receptor
CCND1:	CyclinD1
CTNNB1:	Catenin beta1
STAT3:	Signal transducer and activator of transcription 3
HDAC:	Zinc-dependent histone deacetylases
SIRT:	Sirtuins
SDHA:	Succinate dehydrogenase subunit A.

Data Availability

The data used to support the findings of this study are available from the corresponding authors upon request.

Disclosure

Xiangyu Che, Xiaochen Qi, and Yingkun Xu are co-first authors.

Conflicts of Interest

The authors declare that they have no conflicts of interest.

Authors' Contributions

Guangzhen Wu and Qifei Wang designed the research methods, performed the experiments, and analyzed the data.

Xiangyu Che, Xiaochen Qi, and Yingkun Xu participated in data collection. Xiaochen Qi and Yingkun Xu drafted and revised the manuscript. All authors approved the version of the manuscript to be released and agreed to be responsible for all aspects of the work. Xiangyu Che, Xiaochen Qi, and Yingkun Xu contributed equally to this study.

Acknowledgments

Supplementary Materials

Figure S1: the results of immunohistochemistry experiments on the two molecules PRKAA2 and EIF4EBP1; Table S1: CNV deletion frequency of mTOR pathway genes across 33 cancer types; Table S2: CNV amplification frequency of mTOR pathway genes across 33 cancer types; Table S3: SNV frequency of mTOR pathway genes in 33 cancer types; Table S4: logFCs of mTOR pathway genes across cancer types; Table S5: HRs of mTOR pathway genes across cancer types; Table S6: cluster and mTOR_score information; Table S7: expression of mTOR gene in KIRC; Table S8: uniCox analysis in KIRC; Table S9: multi-Cox analysis in KIRC. (*Supplementary Materials*)

References

[1] J. Ferlay, I. Soerjomataram, R. Dikshit et al., "Cancer incidence and mortality worldwide: sources, methods and major patterns in GLOBOCAN 2012," *International Journal of Cancer*, vol. 136, no. 5, pp. E359–E386, 2015.

[2] H. T. Cohen and F. J. McGovern, "Renal-cell carcinoma," *The New England Journal of Medicine*, vol. 353, no. 23, pp. 2477–2490, 2005.

[3] J. S. Lam, J. T. Leppert, A. S. Belldegrun, and R. A. Figlin, "Novel approaches in the therapy of metastatic renal cell carcinoma," *World Journal of Urology*, vol. 23, no. 3, pp. 202–212, 2005.

[4] R. Rajandram, N. C. Bennett, C. Morais, D. W. Johnson, and G. C. Gobe, "Renal cell carcinoma: resistance to therapy, role of apoptosis, and the prognostic and therapeutic target potential of TRAF proteins," *Medical Hypotheses*, vol. 78, no. 2, pp. 330–336, 2012.

[5] I. J. Frew and H. Moch, "A clearer view of the molecular complexity of clear cell renal cell carcinoma," *Annual Review of Pathology*, vol. 10, no. 1, pp. 263–289, 2015.

[6] A. Kowalewski, M. Zdrenka, D. Grzanka, and Ł. Szylberg, "Targeting the deterministic evolutionary trajectories of clear cell renal cell carcinoma," *Cancers*, vol. 12, no. 11, 2020.

[7] Y. Totoki, K. Tatsuno, K. R. Covington et al., "Trans-ancestry mutational landscape of hepatocellular carcinoma genomes," *Nature Genetics*, vol. 46, no. 12, pp. 1267–1273, 2014.

[8] C. Guichard, G. Amaddeo, S. Imbeaud et al., "Integrated analysis of somatic mutations and focal copy-number changes identifies key genes and pathways in hepatocellular carcinoma," *Nature Genetics*, vol. 44, no. 6, pp. 694–698, 2012.

[9] D. Y. Chiang, A. Villanueva, Y. Hoshida et al., "Focal gains of VEGFA and molecular classification of hepatocellular carcinoma," *Cancer Research*, vol. 68, no. 16, pp. 6779–6788, 2008.

[10] J. Chen, S. Zaidi, S. Rao et al., "Analysis of genomes and transcriptomes of hepatocellular carcinomas identifies mutations and gene expression changes in the transforming growth factor-β pathway," *Gastroenterology*, vol. 154, no. 1, pp. 195–210, 2018.

[11] M. Laplante and D. M. Sabatini, "mTOR signaling in growth control and disease," *Cell*, vol. 149, no. 2, pp. 274–293, 2012.

[12] R. A. Saxton and D. M. Sabatini, "mTOR signaling in growth, metabolism, and disease," *Cell*, vol. 169, no. 2, pp. 361–371, 2017.

[13] R. Watanabe, L. Wei, and J. Huang, "mTOR signaling, function, novel inhibitors, and therapeutic targets," *Journal of Nuclear Medicine*, vol. 52, no. 4, pp. 497–500, 2011.

[14] S. A. Forbes, N. Bindal, S. Bamford et al., "COSMIC: mining complete cancer genomes in the catalogue of somatic mutations in cancer," *Nucleic Acids Research*, vol. 39, no. Database, pp. D945–D950, 2011.

[15] L. Ciuffreda, C. Di Sanza, U. C. Incani, and M. Milella, "The mTOR pathway: a new target in cancer therapy," *Current Cancer Drug Targets*, vol. 10, no. 5, pp. 484–495, 2010.

[16] T. Tian, X. Li, and J. Zhang, "mTOR signaling in cancer and mTOR inhibitors in solid tumor targeting therapy," *International Journal of Molecular Sciences*, vol. 20, no. 3, p. 755, 2019.

[17] F. Conciatori, L. Ciuffreda, C. Bazzichetto et al., "mTOR Cross-Talk in Cancer and Potential for Combination Therapy," *Cancers*, vol. 10, no. 1, p. 23, 2018.

[18] K. Tomczak, P. Czerwińska, and M. Wiznerowicz, "The Cancer Genome Atlas (TCGA): an immeasurable source of knowledge," *Współczesna Onkologia*, vol. 19, no. 1a, pp. A68–A77, 2015.

[19] A. Colaprico, T. C. Silva, C. Olsen et al., "TCGAbiolinks: an R/Bioconductor package for integrative analysis of TCGA data," *Nucleic Acids Research*, vol. 44, no. 8, p. e71, 2016.

[20] J. Lamb, E. D. Crawford, D. Peck et al., "The connectivity map: using gene-expression signatures to connect small molecules, genes, and disease," *Science*, vol. 313, no. 5795, pp. 1929–1935, 2006.

[21] A. Subramanian, R. Narayan, S. M. Corsello et al., "A next generation connectivity map: L1000 platform and the first 1,000,000 profiles," *Cell*, vol. 171, no. 6, pp. 1437–1452.e17, 2017.

[22] P. Geeleher, N. Cox, and R. S. Huang, "pRRophetic: an R package for prediction of clinical chemotherapeutic response from tumor gene expression levels," *PLoS One*, vol. 9, no. 9, article e107468, 2014.

[23] X. Lu, L. Jiang, L. Zhang et al., "Immune signature-based subtypes of cervical squamous cell carcinoma tightly associated with human papillomavirus type 16 expression, molecular features, and clinical outcome," *Neoplasia*, vol. 21, no. 6, pp. 591–601, 2019.

[24] L. Zhang, Y. Zhao, Y. Dai et al., "Immune landscape of colorectal cancer tumor microenvironment from different primary tumor location," *Frontiers in Immunology*, vol. 9, p. 1578, 2018.

[25] K. Chamoto, M. Al-Habsi, and T. Honjo, "Role of PD-1 in immunity and diseases," *Current Topics in Microbiology and Immunology*, vol. 410, pp. 75–97, 2017.

[26] N. Mitsuiki, C. Schwab, and B. Grimbacher, "What did we learn from CTLA-4 insufficiency on the human immune system?," *Immunological Reviews*, vol. 287, no. 1, pp. 33–49, 2019.

[27] J. B. Haanen and C. Robert, "Immune checkpoint inhibitors," *Progress in Tumor Research*, vol. 42, pp. 55–66, 2015.

[28] P. A. Northcott, I. Buchhalter, A. S. Morrissy et al., "The whole-genome landscape of medulloblastoma subtypes," *Nature*, vol. 547, no. 7663, pp. 311–317, 2017.

[29] M. Uhlen, C. Zhang, S. Lee et al., "A pathology atlas of the human cancer transcriptome," *Science*, vol. 357, no. 6352, p. -eaan2507, 2017.

[30] Z. Wang, M. A. Jensen, and J. C. Zenklusen, "A practical guide to the Cancer Genome Atlas (TCGA)," *Methods in Molecular Biology*, vol. 1418, pp. 111–141, 2016.

[31] Y. Nan, H. Guo, L. Guo et al., "MiRNA-451 inhibits glioma cell proliferation and invasion through the mTOR/HIF-1α/VEGF signaling pathway by targeting CAB39," *Human Gene Therapy. Clinical Development*, vol. 29, no. 3, pp. 156–166, 2018.

[32] I. K. Vila, Y. Yao, G. Kim et al., "A UBE2O-AMPKα2 axis that promotes tumor initiation and progression offers opportunities for therapy," *Cancer Cell*, vol. 31, no. 2, pp. 208–224, 2017.

[33] Y. Gao, S. Kim, Y. I. Lee, and J. Lee, "Cellular stress-modulating drugs can potentially be identified by in silico screening with Connectivity Map (CMap)," *International Journal of Molecular Sciences*, vol. 20, no. 22, p. 5601, 2019.

[34] X. Shi, M. Xu, K. Luo, W. Huang, H. Yu, and T. Zhou, "Anticancer activity of bergenin against cervical cancer cells involves apoptosis, cell cycle arrest, inhibition of cell migration and the STAT3 signalling pathway," *Experimental and Therapeutic Medicine*, vol. 17, no. 5, pp. 3525–3529, 2019.

[35] J. Liu, Y. Zhang, C. Yu et al., "Bergenin inhibits bladder cancer progression via activating the PPARγ/PTEN/Akt signal pathway," *Drug Development Research*, vol. 82, no. 2, pp. 278–286, 2021.

[36] S. Qiao, R. Liu, C. Lv et al., "Bergenin impedes the generation of extracellular matrix in glomerular mesangial cells and ameliorates diabetic nephropathy in mice by inhibiting oxidative stress via the mTOR/β-TrcP/Nrf2 pathway," *Free Radical Biology & Medicine*, vol. 145, pp. 118–135, 2019.

[37] D. B. Oien, C. L. Pathoulas, U. Ray, P. Thirusangu, E. Kalogera, and V. Shridhar, "Repurposing quinacrine for treatment-refractory cancer," *Seminars in Cancer Biology*, vol. 68, pp. 21–30, 2021.

[38] C. Guo, A. V. Gasparian, Z. Zhuang et al., "9-Aminoacridine-based anticancer drugs target the PI3K/AKT/mTOR, NF-κB and p53 pathways," *Oncogene*, vol. 28, no. 8, pp. 1151–1161, 2009.

[39] A. K. Murugan, "mTOR: role in cancer, metastasis and drug resistance," *Seminars in Cancer Biology*, vol. 59, pp. 92–111, 2019.

[40] D. Mossmann, S. Park, and M. N. Hall, "mTOR signalling and cellular metabolism are mutual determinants in cancer," *Nature Reviews. Cancer*, vol. 18, no. 12, pp. 744–757, 2018.

[41] A. Kezic, L. Popovic, and K. Lalic, "mTOR inhibitor therapy and metabolic consequences: where do we stand?," *Oxidative Medicine and Cellular Longevity*, vol. 2018, Article ID 2640342, 8 pages, 2018.

[42] H. Hua, Q. Kong, H. Zhang, J. Wang, T. Luo, and Y. Jiang, "Targeting mTOR for cancer therapy," *Journal of Hematology & Oncology*, vol. 12, no. 1, p. 71, 2019.

[43] R. M. Bukowski, "Pazopanib: a multikinase inhibitor with activity in advanced renal cell carcinoma," *Expert Review of Anticancer Therapy*, vol. 10, no. 5, pp. 635–645, 2010.

[44] J. Rawluk and C. F. Waller, "Gefitinib," *Recent Results in Cancer Research*, vol. 211, pp. 235–246, 2018.

[45] J. H. Kong, H. J. Khoury, A. S. Kim, B. G. Hill, and V. Kota, "The safety of bosutinib for the treatment of chronic myeloid leukemia," *Expert Opinion on Drug Safety*, vol. 16, no. 10, pp. 1203–1209, 2017.

[46] M. B. Atkins, E. R. Plimack, I. Puzanov et al., "Axitinib in combination with pembrolizumab in patients with advanced renal cell cancer: a non-randomised, open-label, dose-finding, and dose-expansion phase 1b trial," *The Lancet Oncology*, vol. 19, no. 3, pp. 405–415, 2018.

[47] Z. Chen, H. Yang, Z. Li, Q. Xia, and Y. Nie, "Temsirolimus as a dual inhibitor of retinoblastoma and angiogenesis via targeting mTOR signalling," *Biochemical and Biophysical Research Communications*, vol. 516, no. 3, pp. 726–732, 2019.

[48] R. Mallik and T. A. Chowdhury, "Metformin in cancer," *Diabetes Research and Clinical Practice*, vol. 143, pp. 409–419, 2018.

[49] M. N. A. Kamarudin, M. M. R. Sarker, J. R. Zhou, and I. Parhar, "Metformin in colorectal cancer: molecular mechanism, preclinical and clinical aspects," *Journal of Experimental & Clinical Cancer*, vol. 38, no. 1, p. 491, 2019.

[50] V. Carafa, L. Altucci, and A. Nebbioso, "Dual tumor suppressor and tumor promoter action of sirtuins in determining malignant phenotype," *Frontiers in Pharmacology*, vol. 10, p. 38, 2019.

[51] Y. Tan, B. Li, F. Peng, G. Gong, and N. Li, "Integrative analysis of sirtuins and their prognostic significance in clear cell renal cell carcinoma," *Frontiers in Oncology*, vol. 10, p. 218, 2020.

[52] Z. Li, Y. Tang, S. Zhu et al., "Ethanol extract of *Patrinia scabiosaefolia* induces the death of human renal cell carcinoma 786-O cells via SIRT-1 and mTOR signaling-mediated metabolic disruptions," *Oncology Reports*, vol. 39, no. 2, pp. 764–772, 2018.

[53] Y. Ma, Y. Qi, L. Wang, Z. Zheng, Y. Zhang, and J. Zheng, "SIRT5-mediated SDHA desuccinylation promotes clear cell renal cell carcinoma tumorigenesis," *Free Radical Biology & Medicine*, vol. 134, pp. 458–467, 2019.

[54] S. U. Jeh, J. J. Park, J. S. Lee et al., "Differential expression of the sirtuin family in renal cell carcinoma: aspects of carcinogenesis and prognostic significance," *Urologic Oncology: Seminars and Original Investigations*, vol. 35, no. 12, pp. 675.e9–675.e15, 2017.

[55] M. Haberland, R. L. Montgomery, and E. N. Olson, "The many roles of histone deacetylases in development and physiology: implications for disease and therapy," *Nature Reviews. Genetics*, vol. 10, no. 1, pp. 32–42, 2009.

[56] P. Chun, "Therapeutic effects of histone deacetylase inhibitors on kidney disease," *Archives of Pharmacal Research*, vol. 41, no. 2, pp. 162–183, 2018.

[57] W. H. Xu, Y. Y. Qu, J. Wang et al., "Elevated CD36 expression correlates with increased visceral adipose tissue and predicts poor prognosis in ccRCC patients," *Journal of Cancer*, vol. 10, no. 19, pp. 4522–4531, 2019.

[58] W. H. Xu, Y. Xu, J. Wang et al., "Prognostic value and immune infiltration of novel signatures in clear cell renal cell carcinoma microenvironment," *Aging*, vol. 11, no. 17, pp. 6999–7020, 2019.

[59] H. Zeng, "mTOR signaling in immune cells and its implications for cancer immunotherapy," *Cancer Letters*, vol. 408, pp. 182–189, 2017.

[60] L. Heinzerling, P. A. Ott, F. S. Hodi et al., "Cardiotoxicity associated with CTLA4 and PD1 blocking immunotherapy," *Journal for Immunotherapy of Cancer*, vol. 4, no. 1, p. 50, 2016.

[61] P. J. Thul and C. Lindskog, "The human protein atlas: a spatial map of the human proteome," *Protein Science*, vol. 27, no. 1, pp. 233–244, 2018.

[62] C. Vézina, A. Kudelski, and S. N. Sehgal, "Rapamycin (AY-22,989), a new antifungal antibiotic. I. Taxonomy of the producing streptomycete and isolation of the active principle," *Journal of Antibiotics (Tokyo)*, vol. 28, no. 10, pp. 721–726, 1975.

[63] J. Heitman, N. R. Movva, and M. N. Hall, "Targets for cell cycle arrest by the immunosuppressant rapamycin in yeast," *Science*, vol. 253, no. 5022, pp. 905–909, 1991.

[64] E. J. Brown, M. W. Albers, T. B. Shin et al., "A mammalian protein targeted by G1-arresting rapamycin-receptor complex," *Nature*, vol. 369, no. 6483, pp. 756–758, 1994.

[65] A. Kaur and S. Sharma, "Mammalian target of rapamycin (mTOR) as a potential therapeutic target in various diseases," *Inflammopharmacology*, vol. 25, no. 3, pp. 293–312, 2017.

[66] D. Xu, Y. Sun, C. Wang et al., "Hippocampal mTOR signaling is required for the antidepressant effects of paroxetine," *Neuropharmacology*, vol. 128, pp. 181–195, 2018.

[67] A. Jeong and M. Wong, "mTOR inhibitors in children: current indications and future directions in neurology," *Current Neurology and Neuroscience Reports*, vol. 16, no. 12, p. 102, 2016.

[68] R. Citraro, A. Leo, A. Constanti, E. Russo, and G. De Sarro, "mTOR pathway inhibition as a new therapeutic strategy in epilepsy and epileptogenesis," *Pharmacological Research*, vol. 107, pp. 333–343, 2016.

[69] M. Perluigi, F. Di Domenico, and D. A. Butterfield, "mTOR signaling in aging and neurodegeneration: at the crossroad between metabolism dysfunction and impairment of autophagy," *Neurobiology of Disease*, vol. 84, pp. 39–49, 2015.

[70] F. LiCausi and N. W. Hartman, "Role of mTOR complexes in neurogenesis," *International Journal of Molecular Sciences*, vol. 19, no. 5, p. 1544, 2018.

[71] S. H. Hare and A. J. Harvey, "mTOR function and therapeutic targeting in breast cancer," *American Journal of Cancer Research*, vol. 7, no. 3, pp. 383–404, 2017.

[72] K. Hu, H. B. Dai, and Z. L. Qiu, "mTOR signaling in osteosarcoma: oncogenesis and therapeutic aspects (review)," *Oncology Reports*, vol. 36, no. 3, pp. 1219–1225, 2016.

[73] D. H. Yates, "mTOR treatment in lymphangioleiomyomatosis: the role of everolimus," *Expert Review of Respiratory Medicine*, vol. 10, no. 3, pp. 249–260, 2016.

[74] J. Liu, D. C. Wu, L. H. Qu, H. Q. Liao, and M. X. Li, "The role of mTOR in ovarian neoplasms, polycystic ovary syndrome, and ovarian aging," *Clinical Anatomy*, vol. 31, no. 6, pp. 891–898, 2018.

[75] M. S. Yoon, "The role of mammalian target of rapamycin (mTOR) in insulin signaling," *Nutrients*, vol. 9, no. 11, p. 1176, 2017.

[76] Y. Tuo and M. Xiang, "mTOR: a double-edged sword for diabetes," *Journal of Leukocyte Biology*, vol. 106, no. 2, pp. 385–395, 2019.

[77] V. S. Rodrik-Outmezguine, M. Okaniwa, Z. Yao et al., "Overcoming mTOR resistance mutations with a new-generation mTOR inhibitor," *Nature*, vol. 534, no. 7606, pp. 272–276, 2016.

[78] P. Xia and X. Y. Xu, "PI3K/Akt/mTOR signaling pathway in cancer stem cells: from basic research to clinical application," *American Journal of Cancer Research*, vol. 5, no. 5, pp. 1602–1609, 2015.

[79] P. Wang, X. M. Liu, L. Ding, X. J. Zhang, and Z. L. Ma, "mTOR signaling-related microRNAs and cancer involvement," *Journal of Cancer*, vol. 9, no. 4, pp. 667–673, 2018.

[80] T. Suto and T. Karonitsch, "The immunobiology of mTOR in autoimmunity," *Journal of Autoimmunity*, vol. 110, p. 102373, 2020.

[81] R. Keating and M. A. McGargill, "mTOR regulation of lymphoid cells in immunity to pathogens," *Frontiers in Immunology*, vol. 7, p. 180, 2016.

[82] W. Zhong, C. Huang, J. Lin et al., "Development and validation of nine-RNA binding protein signature predicting overall survival for kidney renal clear cell carcinoma," *Frontiers in Genetics*, vol. 11, p. 568192, 2020.

[83] A. P. Ghosh, C. B. Marshall, T. Coric et al., "Point mutations of the mTOR-RHEB pathway in renal cell carcinoma," *Oncotarget*, vol. 6, no. 20, pp. 17895–17910, 2015.

[84] D. K. Alves-Fernandes and M. G. Jasiulionis, "The role of SIRT1 on DNA damage response and epigenetic alterations in cancer," *International Journal of Molecular Sciences*, vol. 20, no. 13, p. 3153, 2019.

[85] L. M. Zhao and J. H. Zhang, "Histone deacetylase inhibitors in tumor immunotherapy," *Current Medicinal Chemistry*, vol. 26, no. 17, pp. 2990–3008, 2019.

Research Article

Hypoxia Induced by Cobalt Chloride Triggers Autophagic Apoptosis of Human and Mouse Drug-Resistant Glioblastoma Cells through Targeting the PI3K-AKT-mTOR Signaling Pathway

Yuan-Wen Lee,[1,2] Yih-Giun Cherng,[2,3] Shun-Tai Yang,[4,5] Shing-Hwa Liu,[6] Ta-Liang Chen,[2,7] and Ruei-Ming Chen [1,5,7,8]

[1]*Anesthesiology and Health Policy Research Center; Department of Anesthesiology, Taipei Medical University Hospital,*
 Taipei Medical University, Taipei 110, Taiwan
[2]*Department of Anesthesiology, School of Medicine, College of Medicine, Taipei Medical University, Taipei 110, Taiwan*
[3]*Department of Anesthesiology, Shuang Ho Hospital, Taipei Medical University, New Taipei City 235, Taiwan*
[4]*Department of Neurosurgery, Shuang Ho Hospital, Taipei Medical University, New Taipei City 235, Taiwan*
[5]*Graduate Institute of Medical Sciences, College of Medicine, Taipei Medical University, Taipei 110, Taiwan*
[6]*Institute of Toxicology, College of Medicine, National Taiwan University, Taipei 100, Taiwan*
[7]*Cell Physiology and Molecular Image Research Center; Department of Anesthesiology, Wan Fang Hospital,*
 Taipei Medical University, Taipei 116, Taiwan
[8]*TMU Research Center of Cancer Translational Medicine, Taipei 110, Taiwan*

Correspondence should be addressed to Ruei-Ming Chen; rmchen@tmu.edu.tw

Glioblastoma multiforme (GBM) is the most aggressive brain tumor. Drug resistance mainly drives GBM patients to poor prognoses because drug-resistant glioblastoma cells highly defend against apoptotic insults. This study was designed to evaluate the effects of cobalt chloride ($CoCl_2$) on hypoxic stress, autophagy, and resulting apoptosis of human and mouse drug-resistant glioblastoma cells. Treatment of drug-resistant glioblastoma cells with $CoCl_2$ increased levels of hypoxia-inducible factor- (HIF-) 1α and triggered hypoxic stress. In parallel, the $CoCl_2$-induced hypoxia decreased mitochondrial ATP synthesis, cell proliferation, and survival in chemoresistant glioblastoma cells. Interestingly, $CoCl_2$ elevated the ratio of light chain (LC)3-II over LC3-I in TMZ-resistant glioblastoma cells and subsequently induced cell autophagy. Analyses by loss- and gain-of-function strategies further confirmed the effects of the $CoCl_2$-induced hypoxia on autophagy of drug-resistant glioblastoma cells. Furthermore, knocking down HIF-1α concurrently lessened $CoCl_2$-induced cell autophagy. As to the mechanisms, the $CoCl_2$-induced hypoxia decreased levels of phosphoinositide 3-kinase (PI3K) and successive phosphorylations of AKT and mammalian target of rapamycin (mTOR) in TMZ-resistant glioblastoma cells. Interestingly, long-term exposure of human chemoresistant glioblastoma cells to $CoCl_2$ sequentially triggered activation of caspases-3 and -6, DNA fragmentation, and cell apoptosis. However, pretreatment with 3-methyladenine, an inhibitor of autophagy, significantly attenuated the $CoCl_2$-induced autophagy and subsequent apoptotic insults. Taken together, this study showed that long-term treatment with $CoCl_2$ can induce hypoxia and subsequent autophagic apoptosis of drug-resistant glioblastoma cells via targeting the PI3K-AKT-mTOR pathway. Thus, combined with traditional prescriptions, $CoCl_2$-induced autophagic apoptosis can be clinically applied as a *de novo* strategy for therapy of drug-resistant GBM patients.

1. Introduction

Glioblastoma multiforme (GBM) is the most malignant brain tumor. In the clinic, GBM patients are regularly cured with standard surgical resection and successive concurrent chemoradiotherapy [1]. Temozolomide (TMZ) is the first-line chemotherapeutic drug for GBM [2]. Unfortunately, more than 50% of GBM patients will ultimately exhibit drug

resistance and recurrence [3]. Because GBM develops in the brain, this cerebral location limits neurosurgeons' performance of completely removing tumors [4]. Moreover, glioblastoma cells possess unique features of rapid proliferation, migration, and invasion [5]. Following surgery, residual glioblastoma cells existing on the periphery of a brain tumor can speedily proliferate and invade other areas to recur as more-aggressive brain tumors [4]. As a result, GBM patients usually have very poor prognoses. Even if patients are energetically cured, their average survival is only 12~18 months [6]. Until now, chemoresistance is still a key challenge for therapy of glioblastomas. Therefore, establishing *de novo* strategies to overwhelm drug tolerance by GBM is an emergent and necessary issue.

Mammalian cells require an adequate supply of oxygen for energy production in order to support cell activities and functions. Hypoxia is a condition in which there is an insufficient oxygen source in a region of the body [7]. Being related to physiological and pathological situations, hypoxia is highly associated with human health and diseases, especially in the brain [8, 9]. Throughout its entire lifespan, the human brain is often threatened by cerebral hypoxia [10]. For example, prenatal hypoxia that occurs in a key stage of brain formation may cause morphological variations in brain structures that are involved in learning and memory and ultimately affect development of cognitive functions. In ischemic brain diseases, hypoxia can directly disrupt the integrity of the blood-brain barrier (BBB), thus leading to vasogenic edema, brain swelling, and neuronal injury [11]. Moreover, cerebral hypoxia can also be induced by certain diseases, such as asthma, that interfere with breathing and blood oxygenation [12]. More attractively, hypoxia is also detected in solid cancers, particularly in brain tumors [13]. Hypoxic conditions may induce insults to glioblastoma cells. Otherwise, in response to hypoxic stress, glioblastoma cells can produce and excrete vascular endothelial growth factor (VEGF) to stimulate neovascularization from preexisting blood vessels [14]. In response to hypoxic stimuli, hypoxia-induced factor- (HIF-) 1α, a subunit of heterodimeric HIF-1, can be significantly upregulated and then functions as a representative transcription factor to regulate downstream gene expressions [9, 15]. A number of studies disclosed the complexity and importance of the HIF-1α signaling pathway in hypoxia [16]. Accordingly, HIF-1α and its downstream targets are emerging as novel therapeutic options for treating brain tumors.

Autophagy, a process of self-degradation and catabolism, is generally considered to be a survival mechanism in response to nutrient insufficiency-induced stress [17]. In addition, autophagy participates in preventing certain diseases, such as cancer, neuronal disorders, cardiomyopathy, diabetes, liver disease, autoimmune diseases, and infections, by engulfing damaged organelles and intracellular ribosomes and protein aggregates into double-membraned autophagosomes. Hypoxia can induce cell autophagy [18]. In the hypoxic tissue microenvironment, adenosine monophosphate- (AMP-) activated protein kinase (AMPK) is activated due to an increase in the ratio of intracellular AMP and adenosine triphosphate (ATP) [19]. Subsequently, activated AMPK can trigger cell autophagy through directly inducing

autophagy-associated light chain 3 (LC3) and indirectly suppressing activity of the mammalian target of rapamycin (mTOR) [13, 20]. When oxygen deprivation occurs in the tissue microenvironment, HIF-1α is proximately induced and then activated in response to hypoxic stress [21]. HIF-1α can induce cell autophagy via inducing BNIP3 and LC3 expressions [22]. Traditionally, hypoxia-induced autophagy is thought to promote tumor resistance [13]. In addition to autophagy, hypoxic conditions can induce cell apoptosis and necrosis in follicles of mammalian ovaries [18]. Our previous study showed that honokiol, an anticancer drug, induces autophagic insults to neuroblastoma cells via activation of the phosphoinositide 3-kinase- (PI3K-) AKT-mTOR and endoplasmic reticular (ER) stress/extracellular signal-regulated kinase (ERK)1/2 signaling pathways [23]. Moreover, a longer period of treatment with honokiol led to autophagy and the death of glioblastoma cells [24]. Our previous study also demonstrated that cobalt chloride (CoCl$_2$), an inducer of HIF-1α, can be used as a chemical hypoxia model to induce autophagic death of human glioblastoma cells via a p53-dependent mechanism [25]. More than 50% of GBM patients ultimately exhibit chemoresistance, and drug-resistant glioblastoma cells highly defend against apoptotic insults [1]. In this study, we successfully isolated human and mouse TMZ-resistant glioblastoma cells as our experimental models to investigate whether or not a prolonged administration of hypoxia could induce autophagic killing of drug-resistant glioblastoma cells and the possible action mechanisms, focusing on the PI3K-AKT-mTOR signaling pathway.

2. Materials and Methods

2.1. Selection and Culturing of Human and Mouse Drug-Resistant Glioblastoma Cells. TMZ-sensitive human U87 MG and mouse GL261 cells were used for selection of drug-resistant U87 MG-R and GL261-R glioblastoma cells as described previously [26]. In brief, U87 MG and GL261 cells were seeded in 12-well tissue culture plates at a density of 10^5 cells per well and maintained in Dulbecco's modified Eagle's medium (DMEM; Gibco-BRL Life Technologies, Grand Island, NY, USA) with 10% fetal bovine serum, 100 μg/ml streptomycin sulfate, and 100 U/ml penicillin and cultured in a humidified incubator with 5% CO$_2$ at 37°C. Glioblastoma cells were treated with 50 μM TMZ for 2 days. Later, human U87 MG and mouse GL261 cells were trypsinized and diluted 0.2~1.0-fold. Diluted cells were cultured in DMEM with 100 μM TMZ. Surviving cell colonies were dissociated with trypsin and further grown in culture medium containing 100 μM TMZ. After sequential selection of drug-resistant glioblastoma cell colonies, TMZ-tolerant U87 MG-R and GL261-R cells were successfully selected. Human normal astrocytes (HA-h) purchased from ScienCell Research Laboratories (Carlsbad, CA, USA) were cultured in astrocyte medium (ScienCell Research Laboratories).

2.2. Creation of Hypoxic Conditions and Drug Treatment. Hypoxic conditions in drug-resistant U87 MG-R and GL261-R glioblastoma cells were created by inducing HIF-1α

expression following treatment with $CoCl_2$ as described previously [25]. $CoCl_2$, bought from Sigma (St. Louis, MO, USA), was freshly dissolved in phosphate-buffered saline (PBS), containing NaCl (0.14 M), KCl (2.6 mM), Na_2HPO_4 (8 mM), and KH_2PO_4 (1.5 mM). TMZ-resistant U87 MG-R and GL261-R glioblastoma cells were exposed to $100 \mu M$ $CoCl_2$ for 6, 12, and 24 h. Levels of HIF-1α were measured in order to confirm hypoxic conditions in drug-resistant glioblastoma cells. Control cells received PBS only.

2.3. Analyses of Cell Morphology and Survival. Morphologies and survival of human and mouse drug-sensitive and -resistant glioblastoma cells were analyzed according to a previously described method [27]. Drug-resistant glioblastoma cells (10^4 cells/well) were seeded in 12-well tissue culture plates overnight. After drug treatment, cell morphologies were observed and photographed using an inverted light microscope (Nikon, Tokyo, Japan). Then, the cells were trypsinized with 0.1% trypsin-EDTA. After centrifugation, glioblastoma cells were suspended in PBS buffer and stained with a trypan blue dye. Fractions of living cells with white signals were visualized and counted with a light microscope (Nikon).

2.4. Examination of Cell Proliferation. Proliferation of human drug-resistant glioblastoma cells was assayed by analyzing the incorporation of bromodeoxyuridine (BrdU) into genomic DNA as described previously [28]. Glioblastoma cells at 3×10^3 cells/well were seeded in a 96-well cell culture plate. Following $CoCl_2$ treatment, replicating glioblastoma cells were reacted with 10 mM BrdU for a further 2 h. Then, human drug-tolerant glioblastoma cells were fixed with 4% paraformaldehyde. A cell proliferation enzyme-linked immunosorbent assay (ELISA) kit purchased from Roche (Mannheim, Germany) was used in this study to measure amounts of BrdU incorporated into genomic DNA of glioblastoma cells. Signals were read using a microplate photometer (Thermo Fisher Scientific, Tewksbury, MA, USA) and statistically analyzed.

2.5. Assay of Mitochondrial NAD(P)H Oxidoreductase Activity. A colorimetric method was carried out to examine activities of mitochondrial NAD(P)H-dependent oxidoreductase enzymes in human drug-resistant glioblastoma cells as described previously [29]. Briefly, human drug-resistant glioblastoma cells were seeded in 96-well cell culture plates at a density of 10^4 cells/well for 12 h. After exposure to $CoCl_2$, TMZ-tolerant glioblastoma cells were cultured with fresh DMEM containing 0.5 mg/ml 3-(4,5-dimethylthiazol-2-yl)-2,5-diphenyltetrazolium bromide for a further 3 h. The formazan products, metabolized by mitochondrial NAD(P)H oxidoreductases, were then dissolved in DMSO. Dark-brown signals were spectrophotometrically measured at 550 nm using a spectrophotometer (BioTek, Winooski, VT, USA).

2.6. Levels of Cellular ATP. A bioluminescence assay was conducted to measure levels of cellular ATP in human TMZ-resistant glioblastoma cells following the protocol of an ATP determination kit (Molecular Probes, Eugene, OR, USA) as described previously [30]. This assay was based on the luciferase requirement for ATP to produce 560 nm illu-minant signals. A multilabel counter, obtained from BMG Labtech (Offenburg, Germany), was used to measure intensities of the illuminant light. Values were analyzed using the Gen5 software (vers. 3.03, BMG Labtech).

2.7. Quantification of Autophagic Cells. Proportions of autophagic cells were quantified by assessing acidic vesicular organelles in drug-resistant glioblastoma cells as described previously [23]. Following exposure to $CoCl_2$, human and mouse drug-resistant glioblastoma cells at a density of 10^5 cells/well were treated with 1 μg/ml acridine orange for 20 min. After that, these TMZ-tolerant glioblastoma cells were harvested in DMEM without phenol red. A flow cytometer (Beckman Coulter, Fullerton, CA, USA) was used in this study to quantify levels of acridine orange with green and red fluorescence in glioblastoma cells. Intensities of fluorescent signals were analyzed using software from Beckman Coulter. 3-Methyladenine (3-MA), an inhibitor of autophagy, and rapamycin, an inducer of autophagy, were purchased from Sigma. 3-MA and rapamycin were dissolved in dimethyl sulfoxide (DMSO). After pretreatment with 1 mM 3-MA or 0.5 μM rapamycin for 1 h, U87 MG-R and GL261-R glioblastoma cells were then exposed to $CoCl_2$. Control cells received DMSO only.

2.8. Activities of Caspases-3 and -6. A fluorometric substrate assay was conducted to quantify activation of caspases-3 and -6 in human and mouse TMZ-resistant glioblastoma cells as described previously [31]. In brief, after $CoCl_2$ treatment, human and mouse drug-resistant glioblastoma cells were lysed using a buffer containing Nonidet P-40 (1%), NaCl (200 mM), Tris/HCl (pH 7.4, 20 mM), leupeptin (10 mg/ml), aprotinin (0.27 U/ml), and phenylmethylsulfonyl fluoride (PMSF, 100 mM). Cell extracts were incubated with a specific fluorogenic peptide substrate at 50 mM in a cell-free system buffer containing HEPES (pH 7.4, 10 mM), mannitol (220 mM), sucrose (68 mM), NaCl (2 mM), KH_2PO_4 (2.5 mM), ethylene glycol tetraacetic acid (0.5 mM), $MgCl_2$ (2 mM), pyruvate (5 mM), PMSF (0.1 mM), and dithiothreitol (1 mM). DEVD and VEID are specific peptide substrates for, respectively, detecting caspase-3 and -6 enzyme activities. For fluorescent detection, the DEVD and VEID substrates were conjugated with 7-amino-4-(trifluoromethyl)coumarin. A spectrometer (BMG Labtech) was used to measure intensities of the fluorescent products metabolized by caspases-3 and -6. Fluorescent values were examined using software from BMG Labtech and statistically analyzed.

2.9. Quantification of DNA Fragmentation. DNA fragmentation in human and mouse drug-sensitive and -resistant glioblastoma cells was quantified using a cellular ELISA kit (Boehringer Mannheim, Indianapolis, IN, USA) as described previously [32]. In brief, TMZ-tolerant glioblastoma cells were subcultured in 24-well tissue culture plates at a density of 2×10^5 cells/well and labeled with BrdU for 12 h. Human and mouse glioblastoma cells were then harvested and suspended in culture medium. The cell suspension (100 μl per well) was added to 96-well tissue culture plates. Drug-sensitive and -resistant glioblastoma cells were cultured

under hypoxic conditions for various time periods in a humidified incubator with 5% CO_2 at 37°C. Levels of BrdU-labeled DNA in the cytoplasm were measured with a microplate photometer (BMG Labtech) at 450 nm. The data of DNA fragmentation were then analyzed using software from BMG Labtech.

2.10. Assay of Apoptotic Cells. Proportions of drug-sensitive and -resistant glioblastoma cells under apoptotic insults were examined according to a previously described method [33]. After drug administration, glioblastoma cells were harvested and fixed in cold 80% ethanol. Following centrifugation and washing, fixed glioblastoma cells were stained with propidium iodide. A flow cytometer (Beckman Coulter) was used to measure fluorescent signals with a 560 nm dichroic mirror and a 600 nm bandpass filter. Intensities of these fluorescent signals in glioblastoma cells were quantified with software from Beckman Coulter.

2.11. Immunoblot Analysis. Immunoblot analyses were carried out to immunodetect levels of HIF-1α, LC3-I, LC3-II, PI3K, phosphorylated- (p-) and nonphosphorylated AKT and mTOR, vimentin, and β-actin in drug-resistant glioblastoma cells as described previously [34]. After exposure to hypoxia, lysates of drug-resistant glioblastoma cells were prepared in ice-cold radioimmunoprecipitation assay (RIPA) buffer, containing Tris-HCl (pH 7.2, 25 mM), Triton X-100 (1%), sodium dodecylsulfate (SDS, 0.1%), EDTA (1 mM), and NaCl (0.15 M). A mixture of proteinase inhibitors, viz., leupeptin (5 μg/ml), sodium orthovanadate (1 mM), and PMSF (1 mM), was added to ice-cold RIPA buffer to prevent protein degradation. A bicinchonic acid protein assay kit purchased from Pierce (Rockford, IL, USA) was used to quantify protein concentrations. Cell lysates were loaded into SDS-polyacrylamide gel and electrophoretically separated. Then, the proteins were electrophoretically transferred to nitrocellulose membranes. Fiver percentage of on-fat milk was used to block the membranes at 37°C for 1 h. HIF-1α was immunodetected using a mouse monoclonal antibody (mAb) against human HIF-1α (Cell Signaling Technology, Danvers, MA, USA). LC3-I, LC3-II, PI3K, AKT, p-AKT, mTOR, and p-mTOR were recognized using mAbs or polyclonal antibodies (pAbs) purchased from Cell Signaling Technology. Cellular vimentin and β-actin proteins were immunodetected using mouse mAbs against human vimentin and mouse β-actin (Sigma), respectively. These immunoreactive protein bands were quantified with a digital imaging system (Syngene, Cambridge, UK) as described previously [35]. Intensities of these protein bands were analyzed using β-actin as the internal loading control.

2.12. HIF-1α-Knockdown. An RNA interference (RNAi) technique was applied in this study to knock down translation of HIF-1α as described previously [36]. HIF-1α small interfering (si) RNA (sc-35561), scrambled siRNA (sc-37007), and siRNA transfection medium (sc-36868) were purchased from Santa Cruz Biotechnology (Santa Cruz, CA, USA). At first, human TMZ-resistant glioblastoma cells were cultured in antibiotic-free DMEM and maintained in a

humidified incubator with an atmosphere of 5% CO_2 at 37°C for 24 h. After that, the HIF-1α siRNAs were diluted in siRNA transfection medium, and a HIF-1α siRNA duplex solution was added to the cells for transfection for 48 h. After replacing the old medium with normal DMEM, human U87 MG-R cells were exposed to $CoCl_2$. Scrambled siRNA was applied as a negative control.

2.13. Statistical Analysis. Each value represses the mean ± standard deviation (SD) for at least three independent determinations. Statistical analyses were carried out using a two-way analysis of variance (ANOVA) and a post hoc Duncan's multiple-range test. Statistical differences were considered significant at $p < 0.05$.

3. Results

3.1. Selection and Preparation of Human and Mouse Drug-Resistant Glioblastoma Cells. Human and mouse glioblastoma cells that were resistant to TMZ treatment were prepared from their respective drug-sensitive brain tumor cells (Figure 1). No difference in morphologies of human drug-sensitive U87 MG and -resistant U87 MG-R cells was observed (Figure 1(a)). Exposure to TMZ at 25, 50, 75, and 100 μM for 72 h caused significant 19%, 30%, 38%, and 51% decreases in survival of human U87 MG cells, respectively (Figure 1(b)). In contrast, treatment of human U87 MG-R glioblastoma cells with various concentrations of TMZ for 72 h did not change cell survival. Furthermore, exposure of U87 MG cells to 100 μM TMZ for 72 h led to a significant 98% augmentation in DNA fragmentation (Figure 1(c)). The DNA integrity of U87 MG-R glioblastoma cells was not influenced by TMZ. Administration of TMZ at 100 μM for 72 h led to a significant 48% elevation in apoptosis of human U87 MG cells (Figure 1(d)). At the same treated condition, TMZ did not trigger apoptosis of human U87 MG-R cells. Moreover, TMZ induced DNA fragmentation and cell apoptosis in drug-sensitive GL261 glioblastoma cells by 64% and 41%, respectively (Figures 1(e) and 1(f)). In comparison, treatment of mouse drug-resistant GL261-R glioblastoma cells with 100 μM TMZ for 72 h did not trigger DNA fragmentation or cell apoptosis.

3.2. Exposure of Human and Mouse TMZ-Resistant Glioblastoma Cells to $CoCl_2$ Increased Levels of HIF-1α and Led to Cell Death. Effects of $CoCl_2$ on hypoxic insults to human TMZ-tolerant U87 MG-R cells were investigated (Figure 2). Treatment with 100 μM $CoCl_2$ for 6 h augmented levels of HIF-1α in U87 MG-R cells (Figure 2(a), top panel, lane 1). At 12 and 24 h after hypoxic treatment, HIF-1α in U87 MG-R cells were time-dependently elevated (lanes 3 and 4). β-Actin was measured as the internal loading standard (bottom panel). The protein band intensities were statistically analyzed (Figure 2(b)). Exposure to $CoCl_2$ for 6, 12, and 24 h caused respective 2.4-, 2.9-, and 3.8-fold increases in levels of HIF-1α in human U87 MG-R glioblastoma cells. In comparison, exposure of human U87 MG-R cells to $CoCl_2$ for 6, 12, and 24 h did not change levels of vimentin (Fig. S1). Compared to the untreated group,

(a)

(b)

(c)

(d)

(e)

(f)
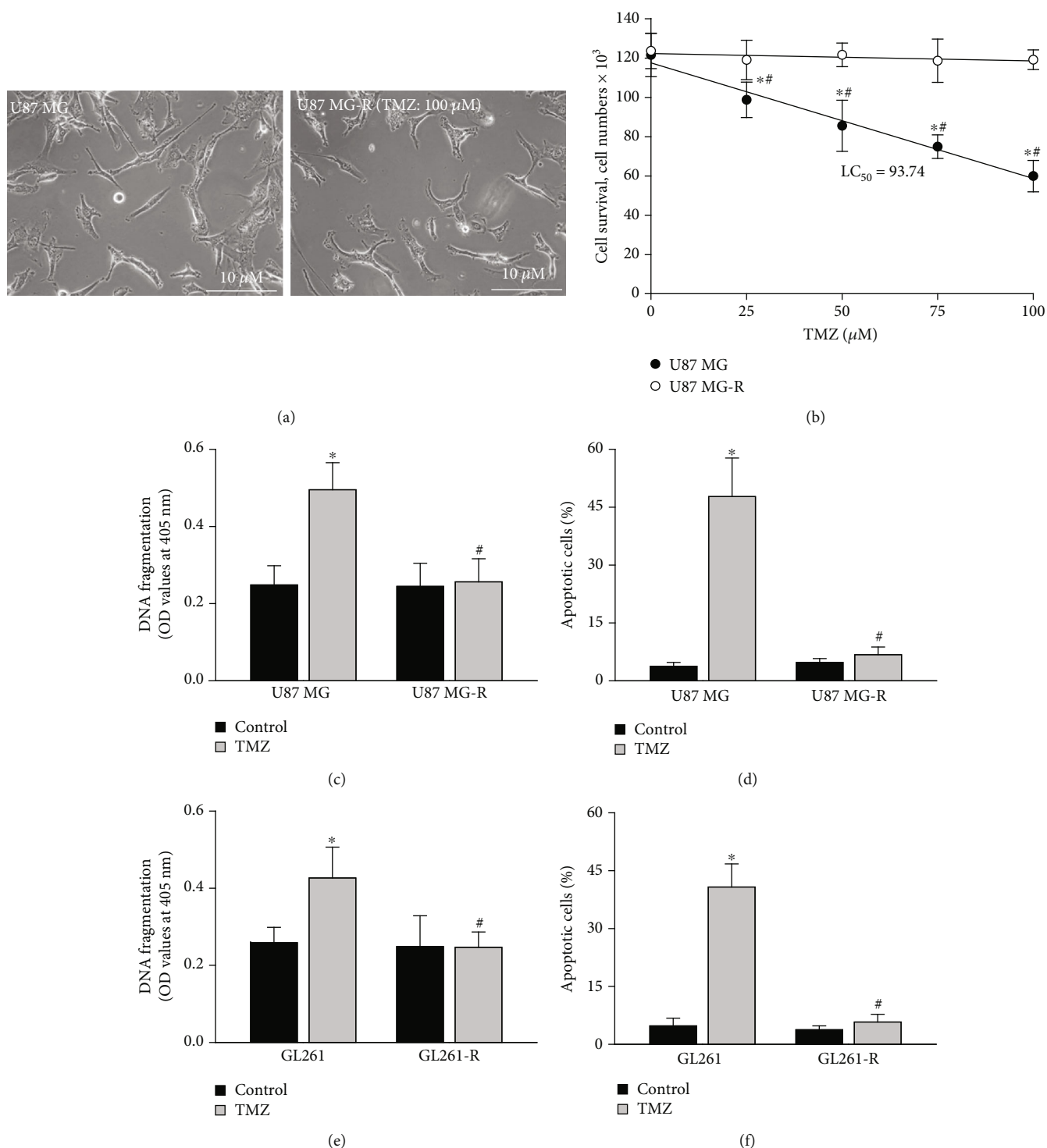
Figure 1: Selection and preparation of human drug-resistant glioblastoma cells. Human TMZ-tolerant U87 MG-R cells were selected from TMZ-sensitive U87 MG cells. (a) Morphologies of U87 MG and U87 MG-R cells are shown. Glioblastoma cells were exposed to TMZ at 25, 50, 75, and 100 μM for 72 h. (b) Cell survival was assayed using a trypan blue exclusion method. (c, d) A cellular ELISA kit and a flow cytometric method were used to quantify DNA fragmentation and apoptotic cells, respectively. Murine GL261 and GL261-R glioblastoma cells were exposed to TMZ at 100 μM. (e, f) DNA fragmentation and apoptotic cells were analyzed. Data are expressed as the mean ± SD for $n = 6$. *$p < 0.05$ vs. control and #$p < 0.05$ vs. U87 MG.

treatment with $CoCl_2$ for 6 h reduced cell numbers (Figure 2(c)). After 12 and 24 h, hypoxia induced more death of human TMZ-tolerant glioblastoma cells. Moreover, our

survival analysis showed that treatment of human U87 MG-R cells with 100 μM $CoCl_2$ for 6, 12, and 24 h, respectively, diminished cell survival by 19%, 31%, and 49%
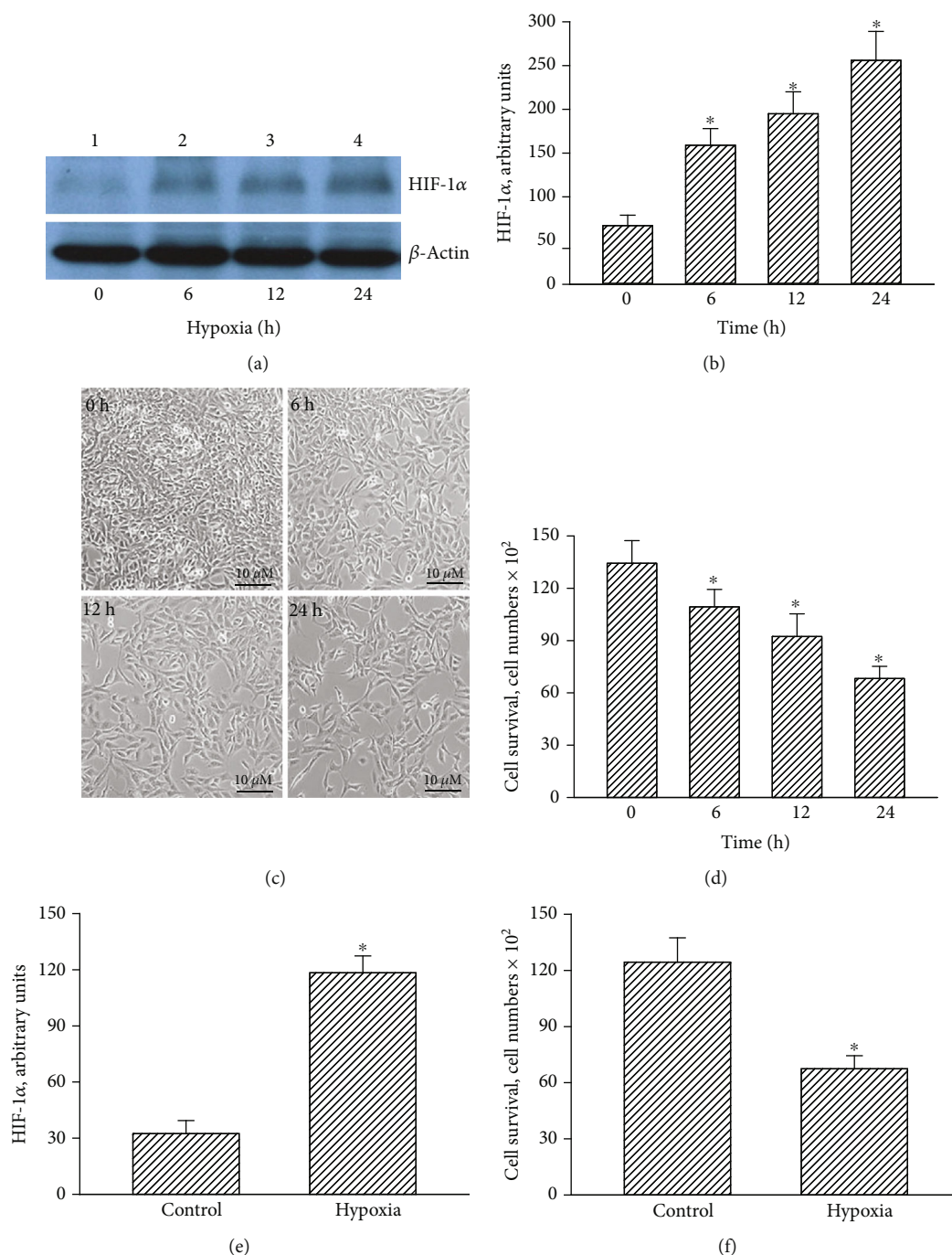
FIGURE 2: Effects of hypoxia induced by $CoCl_2$ on levels of hypoxia-inducible factor- (HIF-) 1α and cell survival in human drug-resistant glioblastoma cells. Human drug-tolerant U87 MG-R cells were selected from TMZ-sensitive U87 MG cells. U87 MG-R cells were treated with hypoxia for 6, 12, and 24 h. (a) Levels of HIF-1α were immunodetected (top panel). β-Actin was analyzed as the internal control (bottom panel). (b) These protein bands were quantified and statistically analyzed. (c) Cell morphology was observed and photographed. (d) Cell survival was assayed with a trypan blue exclusion method. Mouse GL261-R glioblastoma cells were exposed to hypoxia for 24 h. (e, f) Levels of HIF-1α and cell survival were analyzed. Data are expressed as the mean ± SD for $n = 6$. $^*p < 0.05$ vs. control.

(Figure 2(d)). The HIF-1α levels in mouse GL261-R glioblastoma cells increased 3.6-fold following treatment with 100 μM $CoCl_2$ for 24 h (Figure 2(e)). Exposure of mouse GL261-R cells to $CoCl_2$ led to a 46% reduction in cell survival (Figure 2(f)).

3.3. Hypoxia Induced by $CoCl_2$ Triggered Mitochondrial Dysfunction, Proliferation Inhibition, and Cell Autophagy in Human and Mouse Drug-Resistant Glioblastoma Cells.
Effects of the $CoCl_2$-induced hypoxia insults to mitochondrial functions, cell proliferation, and cell autophagy were
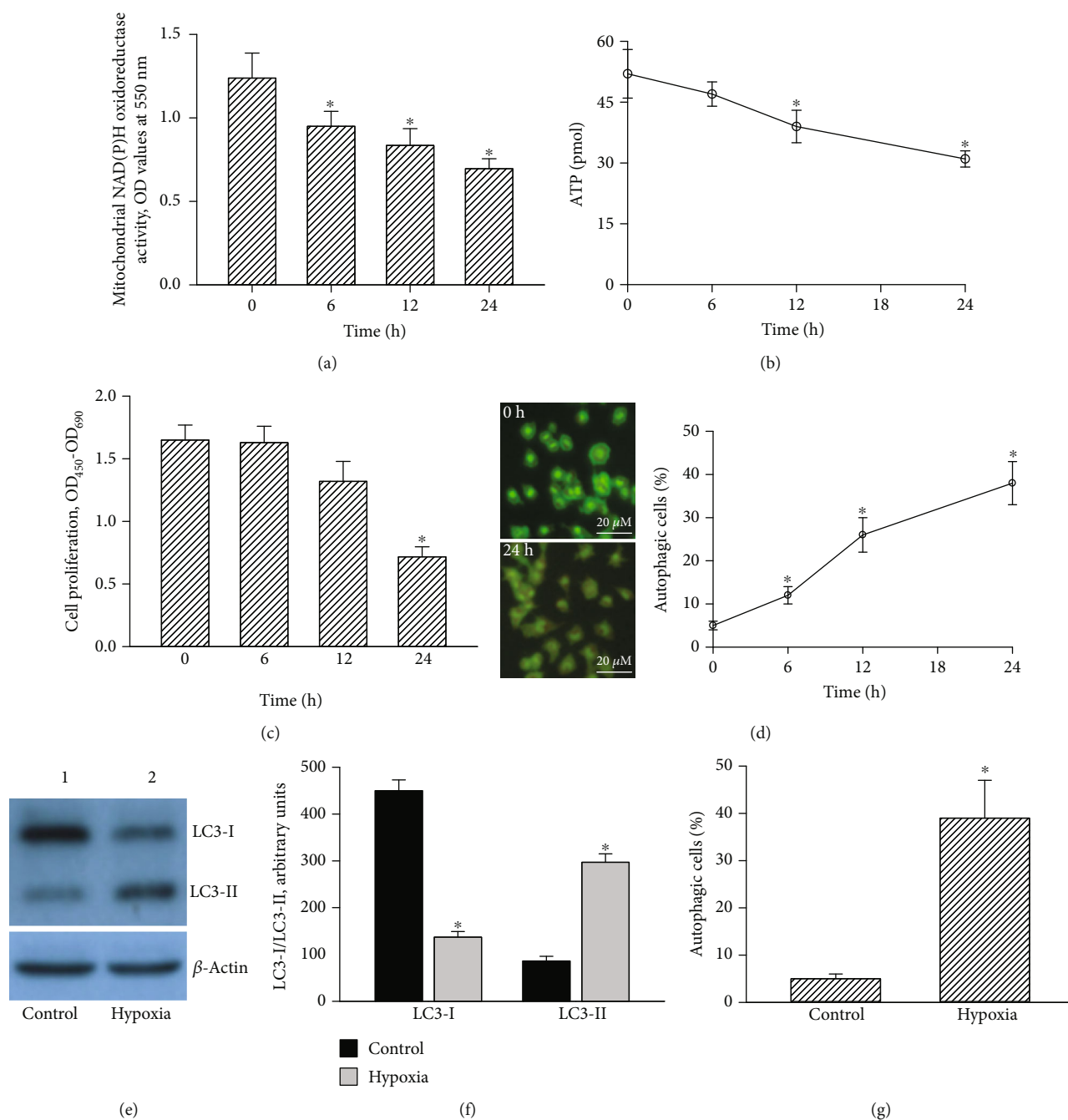
FIGURE 3: Effects of hypoxia induced by $CoCl_2$ on mitochondrial NADH dehydrogenase activity, ATP levels, cell proliferation, cell autophagy, and levels of light chain (LC)3-I and LC3-2 in human drug-resistant glioblastoma cells. Human TMZ-tolerant U87 MG-R cells were selected from TMZ-sensitive U87 MG cells. U87 MG-R glioblastoma cells were treated with hypoxia for 6, 12, and 24 h. (a) Activity of mitochondrial NADH dehydrogenase was assayed using a colorimetric method. (b) Levels of ATP were measured using a bioluminescence assay. (c) Cell proliferation was measured by a thymidine incorporation assay. (d) Autophagic cells with acidic vesicular organelles were observed and photographed using a fluorescent microscope (left panel) and quantified with flow cytometry (right panel). (e) Levels of LC3-I and LC3-II were immunodetected (top panels). β-Actin was measured as the internal control (bottom panels). (f) These protein bands were quantified and statistically analyzed. Mouse GL261-R glioblastoma cells were exposed to hypoxia for 24 h. (g) Autophagic cells were quantified. Data are expressed as the mean ± SD for $n = 6$. *$p < 0.05$ vs. control.

consecutively determined (Figure 3). Activities of mitochondrial NAD(P)H enzymes in U87 MG-R cells decreased by 23%, 32%, and 44% following respective exposure to $CoCl_2$ for 6, 12, and 24 h (Figure 3(a)). Subsequently, treatment with $CoCl_2$ for 12 and 24 h led to respective 25% and 40% reduc-

tions in cellular ATP levels (Figure 3(b)). Moreover, at 24 h after hypoxic administration, proliferation of human TMZ-resistant glioblastoma cells had dropped by 56% (Figure 3(c)).

Remarkably, exposure of human drug-tolerant glioblastoma cells to $CoCl_2$ for 24 h induced the cells with acidic

(a)

(b)

(c)

(d)
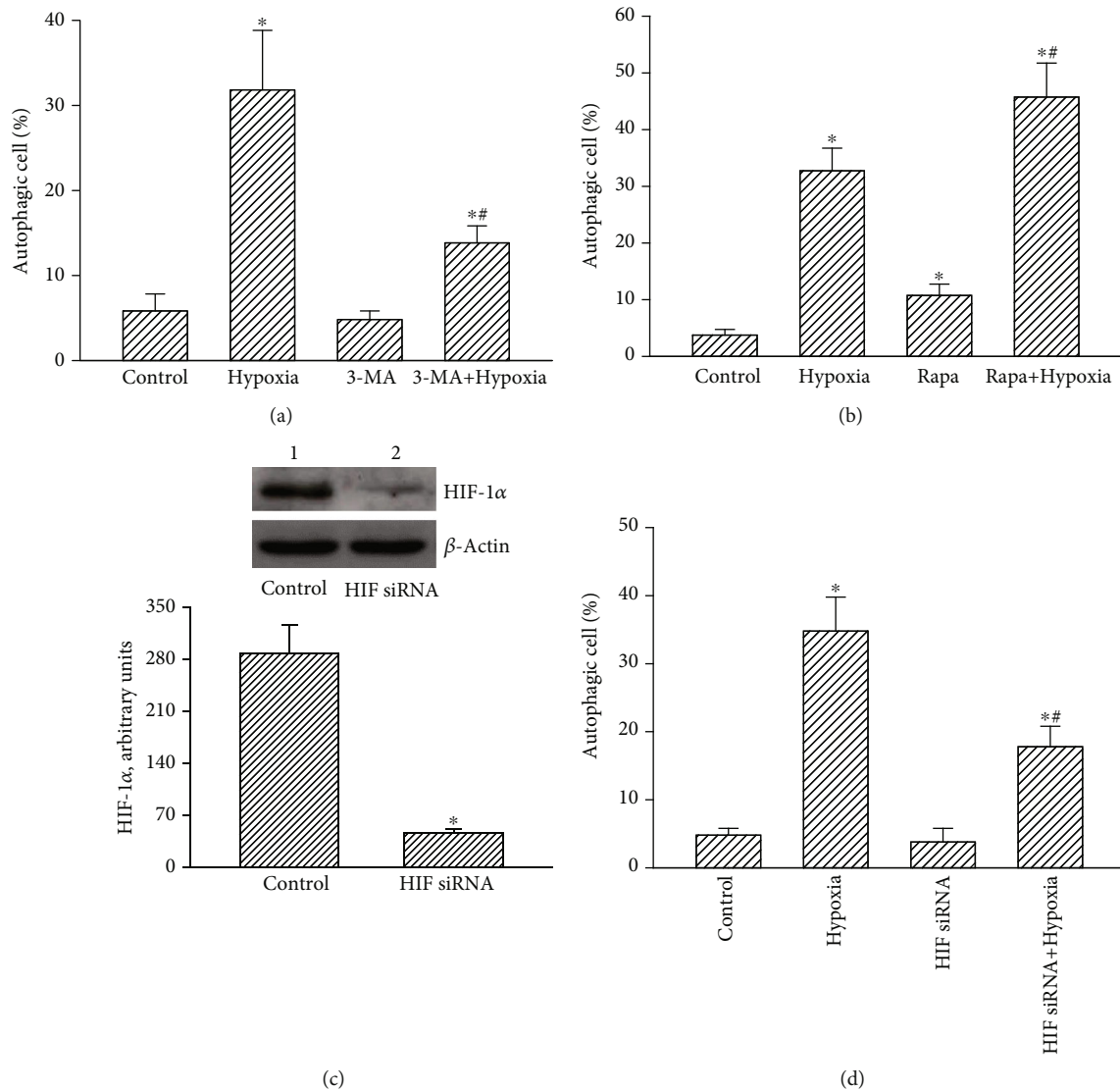
FIGURE 4: Effects of 3-methyladenine (3-MA), rapamycin (Rapa), and hypoxia-inducible factor- (HIF-) 1α knockdown on autophagy of human drug-resistant glioblastoma cells. Human temozolomide- (TMZ-) resistant U87 MG-R glioblastoma cells were selected from TMZ-sensitive U87 MG cells. (a, b) Human U87 MG-R glioblastoma cells were pretreated with 3-MA at 1 mM or Rapa at 0.5 μM for 1 h and then exposed to hypoxia for additional 24 h. Control cells received DMSO only. A flow cytometric method was carried out to quantify autophagic cells. (c) Human U87 MG-R cells were treated with HIF-1α small interfering (si) RNA (HIF siRNA) for 48 h. Scrambled siRNA was applied to control cells as the negative control (control). HIF-1α was immunodetected, and β-actin was analyzed as the internal control. These protein bands were quantified and statistically analyzed. (d) Human U87 MG-R cells were pretreated with HIF-1α siRNA and then exposed to hypoxia. Autophagic cells were quantified using flow cytometry. Data are expressed as the mean ± SD for $n =$ 6. $^{*}p < 0.05$ vs. control and $^{\#}p < 0.05$ vs. U87 MG.

vesicles organelle (Figure 3(d), left panel). A flow cytometric examination revealed that exposure to CoCl$_2$ for 6 h increased acidic vesicular organelles in human drug-tolerant glioblastoma cells by 12% (right panel). Following CoCl$_2$ treatment for 12 and 24 h, autophagic cells were, respectively, increased 26% and 38%. An immunoblot image shows that LC3-I and -II in untreated U87 MG-R cells were detected (Figure 3(e), top panels, lane 1). Administration of CoCl$_2$ for 24 h decreased levels of LC3-I but increased amounts of LC3-II (lane 2). β-Actin was immunodetected as the internal loading standard (bottom panel). Hypoxic treatment decreased of LC3-I by 69% but increased of LC3-II by 240% in TMZ-resistant glio-

blastoma cells (Figure 3(f)). Meanwhile, the CoCl$_2$-induced hypoxia caused 39% of mouse GL261-R cells to undergo autophagy (Figure 3(g)).

3.4. CoCl$_2$ Induced Hypoxic Insults to Human Drug-Resistant Glioblastoma Cells via a HIF-1α-Dependent Mechanism. Loss- and gain-of-function strategies were conducted to confirm the effects of the CoCl$_2$-induced hypoxia on autophagic insults to TMZ-tolerant glioblastoma cells (Figures 4(a) and 4(b)). Administration of CoCl$_2$ induced autophagy of human drug-resistant U87 MG-R cells by 32% (Figure 4(a)). In the control group, pretreatment with 3-MA alone did not trigger

cell autophagy. However, administration of 3-MA attenuated hypoxia-induced autophagic insults to human U87 MG-R cells by 69% (Figure 4(a)). In contrast, pretreatment of human drug-tolerant glioblastoma cells with rapamycin did not influence cell autophagy (Figure 4(b)). Nevertheless, pretreatment with rapamycin increased hypoxia-induced autophagic insults to U87 MG-R cells by 45%.

At the same time, roles of HIF-1α in CoCl$_2$-induced autophagy of human drug-resistant U87 MG-R glioblastoma cells were further investigated (Figures 4(c) and 4(d)). Application of HIF-1α small interfering (si) RNA to human U87 MG-R cells for 48 h caused obvious attenuation of HIF-1α levels compared to untreated cells (Figure 4(c), top panel). Protein bands were quantified using β-actin as the loading control, and the data were statistically analyzed. After application of HIF-1α siRNA, levels of HIF-1α in human U87 MG-R cells were reduced by 83% (Figure 4(c), bottom panel). The CoCl$_2$-induced hypoxia triggered 35% of U87 MG-R cells undergoing autophagy (Figure 4(d)). Application of HIF-1α siRNA to human TMZ-resistant glioblastoma cells did not trigger cell autophagy. In comparison, knocking down HIF-1α translation concurrently suppressed 57% of hypoxia-induced autophagic insults to human U87 MG-R cells (Figure 4(d)).

3.5. The CoCl$_2$-Induced Hypoxia Sequentially Decreased Levels of PI3K and Subsequent Phosphorylation of AKT and mTOR in Human Drug-Resistant Glioblastoma Cells. Molecular mechanisms of CoCl$_2$-induced insults to human TMZ-tolerant glioblastoma cells were further investigated (Figure 5). In the control group, PI3K was immunodetected in human U87 MG-R glioblastoma cells (Figure 5(a), top panel, lane 1). In contrast, administration of CoCl$_2$ to human glioblastoma cells obviously decreased levels of PI3K (lane 2). Intensities of these protein bands were measured using β-actin as a loading standard (bottom panel), and the data were statistically analyzed (Figure 5(b)). Exposure to hypoxia caused a 77% reduction in PI3K levels in human U87 MG-R cells (Figure 5(b)). Consecutively, AKT phosphorylation in U87 MG-R cells was alleviated following exposure to CoCl$_2$ compared to the control group (Figure 5(c), top panel). AKT and β-actin were measured as internal controls (bottom two panels). The CoCl$_2$-induced hypoxia diminished phosphorylation of AKT in human TMZ-resistant glioblastoma cells by 89% (Figure 5(d)). Consequently, hypoxia reduced mTOR phosphorylation in human U87 MG-R cells (Figure 5(e), top panel). mTOR and β-actin were measured as the internal controls (bottom two panels). Exposure of human drug-tolerant glioblastoma cells to hypoxia led to 91% repression of mTOR phosphorylation (Figure 5(f)).

3.6. Hypoxia Induced by CoCl$_2$ Triggered Autophagy and Subsequent Apoptosis of Human and Mouse Drug-Resistant Glioblastoma Cells. Treatment of human drug-resistant glioblastoma cells with CoCl$_2$ enhanced the activity of caspase-3 by 2.5-fold (Figure 6(a)). Pretreatment with 3-MA did change activation of caspase-3. Nonetheless, 3-MA lowered hypoxia-induced caspase-3 activation by 62% (Figure 6(a)). Sequentially, caspase-6 activity in human U87 MG-R glio-

blastoma cells increased 2.5-fold (Figure 6(b)). Pretreatment with 3-MA alone did not affect caspase-6 activity but attenuated CoCl$_2$-triggered activation of caspase-6 by 52%. Exposure to CoCl$_2$ led to a 2.5-fold induction of DNA fragmentation in U87 MG-R cells (Figure 6(c)). In parallel, hypoxia triggered 29% of human U87 MG-R cells to undergo apoptosis (Figure 6(d)). Pretreatment with 3-MA did not affect the DNA integrity or cell apoptosis. In contrast, pretreatment of human TMZ-tolerant glioblastoma cells with 3-MA caused significant 76% and 72% depressions in hypoxia-induced DNA fragmentation and cell apoptosis, respectively (Figures 6(c) and 6(d)). In addition, administration of hypoxia augmented caspase-3 activities by twofold in mouse GL261-R cells (Figure 6(e)). Subsequently, exposure of mouse drug-resistant GL261-R cells to CoCl$_2$ caused a significant 2.3-fold stimulation of DNA fragmentation (Figure 6(f)). Accordingly, apoptotic insults to mouse drug-resistant glioblastoma cells were induced by 31% after CoCl$_2$ administration (Figure 6(g)).

3.7. Exposure to Hypoxia for 96 h Induced Apoptotic Insults to Human Drug-Resistant Glioblastoma Cells without Affecting Human Normal Astrocytes. Treatment of human U87 MG-R cells to CoCl$_2$ for 96 h decreased cell viability by 92% (Figure 7(a)). In addition, exposure to CoCl$_2$ for 96 h caused 16% and 88% of human drug-resistant glioblastoma cells undergoing autophagy and apoptosis, respectively (Figures 7(b) and 7(c)). The safety of CoCl$_2$ to human normal HA-h astrocytes was then evaluated (Figures 7(d)–7(f)). Exposure of HA-h cells to 100 μM CoCl$_2$ for 96 h did not influence cell viability (Figure 7(d)). In contrast, treatment with CoCl$_2$ for 96 h led to a slight 21% induction of HA-h cells undergoing autophagy but did not trigger apoptotic insults (Figures 7(e) and 7(f)).

4. Discussion

Administration of CoCl$_2$ can induce hypoxic conditions and consequent autophagic apoptosis of drug-resistant glioblastoma cells. In this study, we demonstrated that exposure to CoCl$_2$ could trigger hypoxic stress to human and murine TMZ-resistant glioblastoma cells. In parallel, hypoxic conditions disrupted mitochondrial ATP synthesis and induced death of cells of these two drug-resistant glioblastoma cell lines. In addition, hypoxia suppressed proliferation of human TMZ-tolerant glioblastoma cells. GBM is the commonest and most aggressive brain tumor [1]. Inopportunely, GBM patients have very poor prognoses because most patients eventually have become drug-resistant and recurrent [3]. To the present, TMZ is routinely used as the first-line drug for treatment of GBM patients [2]. The malignance of glioblastomas can be elucidated because following surgery, residual glioblastoma cells can rapidly proliferate, migrate, and invade to the other sites for development of new brain tumors. Hypoxia is able to suppress proliferation and viability of drug-sensitive glioblastoma cells [25]. In the present study, we further identified the beneficial actions of the CoCl$_2$-induced hypoxic conditions to suppress proliferation and survival of TMZ-resistant glioblastoma cells. As to the

(a)

(b)

(c)

(d)

(e)

(f)
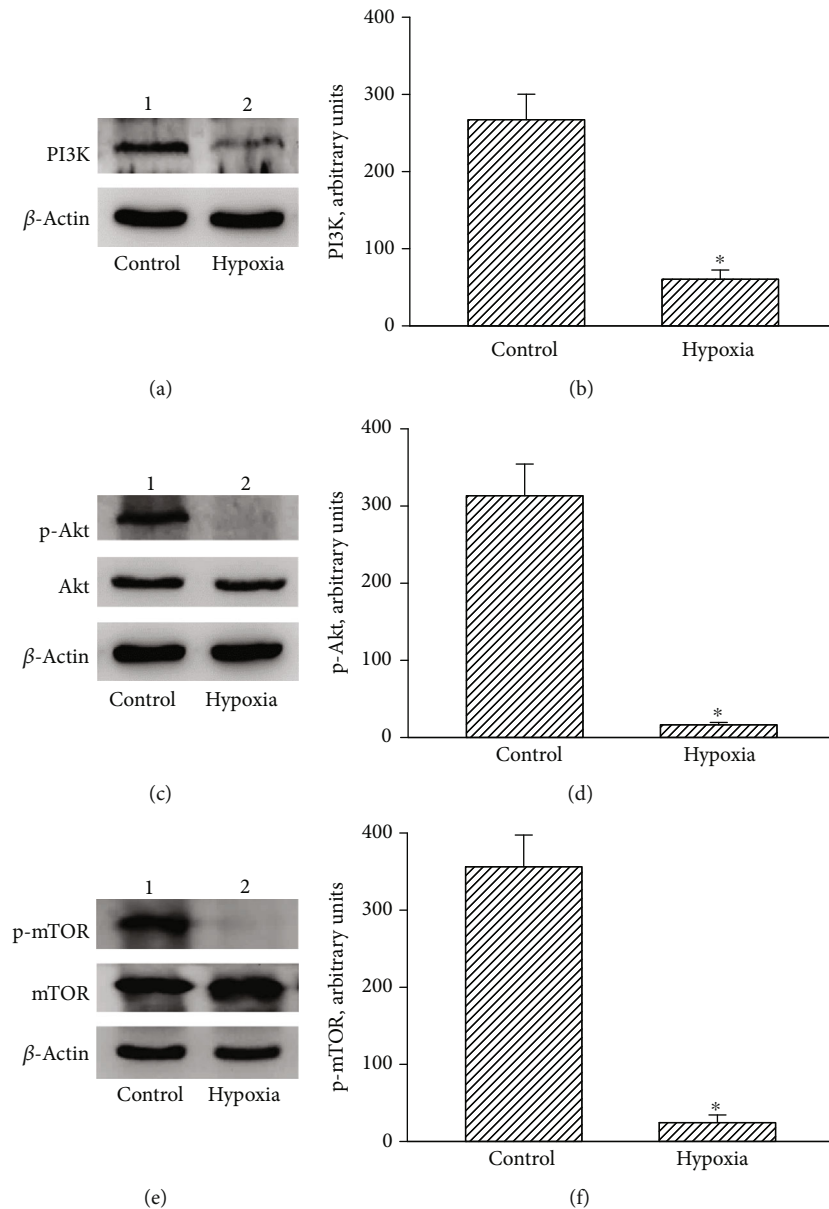
FIGURE 5: Signal-transducing mechanisms involved in hypoxia-induced autophagy of human drug-resistant glioblastoma cells. Human TMZ-tolerant U87 MG-R cells were selected from TMZ-sensitive U87 MG cells. Human U87 MG-R cells were treated with hypoxia for 24 h. (a, c, e) Levels of phosphoinositide 3-kinase (PI3K), phosphorylated- (p-) AKT, and p-mammalian target of rapamycin (mTOR) were immunodetected (top panels). β-Actin, AKT, and mTOR were analyzed as the internal controls for detection of PI3K, p-AKT, and p-mTOR, respectively (bottom panels). (b, d, f) These immunorelated protein bands were quantified and statistically analyzed. Data are expressed as the mean $\pm$ SD for $n = 6$. $^{*}p < 0.05$ vs. control.

mechanisms, administration of hypoxic stress meaningfully induced autophagy and subsequent apoptosis of human and murine drug-resistant glioblastoma cells. In response to malnutrition, cells can temporarily survive by activating a process of self-degradation and catabolism, called autophagy [17]. Autophagic cells will subsequently either survive or proceed to necrosis or apoptosis [17, 18]. Furthermore, autophagy was also shown to be involved in the prevention of certain diseases, including tumors [26]. The drug-resistant glioblastoma cells highly defend against apoptosis. Recently,

we demonstrated advantages of a longer period of hypoxia induced by honokiol, a multifunctional antitumor drug, on the killing of human neuroblastoma cells and glioblastoma cells via an autophagic apoptosis pathway [23–25]. Recently, autophagic cell death has attracted researchers as a potential method for cancer therapy. In this study, we provide serial evidence to show the benefits of $CoCl_2$-induced hypoxia of killing drug-resistant glioblastoma cells through activating an autophagic and subsequent apoptotic mechanism. As a result, longer hypoxia induced by certain agents such as
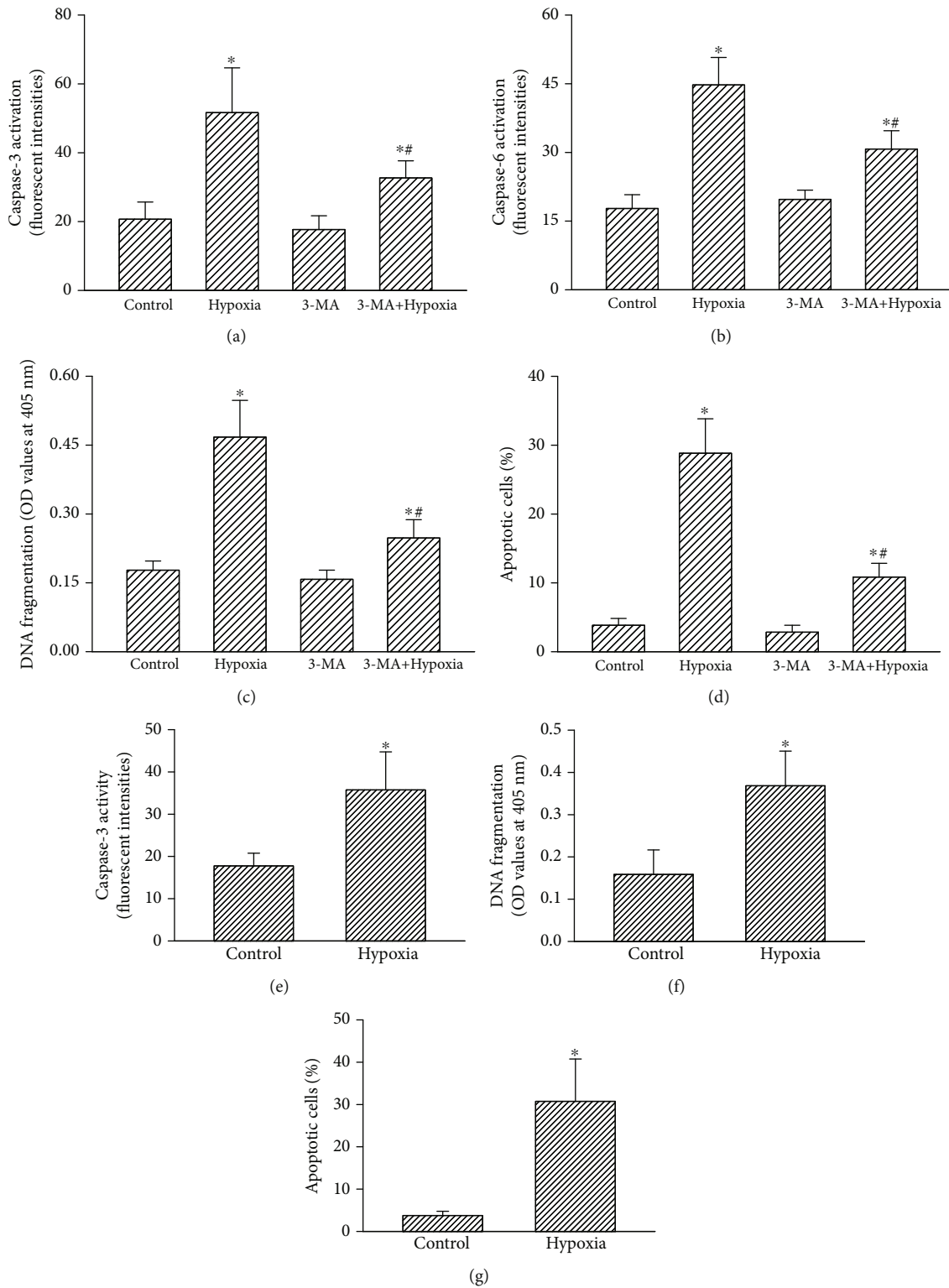
FIGURE 6: Effects of 3-MA on hypoxia-induced cascade activation of caspases-3 and -6, DNA fragmentation, and cell apoptosis in human drug-resistant glioblastoma cells. Human U87 MG-R glioblastoma cells were pretreated with 1 mM 3-MA for 1 h. Then, the cells were treated with hypoxia for 24 h. (a, b) Cascade activation of caspase-3 and caspase-6 were examined with a fluorometric substrate assay. (c, d) DNA fragmentation and apoptotic cells were analyzed. Mouse GL261-R glioblastoma cells were exposed to hypoxia for 24 h. (e–g) Caspase-3 activity, DNA fragmentation, and apoptotic cells were assayed. Data are expressed as the mean ± SD for $n = 6$. $^*p < 0.05$ vs. control and $^\#p < 0.05$ vs. U87 MG.
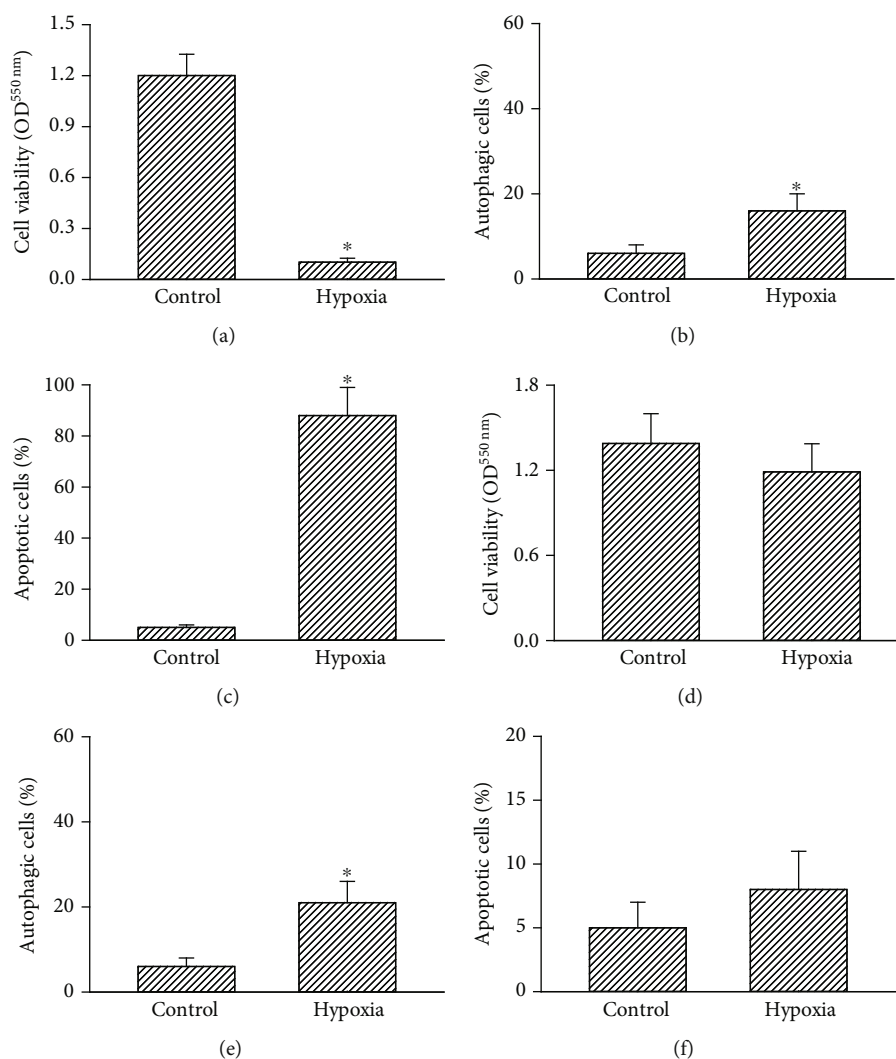
FIGURE 7: Effects of CoCl$_2$ treatment for 96 h on viability, autophagy, and apoptosis of human drug-resistant glioblastoma cells and normal astrocytes. (a–c) Human temozolomide- (TMZ-) resistant U87 MG-R glioblastoma cells and (d–f) human HA-h astrocytes were exposed to CoCl$_2$ for 96 h. (a, d) Cell viability was assayed using a colorimetric method. (b, e) Autophagic and (c, f) apoptotic cells were quantified using flow cytometry. Each value represents the mean ± SD for $n = 3$. The symbol * indicates that a value significantly ($p < 0.05$) differed from the respective control group.

CoCl$_2$ or honokiol may be clinically applied as a *de novo* strategy for treating chemoresistance in malignant and recurrent glioblastomas via an autophagic apoptosis pathway.

Administration of CoCl$_2$ led to hypoxic stress and consequently induced insults to human and murine TMZ-resistant glioblastoma cells. Drug-resistant glioblastoma cells used in this study were prepared according to a continuous selection protocol described in our previous study [37]. Compared to chemosensitive human U87 MZ and mouse GL261 cells, these two TMZ-resistant U87 MZ-R and GL261-R cell lines have similar morphologies. Nevertheless, administration of TMZ induced apoptotic insults to human and mouse TMZ-sensitive glioblastoma cells but did not affect chemoresistant cells. Fascinatingly, exposure to CoCl$_2$ time-dependently raises levels of HIF-1α in drug-resistant glioblastoma cells. In the hypoxic microenvironment, HIF-1/2α, two transcriptional factors, can be massively induced to regulate certain gene expressions in response to oxygen deficiency-induced stress [16]. CoCl$_2$ can chelate Fe^{2+} ions in hemoglobin to decrease the oxygen supply to cells [38]. Additionally, administration of CoCl$_2$ raises levels of cellular HIF-1α by inhibiting the activity of prolyl-4-hydroxylase, a HIF-1α-specific proteinase [39]. Thus, CoCl$_2$ can elevate levels of HIF-1α in human and mouse TMZ-resistant glioblastoma cells and induce intracellular hypoxic stress. At the same time, the CoCl$_2$-induced hypoxia diminished proliferation and survival of drug-resistant glioblastoma cells. In tumorigenesis, hypoxia can stimulate the proliferation of tumor cells via a HIF-1α-dependent transcriptional mechanism [40]. Nonetheless, Dai et al. reported that in a CoCl$_2$-induced hypoxic microenvironment, proliferation and viability of PC-2 cells were lessened, and the cells underwent apoptosis [41]. Our previous studies also demonstrated the oppressive effects CoCl$_2$ on the proliferation and survival of drug-sensitive

glioblastoma cells [25]. In parallel, enzyme activity of mitochondrial NAD(P)H oxidoreductase and levels of cellular ATP in human TMZ-resistant glioblastoma cells were repressed following exposure to hypoxia. Thus, the $CoCl_2$-induced hypoxia suppressed proliferation and survival of drug-resistant glioblastoma cells via lowering mitochondrial ATP synthesis. However, the reasons explain the relation between ATP reductions on suppression of cell proliferation in hypoxia-treated drug-resistant glioblastoma cells need to be further investigated.

Hypoxia induced by $CoCl_2$ can trigger autophagy of human and murine drug-resistant glioblastoma cells via a HIF-1α-dependent pathway. Our flow cytometric analysis of acidic vesicular organelles in human and mouse drug-tolerant glioblastoma cells revealed that administration of $CoCl_2$ time-dependently induced autophagic insults. Simultaneously, the ratio of LC3-II over LC3-I significantly increased after exposure to $CoCl_2$. When the cells are undergoing autophagy, acidic vesicular organelles were formed [23, 42]. At the same time, the ratio of LC3-II over LC3-I was enhanced. In this study, we further used gain- and loss-of-function strategies to confirm the hypoxia-induced autophagy of TMZ-resistant glioblastoma cells. As usual, 3-MA and rapamycin were applied as a respective inhibitor and an inducer of cell autophagy [43]. After administration of 3-MA and rapamycin to chemoresistant glioblastoma cells, hypoxia-induced autophagic insults were, respectively, attenuated and enhanced. Thus, multiple lines of evidence showed the action of the $CoCl_2$-induced hypoxia in inducing autophagy of drug-resistant glioblastoma cells, thereby inducing autophagic insults to TMZ-resistant glioblastoma cells. More interestingly, knocking down HIF-1α concurrently lowered $CoCl_2$-induced autophagic insults to human TMZ-resistant glioblastoma cells. HIF-1α can induce cell autophagy via inducing BNIP3 and LC3 expressions [22]. In addition, a previous study reported that prolonged hypoxia induced mitochondrial autophagy via activation of a HIF-1α/BINP3/-Beclin-1/Atg5 mechanism [44]. In the present study, exposure to $CoCl_2$ led to consequent mitochondrial dysfunction. As a result, one possible mechanism explaining $CoCl_2$-induced autophagy of human drug-resistant glioblastoma cells is via triggering HIF-1α-dependent mitochondrial autophagy. Being a potential target for cancer therapy, autophagy has recently attracted attention of oncologic physicians and researchers [45]. Chemoresistance and recurrence are two critical factors driving malignance and poor prognoses of GBM patients [6]. In this study, we provide *in vitro* evidence to demonstrate the potential effects of prolonged hypoxia induced by $CoCl_2$ for treating GBM by inducing autophagic insults to drug-resistant glioblastomas.

Hypoxia induced by $CoCl_2$ led to autophagy of human drug-resistant glioblastoma cells through targeting the PI3K-AKT-mTOR pathway. After exposure to $CoCl_2$, levels of PI3K in human TMZ-resistant glioblastoma cells were significantly diminished. In tumorigenesis, PI3K is genetically overexpressed or mutated in the brain, breasts, prostate, stomach, colon, and endometrium [46]. So, targeting PI3K was investigated as a new strategy for treating various types of tumors such as breast cancer [47]. AKT is a downstream
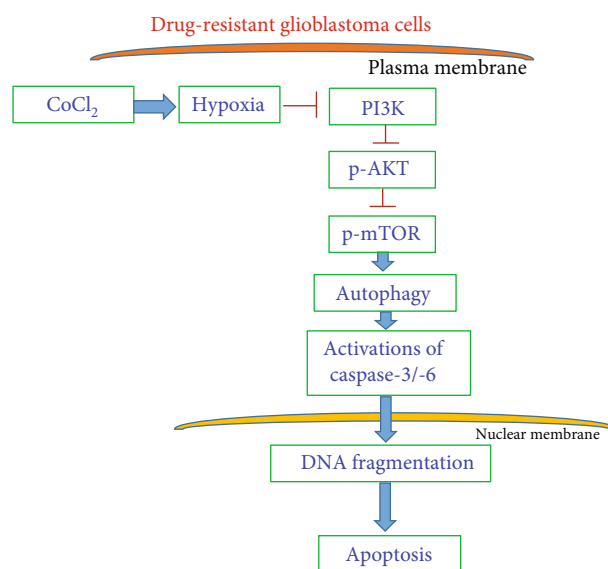
FIGURE 8: Proposed signal-transducing pathways of hypoxia-induced autophagy and subsequently apoptotic killing of human drug-resistant glioblastoma cells. Treatment of human TMZ-resistant glioblastoma cells with $CoCl_2$ induces hypoxic insults by suppressing phosphoinositide 3-kinase- (PI3K-) involved signal-transducing phosphorylations of AKT and mammalian target of rapamycin (mTOR). Consequently, long-period administration of $CoCl_2$ induced cascade activation of caspases-3 and -6, DNA breakage, and apoptotic insults to human drug-resistant glioblastoma cells.

target of PI3K. Our present data reveal that treatment with $CoCl_2$ decreased levels of AKT in human drug-tolerant glioblastoma cells. Hence, the hypoxia-induced downregulation of AKT was due to suppression of PI3K production. Inhibition of the PI3K/AKT pathway is recognized as a new weapon for fighting cancer incidence [46]. Our present data prove the suppressive effects of $CoCl_2$ against the proliferation of human TMZ-resistant glioblastoma cells. Thus, the hypoxia-induced blockage of the PI3K-AKT pathway may be beneficial for inhibiting the growth of chemoresistant glioblastomas. mTOR, a serine/threonine protein kinase, plays a crucial role in the balance between catabolism and anabolism [48]. Phosphorylation of mTOR, activated by the PI3K-AKT pathway, can drive cellular catabolism and depress cell autophagy [49]. In parallel with an interruption of the PI3K/AKT pathway, $CoCl_2$ weakened phosphorylation of mTOR in human TMZ-resistant glioblastoma cells. Hence, one possible mechanism explaining the $CoCl_2$-induced reduction in levels of phosphorylated mTOR in TMZ-resistant glioblastomas is due to disruption of the PI3K-AKT pathway. In addition to HIF-1α, HIF-2α is another factor that can be upregulated by hypoxia [16]. Under hypoxic conditions, the proteasome-dependent stability of HIF-1/2α is involved in regulation of tumor-induced angiogenesis and metastasis via the PI3K/AKT pathway [50]. In aggressive neuroblastomas, Mohlin et al. reported that suppression of HIF-2α by targeting PI3K/mTORC1 can improve therapeutic efficacy [51]. This study demonstrated that knocking down HIF-1α simultaneously attenuated hypoxia-induced

cell autophagy. Therefore, the CoCl$_2$-induced hypoxia can trigger autophagic insults to drug-resistant glioblastoma cells via targeting the PI3K-AKT-mTOR pathway.

Hypoxia induced by CoCl$_2$ triggered autophagic apoptosis of human and murine drug-resistant glioblastoma cells. Prolonged exposure to CoCl$_2$ of human and murine TMZ-resistant glioblastoma cells induced cascade activation of caspases-3 and -6, DNA fragmentation, and cell cycle arrest at the sub-G$_1$ phase. Caspase activation, DNA fragmented damage, and cell cycle arrest are characteristic features indicating that cells are undergoing apoptosis [52, 53]. Interestingly, pretreatment of human TMZ-resistant glioblastoma cells with 3-MA reduced hypoxia-induced autophagy. At the same time, CoCl$_2$-induced cascade activation of caspases-3 and -6, DNA breakage, and apoptosis in human TMZ-tolerant glioblastoma cells were significantly lowered following pretreatment with 3-MA. Autophagic cells will survive or proceed to die [17, 18]. Our present data showed that prolonged administration of CoCl$_2$ can induce autophagic insults to TMZ-resistant glioblastoma cells, resulting in cell death via an apoptotic mechanism. Autophagic cell death is recognized as a separate form of cell death from cell apoptosis and necrosis [54]. Nonetheless, our present study showed that CoCl$_2$ can trigger autophagic apoptosis of human TMZ-tolerant glioblastoma cells. Specific induction of apoptosis of tumor cells can be applied as an anticancer mechanism for cancer therapy [53]. However, GBM is a very aggressive tumor because it is usually hard to induce apoptosis in glioblastoma cells by chemotherapeutic drugs [55]. Therefore, hypoxia-induced autophagic apoptosis has the potential to serve as an alternative strategy for therapy of brain tumors.

5. Conclusions

In this study, we successfully selected human and mouse drug-resistant glioblastoma cells as our experimental models. Exposure of human and mouse TMZ-resistant glioblastoma cells to CoCl$_2$ increased HIF-1α levels and induced hypoxic stress and insults (Figure 8). Subsequently, prolonged hypoxia induced by CoCl$_2$ led to mitochondrial dysfunction. Interestingly, administration of hypoxia elevated proportions of drug-resistant glioblastoma cells with acidic organelles and the ratio of cellular LC3-II over LC3-I. Loss- and gain-of-function strategies were used to further demonstrate that pretreatment with 3-MA and rapamycin, respectively, attenuated and enhanced consequent CoCl$_2$-induced cell autophagy. Importantly, knocking down HIF-1α translation using RNAi concurrently diminished CoCl$_2$-induced cell autophagy. Thus, these manifold lines of evidence showed that prolonged hypoxia induced by CoCl$_2$ could trigger hypoxic insults to human and mouse TMZ-resistant glioblastoma cells via a HIF-1α-dependent mechanism. As to the mechanisms, administration of CoCl$_2$ decreased signal-transducing activation of PI3K and AKT (Figure 8). Successively, levels of phosphorylated mTOR in human drug-resistant glioblastoma cells were reduced by CoCl$_2$. Fascinatingly, prolonged administration of hypoxia sequentially induced cascade activation of caspases-3 and -6, DNA fragmentation, and apoptotic insults in TMZ-tolerant glioblastoma cells (Figure 8). Using 3-MA

to suppress CoCl$_2$-induced autophagy simultaneously defended against apoptotic damage. Therefore, this study showed that prolonged hypoxia induced by CoCl$_2$ can induce autophagic apoptosis of drug-resistant glioblastoma cells via suppression of the PI3K-AKT-mTOR pathway (Figure 8). To the present, chemoresistance and recurrence are the most serious issues and challenges for therapy of GBM patients. CoCl$_2$-induced hypoxia and subsequent autophagic apoptosis may be a *de novo* strategy for treating glioblastomas. We are carrying out a translational study to further confirm our *in vitro* findings.

Data Availability

All data generated or analyzed during this study are included in this article.

Conflicts of Interest

The authors declare that there is no conflict of interest.

Authors' Contributions

Y.-W. Lee and Y.-G. Cherng equally contribute to this scientific work.

Acknowledgments

Supplementary Materials

Figure S1: effects of CoCl$_2$ on levels of vimentin in human drug-resistant glioblastoma cells. Human TMZ-tolerant U87 MG-R cells were selected from TMZ-sensitive U87 MG cells. U87 MG-R glioblastoma cells were treated with hypoxia for 6, 12, and 24 h. (a) Levels of vimentin were immunodetected. β-Actin was analyzed as the internal control. (b) These immunorelated protein bands were quantified and statistically analyzed. Data are expressed as the mean ± SD for $n = 3$. (*Supplementary materials*)

References

[1] C. M. Jackson, J. Choi, and M. Lim, "Mechanisms of immunotherapy resistance: lessons from glioblastoma," *Nature Immunology*, vol. 20, no. 9, pp. 1100–1109, 2019.

[2] F. Sharifzad, S. Ghavami, J. Verdi et al., "Glioblastoma cancer stem cell biology: potential theranostic targets," *Drug Resistance Updates*, vol. 42, pp. 35–45, 2019.

[3] D. Fabian, M. Guillermo Prieto Eibl, I. Alnahhas et al., "Treatment of glioblastoma (GBM) with the addition of tumor-treating fields (TTF): a review," *Cancers*, vol. 11, no. 2, p. 174, 2019.

[4] W. Tomaszewski, L. Sanchez-Perez, T. F. Gajewski, and J. H. Sampson, "Brain tumor microenvironment and host state: implications for immunotherapy," *Clinical Cancer Research*, vol. 25, no. 14, pp. 4202–4210, 2019.

[5] J. Adhikaree, J. Moreno-Vicente, A. P. Kaur, A. M. Jackson, and P. M. Patel, "Resistance mechanisms and barriers to successful immunotherapy for treating glioblastoma," *Cell*, vol. 9, no. 2, p. 263, 2020.

[6] A. Kirstein, T. E. Schmid, and S. E. Combs, "The role of miRNA for the treatment of MGMT unmethylated glioblastoma multiforme," *Cancers*, vol. 12, article E1099, 2020.

[7] B. W. Wong, E. Marsch, L. Treps, M. Baes, and P. Carmeliet, "Endothelial cell metabolism in health and disease: impact of hypoxia," *The EMBO Journal*, vol. 36, no. 15, pp. 2187–2203, 2017.

[8] C. Nyakas, B. Buwalda, and P. G. Luiten, "Hypoxia and brain development," *Progress in Neurobiology*, vol. 49, no. 1, pp. 1–51, 1996.

[9] J. W. Lee, J. Ko, C. Ju, and H. K. Eltzschig, "Hypoxia signaling in human diseases and therapeutic targets," *Experimental & Molecular Medicine*, vol. 51, no. 12, pp. 1–13, 2019.

[10] N. N. Nalivaeva, A. J. Turner, and I. A. Zhuravin, "Role of prenatal hypoxia in brain development, cognitive functions, and neurodegeneration," *Frontiers in Neuroscience*, vol. 12, p. 825, 2018.

[11] R. Kunze and H. H. Marti, "Angioneurins- key regulators of blood-brain barrier integrity during hypoxic and ischemic brain injury," *Progress in Neurobiology*, vol. 178, p. 101611, 2019.

[12] F. Irani, J. M. Barbone, J. Beausoleil, and L. Gerald, "Is asthma associated with cognitive impairments? A meta-analytic review.," *Journal of Clinical and Experimental Neuropsychology*, vol. 39, no. 10, pp. 965–978, 2017.

[13] S. Jawhari, M. H. Ratinaud, and M. Verdier, "Glioblastoma, hypoxia and autophagy: a survival-prone 'ménage-à-trois'," *Cell Death & Disease*, vol. 7, no. 10, article e2434, 2016.

[14] S. Nicolas, S. Abdellatef, M. A. Haddad, I. Fakhoury, and M. El-Sibai, "Hypoxia and EGF stimulation regulate VEGF expression in human glioblastoma multiforme (GBM) cells by differential regulation of the PI3K/Rho-GTPase and MAPK pathways," *Cell*, vol. 8, no. 11, p. 1397, 2019.

[15] G. Gabriely, M. A. Wheeler, M. C. Takenaka, and F. J. Quintana, "Role of AHR and HIF-1α in glioblastoma metabolism," *Trends in Endocrinology and Metabolism*, vol. 28, no. 6, pp. 428–436, 2017.

[16] L. Holmquist-Mengelbier, E. Fredlund, T. Löfstedt et al., "Recruitment of HIF-1α and HIF-2α to common target genes is differentially regulated in neuroblastoma: HIF-2α promotes an aggressive phenotype," *Cancer Cell*, vol. 10, no. 5, pp. 413–423, 2006.

[17] D. Glick, S. Barth, and K. F. Macleod, "Autophagy: cellular and molecular mechanisms," *The Journal of Pathology*, vol. 221, no. 1, pp. 3–12, 2010.

[18] A. K. Yadav, P. K. Yadav, G. R. Chaudhary et al., "Autophagy in hypoxic ovary," *Cellular and Molecular Life Sciences*, vol. 76, no. 17, pp. 3311–3322, 2019.

[19] D. G. Hardie, "Sensing of energy and nutrients by AMP-activated protein kinase," *The American Journal of Clinical Nutrition*, vol. 93, no. 4, pp. 891S–896S, 2011.

[20] F. Chiacchiera and C. Simone, "Inhibition of p38alpha unveils an AMPK-FoxO3A axis linking autophagy to cancer-specific metabolism," *Autophagy*, vol. 5, no. 7, pp. 1030–1033, 2009.

[21] J. Pouyssegur, F. Dayan, and N. M. Mazure, "Hypoxia signalling in cancer and approaches to enforce tumour regression," *Nature*, vol. 441, no. 7092, pp. 437–443, 2006.

[22] G. Bellot, R. Garcia-Medina, P. Gounon et al., "Hypoxia-induced autophagy is mediated through hypoxia-inducible factor induction of BNIP3 and BNIP3L via their BH3 domains," *Molecular and Cellular Biology*, vol. 29, no. 10, pp. 2570–2581, 2009.

[23] P. S. Yeh, W. Wang, Y. A. Chang, C. J. Lin, J. J. Wang, and R. M. Chen, "Honokiol induces autophagy of neuroblastoma cells through activating the PI3K/Akt/mTOR and endoplasmic reticular stress/ERK1/2 signaling pathways and suppressing cell migration," *Cancer Letters*, vol. 370, no. 1, pp. 66–77, 2016.

[24] M. C. Lin, Y. W. Lin, Y. Y. Tseng, Y. W. Lee, J. T. Chen, and R. M. Chen, "Honokiol induces autophagy and successive apoptotic insults to neuroblastomas via a p53-dependent mechanism," *The American Journal of Chinese Medicine*, vol. 47, pp. 859–912, 2019.

[25] B. C. Cheng, J. T. Chen, S. T. Yang, C. C. Chio, S. H. Liu, and R. M. Chen, "Cobalt chloride treatment induces autophagic apoptosis in human glioma cells via a p53-dependent pathway," *International Journal of Oncology*, vol. 50, no. 3, pp. 964–974, 2017.

[26] K. R. Parzych and D. J. Klionsky, "An overview of autophagy: morphology, mechanism, and regulation," *Antioxidants & Redox Signaling*, vol. 20, no. 3, pp. 460–473, 2014.

[27] P. S. Yeh, J. T. Chen, Y. G. Cherng, S. T. Yang, Y. T. Tai, and R. M. Chen, "Methylpiperidinopyrazole attenuates estrogen-induced mitochondrial energy production and subsequent osteoblast maturation via an estrogen receptor alpha-dependent mechanism," *Molecules*, vol. 25, no. 12, p. 2876, 2020.

[28] M. H. Ho, M. H. Liao, Y. L. Lin, C. H. Lai, P. I. Lin, and R. M. Chen, "Improving effects of chitosan nanofiber scaffolds on osteoblast proliferation and maturation," *International Journal of Nanomedicine*, vol. 9, pp. 4293–4304, 2014.

[29] C. J. Lin, Y. A. Chang, Y. L. Lin, C. C. Chio, and R. M. Chen, "Preclinical effects of honokiol on treating glioblastoma multiforme via G1 phase arrest and cell apoptosis," *Phytomedicine*, vol. 23, no. 5, pp. 517–527, 2016.

[30] R. M. Chen, C. H. Wu, H. C. Chang et al., "Propofol suppresses macrophage functions through modulating mitochondrial membrane potential and cellular adenosine triphosphate levels," *Anesthesiology*, vol. 98, no. 5, pp. 1178–1185, 2003.

[31] C. C. Chio, L. Wei, T. G. Chen et al., "Neuron-derived orphan receptor 1 transduces survival signals in neuronal cells in response to hypoxia-induced apoptotic insults," *Journal of Neurosurgery*, vol. 124, no. 6, pp. 1654–1664, 2016.

[32] J. W. Lin, J. T. Chen, C. Y. Hong et al., "Honokiol traverses the blood-brain barrier and induces apoptosis of neuroblastoma cells via an intrinsic Bax-mitochondrion-cytochrome c-caspase protease pathway," *Neuro-Oncology*, vol. 14, no. 3, pp. 302–314, 2012.

[33] C. C. Chio, J. W. Lin, H. A. Cheng et al., "MicroRNA-210 targets antiapoptotic Bcl-2 expression and mediates hypoxia-

induced apoptosis of neuroblastoma cells," *Archives of Toxicology*, vol. 87, pp. 458–468, 2013.

[34] C. J. Lin, T. L. Chen, Y. Y. Tseng et al., "Honokiol induces autophagic cell death in malignant glioma through reactive oxygen species-mediated regulation of the p53/PI3K/Akt/mTOR signaling pathway," *Toxicology and Applied Pharmacology*, vol. 304, pp. 59–69, 2016.

[35] C. C. Chio, Y. T. Tai, M. Mohanraj, S. H. Liu, S. T. Yang, and R. M. Chen, "Honokiol improves temozolomide-induced apoptotic insults to malignant glioma cells via an intrinsic mitochondria-dependent pathway," *Phytomedicine*, vol. 49, pp. 41–51, 2018.

[36] D. P. Sun, Y. W. Lee, J. T. Chen, Y. W. Lin, and R. M. Chen, "The bradykinin-BDKRB1 axis regulates aquaporin 4 gene expression and consequential migration and invasion of malignant glioblastoma cells via a Ca^{2+}-MEK1-ERK1/2-NF-κB mechanism," *Cancers*, vol. 12, no. 3, p. 667, 2020.

[37] C. C. Chio, K. Y. Chen, C. K. Chang et al., "Improved effects of honokiol on temozolomide-induced autophagy and apoptosis of drug-sensitive and -tolerant glioma cells," *BMC Cancer*, vol. 18, no. 1, p. 379, 2018.

[38] M. A. Goldberg and T. J. Schneider, "Similarities between the oxygen-sensing mechanisms regulating the expression of vascular endothelial growth factor and erythropoietin," *The Journal of Biological Chemistry*, vol. 269, no. 6, pp. 4355–4359, 1994.

[39] W. G. Kaelin Jr. and P. J. Ratcliffe, "Oxygen sensing by metazoans: the central role of the HIF hydroxylase pathway," *Molecular Cell*, vol. 30, no. 4, pp. 393–402, 2008.

[40] M. E. Hubbi and G. L. Semenza, "Regulation of cell proliferation by hypoxia-inducible factors," *American Journal of Physiology. Cell Physiology*, vol. 309, no. 12, pp. C775–C782, 2015.

[41] Z. J. Dai, J. Gao, X. B. Ma et al., "Up-regulation of hypoxia inducible factor-1α by cobalt chloride correlates with proliferation and apoptosis in PC-2 cells," *Journal of Experimental & Clinical Cancer Research*, vol. 31, no. 1, p. 28, 2012.

[42] H. Knævelsrud, S. R. Carlsson, and A. Simonsen, "SNX18 tubulates recycling endosomes for autophagosome biogenesis," *Autophagy*, vol. 9, no. 10, pp. 1639–1641, 2013.

[43] S. Ceccariglia, A. Cargnoni, A. R. Silini, and O. Parolini, "Autophagy: a potential key contributor to the therapeutic action of mesenchymal stem cells," *Autophagy*, vol. 16, no. 1, pp. 28–37, 2020.

[44] H. Zhang, M. Bosch-Marce, L. A. Shimoda et al., "Mitochondrial autophagy is an HIF-1-dependent adaptive metabolic response to hypoxia," *The Journal of Biological Chemistry*, vol. 283, no. 16, pp. 10892–10903, 2008.

[45] F. Cuomo, L. Altucci, and G. Cobellis, "Autophagy function and dysfunction: potential drugs as anti-cancer therapy," *Cancers*, vol. 11, no. 10, p. 1465, 2019.

[46] F. M. Elmenier, D. S. Lasheen, and K. A. M. Abouzid, "Phosphatidylinositol 3 kinase (PI3K) inhibitors as new weapon to combat cancer," *European Journal of Medicinal Chemistry*, vol. 183, p. 111718, 2019.

[47] B. Verret, J. Cortes, T. Bachelot, F. Andre, and M. Arnedos, "Efficacy of PI3K inhibitors in advanced breast cancer," *Annals of Oncology*, vol. 30, Supplement 10, pp. x12–x20, 2019.

[48] A. S. Dossou and A. Basu, "The emerging roles of mTORC1 in macromanaging autophagy," *Cancers*, vol. 11, no. 10, p. 1422, 2019.

[49] D. Heras-Sandoval, J. M. Pérez-Rojas, J. Hernández-Damián, and J. Pedraza-Chaverri, "The role of PI3K/AKT/mTOR pathway in the modulation of autophagy and the clearance of protein aggregates in neurodegeneration," *Cellular Signalling*, vol. 26, no. 12, pp. 2694–2701, 2014.

[50] S. Mohlin, A. Hamidian, K. von Stedingk et al., "PI3K-mTORC2 but not PI3K-mTORC1 regulates transcription of HIF2A/EPAS1 and vascularization in neuroblastoma," *Cancer Research*, vol. 75, no. 21, pp. 4617–4628, 2015.

[51] S. Joshi, A. R. Singh, M. Zulcic, and D. L. Durden, "A macrophage-dominant PI3K isoform controls hypoxia-induced HIF1α and HIF2α stability and tumor growth, angiogenesis, and metastasis," *Molecular Cancer Research*, vol. 12, no. 10, pp. 1520–1531, 2014, Epub 2014 Aug 7.

[52] R. M. Chen, Y. L. Lin, and C. W. Chou, "GATA-3 transduces survival signals in osteoblasts through upregulation of bcl-x_L gene expression," *Journal of Bone and Mineral Research*, vol. 25, no. 10, pp. 2193–2204, 2010.

[53] G. Pistritto, D. Trisciuoglio, C. Ceci, A. Garufi, and G. D'Orazi, "Apoptosis as anticancer mechanism: function and dysfunction of its modulators and targeted therapeutic strategies," *Aging*, vol. 8, no. 4, pp. 603–619, 2016.

[54] A. Thorburn, "Apoptosis and autophagy: regulatory connections between two supposedly different processes," *Apoptosis*, vol. 13, no. 1, pp. 1–9, 2008.

[55] A. Escamilla-Ramírez, R. A. Castillo-Rodríguez, S. Zavala-Vega et al., "Autophagy as a potential therapy for malignant glioma," *Pharmaceuticals*, vol. 13, no. 7, p. 156, 2020.

Review Article

Modulation of Autophagy: A Novel "Rejuvenation" Strategy for the Aging Liver

Fengming Xu [ID],[1] Hans-Michael Tautenhahn,[1] Olaf Dirsch,[2] and Uta Dahmen [ID][1]

[1]*Department of General, Visceral and Vascular Surgery, Jena University Hospital, Jena 07747, Germany*
[2]*Institute of Pathology, Klinikum Chemnitz gGmbH, Chemnitz 09111, Germany*

Correspondence should be addressed to Uta Dahmen; uta.dahmen@med.uni-jena.de

Aging is a natural life process which leads to a gradual decline of essential physiological processes. For the liver, it leads to alterations in histomorphology (steatosis and fibrosis) and function (protein synthesis and energy generation) and affects central hepatocellular processes (autophagy, mitochondrial respiration, and hepatocyte proliferation). These alterations do not only impair the metabolic capacity of the liver but also represent important factors in the pathogenesis of malignant liver disease. Autophagy is a recycling process for eukaryotic cells to degrade dysfunctional intracellular components and to reuse the basic substances. It plays a crucial role in maintaining cell homeostasis and in resisting environmental stress. Emerging evidence shows that modulating autophagy seems to be effective in improving the age-related alterations of the liver. However, autophagy is a double-edged sword for the aged liver. Upregulating autophagy alleviates hepatic steatosis and ROS-induced cellular stress and promotes hepatocyte proliferation but may aggravate hepatic fibrosis. Therefore, a well-balanced autophagy modulation strategy might be suitable to alleviate age-related liver dysfunction. *Conclusion.* Modulation of autophagy is a promising strategy for "rejuvenation" of the aged liver. Detailed knowledge regarding the most devastating processes in the individual patient is needed to effectively counteract aging of the liver without causing obvious harm.

1. Introduction

Life expectancy of the population increased substantially. This is due to the development of medical technology and general improvement of sanitary conditions, resulting in an increase of the aging population. In 2019, there were about 703 million (9%) people aged 65 and above in the world. This figure is expected to almost double to 1.5 billion (16%) by 2050 [1].

Age is one of the important risk factors for malignant liver disease. Aging causes changes in hepatic morphology, structure, and function with hepatic steatosis, fibrosis, and impaired liver regeneration being the most prominent features [2–5].

The liver is the pivotal metabolic organ, which is involved in central metabolic activities such as lipid metabolism, gluconeogenesis, and protein synthesis [6, 7]. The age-related changes do not only impair the function of the liver but also

represent a potential risk for the occurrence of malignant liver diseases [2]. Therefore, clinicians face the problem of how to eliminate or mitigate aging-related detrimental changes in the liver.

Autophagy is a crucial mechanism for eukaryocytes to recycle intracellular constituents. During the process of autophagy, misfolded proteins or defective organelles are degraded to basal components via the lysosomal pathway for later reuse [8]. Autophagy contributes to liver homeostasis through its role in ATP synthesis and organelle quality control [9]. However, the level of hepatic autophagy gradually decreases with age [10, 11]. Aging affects autophagy mainly via inhibition of adenosine monophosphate-activated protein kinase (AMPK) activation, hypermethylation of autophagy-related genes, and accumulation of lipofuscin. Lipofuscin is an intracellular brown-yellow pigment granule, which accumulates within the lysosomal compartment during cellular senescence [12–19]. If damaged
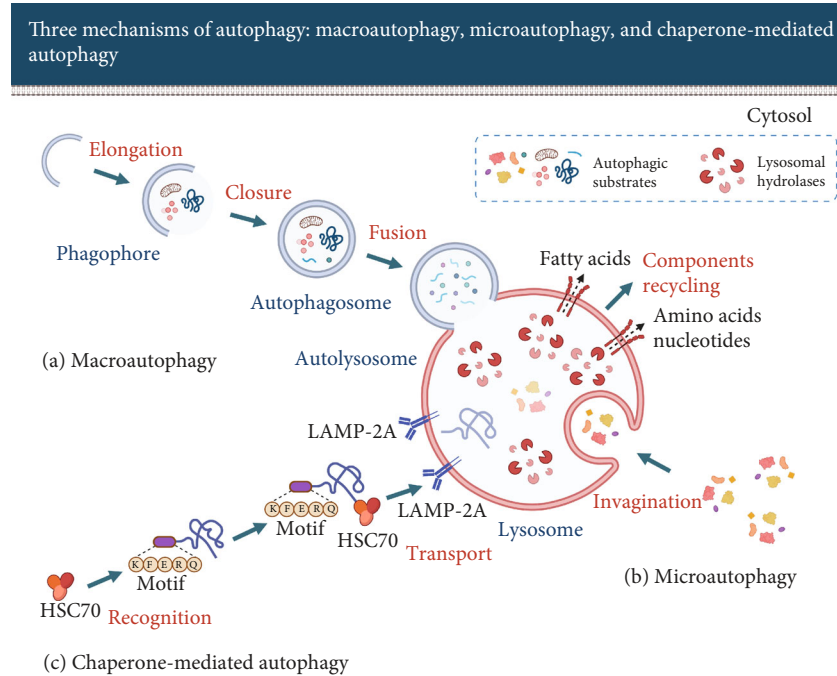
FIGURE 1: Three key types of autophagy in eukaryocytes: macroautophagy, microautophagy, and chaperone-mediated autophagy. They all ultimately transport autophagic substrates to the lysosomes for degradation through different pathways prior to releasing the resulting building blocks such as amino acids, fatty acids, and nucleotides back into the cytosol for cellular reuse.

cellular components or excess reactive oxygen species (ROS) accumulate in cells, cellular homeostasis is disrupted and cellular senescence is further accelerated [20].

In the last ten years, the role of autophagy in liver diseases has attracted more and more attention. Accumulating evidence shows that promoting autophagy effectively mitigates hepatic steatosis, restores impaired liver regeneration, reduces mitochondrial dysfunction, and alleviates ROS-induced cellular injury. However, it may exacerbate the progress of hepatic fibrosis. In this review, we describe the role of autophagy in age-associated liver changes and suggest how to modulate autophagy to rejuvenate the aging liver.

2. Autophagy

Autophagy is an intracellular degradation process. The autophagy-related genes control the process in which eukaryocytes digest their damaged or superfluous components such as misfolded proteins, damaged organelles, and pathogens via the lysosomal pathway [8, 21]. It conveys a prosurvival effect allowing cells to maintain energy homeostasis and accommodate cellular stressors such as excess ROS, anoxia, and nutrient starvation [21, 22]. In contrast, excessive autophagy may lead to cell death [23].

Autophagy can be classified into macroautophagy, microautophagy, and chaperone-mediated autophagy (CMA). The classification is based on the delivery route of autophagy substrates involving different morphological features. All three types of autophagy ultimately deliver substrates to lysosomes for degradation and reutilization (see Figure 1) [24, 25].

2.1. Different Types of Autophagy

2.1.1. Macroautophagy. The first step of macroautophagy is the nucleation of phagophore (see Figure 2). Activation of autophagy signaling molecules such as AMPK, mammalian target of rapamycin (mTOR), or Unc-51 like autophagy activating kinase 1 (ULK1) initiates the process.

The nucleus of the phagophore is derived from a subdomain of the endoplasmic reticulum (ER) called omegasome. Omegasomes are rich in phosphatidylinositol-3-phosphate (PI3P, a crucial lipid messenger for autophagy initiation) [26, 27]. When nucleation is complete, the phagophore enters a rapid growth phase. The most critical step in this phase is membrane acquisition. Phagophores get in contact with other organelles such as plasma membranes [28–30], mitochondria [31], and Golgi complex [32, 33] which may serve as potential membrane sources [34, 35]. Membranes are transported from the donor organelle to the phagophore via Atg9, a crucial transmembrane protein [36].

One of the key regulators that promote the nucleation of phagophore is the ULK1 complex. This complex is composed of ULK1, FAK family kinase interacting protein of 200 kDa (FIP200), autophagy-related protein 13 (Atg13), and Atg101 (see Figure 3) [37]. ULK1, a serine/threonine kinase, has several downstream phosphorylation targets to promote the formation of phagophores. FIP200 is supposed to act as a "scaffolding molecule" in the ULK1 complex. Atg13 acts as an adaptor in the complex to facilitate the interaction between ULK1 and FIP200, and Atg13 boosts the activity of ULK1. Atg101 plays an essential role in the stability and phosphorylation of Atg13 and ULK1 [38, 39]. Moreover, Atg101 promotes the recruitment of downstream autophagic proteins [40].
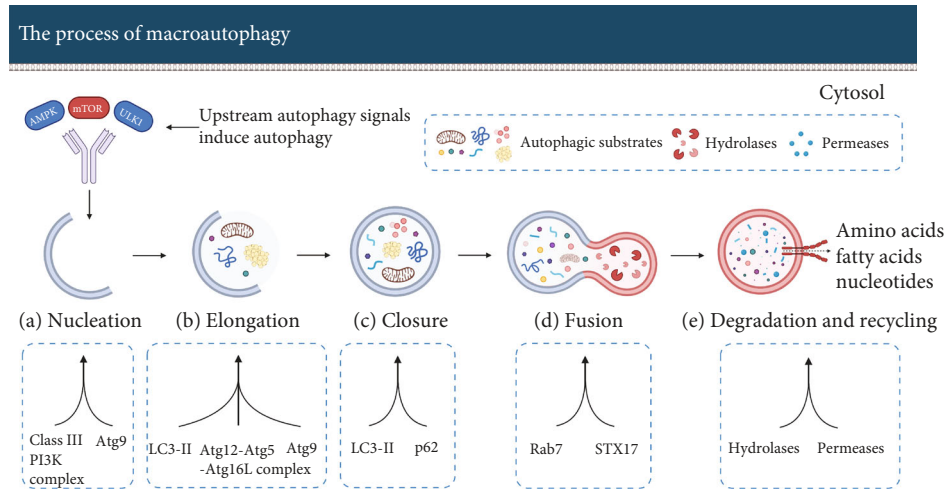
FIGURE 2: Macroautophagy degrades aggregated intracellular proteins or damaged organelles thereby providing the raw material for the production of new intracellular organelles (component-recycling system). (a) The class III PI3K complex induces the initiation of phagophore formation. Atg9 promotes membrane transport from the donor organelle to the phagophore. (b) With the joint action of LC3, Atg12-Atg5-Atg16L complex, and Atg9, the phagophore elongates gradually. (c) LC3 promotes closure of the membranes. p62 interacts with autophagic substrates and delivers the substrates to autophagosomes under the control of LC3. (d) Rab7 and STX17 facilitate the fusion of autophagosome and lysosome. (e) Autophagic substrates are degraded by the action of lysosomal hydrolases into small molecules that are subsequently released by membrane permeases for use in the construction of new organelles.
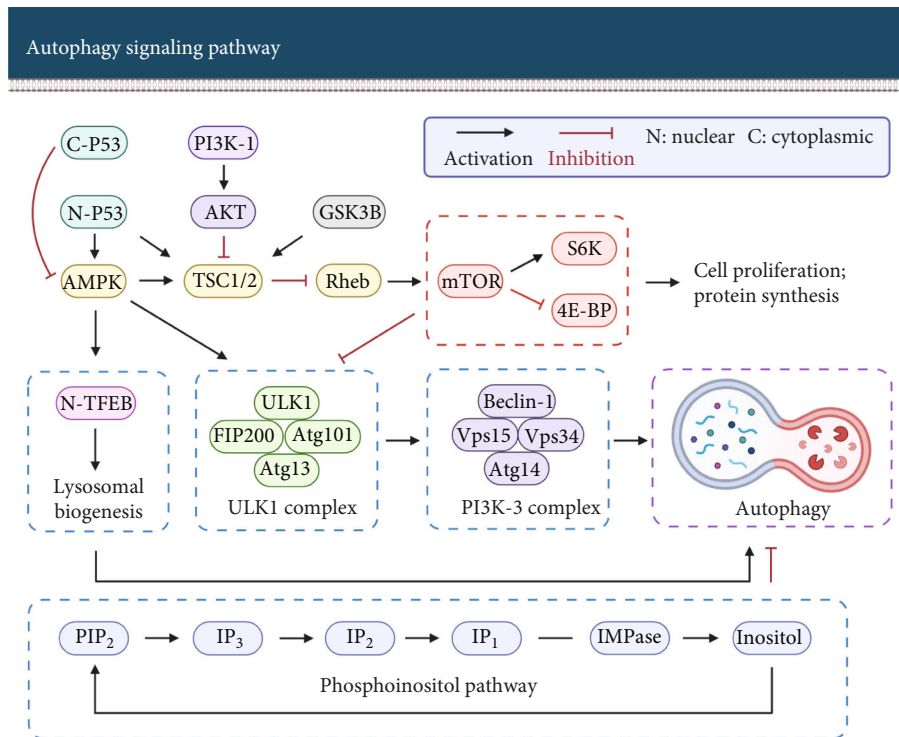
FIGURE 3: Autophagy (encircled in purple) is modulated by multiple signaling pathways; they can be divided into mTOR-dependent (encircled in red) and mTOR-independent autophagy signaling pathways (encircled in blue). mTOR is a central regulatory molecule of autophagy and cell growth. Inducing autophagy by inhibiting mTOR activity impedes protein synthesis and cell proliferation.

The ULK1 complex phosphorylates the components of the class III PI3K (PI3K-3) complex. The PI3K-3 complex is composed of Beclin-1, vacuolar protein sorting 34 (Vps34), Vps15, and Atg14 (see Figure 3). Beclin-1 is a core constituent of the PI3K-3 complex. The phosphorylation of

Beclin-1 via ULK1 is considered to be required for activation of the Atg14-bound Vps34 [41]. Vps34 produces PI3P in phagophores and stabilizes the ULK1 complex. Vps15 is essential for activation and maintaining the function of Vps34 [40, 42]. Atg14 targets the PI3K-3 complex to the

phagophore assembly site and promotes the extension of phagophores [40].

The second step of macroautophagy is autophagosome formation consisting of elongation and closure of the phagophore. The phagophores continuously elongate and capture autophagic substrates in the cytosol. Ultimately, the phagophores form sealed double-membrane autophagosomes.

Microtubule-associated protein light chain 3 (LC3) is a vital protein in this process. Cytosolic LC3 (LC3-I) is covalently bound to phosphatidylethanolamine (PE) to form lipidated LC3-II under the mediation of the Atg12-Atg5-Atg16L complex. The Atg12-Atg5 conjugate enhances the activity of Atg3 to promote the transfer of LC3 from Atg3 to PE. Atg16L specifies the site of the LC3-lipidation reaction. LC3-II locates at the inner and outer membrane and is crucial for the expansion and closure of the isolation membrane [43–45]. Sequestosome-1 (SQSTM1, also known as p62) is an autophagy receptor that recruits autophagic substrates. It interacts with LC3 on the isolation membrane via the LC3 interaction region and targets it to the autophagosome [45–47].

The third step of macroautophagy is the fusion of autophagosomes with lysosomes. Autophagosomes usually fuse with lysosomes directly. However, they can also fuse with late endosomes to form intermediate autophagic vacuoles called amphisomes which then fuse with lysosomes to form autolysosomes [48, 49].

Ras-related protein in brain 7 (Rab7) is a small GTPase that is located in lysosomes and late endosomes [48]. It is one of the key enzymes of membrane trafficking. For autophagy, Rab7 promotes autophagosome clustering in the perinuclear area and the fusion of autophagosomes with lysosomes, but the detailed molecular mechanism is still unclear [50–54]. Syntaxin 17 (STX17) facilitates the fusion process as well. STX17 is a SNARE protein that is located in the outer membrane of completed autophagosomes. It interacts with synaptosomal-associated protein 29 (SNAP-29) and vesicle-associated membrane protein 8 (VAMP8) to form a STX17 complex. This complex facilitates the fusion of autophagosomes and lysosomes [48, 55].

The final step of macroautophagy is degradation and recycling of the enclosed autophagic substrates. The autophagic substrates such as sequestered organelles and aggregated proteins are degraded in autolysosomes via multiple lysosomal hydrolases. After degradation, the resulting monomers such as amino acids, fatty acids, and nucleotides are released to the cytosol through the action of lysosomal permeases for cell reutilization [56].

Depending on the specific autophagy substrate, macroautophagy can be further classified into lipophagy and mitophagy [57], described in detail below. There are also other forms such as pexophagy, nucleophagy, and ribophagy, which we are not explaining here.

The term "lipophagy" is used to describe the process of autophagic degradation for lipid droplets (LDs) [58]. Lipophagy was first observed in the fasting liver and is an important process in lipid metabolism. It contributes to lipid turnover not only in liver cells but also in various other animal cells [59, 60]. Under normal physiological conditions, lipophagy is regulated by the nutritional status of cells via AMPK-mTOR pathways. During periods of starvation, lipophagy is activated, allowing cells to utilize their fat reserves [58].

Similar to the above, mitophagy is the process of selective degradation for damaged or redundant mitochondria via macroautophagy [61, 62]. Mitophagy plays a crucial role in mitochondrial quality control and regeneration [63, 64]. Impaired mitophagy disrupts mitochondrial function, leading to the progressive accumulation of defective mitochondria and eventual cell damage [62]. The Parkin-PINK1 pathway is the critical pathway regulating mitophagy. In general, activated PINK1 facilitates Parkin to bind with depolarized mitochondria to induce mitophagy [65]. We will describe the mechanism of mitophagy mediated by this pathway in detail in a subsequent section (Section 7.2).

2.1.2. Microautophagy. Unlike in macroautophagy, microautophagy does not involve autophagosomes as a vehicle for transporting autophagy substrates. In microautophagy, intracellular substances are directly engulfed by the lysosome membrane via invagination and then degraded within the lysosomal lumen [66, 67]. The major function of microautophagy is to maintain membrane homeostasis and organelle size and promote cell survival under nitrogen restriction [68].

2.1.3. Chaperone-Mediated Autophagy. Chaperone-mediated autophagy regulates the degradation of a selective population of cytosolic proteins containing a specific KFERQ peptide sequence [69]. It is estimated that about 30% of cytosolic proteins contain this sequence motif [70].

Firstly, the molecular chaperone heat-shock cognate protein of 70 kDa (HSC70) recognizes and binds the substrate protein. In a second step, the substrate proteins are transported into the lysosome under the mediation of lysosome-associated membrane protein type 2A (LAMP-2A) for degradation [71]. The selectivity of chaperone-mediated autophagy results in degradation of specific motif proteins only without interfering with other types of proteins. Chaperone-mediated autophagy mainly facilitates protein homeostasis and promotes cellular adaptation to stress [72].

Here, we mainly focus on macroautophagy which is the most relevant form of autophagy within the hepatic aging process.

2.2. Autophagy Participates in a Variety of Physiological Metabolic Activities in the Liver. The role of autophagy in liver physiology was discovered during the past ten years. The main findings can be summarized as follows:

Under homeostatic condition: firstly, hepatic autophagy degrades lipid droplets into free fatty acids (FFAs) which are oxidized in mitochondria to promote ATP synthesis [6, 73]. It facilitates the energy homeostasis of hepatocytes. Secondly, hepatic autophagy promotes the removal of damaged organelles. The accumulation of abnormal organelles leads to hepatocyte swelling and hepatotoxicity [66, 74, 75]. Thirdly, autophagy breaks down misfolded proteins into amino acids which are used in the synthesis of new proteins [76]. Hepatic autophagy may also convert amino acids to glucose via

gluconeogenesis, which is an essential process for maintaining blood glucose concentration [7].

Under stress conditions: the liver maintains a basal level of autophagy which is substantially enhanced in response to cellular metabolic stress. For example, starvation-induced autophagy occurs primarily in the liver [6, 7]. A study on perfused rat livers showed that under basal-nutrient conditions, the rate of protein degradation is about 1.5% of total liver protein per hour, while under starvation, this rate could be increased to about 4.5% [77].

Upon impairment of autophagy process: a number of reports have shown that liver-specific autophagy deficiency leads to significant hepatomegaly and liver injury in animals [74, 75, 78]. In 2-month-old Atg5-deficient mice, the liver to body weight ratio (LBWR) was about 2-fold that of control mice, and the serum alanine aminotransferase (ALT) level was about 8-fold higher [78]. These changes reflect the important role of autophagy in the liver, which may be related to the accumulation of abnormal organelles caused by autophagy deficiency [74, 75].

Upon aging: hepatic autophagy activity gradually decreases with age [10, 11, 79, 80], which may set the stage for the occurrence of age-related liver diseases.

2.3. Autophagic Activity Declines with Age.
Aging, the process of becoming older, leads to spontaneous and inevitable changes in the structure and function of organism over time. This is mainly manifested in the degeneration of biological structures, the decline in physiological functions, and the reduction of stress adaptation [81, 82].

Aging leads to a decline of autophagy in a variety of tissues such as the liver, brain, and ovary [10, 83–85]. For instance, in aged mouse liver, the LC3 protein expression, the number of hepatocytes with autophagic vacuoles, and the total number of autophagic vacuoles in hepatocytes are substantially reduced [86].

2.3.1. Aging Impairs the Activation Capacity of AMPK.
AMPK, the major energy-sensing kinase, activates various catabolic processes. AMPK activation can effectively induce the initiation of the autophagic process. Activated AMPK triggers autophagy to facilitate energy generation in mitochondria and downregulates energy-demanding processes such as cell division and protein synthesis to ensure cellular energy homeostasis [87].

However, aging results in a significant decrease in the activation capacity of AMPK. Reznick et al. [16] observed in the skeletal muscle of old rats that activation of AMPK induced by acute ($5'$-aminoimidazole-4-carboxamide-1-β-D-ribofuranoside, exercise) or chronic (β-guanidinopropionic acid) stimulation was significantly reduced compared with young rats.

The age-related impairment of AMPK activation impedes autophagosome formation, affects cellular homeostasis, and further promotes the aging process via weakening its inhibitory effect on mTOR [17, 18, 88].

2.3.2. Age-Related Lipofuscin Accumulation Impairs the Degradation Efficiency of Lysosome.
Lipofuscin is a brown-yellow and autofluorescent pigment mainly composed of oxidated protein and lipid residues [89]. The formation of lipofuscin is primarily due to iron-catalyzed oxidation of protein and lipid macromolecules [90, 91]. Lipofuscin typically accumulates in the lysosomes of postmitotic cells during senescence.

Lysosomes are acidic organelles that contain multiple hydrolytic enzymes. When lysosomes loaded with lipofuscin accumulate in senescent cells, most of the lysosomal enzymes are drawn from the Golgi apparatus to the lipofuscin-loaded lysosomes. However, lysosomal enzymes degrade proteins but are unable to degrade lipofuscin. As a result, the delivery of enzymes to lipofuscin-loaded lysosomes is ineffective for recycling the aggregated proteins. This imbalanced distribution reduces the availability of lysosomal enzymes in healthy lysosomes, leading to a marked decrease in the lysosomal degradation process [13–15].

Furthermore, the decreased turnover of dysfunctional mitochondria (impaired mitophagy) due to lipofuscin accumulation leads to a substantial increase in the generation of reactive oxygen species (ROS). In turn, the increased oxidative stress impairs autophagy via further impairment in lysosomal function [92–96].

2.3.3. Aging Facilitates Hypermethylation of Autophagic Genes.
As mentioned before, Atg5 and LC3 are pivotal genes governing the autophagic process [45, 97]. So far, it was shown in two different compartments, macrophages and ovaries, but not yet in the liver, that age-related hypermethylation of Atg 5 and LC3 did lead to a downregulation of autophagy.

Khalil et al. [19] observed that mRNA expression of Atg5 and LC3B was significantly reduced in bone marrow-derived macrophages of aged mice. The promoter regions of Atg5 and LC3B were highly methylated compared to those in young mice. Preventing methylation via methyltransferase inhibitor, (2)-epigallocatechin-3-gallate (EGCG), or DNA methyltransferase 2 (DNMT2) siRNA restored the expression of Atg5 and LC3B in the macrophages of aged mice. Li et al. [83] observed also age-related hypermethylation of autophagic genes, albeit in mouse ovaries: the mRNA and protein expression of Atg5 and LC3B were significantly decreased in the ovaries of aged rats. The promoter regions of Atg5 and LC3B were highly methylated compared to those in young rats. The authors pointed out that the observed upregulation of DNA methyltransferase 3A/3B in the ovaries of aged rats may lead to methylation of Atg5 and LC3B, which in return may ultimately decrease autophagy activity.

These results suggest that aging may blunt autophagy activity by promoting the hypermethylation of autophagic genes.

2.4. Main Pathways to Modulate Autophagy.
We first give an explanation of the key molecules regulating autophagy: mTOR and its related complexes mTORC1 and mTORC2. In the second step, we describe the autophagy regulatory pathways.

mTOR is the major regulator of autophagy. It is a serine-threonine kinase, which is involved in the regulation of

multiple cellular activities such as autophagy, cell growth, proliferation, and metabolism [98]. The level of mTOR expression is negatively correlated with the activity of autophagy, e.g., inhibition of mTOR induces autophagy remarkably. mTOR can interact with several binding proteins to form two different protein complexes that are referred to as mTOR complex 1 (mTORC1) and mTOR complex 2 (mTORC2). The activity of mTOR is regulated by multiple upstream factors such as AMPK, AKT, and TSC1/2. Phosphorylation of AMPK and TSC1/2 inhibits the activity of mTORC1, while AKT phosphorylation promotes the activity of mTORC1 [99–101].

mTORC1, a rapamycin-sensitive protein complex, is involved in regulating autophagy, cell growth, protein synthesis, and ribosome biosynthesis [87, 98]. mTORC1 is regulated by AMPK, which is actually one of the most important upstream modulators of mTORC1. mTORC1 senses the cellular energy status through AMPK. In addition, mTORC1 can sense the level of other cellular nutrients as well such as amino acids, growth factors, and oxygen. mTORC1 has three important downstream effectors: p70-S6 kinase (S6K), 4E-binding protein (4E-BP), and ULK1. S6K1 and 4E-BP are closely related to the regulation of protein synthesis and cell growth [87, 98, 102], while ULK1 is an important regulator of autophagosome formation (see Figure 3). In nutrient-rich conditions, mTORC1 is activated and promotes cell growth and proliferation by phosphorylating S6K and 4E-BP. In contrast, activated mTORC1 phosphorylates and inactivates of ULK1 to suppress autophagy [103–106].

mTORC2, a rapamycin-insensitive protein complex, mainly regulates cell survival and modulates the actin cytoskeleton to organize the cell shape [87, 98, 107]. According to Saxton and Sabatini, the critical role of mTORC2 is to phosphorylate and activate AKT which facilitates cellular survival and growth [98]. This view was further confirmed by Kazyken et al. [108]. Kazyken et al. observed that the activation of AMPK phosphorylated and activated mTORC2 in hepatocytes. In his experiments, AMPK-mediated activation of mTORC2 was not induced by AMPK-mediated inhibition of mTORC1, but that AMPK directly phosphorylated mTORC2. The activation of AMPK by starvation stimulated mTORC2 and its substrate AKT to facilitate cell survival. By contrast, inactivation of AMPK, mTORC2, and AKT aggravated cell apoptosis during starvation.

Now, we describe four critical autophagy modulating pathways.

2.4.1. PI3K-AKT-mTOR.

Phosphoinositide 3-kinase (PI3K) is an intracellular phosphatidylinositol kinase. PI3K is involved in a series of cellular events such as autophagy, apoptosis, and proliferation. PI3K activation can effectively activate AKT. AKT is a serine/threonine protein kinase, it plays an important role in cell growth, proliferation, and survival [109]. mTOR acts as a downstream molecule of the PI3K-AKT pathway.

Activation of PI3K by phosphorylation results in the production of a second messenger-phosphatidylinositol-3,4,5-triphosphate (PIP3), which binds to PDK1 (phosphoinositide-dependent kinase-1) and AKT. PDK1 phosphorylates

and activates AKT. There are three ways for activated AKT to regulate mTOR. First, AKT phosphorylates mTOR directly, thereby activating mTOR and inhibiting autophagy. Second, AKT can phosphorylate and inactivate proline-rich AKT substrate of 40 kilodaltons (PRAS40), a downstream target of AKT that inhibits the activity of mTORC1, as well, thereby activating mTORC1. Third, AKT enriches the Ras homolog enriched in the brain (Rheb) via phosphorylating tuberous sclerosis complex 1/2 (TSC1/2). Activated Rheb activates mTOR to inhibit autophagy (see Figure 3) [101, 110–114].

2.4.2. AMPK-mTOR-ULK1.

As mentioned above, AMPK is considered to be a central cellular energy sensor. It is activated in response to energy stress [87].

AMPK regulates mammalian autophagy in two ways. First, AMPK phosphorylation of TSC2 leads to the inactivation of Rheb, which in turn leads to the inactivation of mTOR. mTOR inactivation restores the activity of ULK1 which is a critical initiator of autophagy. Second, AMPK can phosphorylate ULK1 directly, which in turn facilitates the formation of autophagosomes [12, 99, 104, 115–120].

2.4.3. p53-AMPK-mTOR.

p53 is a tumor suppression protein. It is mainly considered as a DNA sequence-specific transcription factor, which is involved in activating proapoptosis, cell-cycle arrest, and proautophagy genes [121, 122].

Emerging evidence suggests that p53 may bidirectionally regulate autophagy based on its subcellular localization. The active p53 tetramer in the nucleus binds to the promoter regions of multiple pro-autophagy-related genes such as AMPK, TSC2, and damage-regulated autophagy modulator (DRAM) to transactivate the expression of proautophagy genes, thereby inducing autophagy [121, 123]. For example, nuclear p53 can trigger autophagy in a DRAM (a lysosomal protein that induces macroautophagy)-dependent way [124]. Furthermore, nuclear p53 can inhibit mTOR via the phosphorylation and activation of AMPK to induce autophagy [125], whereas cytoplasmic p53 inhibits autophagy [123, 126].

Furthermore, p53 plays an important role in cell senescence and proliferation. Activated p53 triggers the expression of its downstream prosenescence molecules such as p21 and E2F Transcription Factor 7 (E2F7). p21 is a cyclin-dependent kinase (CDK) inhibitor that leads to p53-dependent cell-cycle arrest and induces cell senescence. E2F7 is a transcriptional repressor of E2F target genes and is substantially upregulated during cellular senescence. E2F7 inhibits the expression of mitogenic genes and cooperates with retinoblastoma protein (RB) to promote cell cycle arrest [123, 127–130].

2.4.4. Phosphoinositol Pathway.

Inositol or inositol 1,4,5-tris-phosphate (IP_3) elimination can induce autophagy as well [131, 132]. The activation of autophagy may be related to the role of Ca^{2+} in energy metabolism.

The ER stores most of the intracellular Ca^{2+}. After IP_3 binds to the membrane IP_3 receptor on the ER surface, Ca^{2+} can be released from the ER. This process is thought to be a requirement for maintaining the energy state of

mitochondria since providing Ca^{2+} to mitochondria promotes the production of nicotinamide adenine dinucleotide (NADH) and energy. Conversely, inhibition of IP_3 or IP_3 receptors will result in a decrease in energy production. The reduced energy level stimulates AMPK and triggers autophagy through an mTOR-independent mechanism to maintain cellular energy balance [12, 133, 134].

3. Age-Related Common Alterations in the Liver

The liver is the largest solid organ of the human body, and it is mainly composed of 4 types of cells: hepatocytes, hepatic stellate cells (HSCs), Kupffer cells (KCs), and liver sinusoidal endothelial cells (LSECs).

Hepatocytes are the major parenchymal and functional cells of the liver, accounting for about 70% of the total liver cells. They perform multiple functions such as metabolic (lipid, carbohydrate, and protein), detoxifying (xenobiotics), and secretory (bile) functions to ensure metabolic homeostasis.

The remaining 30% of hepatic cells are primarily HSCs, LSECs, and KCs [135, 136]. HSCs are mainly involved in the storage of vitamin A in lipid droplets (LDs) and regulation of extracellular matrix and may affect sinusoidal blood flow via their contractile properties [4, 137]. LSECs constitute a permeable barrier within the liver sinusoids. They can promote the exchange of substances between the blood flow in the sinusoids and the surrounding tissues [138, 139]. KCs are resident hepatic macrophages. They are considered to act as "pathogen-scavengers" that play a major role in the immune and inflammatory response of the liver [140].

3.1. The Influence of Aging on Liver Cells.
With age, the number of hepatocytes gradually decreases, the genome of hepatocytes becomes unstable, and the number of polyploid hepatocytes increases. Moreover, lipofuscin accumulation and mitochondrial dysfunction also appear in senescent hepatocytes [4, 141].

In addition, the number of HSCs increases, and the number of activated stellate cells, staining positive for α-smooth muscle actin (αSMA, a stellate cell activation marker), increases as well [4]. In LSECs, aging leads to a decrease in the number and size of fenestrations, an increase in the deposition of basal collagen, and thickening of the endothelium [142] compromising the intercellular molecular exchange. Moreover, the implications of aging on macrophages include a decrease in phagocytosis and an increase in the secretion of cytokines that lead to an inflammatory phenotype [4].

3.2. The Influence of Aging on Liver Morphology and Structure.
The molecular changes described above also lead to changes on the macroscopical level. Age-associated accumulation of lipofuscin in hepatocytes leads to a gradual change in the color of the liver from light brown to dark brown [143].

Age-associated decrease in the number and quality of hepatocytes seems to cause a gradual decrease in the size and perfusion of the liver [4, 143]. Wynne et al. [144] reported a reduction of more than 40% when comparing a young with an old liver (24 years versus 91 years).

Aging also affects hepatic morphology and liver regeneration as mentioned before. Steatosis and fibrosis progressively appear in the aged liver [2–5]. A number of authors (see Tables 1–4) are giving evidence that there is a close link between autophagy and age-related diseases of the liver. Autophagy plays an important role in these hepatic diseases such as nonalcoholic fatty liver disease (NAFLD) and hepatic cirrhosis but also in posthepatectomy liver failure due to inadequate liver regeneration.

4. Liver Steatosis

The liver is the major organ of lipid metabolism. Hepatic lipid metabolism is of central importance for the synthesis, storage, secretion, and catabolism of triglycerides and fatty acids [145]. Liver steatosis occurs upon disturbances of the hepatic lipid metabolism, e.g., increased lipid synthesis or decreased lipid degradation in the liver. Steatosis can induce progressive hepatic pathological alterations, including lobular inflammation, ballooning degeneration, and fibrosis [146–149].

4.1. Aging is Associated with Development of Hepatic Steatosis.
The lipid metabolism capacity of the liver graduate declines with age [150]. Steatosis can be observed in mouse livers above the age of 12 months [151]. Steatosis and especially nonalcoholic fatty liver disease (NAFLD) are also often observed in the human elderly population. NAFLD is characterized as the presence of more than 5% of fat-laden hepatocytes in the absence of a competing cause of liver steatosis [147]. According to a 2012 Rotterdam study, the overall prevalence of NAFLD was 35.1% in the elderly population aged over 65 years old [152]. NAFLD may progress to nonalcoholic steatohepatitis (NASH), liver cirrhosis, and eventually liver cancer without effective intervention [153].

4.2. Hepatic Steatosis Also Impairs Autophagy.
As mentioned before, the autophagy activity declines with age [10, 11, 80]. The age-related accumulation of hepatic lipids, described above, further impairs autophagic activity. This was nicely illustrated in the study of Inami et al. [154]. They observed in a mouse model of genetically induced obesity (ob/ob mouse) that the p62 expression level was significantly increased in the steatotic liver compared to the control group. Furthermore, the rate of degradation for long-lived proteins, the activity of cathepsin B/L (lysosomal proteases), and the ratio of lysotracker red-stained autophagosomes were significantly lower in hepatocytes from ob/ob mice compared to control mice. These results suggest that hepatic steatosis impaired autophagy by impeding autophagosome acidification and expression of proteolytic enzymes.

Moreover, autophagy is involved in the regulation of cellular energy and nutrient metabolism. Conversely, energy and nutrient levels modulate autophagy as well. For example, during a period of starvation, lipophagy is activated to provide the needed FFAs for ATP synthesis. In contrast, adequate nutrition inhibits lipophagy since cells do not

TABLE 1: Induction of autophagy reduces hepatic steatosis.

			Recent scientific evidence that activating autophagy improves liver steatosis				
Author year	Research model	Autophagy pathway	Autophagy modulation	Enhanced autophagy	Reduced steatosis	Reduced autophagy	Increased steatosis
Tong et al. [179] 2019	HFD-fed C57BL/6 mice; ob/ob mice; primary mouse hepatocytes; HepG2 cells	AMPK-mTOR	PPARδ Chloroquine Atg5-KD	LC3-II: +++ P62: —	TG: — HE: —	P62: +++	TG: +++ HE: +++
Ren et al. [176] 2019	HFD-fed C57BL/6 mice; ob/ob mice; Palmitate-stimulated HepG2 cells	AMPK-TFEB	Catalpol Chloroquine	LC3-II: +++ P62: —	TG: — TC: — HE: — Oil Red O: —		TG: +++ TC: +++ Oil Red O: +++
Wang et al. [180] 2019	HFD and MCDD-fed C57BL/6J mice; Palmitate-stimulated primary mouse hepatocytes and HepG2 cells	AMPK-SIRT1	Tangshen formula SIRT1-KD	LC3-II: +++ P62: —	TG: — TC: — HE: — Oil Red O: —	LC3-II: — P62: +++	LDs: +++
Chu et al. [181] 2019	Oleic acid-stimulated HepG2 and LO2 cells	AMPK-mTOR Akt-mTOR	Cherry anthocyanins 3-Methyladenine; Atg5-KD	LC3-II: +++ P62: —	TG: — TC: — Oil Red O: —	LC3-II: —	TG: +++ TC: +++ Oil Red O: +++
Ohashi et al. [182] 2019	HFD-fed male BALB/c mice	Not investigated	Conophylline	LC3-II: +++ P62: —	TG: — HE: — Oil Red O: —		
Liu et al. [183] 2018	HFD-fed male SD rats; Palmitate-stimulated L02 cells	COX-2	Celecoxib Rapamycin Chloroquine	LC3-II: +++ P62: —	TG: — Oil Red O: —	LC3-II: — P62: +++	TG: +++ Oil Red O: +++
Hong et al. [184] 2018	Male ob/ob and C57BL/6 mice; Palmitate-stimulated HepG2 cells and primary hepatocytes	SIRT1	Erythropoietin SIRT1-KD	LC3-II: +++	TG: — Oil Red O: —	LC3-II: —	TG: +++ Oil Red O: +++
Balachander et al. [185] 2018	Oleic acid-stimulated HepG2 cells	Not investigated	Rosmarinic acid	LC3-II: +++	TG: — TC: — Oil Red O: —		
Li et al. [186] 2017	HFD-fed male C57BL/6 mice; free fatty acid-stimulated HepG2 cells	Atg16L1-mediated	1,25(OH)$_2$D$_3$ 3-Methyladenine Atg16L1-KD	LC3-II: +++ P62: —	TG: — TC: — HE: — Oil Red O: —	LC3-II: —	TG: +++ TC: +++ Oil Red O: +++
Tang et al. [173] 2016	Chronic ethanol-fed male C57BL/6J mice; oleic acid and alcohol-stimulated HepG2 cells	Not investigated	Resveratrol 3-Methyladenine	LC3-II: +++ P62: —	TG: — HDL-C: +++ LDL-C: — LDs: — HE: — Oil Red O: —	LC3-II: — P62: +++	TG: +++ Oil Red O: +++
Jung et al. [187] 2015	HFD-fed male C57BL/6J mice; Palmitate or tunicamycin-stimulated HepG2 cells and human primary hepatocytes	AMPK-mediated	C1q/TNF-related protein 9 Compound C 3-Methyladenine	LC3-II: +++ P62: —	TG: — HE: — Oil Red O: —	LC3-II: — P62: +++	TG: +++ Oil Red O: +++
Zhang et al. [188] 2015	HFD-fed 129/SvJ mice; Palmitate-stimulated HepG2 cells	cAMP-PRKA-AMPK-SIRT1	Resveratrol 3-Methyladenine	LC3-II: +++ P62: —	TG: — Oil Red O: —	LC3-II: — P62: +++	TG: +++

+++: increase; —: decrease; KO: knockout; KD: knockdown; HFD: high-fat diet; MCDD: methionine choline-deficient diet; TG: triglyceride; TC: total cholesterol; HDL-C: high-density lipoprotein cholesterol; LDL-C: low-density lipoprotein cholesterol; LDs: lipid droplets; PPARδ: peroxisome proliferator-activated receptor δ; TFEB: transcription factor EB; cAMP: cyclic adenosine monophosphate; PRKA: protein kinase A; SIRT1: sirtuin 1; HE: hematoxylin and eosin stain; Oil Red O: Oil Red O stain.

need FFAs as energy sources [58]. Overnutrition and obesity can activate mTOR by inactivating AMPK, which may blunt the ULK1 kinase complex and in turn inhibit autophagy [155, 156].

4.3. Impaired Lipophagy Contributes to Accumulation of Lipid Droplets in Hepatocytes. The process of converting lipid droplets into FFAs, called lipolysis, includes two different types: neutral lipolysis and acid lipolysis (also referred to as lipophagy). Neutral lipolysis refers to that lipid droplet-related triacylglycerols are hydrolysed by cytoplasmic lipases at pH 7. In contrast, acid lipolysis refers to that LD-related triacylglycerols are hydrolysed by lysosomal acid lipase at pH 4.5-5 [157].

Singh et al. [158] observed that inhibition of hepatic autophagy via 3-methyladenine (3-MA) treatment or Atg5

TABLE 2: Autophagy performs a dual role in liver fibrosis.

(a) Recent scientific evidence that activating autophagy aggravates liver fibrosis

Author year	Research model	Autophagy pathway	Autophagy modulation	Enhanced autophagy	Increased fibrosis	Reduced autophagy	Reduced fibrosis
Ma et al. [217] 2020	CCl$_4$-stimulated male Norway rats; platelet-derived growth factor-BB (PDGF-BB) stimulated LX-2 cells	Not investigated	Small heterodimer partner			P62: +++ Atg12: —	SMA: —
Liu et al. [218] 2019	CCl$_4$ and BDL-stimulated male C57 mice	TGF-β1-Smad3	Isorhamnetin CCl$_4$ BDL	LC3-II: +++ Beclin-1: +++	α-SMA: +++ Hydroxyproline: +++ PPAR-γ: — HE: +++ Masson: +++	LC3-II: — Beclin-1: —	α-SMA: — Hydroxyproline: — PPAR-γ: +++ HE: — Masson:—
Meng et al. [219] 2018	LX-2 cells	Not investigated	Carvedilol Rapamycin	LC3-II/I: +++	Cleaved PARP: —	Autophagic flux: —	α-SMA: — CCK-8: — Bcl-2: — Bax: +++ Cleaved PARP: +++
Feng et al. [220] 2018	CCl$_4$ and BDL-stimulated male C57 mice	TGFβ1-Smad3	Salidroside CCl$_4$ BDL	LC3-II: +++ P62: — Beclin-1: +++	α-SMA: +++ Hydroxyproline: +++ HE: +++ Masson:+++	LC3-II: — P62: +++ Beclin-1: —	α-SMA: — Hydroxyproline: — HE: — Masson:—
Wang et al. [221] 2017	CCl$_4$-stimulated female BALB/c mice; LX-2 cells	NF-κB	3-Methyladenine Atg5-KD Rapamycin CCl$_4$	LC3-II: +++ Beclin-1: +++	α-SMA: +++ TGF-β: +++ HE: +++ Masson: +++	LC3-II: — Beclin-1: —	α-SMA: — TGF-β: — HE: — Masson: —
Wu et al. [222] 2017	CCl$_4$ and BDL-stimulated male C57 mice	TGF-β1-Smads PI3K-AKT	Quercetin CCl$_4$ BDL	LC3-II: +++ P62: — Beclin-1: +++	α-SMA: +++ Hydroxyproline: +++ HE: +++ Masson: +++	LC3-II: — P62: +++ Beclin-1: —	α-SMA: — Hydroxyproline: — HE: — Masson: —
Mao et al. [223] 2015	CCl$_4$ and BDL-stimulated male C57BL/6 mice; HSC cell line	Not investigated	Ghrelin CCl$_4$ BDL	LC3-II: +++ P62: —	α-SMA: +++ Hydroxyproline: +++ HE: +++ Masson: +++	LC3-II: — P62: +++	α-SMA: — Hydroxyproline: — HE: — Masson: —
Hernández-Gea et al. [201] 2012	CCl$_4$ or TAA-stimulated C57BL/6 mice; mouse hepatic stellate cells; mouse stellate cell line JS1	Not investigated	3-Methyladenine Chloroquine Atg5/7-KD CCl$_4$ TAA	LC3-II: +++ P62: —	IPF: +++	LC3-II: — P62: +++	α-SMA: — Sirius Red: —
Thoen et al. [198] 2011	Balb/c mouse; human and mouse HSCs	Not investigated	Bafilomycin A1 CCl$_4$	Autophagic flux: +++	a-SMA:+++	Autophagic flux: —	SMA: — PDGFR-β: — EdU: —

(b) Activating autophagy alleviates liver fibrosis

Author year	Research model	Autophagy pathway	Autophagy modulation	Enhanced autophagy	Reduced fibrosis	Reduced autophagy	Increased fibrosis
Liu et al. [224] 2018	CCl$_4$-stimulated male SD rats; primary HSCs	Not investigated	Catalpol	LC3-II: +++ P62: — Beclin-1: +++ Atg5: +++	α-SMA: — Hydroxyproline: — HE: — Masson: — Sirius Red: —		
Ruart et al. [214] 2018	CCl$_4$-stimulated C57BL/6 mice; LSECs	Not investigated	Atg7-KO			LC3-II/I: — P62: +++	α-SMA: +++ Hydroxyproline: +++ Sirius Red: +++
Lodder et al. [213] 2015	CCl$_4$-stimulated mice; Kupffer cells	Not investigated	Atg5-KO			LC3-II: — P62: +++	α-SMA: +++ Sirius Red: +++

+++: increase; —: decrease; KO: knockout; KD: knockdown; CCl$_4$: carbon tetrachloride; TAA: thioacetamide; BDL: bile duct ligation; α-SMA: α-smooth muscle actin; PPAR-γ: peroxisome proliferator-activated receptor γ; PARP: poly(ADP-ribose) polymerase; HE: hematoxylin and eosin stain; Masson: Masson's trichrome stain; PDGFR-β: platelet-derived growth factor receptor type-b; IPF: idiopathic pulmonary fibrosis; EdU: 5-ethynyl-2$'$-deoxyuridine; LSECs: liver sinusoidal endothelial cells.

knockdown resulted in excessive accumulation of hepatic lipids and triglycerides in mouse liver. Furthermore, they investigated the rate of β-oxidation which is reflecting the level of FFA produced by triglyceride (TG) hydrolysis. The relative ratio of β-oxidation in Atg5-knockdown cells was significantly reduced compared with control cells. This result was consistent with the previous reduction in lipolysis. To further prove that autophagy regulated liver lipid metabolism, the authors measured the TG and cholesterol content in hepatocytes of mice with hepatocyte-specific Atg7 knockdown. They observed a significant increase in hepatic total cholesterol and TG accumulation. In contrast, the ratio of cholesterol in the lysosome was significantly reduced.

Subsequently, the role of lipophagy in promoting lipid metabolism was also confirmed in zebrafish liver cells. Wang et al. [159] observed the sequestered LDs in autophagic vacuoles of zebrafish liver cells by electron microscopy, thus confirming the occurrence of lipophagy. Inhibition of autophagy by chloroquine, a lysosomal acidification inhibitor that blocks the fusion of autophagosomes and lysosomes [160], significantly increased the LDs and TG content of the liver cells. Moreover, the chloroquine-induced lipophagy inhibition did also reduce the rate of β-oxidation significantly.

The decline of lipophagy in the aged or steatotic liver hinders the degradation of accumulated lipids in the liver and reduces the supply of FFAs for lipid metabolism, both further compromising cellular function [161, 162].

4.4. Impaired Mitophagy Leads to Decreased Mitochondrial Turnover and Increased ROS Production.
Hepatocytes are rich in mitochondria which are the crucial organelles for lipid metabolism. Each hepatocyte includes about 800 mitochondria [163, 164]. Mitochondria act as the "energy plant" of the cells. Fatty acids can undergo β-oxidation to generate Coenzyme A (CoA), which enters the citric acid cycle (CAC) and produces abundant NADH and flavin adenine dinucleotide (FADH2). Both NADH and FADH2 enter the oxidative phosphorylation process and generate large amounts of ATP [163].

Ogrodnik et al. [165] observed that hepatocyte senescence caused mitochondrial dysfunction and impaired the capacity of fatty acid oxidation. This in return facilitated lipid accumulation and promoted age-related hepatic steatosis. Age-related mitochondrial dysfunction does not only affect lipid metabolism and ATP synthesis but also leads to the production of large amounts of reactive oxygen species (ROS).

Under normal physiological conditions, about 2% of oxygen is used for the production of reactive oxygen species [163, 166]. A basal level of ROS promotes cell survival and repair. However, high levels of ROS are detrimental, since they initiate fibrotic changes leading to structural impairment of the liver. For example, ROS and other lipid peroxidation products are activating hepatic stellate cells to produce extracellular matrix proteins ultimately contributing to the development of hepatic fibrosis. Besides, the increased ROS levels further aggravate the impairment of lipid metabolism finally resulting in hepatocyte apoptosis and hepatic inflammation [167–169].

In brief, normal mitochondrial function is an important basis for maintaining hepatic metabolism. However, the age-associated impaired mitophagy in the liver leads to a decrease in mitochondrial turnover rate [170]. The number of dysfunctional mitochondria is increasing, which upregulates ROS production and ultimately aggravates hepatic steatosis (see Figure 4).

4.5. Restoring Autophagy Is Beneficial to Reduce Liver Steatosis.
Numerous studies demonstrated that promotion of autophagy can effectively reduce lipid accumulation in the liver (see Table 1). Therefore, promoting autophagy may result in a novel therapeutic strategy to mitigate hepatic steatosis [158, 171, 172].

The following studies focused on inducing autophagy to reduce fat accumulation by using Resveratrol, Trehalose, and Catalpol, but also commonly known autophagy inducers such as rapamycin and carbamazepine.

Resveratrol is a natural polyphenol commonly found in grapes. Tang et al. [173] observed that Resveratrol treatment significantly enhanced the protein expression of LC3-II and

TABLE 3: The role of autophagy in liver regeneration remains controversial.

(a) Activating autophagy via the mTOR-independent pathway facilitates liver regeneration

Author year	Research model	Autophagy pathway	Autophagy modulation	Enhanced autophagy	Increased regeneration	Reduced autophagy	Reduced regeneration
Guha et al. [266] 2019	Mice; MEFs; HEK293T cells	IPMK-AMPK-ULK1; IPMK-AMPK-SIRT1	IPMK-KO			LC3-II: —	Ki-67: — Edu: —
Jia et al. [267] 2019	Male SD rats	Not investigated	70% PVL	LC3-II: +++	Cyclin D1: +++		
Liu et al. [10] 2018	Male SD rats, primary rat hepatocytes	Not investigated	Young plasma Wortmannin 3-Methyladenine	LC3-II: +++ p62: —	Ki-67: +++	LC3-II: —	Ki-67: —
Wang et al. [268] 2017	Male C57BL/6 mice; AML12 cell line	Not investigated	TSG-6 3-Methyladenine	LC3-II: +++ Atg3: +++ Atg7: +++	Ki-67: +++ LBWR: +++	LC3-II: — Atg3: — Atg7: —	CellTiter Proliferation Assay: — LBWR: —
Lin et al. [265] 2015	Male C57BL/6 mice	mTOR-independent	Amiodarone Atg7-KD	LC3-II: +++ p62: —	Ki-67: +++ LBWR: +++	LC3-II: — Atg7: —	Ki-67: — LBWR: —
Cheng et al. [251] 2015	Liver progenitor cells	Not investigated	Beclin-1 overexpression Beclin-1-KD Atg5-KD	LC3-II: +++	PAS: +++	LC3-II: — p62: +++ Beclin-1: — Atg5: —	PAS: — CCK-8: —
Toshima et al. [257] 2014	Mice	Not investigated	Atg5-KO			LC3-II: — p62: +++ Atg5: —	BrdU: —

(b) Activating autophagy via the mTOR-dependent pathway impairs liver regeneration

Author year	Research model	Autophagy pathway	Autophagy modulation	Enhanced autophagy	Reduced regeneration	Reduced autophagy	Increased regeneration
Shi et al. [269] 2018	Balb/c mice	mTOR-dependent	Rapamycin ASPP2-haploinsufficient	LC3-II: +++	PCNA: — LBWR: —	LC3-II: — p62: +++	PCNA: +++ LBWR: +++
Fouraschen et al. [208] 2013	Male C57BL/6J mice	mTOR-dependent	Rapamycin & steroid dexamethasone	LC3-II: +++	PCNA: — BrdU: — LWRR: —		
Kawaguchi et al. [260] 2013	Male C57BL/6J mice	mTOR-dependent	Temsirolimus		PCNA: — LBWR: —		
Espeillac et al. [102] 2011	Male C57BL/6J mice	mTOR-dependent	Temsirolimus		BrdU: —		
Palmes et al. [258] 2008	Male Lewis rats	mTOR-dependent	Rapamycin		Ki-67: —		
Jiang et al. [259] 2001	Male SD rats	mTOR-dependent	Rapamycin		LWRR: —		

+++: increase; —: decrease; KO: knockout; KD: knockdown; IPMK: inositol polyphosphate multikinase; SIRT1: sirtuin 1; ULK1: Unc-51 like autophagy activating kinase 1; PVL: portal vein ligation; LBWR: liver to body weight ratio; LWRR: liver-weight recovery rate; TSG-6: tumor necrosis factor-inducible gene 6 protein; PAS: periodic acid–Schiff stain.

Beclin-1, while p62 was reduced in C57BL/6J mice subjected to ethanol diet, indicating that autophagy was activated. In contrast, ethanol-induced steatosis was significantly alleviated in Resveratrol-treated mice, mainly manifested by a decrease of triglyceride, low density-lipoprotein cholesterol, and an increase of high-density lipoprotein cholesterol.

Trehalose is a natural disaccharide, which is usually used as a medical desiccant. Nowadays, it has attracted much attention as a mTOR-independent autophagy inducer [12, 174]. DeBosch et al. [175] observed that Trehalose prevented cells from taking up glucose via blocking glucose transporters in the plasma membrane. Doing so, Trehalose treatment induced a "starvation-like" condition triggering autophagy even in the presence of nutrients. Activation of autophagy alleviated accumulation of LDs in hepatocytes. This effect was attributed at least partly to preventing hexose uptake

TABLE 4: Induction of autophagy alleviates hepatic mitochondrial dysfunction.

Author year	Research model	Autophagy pathway	Autophagy modulation	Enhanced autophagy	Improved mitochondrial function	Reduced autophagy	Increased mitochondrial dysfunction
Recent scientific evidence that activating autophagy improves liver mitochondrial dysfunction							
Li et al. [307] 2020	HFD-fed male mice; palmitic acid-stimulated AML-12 cells; primary human hepatocytes	PINK1-Parkin	Cyanidin-3-O-glucoside	PINK1: +++ Parkin: +++ p62: —	CPT1A: +++ SOD: +++ GSH-PX: +++ H_2O_2: — MDA: — IL-1B: —		
Shan et al. [308] 2019	Acetaminophen-stimulated male C57/BL6 mice	PINK1-Parkin	Rapamycin Chloroquine	LC3-II/I: +++ p62: —	MA: — IL-1B: — NLRP3: —	p62: +++	IL-1B: +++ NLRP3: +++
Yu et al. [309] 2019	Palmitic acid and lipopolysaccharide-stimulated HepG2 cells	PINK1	Liraglutide 3-Methyladenine PINK1-KD	PINK1-FL: +++ Parkin: +++	ROS: — IL-1B: — NLRP3: — ATP: +++	PINK1: —	NLRP3: +++
Zhou et al. [310] 2019	HFD-fed male mice; palmitic acid-stimulated primary hepatocytes	AMPK-Parkin	Macrophage stimulating 1-KO	LC3-II/I: +++ Parkin: +++	$\Delta\Psi$m: +++ ROS: —		
Liu et al. [311] 2018	HFD-fed male C57BL/J mice; oleate/palmitate-stimulated HepG2 cells	PINK1-Parkin	Quercetin	LC3-II: +++ Parkin: +++	CPT1: +++ RCR: +++ $\Delta\Psi$m: +++ MA: —		
Zhou et al. [300] 2018	HFD-fed C57BL/6J mice; palmitic acid-stimulated primary hepatocytes	Bnip3	Melatonin	LC3-II: +++ Atg5: +++ Beclin1: +++	ATP: +++ $\Delta\Psi$m: +++ OCR: +++		
Yu et al. [299] 2016	Ethanol diet-fed male C57BL/6J mice	AMPK-ERK2	Quercetin	Parkin: +++ VDAC1: +++	$\Delta\Psi$m: +++ MA: —		
Williams et al. [312] 2015	Ethanol administration C57BL/6J mice	Parkin	Parkin-KO			MPG: —	RCR: — COX: — MA: —

+++: increase; —: decrease; KO: knockout; KD: knockdown; MA: morphological abnormalities; ERK2: extracellular signal-regulated kinase 2; VDAC1: voltage-dependent anion channel 1; CPT1/1A: carnitine palmitoyltransferase 1/1A; PINK1-FL: PINK1 precursor; NLRP3: nucleotide-binding oligomerization domain, leucine-rich repeat-containing receptor-containing pyrin domain 3; RCR: respiratory control ratio; COX: cytochrome c oxidase; MPG: mitophagosomes; Bnip3: Bcl-2/E1B-19KD-interacting protein 3; OCR: oxygen consumption rate; H_2O_2: hydrogen peroxide; SOD: superoxide dismutase; GSH-PX: glutathione peroxidase; MDA: malondialdehyde; GSSG: glutathione disulfide.

and subsequently triggering the AMPK-ULK1 pathway. Moreover, Trehalose significantly mitigated the accumulation of triglycerides induced by fructose in primary hepatocytes. Similar results were observed in independent experiments using the HepG2 cell line and mouse liver.

Catalpol is an iridoid glucoside mainly obtained from the root of Rehmannia glutinosa. This drug is commonly used for neurodegenerative diseases, e.g., Alzheimer's disease. Catalpol administration alleviated hepatic steatosis via enhancing autophagy in both ob/ob mice and mice subjected to a high-fat diet (HFD) as observed by Ren et al. [176]. They also reported that Catalpol mitigated Palmitate-induced lipid accumulation in HepG2 cells by activating autophagy via the AMPK-Transcription Factor EB (TFEB) pathway. In contrast, treatment with the AMPK inhibitor (Compound C) almost abolished the protective effect of Catalpol on lipid accumulation in HepG2 cells, supporting the crucial role of autophagy in hepatic steatosis.

Using other autophagy inducers as done by Lin et al. [177] resulted in similar observations: they reported that rapamycin and carbamazepine also relieved hepatic steatosis in C57BL/6 mice by inducing autophagy. In contrast, treatment of mice with autophagy inhibitors (chloroquine) exacerbated hepatic steatosis and injury.

To our knowledge, there is no widely accepted pharmacological strategy for fatty liver disease. Many clinical guidelines recommended that exercise is an effective way to improve nonalcoholic fatty liver disease. Recent studies demonstrated that exercise may improve NAFLD through enhancing autophagy as well. Chun et al. [178] reported that exercise may trigger hepatic autophagy via regulating muscle-derived myokines. First, postexercise reduction of C1q/TNF-related protein 5 (CTRP5) inhibited the activity of the mTORC1 to induce autophagy. Second, the increase of irisin, a myokine secreted by skeletal muscle after exercise, promoted the stimulation of AMPK. The subsequent
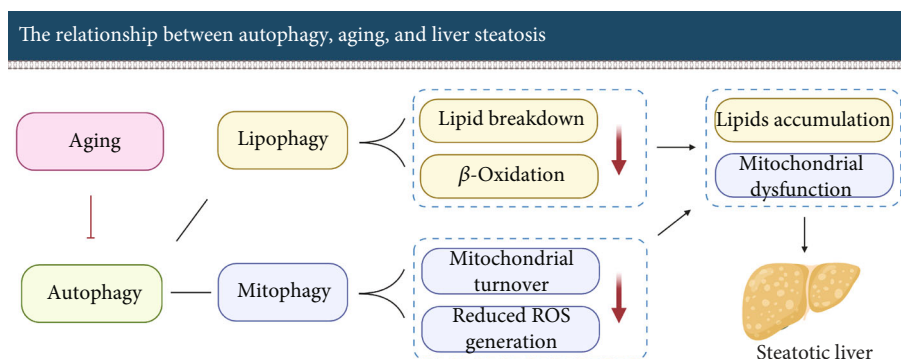
FIGURE 4: Aging-related decline of autophagy activity leads to impaired lipid metabolism in the liver. Impaired autophagy results in decreased lipid metabolism and in reduced mitochondrial turnover. These changes lead to the accumulation of lipid droplets in the hepatocytes and an increase of ROS production, which contributes to the accumulation of fat in the liver ultimately resulting in hepatic steatosis.

activation of AMPK activated ULK1 resulting in enhanced autophagy. Besides, exercise can also induce autophagy via releasing Beclin-1 from its complex with B-cell lymphoma-2 (Bcl2). As mentioned before, Beclin-1 can promote autophagy via forming a PI3K-3 complex which is crucial for the initiation of autophagosomes [133].

To sum up, activating autophagy removes dysfunctional mitochondria, reduces ROS production, degrades excess lipids, and promotes β-oxidation in the steatotic liver. Therefore, modulating autophagy seems to be an effective strategy in alleviating liver steatosis and preventing the development of fatty liver diseases, possibly also suitable to treat age-related steatosis.

5. Liver Fibrosis

Liver fibrosis is the consequence of an imbalance in the generation and degradation of extracellular matrix (ECM), which is usually caused by acute or chronic liver damage [189]. In essence, liver fibrosis is a wound healing response to various liver injuries. Aging is considered as one of the important risk factors for liver fibrosis [190]. Liver fibrosis may gradually progress to liver cirrhosis in case of chronic liver damage. At present, there is no effective clinical treatment for liver fibrosis.

Hepatic stellate cells (HSCs) reside in the space of Disse and account for about 5-8% of the total number of liver cells. In a normal liver, most of the HSCs are at a quiescent state with low proliferative activity [191, 192]. Activation of hepatic stellate cells (HSCs) is now widely recognized as a major driver for the initiation and progression of hepatic fibrosis in rodents and humans [193]. Hepatic stellate cells are usually activated when the liver undergoes injury. Activated HSCs are characterized by increasing proliferation, chemotaxis, and contractility. Upon activation, they secrete large amounts of fibrogenic factors that facilitate the generation of collagen. Excessive deposition of the extracellular matrix is indicative of hepatic fibrosis [194–197].

Quiescent HSCs contain high amounts of cytoplasmic LDs with triglyceride and retinyl esters. During the process of HSC activation, LDs are degraded and activate HSCs to secrete excessive amounts of the extracellular matrix proteins such as collagen and fibronectin. Upon activation, HSCs undergo a transformation from LD-rich cells to myofibroblast-like cells, a process which is accompanied by an upregulation of autophagic flux [198–200].

5.1. Autophagy Provides Energy for Activation of Hepatic Stellate Cells via Lipid Degradation. Autophagy may provide energy to promote the activation of HSCs [198–200]. This view is supported by several independent authors.

Hepatic injury triggers autophagy which in turn promoted ATP-production. Hernández-Gea et al. [201] observed that hepatic injury induced by carbon tetrachloride (CCl$_4$) or thioacetamide (TAA) enhanced the autophagy level in C57BL/6 mice. They established HSC-specific Atg7-knockdown mice. After inducing chronic fibrosis using CCl$_4$ for 6 weeks in genetically modified and wild-type mice, the collagen accumulation in Atg7-knockdown mice was significantly decreased compared with control mice. Interestingly, the number of α-SMA positive HSCs in Atg7-knockdown animals was not significantly different from that in control mice. However, the expression of total α-SMA protein in HSCs of Atg7-knockdown animals was significantly reduced, indicating that the absence of Atg7 reduced the expression of α-SMA in each HSC instead of affecting the number of HSCs. In addition, Atg5/7 knockdown, as well as pharmacological inhibition of autophagy through administration (3-MA or chloroquine), substantially reduced fibrogenic mediators in mouse stellate cells. It is worth noting that there was a significant increase in the number of LDs in mouse stellate cells obtained after Atg5/7 knockdown, respectively, 3-MA treatment.

Furthermore, 3-MA-mediated inhibition of autophagy caused a substantial decrease in ATP levels of the cells. In contrast, the administration of oleic acid in mouse stellate cells enhanced ATP levels and abolished the reduction of fibrogenesis mediated via inhibition of autophagy. These results imply that autophagy facilitated the breakdown of lipid droplets into FFAs in mouse stellate cells. Subsequently, these FFAs are oxidized in mitochondria to generate ATP needed for the activation of mouse stellate cells.

Moreover, Thoen et al. [198] found a significant elevation in autophagy levels during HSC activation. In contrast,

inhibition of autophagy prevented HSC activation. In more detail, they treated HSCs with Bafilomycin A1, a V-ATPase inhibitor preventing the acidification of lysosome and the fusion of the autophagosome with lysosome [202, 203]. Bafilomycin A1 treatment of HSCs resulted in a significant decrease in α-SMA. The proliferation rate of Bafilomycin A1-treated HSCs was reduced by approximately 6-fold compared to control HSCs. In contrast, HSCs responded to activation when Bafilomycin A1 treatment was discontinued.

Inhibition of autophagy using chloroquine resulted in similar observations. He et al. [204] demonstrated that chloroquine attenuated CCl_4-induced liver fibrosis in Sprague-Dawley rats by inhibiting autophagy and thereby HSC activation. Compared with the animals of the control group, the expression levels of serum ALT, aspartate aminotransferase (AST), hydroxyproline (an extracellular matrix marker), and α-SMA were significantly decreased in the chloroquine group. In contrast to Hernández-Gea et al.'s findings, He et al. observed that chloroquine-mediated autophagy inhibition improved liver injury as well. This additional finding may be related to the fact that they did not only use a different modeling method but also a different species of animals.

Taken together, these studies imply that induction of autophagy promotes the initiation of liver fibrosis by degrading intracellular lipids to provide the energy needed for HSC activation.

However, rapamycin, an autophagy inducer known for its antiproliferative effect, had an opposite effect and reduced hepatic fibrosis. In this case, the effect was attributed to the antiproliferative effect on HSCs rather than to the autophagy-inducing capacity suggesting the promotion of fibrosis. For better illustration of this seemingly contradictory effect, we describe the experimental observations reported by Zhu et al. [205]. They investigated the effect of rapamycin on hepatic stellate cells in Sprague-Dawley rats with CCl_4-induced liver fibrosis. In their hands, rapamycin treatment reduced the extent of rat liver fibrosis induced by CCl_4 compared to the control group.

Further experiments revealed that rapamycin significantly inhibited the proliferation of HSCs stimulated by the platelet-derived growth factor. However, treating HSCs with rapamycin did not significantly affect the expression of ECM-related proteins. The inhibition of HSC proliferation by rapamycin appeared to be the main reason for its alleviation of liver fibrosis. This antiproliferative effect of rapamycin on various cell types has been confirmed repeatedly in different studies [206–208].

We will elucidate the mechanism conveying its antiproliferative effect in the next section dedicated to explain the impact of aging and autophagy on liver regeneration later in this review (Section 6.4).

5.2. Autophagy May Indirectly Reduce Fibrosis by Ameliorating Liver Injury.
Hepatic fibrosis is a common result of different liver diseases such as NAFLD, alcoholic hepatitis, and drug intoxication. Induction of autophagy is currently considered to exert a therapeutic effect on these hepatic diseases causing liver injury. For example, alcohol abuse increases liver metabolic burden, induces accumula-

tion of lipid droplets, and impairs mitochondrial function leading to increased oxidative stress. Autophagy may alleviate alcohol-induced hepatic injury by selectively eliminating dysfunctional mitochondria (mitophagy) and lipid droplets (lipophagy) [209].

Moreover, intoxication with acetaminophen, a commonly antipyretic drug, can cause severe liver damage such as acute hepatocyte necrosis and mitochondrial damage [210]. Ni et al. [210] observed that rapamycin-induced autophagy mitigated acetaminophen-induced hepatotoxicity via eliminating impaired mitochondria in C57BL/6 mice. In contrast, inhibition of autophagy using chloroquine aggravated acetaminophen-induced hepatotoxicity.

5.3. The Effect of Modulating Autophagy on Liver Fibrosis Is Dependent on Cell Types.
Inhibition of autophagy may mitigate hepatic fibrosis by alleviating hepatocyte injury, by reducing endothelial dysfunction, and by decreasing inflammatory cytokines synthesized and released from macrophages (see Figure 5) [211–214].

Here, we present the experiments of Lodder et al. [213] for further illustration that autophagy inhibition via Atg5-knockout aggravated fibrosis. Lodder et al. stated that macrophages were involved in promoting both inflammatory and liver fibrogenesis by secreting cytokines such as ROS-induced IL-1A/B. Compared with wild-type mice, Atg5-knockdown mice subjected to treatment with CCl_4 demonstrated higher levels of proinflammatory cytokines IL-1A/B in the liver. Furthermore, mice with Atg5-knockdown developed a higher degree of fibrosis compared to wild-type animals. These mice also showed higher protein level of fibrosis-related proteins such as α-SMA and mRNA expression of fibrogenic-related genes such as matrix metallopeptidase 9 (Mmp9), transforming growth factor beta 1 (TGF-β1), and serpine 1 in the liver. Administration of the Atg5-knockout mice with recombinant interleukin-1 receptor antagonist (IL-1RN) substantially reduced CCl_4-induced liver injury and fibrosis. Taken together, these results illustrate that autophagy attenuates liver fibrosis by reducing the release of IL-1A/B.

Similarly, Ruart et al. [214] demonstrated that selective autophagy suppression by cell-specific Atg7 knockdown in endothelial cells exacerbated CCl_4-induced liver fibrosis in mice. Autophagy suppression decreased the ability of LSECs to respond to oxidative stress and led to endothelial dysfunction, which in turn activated HSCs. The authors observed a marked reduction in the porosity and number of fenestrae in LSECs of Atg7-knockdown mice via scanning electron microscopy. Besides, hydroxyproline and α-SMA expression in mouse liver was increased, but there was no difference in the expression of platelet-derived growth factor receptor beta (PDGFR-β, a proliferation marker of HSCs). These results reflected that the aggravation of liver fibrosis in Atg7-knockdown mice may be due to EC-mediated activation rather than proliferation of HSCs.

5.4. Selective Inhibition of Autophagy in HSC Appears to Be a Promising Antifibrosis Strategy for the Aging Liver.
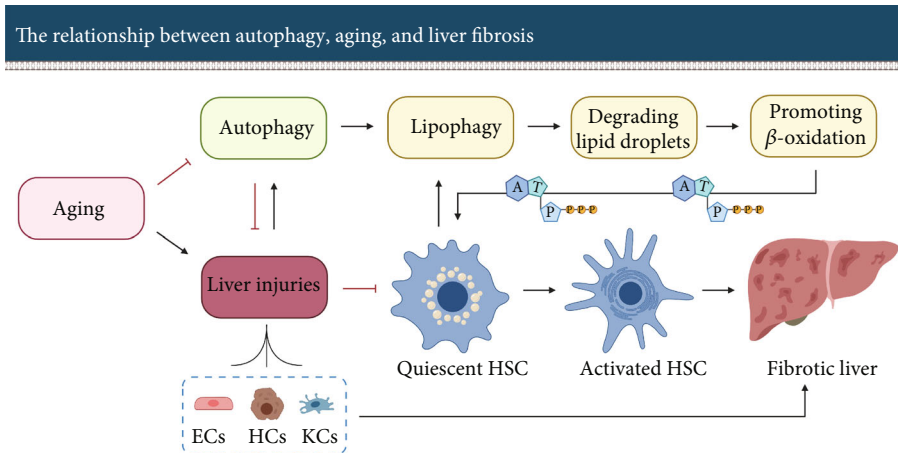As explained above, autophagy has a dual role in the process of

FIGURE 5: Autophagy plays a dual role in liver fibrosis. First, it promotes the initiation of fibrosis by providing the energy required for activation of hepatic stellate cells. On the other hand, it alleviates liver fibrosis by improving the function and status of other hepatic cells such as hepatocytes, endotheliocytes, and macrophages. ECs: endotheliocytes; HCs: hepatocytes; KCs: Kupffer cells.

liver fibrosis (see Table 2). On the one hand, upregulation of autophagy induces HSC activation, leading to the initiation and progression of hepatic fibrosis. On the other hand, upregulation of autophagy may also result in an antifibrotic effect. However, the profibrotic effect of inducing autophagy and thereby providing energy for HSC activation seems to be more pronounced than the antifibrotic effect exerted by relieving cellular oxidative stress and inflammation.

It is worth noting that basal autophagy takes place continuously in eukaryotes as it is essential for intracellular homeostasis and cellular self-renewal [215, 216]. As the autophagy activity in the aged liver declines, further inhibition of autophagy may cause serious adverse effects for the liver and other organs. Therefore, only selective inhibition of autophagy in HSCs appears to be a potentially effective antifibrotic strategy.

6. Impaired Liver Regeneration

Unlike other visceral organs, the liver has an amazing capacity for regeneration. It is the pathophysiological basis for successful surgery such as liver resection and partial liver transplantation. After rodents undergo 2/3 partial hepatectomy (PH), the remaining liver tissue is almost restored to its original volume and function in about 1-2 weeks [225, 226].

6.1. Liver Regeneration Is Mainly Accomplished by Two Different Regenerative Mechanisms. Liver regeneration is mainly achieved by two regenerative mechanisms: first, the division of mature hepatocytes; second, the renewal and differentiation of liver progenitor cells (LPCs) [12, 227].

The first mechanism of liver regeneration consists of well-orchestrated hepatocyte proliferation, a sophisticated process that includes three phases: the priming stage, proliferation stage, and termination stage. In the priming stage, quiescent hepatocytes shift from G0 to G1 phase within 4 hours after PH-induced stimulation in rodents [228]. In the

proliferation stage, hepatocytes are stimulated by several mitogens such as hepatocyte growth factor (HGF) and transforming growth factor-alpha (TGF-α) to cross the restriction point of the G1 phase. Then, they enter the synthesis and mitotic phase [229–234]. The termination stage starts once liver mass is almost restored to its original level. Hepatocyte proliferation ceases under the regulation of transforming growth factor beta (TGF-β), activin, and interleukin-1A/B (IL-1A/B) [226, 235–245].

The second mechanism is based on LPCs, which are involved in the regeneration of animal livers under certain conditions [246, 247]. LPCs are bipotent progenitor cells that reside in the canal of Hering. When the liver is severely injured or is chronically damaged, the remaining hepatocytes may not be able to meet the regenerative demand. Then, LPCs will be activated and promote liver regeneration via renewing and differentiating into hepatocytes and cholangiocytes [248–251].

6.2. Aging Significantly Impairs Liver Regeneration. Aging leads to a significant decrease in the regenerative capacity of the liver in respect to hepatocyte proliferation as well as LPC division and differentiation. In the aged liver, there are fewer hepatocytes entering the S phase (about 30%) compared with the young liver (90%-100%). Furthermore, senescent hepatocytes enter the S phase more slowly [252].

Also, the responsiveness of LPCs to liver injury decreases with age. For example, Cheng et al. reported that LPCs of young mice are activated to proliferate following chronic liver injury induced by a choline-deficient, ethionine-supplemented (CDE) diet. However, LPCs in aged mice did not respond effectively to the injury, leading to defective liver regeneration. According to Cheng et al., hepatic stellate cells of aged mice secreted more chemokine (C-X-C motif) ligand 7 (CXCL7) than those of young mice, attracting more neutrophils to infiltrate the liver. Neutrophil infiltration resulted in excessive ROS production, thereby restraining the activation and proliferation of LPCs, which further impaired liver regeneration [247].
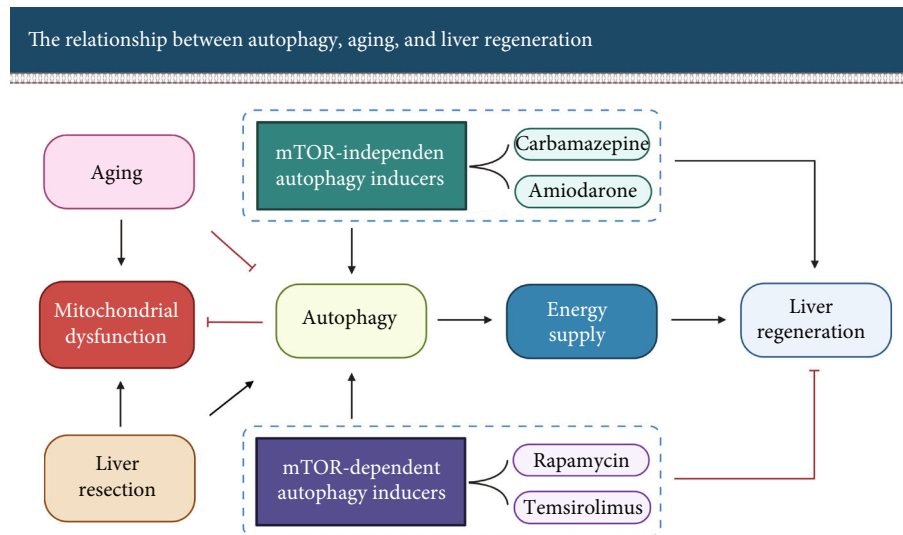
FIGURE 6: The effect of autophagy on liver regeneration in the aged individual. Liver resection and aging lead to mitochondrial dysfunction. Autophagy can degrade dysfunctional mitochondria and other cellular components to promote the synthesis of new organelles and energy production, thereby facilitating liver regeneration. However, the induction of autophagy through the mTOR pathway impedes cell proliferation. Therefore, inducing autophagy via the mTOR-independent pathway is more appropriate for promoting liver regeneration.

As described before, aging causes structural changes of the liver such as steatosis and fibrosis. Both can be further aggravated by the lifestyle of the patients, e.g., dietary overload or extensive alcohol consumption leading to NAFLD and/or alcoholic fibrosis and even cirrhosis. Both NAFLD and alcoholic cirrhosis are further impairing liver regeneration substantially [253, 254]. The overall impaired regenerative capacity of the aged liver leads to a remarkably increased risk of hepatic failure after partial hepatectomy [255].

6.3. Autophagy Provides the Necessary Energy for Liver Regeneration. Liver regeneration is an energy-intensive process. The division and growth of hepatocytes require abundant energy supply [256]. Hepatocytes are rich in mitochondria, but liver resection can cause substantial mitochondrial damage and decrease hepatocyte ATP synthesis. Correspondingly, Toshima et al. reported a significant decrease in ATP reserves within 6 h after liver resection [257].

During the initial stage of liver regeneration, autophagy, particularly mitophagy, is crucial for maintaining healthy mitochondria to generate ATP. Mitophagy can selectively eliminate dysfunctional mitochondria in order to reduce ROS production, promote mitochondrial regeneration, and facilitate ATP synthesis [62–64, 215]. This process contributes to the required energy and environment for liver regeneration (see Figure 6). However, the autophagy level in the aged liver is significantly reduced. Therefore, appropriate induction of autophagy seems to be a promising strategy to promote regeneration, especially of the aged liver.

6.4. Autophagy Induced through the mTOR-Dependent Pathway Impairs Liver Regeneration. As mentioned above, autophagy can be activated by both mTOR-dependent pathways and mTOR-independent pathways. However, mTOR is not only an essential regulator of autophagy but also a key

regulator of cell proliferation [12, 98]. Inhibiting mTOR induces autophagy, but it also significantly impairs cell proliferation.

For example, rapamycin, a classic mTOR inhibitor, induces autophagy by inhibiting mTOR activity. Rapamycin inhibits mTORC1 by forming a complex with FK506-binding protein 12. This complex acts on downstream targets to restrain protein synthesis and causes cell-cycle arrest by preventing the transition from G1 to S phase [87, 258]. The antiproliferative effect has been demonstrated in several independent experiments regarding liver regeneration [208, 259]. Similar results have also been observed with other mTOR inhibitors such as Temsirolimus [260]. Therefore, activating autophagy by inhibiting mTOR activity does not seem to be appropriate for facilitating liver regeneration (see Figure 6).

6.5. Autophagy Induced through the mTOR-Independent Pathway Appears to Promote Liver Regeneration. Activation of autophagy without suppression of cell proliferation is a better option for liver regeneration. Therefore, inducing autophagy via the mTOR-independent pathway seems promising in promoting liver regeneration (for more molecular details, see also Xu et al. [12]). By now, the role of this pathway for liver regeneration has been investigated by a number of authors (see Table 3). They demonstrated that the use of different mTOR-independent autophagy inducers such as carbamazepine and amiodarone promoted liver regeneration.

Carbamazepine is a common antiepileptic medication that can be used to prevent and control seizures. It has recently been shown to induce autophagy through depletion of cytosolic inositol and AMPK activation. The depletion of cytosolic inositol causes a decrease in basal IP_3, which reduces energy production via blocking mitochondrial

calcium influx. The reduced energy level activates the AMPK-ULK1 pathway to enhance autophagy [261, 262].

In 2013, Kawaguchi et al. [260] observed that carbamazepine treatment substantially promoted hepatocyte proliferation after PH in mice through activation of mTOR and its downstream factor S6K. Three proliferation indices, Ki-67, 5-Bromo-2′-Deoxyuridine (BrdU), and the Proliferating Cell Nuclear Antigen (PCNA) index as well the LBWR levels, were significantly increased on postoperative day 2 (POD2) in carbamazepine-treated animals compared to control animals. On the contrary, the application of mTOR inhibitor Temsirolimus abolished the effect of carbamazepine in promoting hepatocyte proliferation, indicated by a marked decrease in the protein expression of PCNA and LBWR of animals on POD2.

Amiodarone is a potent antiarrhythmic medication that is mainly used to promote the restoration of normal heart rhythm. It is currently obtaining attention as an autophagy inducer. Amiodarone treatment decreases intracellular Ca^{2+} concentration by inhibiting L-type Ca^{2+} channels at the plasma membrane to block extracellular Ca^{2+} entry. Reducing intracellular Ca^{2+} concentration can induce autophagy [132, 263, 264]. In 2015, Lin et al. [265] observed that amiodarone could significantly induce autophagy via the mTOR-independent pathway and boost liver regeneration. After PH, LC3-II was significantly higher and p62 level lower in the amiodarone-treated mice compared to the control mice. The Ki-67, PCNA, cyclin D1 levels, and LBWR were substantially increased, but the level of p21 decreased significantly in amiodarone-treated mice, altogether demonstrating an improved hepatic proliferative response. As a contrast, inhibition of autophagy via chloroquine pretreatment or Atg7 knockdown deteriorated liver regeneration. Correspondingly, decreased Ki-67, PCNA, cyclin D1, and LBWR and increased TGF-β1 were observed in the autophagy-suppressed mice.

Overall, selecting the appropriate pathway to induce autophagy is essential for promoting liver regeneration. Enhancing autophagy through the mTOR-dependent pathway alone seems to be rather harmful to liver regeneration. In contrast, inducing autophagy through the mTOR-independent pathway does not affect cell proliferation. Therefore, exploring novel mTOR-independent autophagy inducers without obvious side effects has the great potential to improve liver regeneration, especially in aged patients with reduced autophagy.

7. Mitochondrial Dysfunction

Mitochondria are the sites of oxidative phosphorylation in cells [270]. The synthesis of ATP through oxidative phosphorylation is one of the key functions of mitochondria. This process is regulated by four respiratory chain complexes, type I NADH dehydrogenase (complex I), succinate dehydrogenase (complex II), CoQH2-cytochrome c reductase (complex III), cytochrome c oxidase (complex IV), and another ATP synthase (complex V). All these complexes are located on the inner membrane of mitochondria [271–273]. Mitochondrial bioenergy is pivotal to maintain liver function. Mitochondrial dysfunction can lead to impaired energy metabolism and increased production of reactive oxygen species, which in turn triggers cell senescence and apoptosis [20, 274].

7.1. Aging Impairs the Function of Hepatic Mitochondria.
Evidence in human and animal liver manifests that aging results in increased oxidative stress and decreased mitochondrial bioenergetics. Actually, mitochondrial dysfunction is considered to be one of the crucial features of the aging process.

One feature of mitochondrial dysfunction is the loss of activity of mitochondrial enzymes. To give one example, Navarro and Boveris [275] observed in aged rat livers that the activity of key enzymes indicative of mitochondrial function decreased substantially compared to young rats. They investigated type I NADH dehydrogenase (complex I), cytochrome oxidase (complex IV), mitochondrial nitric oxide synthase, and Mn-superoxide dismutase and reported a loss of activity in these enzymes of about 30%, 24%, 47%, and 46%, respectively. The reduced activity of respiratory chain complexes impaired energy synthesis of mitochondria in the hepatocytes from aged rats. Yen et al. [276] used human livers and confirmed that mitochondrial respiration was also deficient in isolated mitochondria from the aging human liver.

Other features of mitochondrial dysfunction are the reduction of the mitochondrial membrane potential ($\Delta\Psi$m) and the increase of peroxide production. Sastre et al. [277] used liver cells from aged Wistar rats in comparison to young rats and observed a 30% reduction in mitochondrial membrane potential and a 23% increase in mitochondrial peroxide production. This was accompanied by an age-related increase in size.

7.1.1. Age-Related Mitochondrial Dysfunction Is Associated with the Accumulation of mtDNA Mutations.
Mitochondria contain their own genome, a 16.5 kb double-stranded circular molecule (mtDNA) which encodes 2 mammalian ribosomal RNAs, 22 transfer RNAs, and 13 proteins. The 13 proteins encoded by mtDNA are the constituent of respiratory chain enzymes [273, 278]. Mitochondrial dysfunction is usually associated with mitochondrial DNA (mtDNA) mutations.

mtDNA is located near the main site of ROS generation—the respiratory chain. ROS are a byproduct of oxidative metabolism. It can induce oxidative damage to mtDNA and is thought to be responsible for mtDNA mutations that accumulate with aging [279, 280]. Vermulst et al. [281] established a genetically modified animal that enhances the expression of human catalase (a ROS scavenger). The level of mtDNA mutations in heart and mouse embryonic fibroblasts (MEFs) of these animals was significantly lower than in WT animals. This result demonstrated that oxidative stress plays a negative role in mtDNA mutations. The cumulative effect of ROS affects genetic information of mtDNA causing point mutations, deletions, or duplications of mtDNA [282]. Ultimately, the accumulation of mtDNA
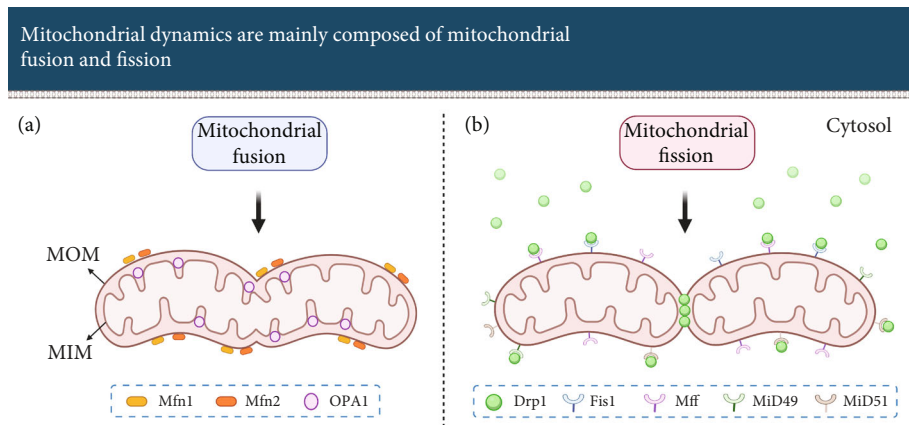
FIGURE 7: Mitochondrial dynamics mainly include mitochondrial fusion and fission. Mitochondria perform fusion and fission under the joint regulation of multiple signals. (a) Mfn1 and Mfn2 regulate mitochondrial outer membrane fusion; OPA1 regulates mitochondrial inner membrane fusion. (b) Fis1, Mff, MiD49, and MiD51 are anchored at the mitochondrial outer membrane to recruit Drp1 from the cytosol, which facilitates that mitochondria contract and split into several mitochondria. MOM: mitochondrial outer membrane; MIM: mitochondrial inner membrane.

mutations and ROS leads to impaired respiratory chain activity and energy production [283].

In 2004, Trifunovic et al. [284] established mtDNA mutator mice that express a checking-deficient version of PolgA (mtDNA polymerase gamma). The mtDNA mutator mice successfully express a mtDNA mutant phenotype with an about 4-fold increase in point mutations in the liver and a concomitant increase of deleted mtDNAs. The lifespan of mtDNA mutant mice was significantly shorter compared to control animals. Phenotypic features related to aging such as fertility did decline. In contrast, age-related impairments like osteoporosis and anaemia did appear prematurely in these animals. Moreover, the enzymatic activity of the respiratory chain was decreased. These results suggest that mtDNA mutations cause mitochondrial dysfunction and aggravate the aging process.

But this view has also been challenged. In 2007, Vermulst et al. [281] could not confirm that mtDNA mutations shortened the longevity of wild-type mice. Although the point mutations of mtDNA in wild-type mice increased about 11-fold with age, mitochondrial mutator mice could tolerate a 500-fold higher mutational burden than control mice without any evident accelerated aging characteristics. It is worth noting the authors pointed out that their technique can only detect small deletion of mtDNA but not the large-scale deletion of mtDNA.

Overall, the age-related ROS increase is considered to be an important causal factor of mtDNA mutations. mtDNA mutations substantially impair the efficiency of the respiratory chain and contribute to mitochondrial dysfunction. However, whether mtDNA mutations directly accelerate the aging process and affect human lifespan still needs further investigation.

7.1.2. Aging Impairs Mitochondrial Dynamics.
Mitochondria are dynamic organelles that constantly undergo fission and fusion to form network structures in cells. This process usually is termed mitochondrial dynamics (see Figure 7) [285,

286]. It is involved in regulating the morphology, distribution, and property of mitochondria [285, 287, 288].

Mammalian mitochondrial fusion is mainly mediated by mitofusin 1 (Mfn1), Mfn2, and optic atrophy 1 (OPA1). All of them are dynamin-related GTPases, but their function is different during mitochondrial dynamics. Mfn1 and Mfn2 are involved in fusing the outer membranes of mitochondria, while OPA1 is in charge of fusing the inner membranes of mitochondria. Mammalian mitochondrial fission is mainly regulated by dynamin-related protein 1 (Drp1). It interacts with his receptor proteins, mitochondrial dynamics protein of 49 kDa (MiD49), MiD51, fission 1 (Fis1), and mitochondrial fission factor (Mff), to promote the constriction of mitochondrial membrane and mitochondrial fission [285, 289].

Mitochondrial dynamics plays a vital role in mitochondrial quality control. Malfunctioning mitochondria may lose their fusing capacity to prevent damaged mitochondria from merging back into the mitochondrial network [289]. These dysfunctional mitochondria will be degraded by mitophagy. However, the age-dependent decline of mitophagy not only inhibits the clearance of dysfunctional mitochondria but also affects the mitochondrial biogenesis, leading to the gradual accumulation of dysfunctional mitochondria [290].

7.2. Mitophagy Effectively Promotes Mitochondrial Turnover.
Dysfunctional mitochondria promote ROS generation. Mitophagy can selectively degrade damaged mitochondria, reduce excessively produced ROS, facilitate mitochondrial regeneration, and promote the survival of cells in stressful environments [291, 292]. The serine/threonine kinase PTEN-induced kinase 1(PINK1) and E3 ubiquitin ligase Parkin are considered to be two crucial factors that mediate mitophagy.

PINK1 is thought to sense mitochondrial quality. It includes a mitochondrial targeting sequence (MTS) and can be recruited into mitochondria. In normal mitochondria, PINK1 is translocated into the outer mitochondrial
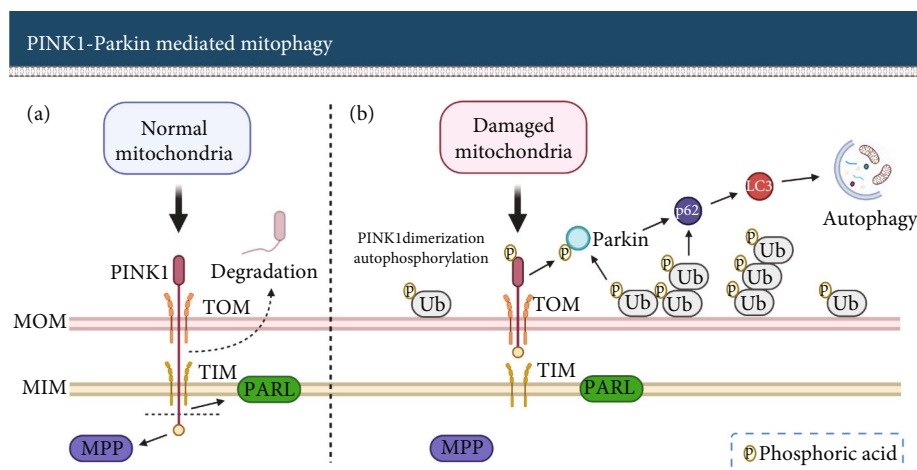
FIGURE 8: PINK1-Parkin-mediated mitochondrial autophagy (mitophagy) eliminates damaged mitochondria. (a) In the case of normal mitochondria, Pink1 is cleaved twice by MPP and PARL then decomposed by the proteasome system. (b) When mitochondria are damaged, due to changes such as the dissipation of membrane potential ($\Delta\Psi$m), PINK1 aggregates in the outer mitochondrial membrane to undergo dimerization and autophosphorylation. Parkin and ubiquitin are phosphorylated via PINK1. PINK1-Parkin facilitates mitophagy via the recruitment of autophagy receptor proteins and mitochondrial ubiquitination. MOM: mitochondrial outer membrane; MIM: mitochondrial inner membrane; TOM: translocase outer membrane; TIM: translocase inner membrane.

membrane through the translocase outer membrane (TOM) complex and into the inner mitochondrial membrane with the mediation of the translocase inner membrane (TIM) complex. The MTS fragment of PINK1 is cleaved by the mitochondrial processing peptidase (MPP) in the matrix. Then, PINK1 is degraded by the proteasome system controlled by presenilin-associated rhomboid-like protease (PARL). This process regulates the concentration of PINK1 in normal mitochondria.

In damaged mitochondria, mitochondria depolarize due to various injuries. This membrane potential is crucial for TIM-mediated protein translocation. Based on that, most of PINK1 is unable to enter the inner membrane and cannot be degraded by PARL-mediated degradation. In consequence, PINK1 accumulates on the outer mitochondrial membrane and phosphorylates ubiquitin. Then, accumulated PINK1 is activated via dimerization and autophosphorylation. Autophosphorylation of the PINK1 at S228 and 402 sites occurs after mitochondrial depolarization, which is thought to be a precondition for recruiting Parkin. PINK1 phosphorylates Parkin at the S65 site. PINK1/Parkin triggers autophagy via recruitment of the autophagic-substrate proteins such as p62 and mitochondrial ubiquitination [65, 289, 293–298] to eliminate damaged mitochondria (see Figure 8).

7.3. Enhancing Autophagy Is a Promising Way to Improve Mitochondrial Function in the Aged Liver.

Recent studies revealed a number of interesting approaches in different model organisms (see Table 4) suitable to improve mitochondrial function via enhancing autophagy. Here, we are presenting the results of pharmacological upregulation using quercetin, melatonin, urolithin 1, and tomatidine, and via mTOR knockdown. Interestingly, they also improved the longevity of the model organisms.

Quercetin administration upregulates mitophagy thereby effectively reducing the impact of mitochondrial injuries as reported by Yu et al. [299]. They observed that chronic ethanol diet administration caused significant damage to hepatic mitochondria of C57BL/6J mice. Mitochondrial injury mainly manifested as mitochondrial swelling, internal membrane destruction, lack of cristae, rupture of the endoplasmic reticulum, and decrease of mitochondrial membrane potential. Quercetin administration effectively reduced these mitochondrial injuries by activating mitophagy. The mRNA and protein expression of Parkin was significantly decreased in the ethanol diet administration mice compared with control mice, while Parkin expression was significantly increased after quercetin coadministration. These results reflect that mitophagy activation exerts a crucial role in improving hepatic mitochondrial dysfunction.

Melatonin, a hormone that is usually used to enhance sleep quality, improved hepatic mitochondria function by activating mitophagy as reported by Zhou et al. [300]. They found that the protein expression of mitochondrial-LC3-II, Atg5, and Beclin-1 in mouse primary hepatocytes was substantially decreased after treatment with palmitic acid but significantly increased after treatment with melatonin. Palmitic acid caused mitochondrial damage indicated by a reduced oxygen consumption rate, decreased ATP synthesis, and dissipation of mitochondrial membrane potential, while melatonin effectively alleviated the above mitochondrial dysfunctions.

Urolithin A, a bacterial metabolite of ellagic acids [301], could trigger mitophagy in vivo and in vitro, as observed by Ryu et al. [302, 303]. Urolithin A prevented the age-related accumulation of damaged mitochondria in C. elegans, a model organism used frequently in aging research, and prolonged their lifespan. In mammalian cells, urolithin A was able to induce mitophagy and lead to an increase of phospho-AMPKα. Furthermore, in rodents, urolithin A promoted mitophagy leading to improved mitochondrial biogenesis and mitochondrial function, which was indicated
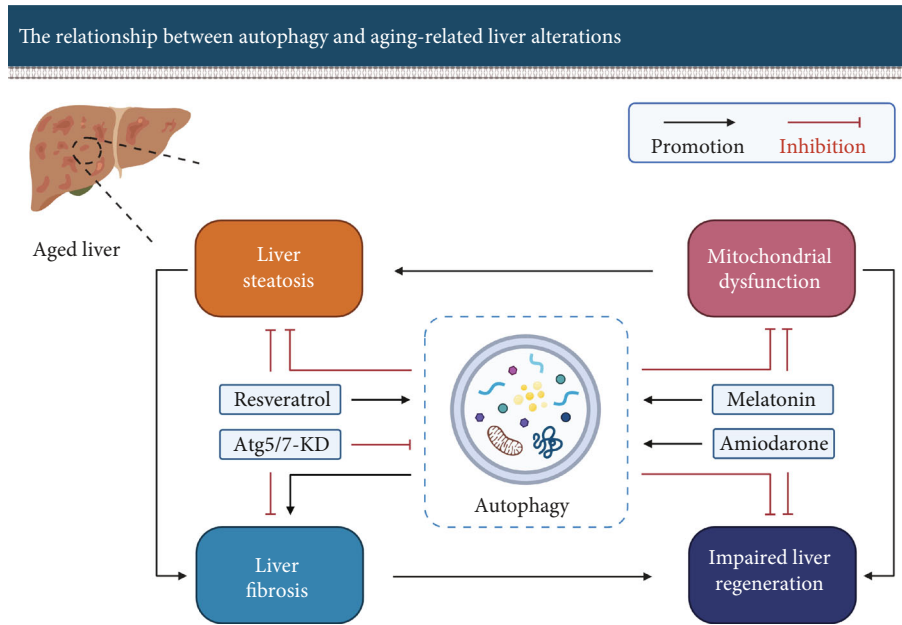
FIGURE 9: Autophagy plays different roles in age-related liver alterations. Enhancing autophagy may ameliorate aging-induced liver steatosis, mitochondrial dysfunction, and the impaired regenerative capacity but may aggravate liver fibrosis injury. KD: knockdown.

by the enhanced aerobic endurance and grip strength of the animals.

Similarly, tomatidine, a steroidal alkaloid from unripe tomato [304], did enhance longevity in C. elegans by inducing mitophagy, as reported by Fang et al. [305]. Tomatidine sustained mitochondrial homeostasis via regulating PINK-1/DCT-1-dependent mitophagy and mitochondrial biogenesis. Besides, tomatidine could effectively relieve age-related changes in C. elegans. For example, tomatidine substantially improved the decline in age-related swimming scores in aged C. elegans. Compared with the vehicle group, the score increased by 48%.

Reducing mTOR expression via mTOR knockdown in mice as performed by Wu et al. [306] prolonged the overall lifespan by 20% compared to control animals. The mRNA expression of p16 in the liver of aged mTOR-knockdown mice was significantly lower than that of control animals.

These results from strikingly different experiments all suggest that upregulation of autophagy seems to be effective to alleviate age-related impairment.

8. Conclusion

Aging is a natural phenomenon that occurs in all eukaryotic organisms. The aging process predisposes the liver to certain histopathological lesions, to decreased metabolic function, and to an impaired regenerative capacity. Accumulating evidence suggests that autophagy is involved in a variety of physiological and pathological events in the liver. Of concern is that modulation of autophagy has different effects on aging-induced changes in the liver (see Figure 9).

For liver steatosis: an appropriate boost in autophagy can effectively promote lipid metabolism and reduce lipid accumulation in hepatocytes. Inducing autophagy, e.g., Resveratrol may contribute to relieving the metabolic burden of the aging liver as well as prevent or slow down the initiation and progression of NAFLD, especially in elderly patients with impaired autophagy.

For liver fibrosis: upregulation of autophagy appears to provide the energy required for activation of hepatic stellate cells in case of hepatic injury. However, the induction of autophagy is also thought to be beneficial in reducing liver cell injury. Reduction of liver cell injury may improve fibrosis, which is relatively limited compared to the direct profibrosis effect. Therefore, selective inhibition of autophagy in hepatic stellate cells using, e.g., Atg5/7 knockdown seems to be a promising experimental strategy to counteract liver fibrosis in aged livers.

For impaired liver regenerative capacity: enhancement of autophagy via the mTOR-independent pathway, e.g., amiodarone, seems to be helpful. In this case, cell proliferation is not affected but the energy required for hepatocyte division and growth provided, thereby promoting liver regeneration. This is of utmost benefit for elderly patients who desperately need a life-saving liver resection.

For mitochondrial dysfunction: activation of autophagy can effectively eliminate dysfunctional mitochondria and promote mitochondrial regeneration. Both are of equal importance for reducing ROS and facilitating hepatocyte survival. Adequate and healthy mitochondria in turn facilitate the breakdown of hepatic lipids and provide energy to maintain liver function. Prevention or reversing mitochondrial dysfunction by inducing autophagy, e.g., melatonin, could be a promising therapeutic approach to improve mitochondrial respiration, especially for elderly patients.

With the development of autophagy research in the past decade, numerous autophagy modulators have emerged. Understanding the relationship between autophagy and age-related hepatic changes may lead to novel strategies to "rejuvenate" the aged liver. However, modulation of

autophagy via pharmacological intervention is a promising but double-edged treatment strategy. Therefore, to effectively counteract liver aging without causing obvious harm, it is necessary to evaluate the most destructive process in the individual patient before modulating autophagy.

Conflicts of Interest

The authors declare that there is no conflict of interest regarding the publication of this paper.

Authors' Contributions

Fengming Xu generated the original manuscript and the graphics; Fengming Xu and Uta Dahmen conceived and designed the structure of the manuscript; Hans-Michael Tautenhahn, Olaf Dirsch, and Uta Dahmen reviewed the manuscript; Uta Dahmen managed the project.

Acknowledgments

References

[1] D. o. E. a. S. A. United Nations, Population Division, *World Population Ageing 2019 Highlights*, United Nations, 2019.

[2] F. Sheedfar, S. Di Biase, D. Koonen, and M. Vinciguerra, "Liver diseases and aging: friends or foes?," *Aging Cell*, vol. 12, no. 6, pp. 950–954, 2013.

[3] M. Pibiri, "Liver regeneration in aged mice: new insights," *Aging*, vol. 10, no. 8, pp. 1801–1824, 2018.

[4] N. J. Hunt, S. W. S. Kang, G. P. Lockwood, D. G. Le Couteur, and V. C. Cogger, "Hallmarks of aging in the liver," *Computational and Structural Biotechnology Journal*, vol. 17, pp. 1151–1161, 2019.

[5] I. H. Kim, T. Kisseleva, and D. A. Brenner, "Aging and liver disease," *Current Opinion in Gastroenterology*, vol. 31, no. 3, pp. 184–191, 2015.

[6] M. J. Czaja, W.-X. Ding, T. M. Donohue Jr. et al., "Functions of autophagy in normal and diseased liver," *Autophagy*, vol. 9, no. 8, pp. 1131–1158, 2014.

[7] J. Ezaki, N. Matsumoto, M. Takeda-Ezaki et al., "Liver autophagy contributes to the maintenance of blood glucose and amino acid levels," *Autophagy*, vol. 7, no. 7, pp. 727–736, 2014.

[8] Y. Chun and J. Kim, "Autophagy: an essential degradation program for cellular homeostasis and life," *Cell*, vol. 7, no. 12, p. 278, 2018.

[9] R. Weiskirchen and F. Tacke, "Relevance of autophagy in parenchymal and non-parenchymal liver cells for health and disease," *Cell*, vol. 8, no. 1, p. 16, 2019.

[10] A. Liu, E. Guo, J. Yang et al., "Young plasma reverses age-dependent alterations in hepatic function through the restoration of autophagy," *Aging Cell*, vol. 17, no. 1, 2018.

[11] K. A. Escobar, N. H. Cole, C. M. Mermier, and T. A. VanDusseldorp, "Autophagy and aging: Maintaining the proteome through exercise and caloric restriction," *Aging Cell*, vol. 18, no. 1, p. e12876, 2019.

[12] F. Xu, C. Hua, H. M. Tautenhahn, O. Dirsch, and U. Dahmen, "The role of autophagy for the regeneration of the aging liver," *International Journal of Molecular Sciences*, vol. 21, no. 10, p. 3606, 2020.

[13] A. Terman and U. T. Brunk, "Autophagy in cardiac myocyte homeostasis, aging, and pathology," *Cardiovascular Research*, vol. 68, no. 3, pp. 355–365, 2005.

[14] A. M. Cuervo, E. Bergamini, U. T. Brunk, W. Dröge, M. Ffrench, and A. Terman, "Autophagy and aging: the importance of maintaining "clean" cells," *Autophagy*, vol. 1, no. 3, pp. 131–140, 2014.

[15] U. T. Brunk and A. Terman, "The mitochondrial-lysosomal axis theory of aging," *European Journal of Biochemistry*, vol. 269, no. 8, pp. 1996–2002, 2002.

[16] R. M. Reznick, H. Zong, J. Li et al., "Aging-associated reductions in AMP-activated protein kinase activity and mitochondrial biogenesis," *Cell Metabolism*, vol. 5, no. 2, pp. 151–156, 2007.

[17] A. Salminen, K. Kaarniranta, and A. Kauppinen, "Age-related changes in AMPK activation: role for AMPK phosphatases and inhibitory phosphorylation by upstream signaling pathways," *Ageing Research Reviews*, vol. 28, pp. 15–26, 2016.

[18] A. Salminen and K. Kaarniranta, "AMP-activated protein kinase (AMPK) controls the aging process via an integrated signaling network," *Ageing Research Reviews*, vol. 11, no. 2, pp. 230–241, 2012.

[19] H. Khalil, M. Tazi, K. Caution et al., "Aging is associated with hypermethylation of autophagy genes in macrophages," *Epigenetics*, vol. 11, no. 5, pp. 381–388, 2016.

[20] P. Davalli, T. Mitic, A. Caporali, A. Lauriola, and D. D'Arca, "ROS, cell senescence, and novel molecular mechanisms in aging and age-related diseases," *Oxidative Medicine and Cellular Longevity*, vol. 2016, Article ID 3565127, 18 pages, 2016.

[21] D. Glick, S. Barth, and K. F. Macleod, "Autophagy: cellular and molecular mechanisms," *The Journal of Pathology*, vol. 221, no. 1, pp. 3–12, 2010.

[22] C. He and D. J. Klionsky, "Regulation mechanisms and signaling pathways of autophagy," *Annual Review of Genetics*, vol. 43, no. 1, pp. 67–93, 2009.

[23] S. Bialik, S. K. Dasari, and A. Kimchi, "Autophagy-dependent cell death – where, how and why a cell eats itself to death," *Journal of Cell Science*, vol. 131, no. 18, article jcs215152, 2018.

[24] R. Ghosh and J. S. Pattison, "Macroautophagy and chaperone-mediated autophagy in heart failure: the known and the unknown," *Oxidative Medicine and Cellular Longevity*, vol. 2018, Article ID 8602041, 22 pages, 2018.

[25] K. R. Parzych and D. J. Klionsky, "An Overview of Autophagy: Morphology, Mechanism, and Regulation," *Antioxidants & Redox Signaling*, vol. 20, no. 3, pp. 460–473, 2014.

[26] E. L. Axe, S. A. Walker, M. Manifava et al., "Autophagosome formation from membrane compartments enriched in phosphatidylinositol 3-phosphate and dynamically connected to the endoplasmic reticulum," *Journal of Cell Biology*, vol. 182, no. 4, pp. 685–701, 2008.

[27] X. Tan, N. Thapa, Y. Liao, S. Choi, and R. A. Anderson, "PtdIns(4,5)P2 signaling regulates ATG14 and autophagy," *Proceedings of the National Academy of Sciences of the United States of America*, vol. 113, no. 39, pp. 10896–10901, 2016.

[28] B. Ravikumar, K. Moreau, and D. C. Rubinsztein, "Plasma membrane helps autophagosomes grow," *Autophagy*, vol. 6, no. 8, pp. 1184–1186, 2014.

[29] B. Ravikumar, K. Moreau, L. Jahreiss, C. Puri, and D. C. Rubinsztein, "Plasma membrane contributes to the formation of pre-autophagosomal structures," *Nature Cell Biology*, vol. 12, no. 8, pp. 747–757, 2010.

[30] A. M. Cuervo, "The plasma membrane brings autophagosomes to life," *Nature Cell Biology*, vol. 12, no. 8, pp. 735–737, 2010.

[31] D. W. Hailey, A. S. Rambold, P. Satpute-Krishnan et al., "Mitochondria supply membranes for autophagosome biogenesis during starvation," *Cell*, vol. 141, no. 4, pp. 656–667, 2010.

[32] A. van der Vaart, J. Griffith, and F. Reggiori, "Exit from the Golgi Is Required for the Expansion of the Autophagosomal Phagophore in Yeast Saccharomyces cerevisiae," *Molecular Biology of the Cell*, vol. 21, no. 13, pp. 2270–2284, 2010.

[33] A. van der Vaart and F. Reggiori, "The Golgi complex as a source for yeast autophagosomal membranes," *Autophagy*, vol. 6, no. 6, pp. 800-801, 2014.

[34] J. Biazik, P. Ylä-Anttila, H. Vihinen, E. Jokitalo, and E.-L. Eskelinen, "Ultrastructural relationship of the phagophore with surrounding organelles," *Autophagy*, vol. 11, no. 3, pp. 439–451, 2015.

[35] A. Bernard and D. J. Klionsky, "Autophagosome formation: tracing the source," *Developmental Cell*, vol. 25, no. 2, pp. 116-117, 2013.

[36] Y. Feng and D. J. Klionsky, "Autophagic membrane delivery through ATG9," *Cell Research*, vol. 27, no. 2, pp. 161-162, 2017.

[37] M. G. Lin and J. H. Hurley, "Structure and function of the ULK1 complex in autophagy," *Current Opinion in Cell Biology*, vol. 39, pp. 61–68, 2016.

[38] N. Hosokawa, T. Sasaki, S. Iemura, T. Natsume, T. Hara, and N. Mizushima, "Atg101, a novel mammalian autophagy protein interacting with Atg13," *Autophagy*, vol. 5, no. 7, pp. 973–979, 2014.

[39] B.-W. Kim, Y. Jin, J. Kim et al., "The C-terminal region of ATG101 bridges ULK1 and PtdIns3K complex in autophagy initiation," *Autophagy*, vol. 14, no. 12, pp. 2104–2116, 2018.

[40] I. Dikic and Z. Elazar, "Mechanism and medical implications of mammalian autophagy," *Nature Reviews Molecular Cell Biology*, vol. 19, no. 6, pp. 349–364, 2018.

[41] R. C. Russell, Y. Tian, H. Yuan et al., "ULK1 induces autophagy by phosphorylating Beclin-1 and activating VPS34 lipid kinase," *Nature Cell Biology*, vol. 15, no. 7, pp. 741–750, 2013.

[42] J. H. Stack, D. B. DeWald, K. Takegawa, and S. D. Emr, "Vesicle-mediated protein transport: regulatory interactions between the Vps15 protein kinase and the Vps34 PtdIns 3-kinase essential for protein sorting to the vacuole in yeast," *The Journal of Cell Biology*, vol. 129, no. 2, pp. 321–334, 1995.

[43] T. Hanada, N. N. Noda, Y. Satomi et al., "The Atg12-Atg5 Conjugate Has a Novel E3-like Activity for Protein Lipidation in Autophagy," *The Journal of Biological Chemistry*, vol. 282, no. 52, pp. 37298–37302, 2007.

[44] N. Fujita, T. Itoh, H. Omori, M. Fukuda, T. Noda, and T. Yoshimori, "The Atg16L complex specifies the site of LC3 lipidation for membrane biogenesis in autophagy," *Molecular Biology of the Cell*, vol. 19, no. 5, pp. 2092–2100, 2008.

[45] M. Komatsu and Y. Ichimura, "Physiological significance of selective degradation of p62 by autophagy," *FEBS Letters*, vol. 584, no. 7, pp. 1374–1378, 2010.

[46] N. Mizushima and M. Komatsu, "Autophagy: renovation of cells and tissues," *Cell*, vol. 147, no. 4, pp. 728–741, 2011.

[47] V. Cohen-Kaplan, I. Livneh, N. Avni et al., "p62- and ubiquitin-dependent stress-induced autophagy of the mammalian 26S proteasome," *Proceedings of the National Academy of Sciences*, vol. 113, no. 47, pp. E7490–E7499, 2016.

[48] S. Nakamura and T. Yoshimori, "New insights into autophagosome–lysosome fusion," *Journal of Cell Science*, vol. 130, no. 7, pp. 1209–1216, 2017.

[49] T. O. Berg, M. Fengsrud, P. E. Strømhaug, T. Berg, and P. O. Seglen, "Isolation and characterization of rat liver amphisomes: evidence for fusion of autophagosomes with both early and late endosomes," *The Journal of Biological Chemistry*, vol. 273, no. 34, pp. 21883–21892, 1998.

[50] P. Lőrincz and G. Juhász, "Autophagosome-lysosome fusion," *Journal of Molecular Biology*, vol. 432, no. 8, pp. 2462–2482, 2020.

[51] M. G. Gutierrez, D. B. Munafó, W. Berón, and M. I. Colombo, "Rab7 is required for the normal progression of the autophagic pathway in mammalian cells," *Journal of Cell Science*, vol. 117, no. 13, pp. 2687–2697, 2004.

[52] T. Wang, Z. Ming, W. Xiaochun, and W. Hong, "Rab7: role of its protein interaction cascades in endo-lysosomal traffic," *Cellular Signalling*, vol. 23, no. 3, pp. 516–521, 2011.

[53] F. Guerra and C. Bucci, "Multiple roles of the small GTPase Rab7," *Cell*, vol. 5, no. 3, p. 34, 2016.

[54] S. Jäger, C. Bucci, I. Tanida et al., "Role for Rab7 in maturation of late autophagic vacuoles," *Journal of Cell Science*, vol. 117, no. 20, pp. 4837–4848, 2004.

[55] E. Itakura, C. Kishi-Itakura, and N. Mizushima, "The hairpin-type tail-anchored SNARE syntaxin 17 targets to autophagosomes for fusion with endosomes/lysosomes," *Cell*, vol. 151, no. 6, pp. 1256–1269, 2012.

[56] J. D. Rabinowitz and E. White, "Autophagy and metabolism," *Science*, vol. 330, no. 6009, pp. 1344–1348, 2010.

[57] J. Zhang, "Autophagy and mitophagy in cellular damage control," *Redox Biology*, vol. 1, no. 1, pp. 19–23, 2013.

[58] K. Kounakis, M. Chaniotakis, M. Markaki, and N. Tavernarakis, "Emerging roles of lipophagy in health and disease," *Frontiers in Cell and Development Biology*, vol. 7, no. 185, 2019.

[59] K. Zhou, P. Yao, J. He, and H. Zhao, "Lipophagy in nonliver tissues and some related diseases: pathogenic and therapeutic implications," *Journal of Cellular Physiology*, vol. 234, no. 6, pp. 7938–7947, 2019.

[60] W. Cui, A. Sathyanarayan, M. Lopresti, M. Aghajan, C. Chen, and D. G. Mashek, "Lipophagy-derived fatty acids undergo extracellular efflux via lysosomal exocytosis," *Autophagy*, pp. 1–16, 2020.

[61] S. A. Killackey, D. J. Philpott, and S. E. Girardin, "Mitophagy pathways in health and disease," *Journal of Cell Biology*, vol. 219, no. 11, 2020.

[62] K. Palikaras, E. Lionaki, and N. Tavernarakis, "Mechanisms of mitophagy in cellular homeostasis, physiology and pathology," *Nature Cell Biology*, vol. 20, no. 9, pp. 1013–1022, 2018.

[63] P.-Y. Ke, "Mitophagy in the pathogenesis of liver diseases," *Cell*, vol. 9, no. 4, p. 831, 2020.

[64] S. Pickles, P. Vigié, and R. J. Youle, "Mitophagy and quality control mechanisms in mitochondrial maintenance," *Current Biology*, vol. 28, no. 4, pp. R170–R185, 2018.

[65] S. M. Jin and R. J. Youle, "PINK1- and Parkin-mediated mitophagy at a glance," *Journal of Cell Science*, vol. 125, no. 4, pp. 795–799, 2012.

[66] J. L. Schneider and A. M. Cuervo, "Liver autophagy: much more than just taking out the trash," *Nature Reviews. Gastroenterology & Hepatology*, vol. 11, no. 3, pp. 187–200, 2014.

[67] S. Schuck, "Microautophagy – distinct molecular mechanisms handle cargoes of many sizes," *Journal of Cell Science*, vol. 133, no. 17, article jcs246322, 2020.

[68] W.-w. Li, J. Li, and J.-k. Bao, "Microautophagy: lesser-known self-eating," *Cellular and Molecular Life Sciences*, vol. 69, no. 7, pp. 1125–1136, 2012.

[69] S. Kaushik, U. Bandyopadhyay, S. Sridhar et al., "Chaperone-mediated autophagy at a glance," *Journal of Cell Science*, vol. 124, no. 4, pp. 495–499, 2011.

[70] N. R. Romero and P. Agostinis, "Chapter 12 - Molecular mechanisms underlying the activation of autophagy pathways by reactive oxygen species and their relevance in cancer progression and therapy," *Autophagy: Cancer, Other Pathologies, Inflammation, Immunity, Infection, and Aging*, vol. 1, pp. 159–178, 2014.

[71] A. M. Cuervo and E. Wong, "Chaperone-mediated autophagy: roles in disease and aging," *Cell Research*, vol. 24, no. 1, pp. 92–104, 2014.

[72] E. Arias, "Methods to Study Chaperone-Mediated Autophagy," *Methods in Enzymology*, vol. 588, pp. 283–305, 2017.

[73] N. Martinez-Lopez and R. Singh, "Autophagy and lipid droplets in the liver," *Annual Review of Nutrition*, vol. 35, no. 1, pp. 215–237, 2015.

[74] M. Komatsu, S. Waguri, T. Ueno et al., "Impairment of starvation-induced and constitutive autophagy in Atg7-deficient mice," *Journal of Cell Biology*, vol. 169, no. 3, pp. 425–434, 2005.

[75] R. H. Bhogal and S. C. Afford, "Autophagy and the liver," in *Autophagy-A Double-Edged Sword-Cell Survival or Death*, pp. 165–185, INTECH, 2013.

[76] R. Singh and A. M. Cuervo, "Autophagy in the cellular energetic balance," *Cell Metabolism*, vol. 13, no. 5, pp. 495–504, 2011.

[77] C. M. Schworer, K. A. Shiffer, and G. E. Mortimore, "Quantitative relationship between autophagy and proteolysis during graded amino acid deprivation in perfused rat liver.," *The Journal of Biological Chemistry*, vol. 256, no. 14, pp. 7652–7658, 1981.

[78] H. M. Ni, N. Boggess, M. R. McGill et al., "Liver-specific loss of Atg5 causes persistent activation of Nrf2 and protects against acetaminophen-induced liver injury," *Toxicological Sciences*, vol. 127, no. 2, pp. 438–450, 2012.

[79] J. Bi, L. Yang, T. Wang et al., "Irisin improves autophagy of aged hepatocytes via increasing telomerase activity in liver injury," *Oxidative Medicine and Cellular Longevity*, vol. 2020, Article ID 6946037, 13 pages, 2020.

[80] A. D. Liu, J. K. Yang, Q. Hu et al., "Young plasma attenuates age-dependent liver ischemia reperfusion injury," *FASEB Journal*, vol. 33, no. 2, pp. 3063–3073, 2018.

[81] T. Flatt, "A new definition of aging?," *Frontiers in Genetics*, vol. 3, pp. 148–148, 2012.

[82] M. A. Mori, "Aging: a new perspective on an old issue," *Anais da Academia Brasileira de Ciências*, vol. 92, no. 2, article e20200437, 2020.

[83] Q. Li, M. Cai, J. Wang et al., "Decreased ovarian function and autophagy gene methylation in aging rats," *Journal of Ovarian Research*, vol. 13, no. 1, p. 12, 2020.

[84] M. M. Lipinski, B. Zheng, T. Lu et al., "Genome-wide analysis reveals mechanisms modulating autophagy in normal brain aging and in Alzheimer's disease," *Proceedings of the National Academy of Sciences*, vol. 107, no. 32, pp. 14164–14169, 2010.

[85] D. C. Rubinsztein, G. Mariño, and G. Kroemer, "Autophagy and aging," *Cell*, vol. 146, no. 5, pp. 682–695, 2011.

[86] M. N. Uddin, N. Nishio, S. Ito, H. Suzuki, and K.-i. Isobe, "Autophagic activity in thymus and liver during aging," *Age*, vol. 34, no. 1, pp. 75–85, 2012.

[87] S. Wullschleger, R. Loewith, and M. N. Hall, "TOR signaling in growth and metabolism," *Cell*, vol. 124, no. 3, pp. 471–484, 2006.

[88] M. V. Blagosklonny, "TOR-driven aging: speeding car without brakes," *Cell Cycle*, vol. 8, no. 24, pp. 4055–4059, 2014.

[89] K. L. Double, V. N. Dedov, H. Fedorow et al., "The comparative biology of neuromelanin and lipofuscin in the human brain," *Cellular and Molecular Life Sciences*, vol. 65, no. 11, pp. 1669–1682, 2008.

[90] A. Terman and U. T. Brunk, "Lipofuscin: mechanisms of formation and increase with age," *APMIS*, vol. 106, no. 1-6, pp. 265–276, 1998.

[91] A. Höhn and T. Grune, "Lipofuscin: formation, effects and role of macroautophagy," *Redox Biology*, vol. 1, no. 1, pp. 140–144, 2013.

[92] A. Terman, T. Kurz, M. Navratil, E. A. Arriaga, and U. T. Brunk, "Mitochondrial turnover and aging of long-lived postmitotic cells: the mitochondrial-lysosomal axis theory of aging," *Antioxidants & Redox Signaling*, vol. 12, no. 4, pp. 503–535, 2010.

[93] M. Perše, R. Injac, and A. Erman, "Oxidative status and lipofuscin accumulation in urothelial cells of bladder in aging mice," *PLoS One*, vol. 8, no. 3, article e59638, 2013.

[94] A. Terman, B. Gustafsson, and U. T. Brunk, "Autophagy, organelles and ageing," *The Journal of Pathology*, vol. 211, no. 2, pp. 134–143, 2007.

[95] A. Moreno-García, A. Kun, O. Calero, M. Medina, and M. Calero, "An overview of the role of lipofuscin in age-related neurodegeneration," *Frontiers in Neuroscience*, vol. 12, pp. 464–464, 2018.

[96] Y. Yuan, Y. Chen, T. Peng et al., "Mitochondrial ROS-induced lysosomal dysfunction impairs autophagic flux and contributes to M1 macrophage polarization in a diabetic condition," *Clinical Science*, vol. 133, no. 15, pp. 1759–1777, 2019.

[97] Z.-H. Liu and J. C. He, "Podocytopathy," *Contributions to Nephrology*, vol. 183, pp. 83–100, 2014.

[98] R. A. Saxton and D. M. Sabatini, "mTOR signaling in growth, metabolism, and disease," *Cell*, vol. 168, no. 6, pp. 960–976, 2017.

[99] K. Inoki, T. Zhu, and K. L. Guan, "TSC2 mediates cellular energy response to control cell growth and survival," *Cell*, vol. 115, no. 5, pp. 577–590, 2003.

[100] R. J. Shaw, "LKB1 and AMP-activated protein kinase control of mTOR signalling and growth," *Acta Physiologica*, vol. 196, no. 1, pp. 65–80, 2009.

[101] R. M. Gunn and H. C. Hailes, "Insights into the PI3-K-PKB-mTOR signalling pathway from small molecules," *Journal of Chemical Biology*, vol. 1, no. 1-4, pp. 49–62, 2008.

[102] C. Espeillac, C. Mitchell, S. Celton-Morizur et al., "S6 kinase 1 is required for rapamycin-sensitive liver proliferation after mouse hepatectomy," *The Journal of Clinical Investigation*, vol. 121, no. 7, pp. 2821–2832, 2011.

[103] Y. Rabanal-Ruiz, E. G. Otten, and V. I. Korolchuk, "mTORC1 as the main gateway to autophagy," *Essays in Biochemistry*, vol. 61, no. 6, pp. 565–584, 2017.

[104] J. Kim, M. Kundu, B. Viollet, and K.-L. Guan, "AMPK and mTOR regulate autophagy through direct phosphorylation of Ulk1," *Nature Cell Biology*, vol. 13, no. 2, pp. 132–141, 2011.

[105] D. Meng and J. L. Jewell, "Clearing debris," *Nature Chemical Biology*, vol. 15, no. 8, pp. 760-761, 2019.

[106] D. Egan, J. Kim, R. J. Shaw, and K.-L. Guan, "The autophagy initiating kinase ULK1 is regulated via opposing phosphorylation by AMPK and mTOR," *Autophagy*, vol. 7, no. 6, pp. 643-644, 2014.

[107] E. Jacinto, R. Loewith, A. Schmidt et al., "Mammalian TOR complex 2 controls the actin cytoskeleton and is rapamycin insensitive," *Nature Cell Biology*, vol. 6, no. 11, pp. 1122–1128, 2004.

[108] D. Kazyken, B. Magnuson, C. Bodur et al., "AMPK directly activates mTORC2 to promote cell survival during acute energetic stress," *Science Signaling*, vol. 12, no. 585, article eaav3249, 2019.

[109] B. D. Manning and A. Toker, "AKT/PKB signaling: navigating the network," *Cell*, vol. 169, no. 3, pp. 381–405, 2017.

[110] Y. Li, K. Inoki, R. Yeung, and K.-L. Guan, "Regulation of TSC2 by 14-3-3 Binding," *The Journal of Biological Chemistry*, vol. 277, no. 47, pp. 44593–44596, 2002.

[111] M. Nellist, M. A. Goedbloed, C. de Winter et al., "Identification and Characterization of the Interaction between Tuberin and 14-3-3ζ," *The Journal of Biological Chemistry*, vol. 277, no. 42, pp. 39417–39424, 2002.

[112] R. A. Nixon, "The role of autophagy in neurodegenerative disease," *Nature Medicine*, vol. 19, no. 8, pp. 983–997, 2013.

[113] B. T. Navé, D. M. Ouwens, D. J. Withers, D. R. Alessi, and P. R. Shepherd, "Mammalian target of rapamycin is a direct target for protein kinase B: identification of a convergence point for opposing effects of insulin and amino-acid deficiency on protein translation," *Biochemical Journal*, vol. 344, no. 2, pp. 427–431, 1999.

[114] B. A. Hemmings and D. F. Restuccia, "PI3K-PKB/Akt pathway," *Cold Spring Harbor Perspectives in Biology*, vol. 4, no. 9, pp. a011189–a011189, 2012.

[115] I. G. Ganley, D. H. Lam, J. Wang, X. Ding, S. Chen, and X. Jiang, "ULK1·ATG13·FIP200 Complex Mediates mTOR Signaling and Is Essential for Autophagy," *The Journal of Biological Chemistry*, vol. 284, no. 18, pp. 12297–12305, 2009.

[116] C. H. Jung, C. B. Jun, S.-H. Ro et al., "ULK-Atg13-FIP200 complexes mediate mTOR signaling to the autophagy machinery," *Molecular Biology of the Cell*, vol. 20, no. 7, pp. 1992–2003, 2009.

[117] N. Hosokawa, T. Hara, T. Kaizuka et al., "Nutrient-dependent mTORC1 association with the ULK1-Atg13-FIP200 complex required for autophagy," *Molecular Biology of the Cell*, vol. 20, no. 7, pp. 1981–1991, 2009.

[118] Y. Kamada, K.-i. Yoshino, C. Kondo et al., "Tor directly controls the Atg1 kinase complex to regulate autophagy," *Molecular and Cellular Biology*, vol. 30, no. 4, pp. 1049–1058, 2010.

[119] M. Segatto, P. Rosso, M. Fioramonti et al., "AMPK in the central nervous system: physiological roles and pathological implications," *Research and Reports in Biology*, vol. 7, pp. 1–13, 2016.

[120] P. J. Roach, "AMPK→ uLK1→ autophagy," *Molecular and Cellular Biology*, vol. 31, no. 15, pp. 3082–3084, 2011.

[121] M. C. Maiuri, E. Tasdemir, A. Criollo et al., "Control of autophagy by oncogenes and tumor suppressor genes," *Cell Death and Differentiation*, vol. 16, no. 1, pp. 87–93, 2009.

[122] E. White, "Autophagy and p53," *Cold Spring Harbor Perspectives in Medicine*, vol. 6, no. 4, article a026120, 2016.

[123] M. C. Maiuri, L. Galluzzi, E. Morselli, O. Kepp, S. A. Malik, and G. Kroemer, "Autophagy regulation by p53," *Current Opinion in Cell Biology*, vol. 22, no. 2, pp. 181–185, 2010.

[124] D. Crighton, S. Wilkinson, J. O'Prey et al., "DRAM, a p53-induced modulator of autophagy, is critical for apoptosis," *Cell*, vol. 126, no. 1, pp. 121–134, 2006.

[125] Z. Feng, H. Zhang, A. J. Levine, and S. Jin, "The coordinate regulation of the p53 and mTOR pathways in cells," *Proceedings of the National Academy of Sciences of the United States of America*, vol. 102, no. 23, pp. 8204–8209, 2005.

[126] E. Tasdemir, M. C. Maiuri, L. Galluzzi et al., "Regulation of autophagy by cytoplasmic p53," *Nature Cell Biology*, vol. 10, no. 6, pp. 676–687, 2008.

[127] R. I. Martínez-Zamudio, L. Robinson, P.-F. Roux, and O. Bischof, "SnapShot: cellular senescence pathways," *Cell*, vol. 170, no. 4, pp. 816–816.e1, 2017.

[128] A. Rufini, P. Tucci, I. Celardo, and G. Melino, "Senescence and aging: the critical roles of p53," *Oncogene*, vol. 32, no. 43, pp. 5129–5143, 2013.

[129] O. Aksoy, A. Chicas, T. Zeng et al., "The atypical E2F family member E2F7 couples the p53 and RB pathways during cellular senescence," *Genes & Development*, vol. 26, no. 14, pp. 1546–1557, 2012.

[130] A. S. Coutts, S. Munro, and N. B. La Thangue, "Functional interplay between E2F7 and ribosomal rRNA gene transcription regulates protein synthesis," *Cell Death & Disease*, vol. 9, no. 5, p. 577, 2018.

[131] S. Sarkar, R. A. Floto, Z. Berger et al., "Lithium induces autophagy by inhibiting inositol monophosphatase," *The Journal of Cell Biology*, vol. 170, no. 7, pp. 1101–1111, 2005.

[132] S. Sarkar, B. Ravikumar, R. A. Floto, and D. C. Rubinsztein, "Rapamycin and mTOR-independent autophagy inducers ameliorate toxicity of polyglutamine-expanded huntingtin and related proteinopathies," *Cell Death and Differentiation*, vol. 16, no. 1, pp. 46–56, 2009.

[133] E. Kania, G. Roest, T. Vervliet, J. B. Parys, and G. Bultynck, "IP3 receptor-mediated calcium signaling and its role in autophagy in cancer," *Frontiers in Oncology*, vol. 7, pp. 140–140, 2017.

[134] C. Cárdenas, R. A. Miller, I. Smith et al., "Essential regulation of cell bioenergetics by constitutive InsP$_3$ receptor Ca^{2+} transfer to mitochondria," *Cell*, vol. 142, no. 2, pp. 270–283, 2010.

[135] C. Ding, Y. Li, F. Guo et al., "A Cell-type-resolved Liver Proteome," *Molecular & cellular proteomics : MCP*, vol. 15, no. 10, pp. 3190–3202, 2016.

[136] V. Racanelli and B. Rehermann, "The liver as an immunological organ," *Hepatology*, vol. 43, no. S1, pp. S54–S62, 2006.

[137] H. Senoo, N. Kojima, and M. Sato, "Vitamin A-Storing Cells (Stellate Cells)," *Vitamins and Hormones*, vol. 75, pp. 131–159, 2007.

[138] P. A. Knolle and D. Wohlleber, "Immunological functions of liver sinusoidal endothelial cells," *Cellular & Molecular Immunology*, vol. 13, no. 3, pp. 347–353, 2016.

[139] Y. Ni, J. M. Li, M. K. Liu et al., "Pathological process of liver sinusoidal endothelial cells in liver diseases," *World Journal of Gastroenterology*, vol. 23, no. 43, pp. 7666–7677, 2017.

[140] L. J. Dixon, M. Barnes, H. Tang, M. T. Pritchard, and L. E. Nagy, "Kupffer cells in the liver," *Comprehensive Physiology*, vol. 3, no. 2, pp. 785–797, 2013.

[141] A. Basso, L. Piantanelli, G. Rossolini, and G. S. Roth, "Reduced DNA synthesis in primary cultures of hepatocytes from old mice is restored by thymus grafts," *The Journals of Gerontology: Series A*, vol. 53A, no. 2, pp. B111–B116, 1998.

[142] V. C. Cogger, A. Warren, R. Fraser, M. Ngu, A. J. McLean, and D. G. Le Couteur, "Hepatic sinusoidal pseudocapillarization with aging in the non-human primate," *Experimental Gerontology*, vol. 38, no. 10, pp. 1101–1107, 2003.

[143] D. Stell and W. J. Wall, "The impact of aging on the liver," *Geriatrics and Aging*, vol. 6, pp. 36-37, 2003.

[144] H. A. Wynne, L. H. Cope, E. Mutch, M. D. Rawlins, K. W. Woodhouse, and O. F. W. James, "The effect of age upon liver volume and apparent liver blood flow in healthy man," *Hepatology*, vol. 9, no. 2, pp. 297–301, 1989.

[145] A. P. L. Jensen-Urstad and C. F. Semenkovich, "Fatty acid synthase and liver triglyceride metabolism: housekeeper or messenger?," *Biochimica et Biophysica Acta (BBA) - Molecular and Cell Biology of Lipids*, vol. 1821, no. 5, pp. 747–753, 2012.

[146] P. Angulo, "Treatment of nonalcoholic fatty liver disease," *Annals of Hepatology*, vol. 1, no. 1, pp. 12–19, 2002.

[147] Z. M. Younossi, A. B. Koenig, D. Abdelatif, Y. Fazel, L. Henry, and M. Wymer, "Global epidemiology of nonalcoholic fatty liver disease-meta-analytic assessment of prevalence, incidence, and outcomes," *Hepatology*, vol. 64, no. 1, pp. 73–84, 2016.

[148] M. M. Yeh and E. M. Brunt, "Pathology of nonalcoholic fatty liver disease," *American Journal of Clinical Pathology*, vol. 128, no. 5, pp. 837–847, 2007.

[149] V. Manne, P. Handa, and K. V. Kowdley, "Pathophysiology of nonalcoholic fatty liver disease/nonalcoholic steatohepatitis," *Clinics in Liver Disease*, vol. 22, no. 1, pp. 23–37, 2018.

[150] D. Luo, J. Li, K. Chen et al., "Study on metabolic trajectory of liver aging and the effect of Fufang Zhenzhu Tiaozhi on aging mice," *Frontiers in Pharmacology*, vol. 10, no. 926, 2019.

[151] P. Nguyen, L. Valanejad, A. Cast et al., "Elimination of age-associated hepatic steatosis and correction of aging phenotype by inhibition of cdk4-C/EBPα-p300 axis," *Cell Reports*, vol. 24, no. 6, pp. 1597–1609, 2018.

[152] E. M. Koehler, J. N. L. Schouten, B. E. Hansen et al., "Prevalence and risk factors of non-alcoholic fatty liver disease in the elderly: results from the Rotterdam study," *Journal of Hepatology*, vol. 57, no. 6, pp. 1305–1311, 2012.

[153] I. Pierantonelli and G. Svegliati-Baroni, "Nonalcoholic fatty liver disease: basic pathogenetic mechanisms in the progression from NAFLD to NASH," *Transplantation*, vol. 103, no. 1, pp. e1–e13, 2019.

[154] Y. Inami, S. Yamashina, K. Izumi et al., "Hepatic steatosis inhibits autophagic proteolysis via impairment of autophagosomal acidification and cathepsin expression," *Biochemical and Biophysical Research Communications*, vol. 412, no. 4, pp. 618–625, 2011.

[155] H. Chen, "Nutrient mTORC1 signaling contributes to hepatic lipid metabolism in the pathogenesis of nonalcoholic fatty liver disease," *Liver Research*, vol. 4, no. 1, pp. 15–22, 2020.

[156] G. Jia and J. R. Sowers, "Autophagy: a housekeeper in cardiorenal metabolic health and disease," *Biochimica et Biophysica Acta (BBA) - Molecular Basis of Disease*, vol. 1852, no. 2, pp. 219–224, 2015.

[157] R. Zechner, F. Madeo, and D. Kratky, "Cytosolic lipolysis and lipophagy: two sides of the same coin," *Nature Reviews Molecular Cell Biology*, vol. 18, no. 11, pp. 671–684, 2017.

[158] R. Singh, S. Kaushik, Y. Wang et al., "Autophagy regulates lipid metabolism," *Nature*, vol. 458, no. 7242, pp. 1131–1135, 2009.

[159] J. Wang, S.-L. Han, D.-L. Lu et al., "Inhibited lipophagy suppresses lipid metabolism in zebrafish liver cells," *Frontiers in Physiology*, vol. 10, no. 1077, 2019.

[160] P. Maycotte, S. Aryal, C. T. Cummings, J. Thorburn, M. J. Morgan, and A. Thorburn, "Chloroquine sensitizes breast cancer cells to chemotherapy independent of autophagy," *Autophagy*, vol. 8, no. 2, pp. 200–212, 2014.

[161] K. Liu and M. J. Czaja, "Regulation of lipid stores and metabolism by lipophagy," *Cell Death and Differentiation*, vol. 20, no. 1, pp. 3–11, 2013.

[162] J. Madrigal-Matute and A. M. Cuervo, "Regulation of liver metabolism by autophagy," *Gastroenterology*, vol. 150, no. 2, pp. 328–339, 2016.

[163] F. Nassir and J. A. Ibdah, "Role of mitochondria in nonalcoholic fatty liver disease," *International Journal of Molecular Sciences*, vol. 15, no. 5, pp. 8713–8742, 2014.

[164] M. Scharwey, T. Tatsuta, and T. Langer, "Mitochondrial lipid transport at a glance," *Journal of Cell Science*, vol. 126, no. 23, pp. 5317–5323, 2013.

[165] M. Ogrodnik, S. Miwa, T. Tchkonia et al., "Cellular senescence drives age-dependent hepatic steatosis," *Nature Communications*, vol. 8, no. 1, article 15691, 2017.

[166] A. Boveris and B. Chance, "The mitochondrial generation of hydrogen peroxide. General properties and effect of hyperbaric oxygen," *The Biochemical Journal*, vol. 134, no. 3, pp. 707–716, 1973.

[167] L. Cao, X.-B. Quan, W.-J. Zeng, X.-O. Yang, and M.-J. Wang, "Mechanism of hepatocyte apoptosis," *Journal of Cell Death*, vol. 9, pp. 19–29, 2016.

[168] G. H. Koek, P. R. Liedorp, and A. Bast, "The role of oxidative stress in non-alcoholic steatohepatitis," *Clinica Chimica Acta*, vol. 412, no. 15-16, pp. 1297–1305, 2011.

[169] Z. Chen, R. Tian, Z. She, J. Cai, and H. Li, "Role of oxidative stress in the pathogenesis of nonalcoholic fatty liver disease," *Free Radical Biology and Medicine*, vol. 152, pp. 116–141, 2020.

[170] N. Sun, J. Yun, J. Liu et al., "Measuring in vivo mitophagy," *Molecular Cell*, vol. 60, no. 4, pp. 685–696, 2015.

[171] R. Singh, "Autophagy and regulation of lipid metabolism," *Results and Problems in Cell Differentiation*, vol. 52, pp. 35–46, 2010.

[172] J. Xiong, K. Wang, J. He, G. Zhang, D. Zhang, and F. Chen, "TFE3 alleviates hepatic steatosis through autophagy-induced lipophagy and PGC1α-mediated fatty acid β-Oxidation," *International Journal of Molecular Sciences*, vol. 17, no. 3, p. 387, 2016.

[173] L. Tang, F. Yang, Z. Fang, and C. Hu, "Resveratrol ameliorates alcoholic fatty liver by inducing autophagy," *The American Journal of Chinese Medicine*, vol. 44, no. 6, pp. 1207–1220, 2016.

[174] F. Manai, A. Azzalin, M. Morandi et al., "Trehalose modulates autophagy process to counteract gliadin cytotoxicity in an in vitro celiac disease model," *Cell*, vol. 8, no. 4, p. 348, 2019.

[175] B. J. DeBosch, M. R. Heitmeier, A. L. Mayer et al., "Trehalose inhibits solute carrier 2A (SLC2A) proteins to induce autophagy and prevent hepatic steatosis," *Science Signaling*, vol. 9, no. 416, p. ra21, 2016.

[176] H. Ren, D. Wang, L. Zhang et al., "Catalpol induces autophagy and attenuates liver steatosis in ob/ob and high-fat diet-induced obese mice," *Aging*, vol. 11, no. 21, pp. 9461–9477, 2019.

[177] C.-W. Lin, H. Zhang, M. Li et al., "Pharmacological promotion of autophagy alleviates steatosis and injury in alcoholic and non-alcoholic fatty liver conditions in mice," *Journal of Hepatology*, vol. 58, no. 5, pp. 993–999, 2013.

[178] S. K. Chun, S. Lee, M. J. Yang, C. Leeuwenburgh, and J. S. Kim, "Exercise-induced autophagy in fatty liver disease," *Exercise and Sport Sciences Reviews*, vol. 45, no. 3, pp. 181–186, 2017.

[179] L. Tong, L. Wang, S. Yao et al., "PPARδ attenuates hepatic steatosis through autophagy-mediated fatty acid oxidation," *Cell Death & Disease*, vol. 10, no. 3, p. 197, 2019.

[180] Y. Wang, H. Zhao, X. Li et al., "Tangshen formula alleviates hepatic steatosis by inducing autophagy through the AMPK/SIRT1 pathway," *Frontiers in Physiology*, vol. 10, p. 494, 2019.

[181] Q. Chu, S. Zhang, M. Chen et al., "Cherry anthocyanins regulate NAFLD by promoting autophagy pathway," *Oxidative Medicine and Cellular Longevity*, vol. 2019, Article ID 4825949, 16 pages, 2019.

[182] T. Ohashi, Y. Nakade, M. Ibusuki et al., "Conophylline inhibits high fat diet-induced non-alcoholic fatty liver disease in mice," *PLoS One*, vol. 14, no. 1, article e0210068, 2019.

[183] C. Liu, L. Liu, H.-D. Zhu et al., "Celecoxib alleviates nonalcoholic fatty liver disease by restoring autophagic flux," *Scientific Reports*, vol. 8, no. 1, article 4108, 2018.

[184] T. Hong, Z. Ge, R. Meng et al., "Erythropoietin alleviates hepatic steatosis by activating SIRT1-mediated autophagy," *Biochimica et Biophysica Acta (BBA) - Molecular and Cell Biology of Lipids*, vol. 1863, no. 6, pp. 595–603, 2018.

[185] G. J. Balachander, S. Subramanian, and K. Ilango, "Rosmarinic acid attenuates hepatic steatosis by modulating ER stress and autophagy in oleic acid-induced HepG2 cells," *RSC Advances*, vol. 8, no. 47, pp. 26656–26663, 2018.

[186] R. Li, E. Guo, J. Yang et al., "1,25(OH)$_2$D$_3$ attenuates hepatic steatosis by inducing autophagy in mice," *Obesity*, vol. 25, no. 3, pp. 561–571, 2017.

[187] T. W. Jung, H. C. Hong, H.-J. Hwang, H. J. Yoo, S. H. Baik, and K. M. Choi, "C1q/TNF-related protein 9 (CTRP9) attenuates hepatic steatosis via the autophagy-mediated inhibition of endoplasmic reticulum stress," *Molecular and Cellular Endocrinology*, vol. 417, pp. 131–140, 2015.

[188] Y. Zhang, M.-l. Chen, Y. Zhou et al., "Resveratrol improves hepatic steatosis by inducing autophagy through the cAMP signaling pathway," *Molecular Nutrition & Food Research*, vol. 59, no. 8, pp. 1443–1457, 2015.

[189] J. Jiao, S. L. Friedman, and C. Aloman, "Hepatic fibrosis," *Current Opinion in Gastroenterology*, vol. 25, no. 3, pp. 223–229, 2009.

[190] E. C. Stahl, M. J. Haschak, B. Popovic, and B. N. Brown, "Macrophages in the aging liver and age-related liver disease," *Frontiers in Immunology*, vol. 9, article 2795, 2018.

[191] Netinbag, "What are stellate cells?," 2020, August 2020, https://www.netinbag.com/en/physiology/what-are-stellate-cells.html.

[192] F. Marra and M. Pinzani, "Role of hepatic stellate cells in the pathogenesis of portal hypertension," *Nefrología*, vol. 22, Supplement 5, pp. 34–40, 2002.

[193] T. Tsuchida and S. L. Friedman, "Mechanisms of hepatic stellate cell activation," *Nature Reviews Gastroenterology & Hepatology*, vol. 14, no. 7, pp. 397–411, 2017.

[194] F. J. Eng and S. L. Friedman, "Fibrogenesis I. New insights into hepatic stellate cell activation: the simple becomes complex," *American Journal of Physiology - Gastrointestinal and Liver Physiology*, vol. 279, no. 1, pp. G7–G11, 2000.

[195] C.-Y. Zhang, W.-G. Yuan, P. He, J. H. Lei, and C. X. Wang, "Liver fibrosis and hepatic stellate cells: etiology, pathological hallmarks and therapeutic targets," *World Journal of Gastroenterology*, vol. 22, no. 48, pp. 10512–10522, 2016.

[196] U. E. Lee and S. L. Friedman, "Mechanisms of hepatic fibrogenesis," *Best Practice & Research Clinical Gastroenterology*, vol. 25, no. 2, pp. 195–206, 2011.

[197] M. Fausther, M. T. Pritchard, Y. V. Popov, and K. Bridle, "Contribution of liver nonparenchymal cells to hepatic fibrosis: interactions with the local microenvironment," *BioMed Research International*, vol. 2017, Article ID 6824762, 4 pages, 2017.

[198] L. F. R. Thoen, E. L. M. Guimarães, L. Dollé et al., "A role for autophagy during hepatic stellate cell activation," *Journal of Hepatology*, vol. 55, no. 6, pp. 1353–1360, 2011.

[199] N. Testerink, M. Ajat, M. Houweling et al., "Replacement of retinyl esters by polyunsaturated triacylglycerol species in lipid droplets of hepatic stellate cells during activation," *PLoS One*, vol. 7, no. 4, article e34945, 2012.

[200] Y. Song, Y. Zhao, F. Wang, L. Tao, J. Xiao, and C. Yang, "Autophagy in hepatic fibrosis," *BioMed Research International*, vol. 2014, Article ID 436242, 8 pages, 2014.

[201] V. Hernández–Gea, Z. Ghiassi–Nejad, R. Rozenfeld et al., "Autophagy releases lipid that promotes fibrogenesis by activated hepatic stellate cells in mice and in human tissues," *Gastroenterology*, vol. 142, no. 4, pp. 938–946, 2012.

[202] A. Yamamoto, Y. Tagawa, T. Yoshimori, Y. Moriyama, R. Masaki, and Y. Tashiro, "Bafilomycin A1 prevents maturation of autophagic vacuoles by inhibiting fusion between autophagosomes and lysosomes in rat hepatoma cell line, H-4-II-E cells," *Cell Structure and Function*, vol. 23, no. 1, pp. 33–42, 1998.

[203] M. Redmann, G. A. Benavides, T. F. Berryhill et al., "Inhibition of autophagy with bafilomycin and chloroquine decreases mitochondrial quality and bioenergetic function in primary neurons," *Redox Biology*, vol. 11, pp. 73–81, 2017.

[204] W. He, B. Wang, J. Yang et al., "Chloroquine improved carbon tetrachloride-induced liver fibrosis through its inhibition

of the activation of hepatic stellate cells: role of autophagy," *Biological & Pharmaceutical Bulletin*, vol. 37, no. 9, pp. 1505–1509, 2014.

[205] J. Zhu, J. Wu, E. Frizell et al., "Rapamycin inhibits hepatic stellate cell proliferation in vitro and limits fibrogenesis in an in vivo model of liver fibrosis," *Gastroenterology*, vol. 117, no. 5, pp. 1198–1204, 1999.

[206] Y. Akselband, M. W. Harding, and P. A. Nelson, "Rapamycin inhibits spontaneous and fibroblast growth factor beta-stimulated proliferation of endothelial cells and fibroblasts," *Transplantation Proceedings*, vol. 23, no. 6, pp. 2833–2836, 1991.

[207] X. Lin, L. Han, J. Weng, K. Wang, and T. Chen, "Rapamycin inhibits proliferation and induces autophagy in human neuroblastoma cells," *Bioscience Reports*, vol. 38, no. 6, article BSR20181822, 2018.

[208] S. M. Fouraschen, P. E. de Ruiter, J. Kwekkeboom et al., "mTOR signaling in liver regeneration: rapamycin combined with growth factor treatment," *World Journal of Transplantation*, vol. 3, no. 3, pp. 36–47, 2013.

[209] W.-X. Ding, S. Manley, and H.-M. Ni, "The emerging role of autophagy in alcoholic liver disease," *Experimental Biology and Medicine*, vol. 236, no. 5, pp. 546–556, 2011.

[210] H.-M. Ni, A. Bockus, N. Boggess, H. Jaeschke, and W. X. Ding, "Activation of autophagy protects against acetaminophen-induced hepatotoxicity," *Hepatology*, vol. 55, no. 1, pp. 222–232, 2012.

[211] M. Allaire, P.-E. Rautou, P. Codogno, and S. Lotersztajn, "Autophagy in liver diseases: time for translation?," *Journal of Hepatology*, vol. 70, no. 5, pp. 985–998, 2019.

[212] A. Hammoutene, J. Lasselin, A. C. Vion et al., "Defective autophagy in liver sinusoidal endothelial cells promotes non alcoholic steatohepatitis and fibrosis development," *Journal of Hepatology*, vol. 68, p. S29, 2018.

[213] J. Lodder, T. Denaës, M.-N. Chobert et al., "Macrophage autophagy protects against liver fibrosis in mice," *Autophagy*, vol. 11, no. 8, pp. 1280–1292, 2015.

[214] M. Ruart, L. Chavarria, G. Campreciós et al., "Impaired endothelial autophagy promotes liver fibrosis by aggravating the oxidative stress response during acute liver injury," *Journal of Hepatology*, vol. 70, no. 3, pp. 458–469, 2019.

[215] N. Mizushima, "Autophagy: process and function," *Genes & Development*, vol. 21, no. 22, pp. 2861–2873, 2007.

[216] J. S. Pattison, H. Osinska, and J. Robbins, "Atg7 induces basal autophagy and rescues autophagic deficiency in CryABR120GCardiomyocytes," *Circulation Research*, vol. 109, no. 2, pp. 151–160, 2011.

[217] W. Ma, L. S. Cheng, W. Jiang, and S. D. Wu, "The small heterodimer partner inhibits activation of hepatic stellate cells via autophagy," *Advances in Clinical and Experimental Medicine*, vol. 29, no. 6, pp. 683–693, 2020.

[218] N. Liu, J. Feng, X. Lu et al., "Isorhamnetin inhibits liver fibrosis by reducing autophagy and inhibiting extracellular matrix formation via the TGF-β1/Smad3 and TGF-β1/p38 MAPK pathways," *Mediators of Inflammation*, vol. 2019, Article ID 6175091, 14 pages, 2019.

[219] D. Meng, Z. Li, G. Wang, L. Ling, Y. Wu, and C. Zhang, "Carvedilol attenuates liver fibrosis by suppressing autophagy and promoting apoptosis in hepatic stellate cells," *Biomedicine & Pharmacotherapy*, vol. 108, pp. 1617–1627, 2018.

[220] J. Feng, K. Chen, Y. Xia et al., "Salidroside ameliorates autophagy and activation of hepatic stellate cells in mice via NF-κB and TGFβ1/Smad3 pathways," *Drug Design, Development and Therapy*, vol. 12, pp. 1837–1853, 2018.

[221] B. Wang, H. Yang, Y. Fan et al., "3-Methyladenine ameliorates liver fibrosis through autophagy regulated by the NF-κB signaling pathways on hepatic stellate cell," *Oncotarget*, vol. 8, no. 64, pp. 107603–107611, 2017.

[222] L. Wu, Q. Zhang, W. Mo et al., "Quercetin prevents hepatic fibrosis by inhibiting hepatic stellate cell activation and reducing autophagy via the TGF-β1/Smads and PI3K/Akt pathways," *Scientific Reports*, vol. 7, no. 1, article 9289, 2017.

[223] Y. Mao, S. Zhang, F. Yu, H. Li, C. Guo, and X. Fan, "Ghrelin attenuates liver fibrosis through regulation of TGF-β1 expression and autophagy," *International Journal of Molecular Sciences*, vol. 16, no. 9, pp. 21911–21930, 2015.

[224] Z. Liu, P. Zhu, L. Zhang et al., "Autophagy inhibition attenuates the induction of anti-inflammatory effect of catalpol in liver fibrosis," *Biomedicine & Pharmacotherapy*, vol. 103, pp. 1262–1271, 2018.

[225] G. K. Michalopoulos and M. C. DeFrances, "Liver regeneration," *Science*, vol. 276, no. 5309, pp. 60–66, 1997.

[226] R. Taub, "Liver regeneration: from myth to mechanism," *Nature Reviews. Molecular Cell Biology*, vol. 5, no. 10, pp. 836–847, 2004.

[227] J. So, A. Kim, S.-H. Lee, and D. Shin, "Liver progenitor cell-driven liver regeneration," *Experimental & Molecular Medicine*, vol. 52, no. 8, pp. 1230–1238, 2020.

[228] N. Fausto, "Liver regeneration," *Journal of Hepatology*, vol. 32, 1 Supplement, pp. 19–31, 2000.

[229] T. Nakamura and S. Mizuno, "The discovery of hepatocyte growth factor (HGF) and its significance for cell biology, life sciences and clinical medicine," *Proceedings of the Japan Academy. Series B, Physical and Biological Sciences*, vol. 86, no. 6, pp. 588–610, 2010.

[230] G. Michalopoulos, "HGF and liver regeneration," *Gastroenterologia Japonica*, vol. 28, no. S4, Supplement 4, pp. 36–39, 1993.

[231] P. M. Lindroos, R. Zarnegar, and G. K. Michalopoulos, "Hepatocyte growth factor (hepatopoietin A) rapidly increases in plasma before DNA synthesis and liver regeneration stimulated by partial hepatectomy and carbon tetrachloride administration," *Hepatology*, vol. 13, no. 4, pp. 743–750, 1991.

[232] I. Zambreg, B. Assouline, C. Housset, and E. Schiffer, "Overexpression of TGF-α and EGFR, a key event in liver carcinogenesis, is induced by hypoxia specifically in hepatocytes," *Gastroenterology, Hepatology and Endoscopy*, vol. 4, no. 3, 2019.

[233] T. Tomiya, I. Ogata, and K. Fujiwara, "Transforming Growth Factor α Levels in Liver and Blood Correlate Better than Hepatocyte Growth Factor with Hepatocyte Proliferation during Liver Regeneration," *The American Journal of Pathology*, vol. 153, no. 3, pp. 955–961, 1998.

[234] J. E. Mead and N. Fausto, "Transforming growth factor alpha may be a physiological regulator of liver regeneration by means of an autocrine mechanism," *Proceedings of the National Academy of Sciences of the United States of America*, vol. 86, no. 5, pp. 1558–1562, 1989.

[235] K. Breitkopf, P. Godoy, L. Ciuclan, M. Singer, and S. Dooley, "TGF-β/Smad signaling in the injured liver," *Zeitschrift für Gastroenterologie*, vol. 44, no. 1, pp. 57–66, 2006.

[236] Y. Tao, M. Wang, E. Chen, and H. Tang, "Liver regeneration: analysis of the main relevant signaling molecules," *Mediators of Inflammation*, vol. 2017, Article ID 4256352, 9 pages, 2017.

[237] L. Braun, J. E. Mead, M. Panzica, R. Mikumo, G. I. Bell, and N. Fausto, "Transforming growth factor beta mRNA increases during liver regeneration: a possible paracrine mechanism of growth regulation," *Proceedings of the National Academy of Sciences of the United States of America*, vol. 85, no. 5, pp. 1539–1543, 1988.

[238] M. Macías-Silva, W. Li, J. I. Leu, M. A. S. Crissey, and R. Taub, "Up-regulated Transcriptional Repressors SnoN and Ski Bind Smad Proteins to Antagonize Transforming Growth Factor-β Signals during Liver Regeneration," *The Journal of Biological Chemistry*, vol. 277, no. 32, pp. 28483–28490, 2002.

[239] S. Werner and C. Alzheimer, "Roles of activin in tissue repair, fibrosis, and inflammatory disease," *Cytokine & Growth Factor Reviews*, vol. 17, no. 3, pp. 157–171, 2006.

[240] A. Zimmermann, "Regulation of liver regeneration," *Nephrology, Dialysis, Transplantation*, vol. 19, Supplement_4, pp. iv6–iv10, 2004.

[241] K. Takamura, K. Tsuchida, H. Miyake, S. Tashiro, and H. Sugino, "Activin and activin receptor expression changes in liver regeneration in rat," *The Journal of Surgical Research*, vol. 126, no. 1, pp. 3–11, 2005.

[242] L. Chen, W. Zhang, H.-f. Liang et al., "Activin A induces growth arrest through a SMAD- dependent pathway in hepatic progenitor cells," *Cell Communication and Signaling: CCS*, vol. 12, no. 1, pp. 18–18, 2014.

[243] J. R. Hully, L. Chang, R. H. Schwall, H. R. Widmer, T. G. Terrell, and N. A. Gillett, "Induction of apoptosis in the murine liver with recombinant human activin A," *Hepatology*, vol. 20, no. 4, pp. 854–862, 1994.

[244] R. Boulton, A. Woodman, D. Calnan, C. Selden, F. Tam, and H. Hodgson, "Nonparenchymal cells from regenerating rat liver generate interleukin- 1alpha and -1beta: A mechanism of negative regulation of hepatocyte proliferation," *Hepatology*, vol. 26, no. 1, pp. 49–58, 1997.

[245] T. Nakamura, R. Arakaki, and A. Ichihara, "Interleukin-1β is a potent growth inhibitor of adult rat hepatocytes in primary culture," *Experimental Cell Research*, vol. 179, no. 2, pp. 488–497, 1988.

[246] R. P. Evarts, P. Nagy, E. Marsden, and S. S. Thorgeirsson, "A precursor-product relationship exists between oval cells and hepatocytes in rat liver," *Carcinogenesis*, vol. 8, no. 11, pp. 1737–1740, 1987.

[247] Y. Cheng, X. Wang, B. Wang et al., "Aging-associated oxidative stress inhibits liver progenitor cell activation in mice," *Aging*, vol. 9, no. 5, pp. 1359–1374, 2017.

[248] T. Itoh and A. Miyajima, "Liver regeneration by stem/progenitor cells," *Hepatology*, vol. 59, no. 4, pp. 1617–1626, 2014.

[249] S. S. Thorgeirsson, "Hepatic stem cells in liver regeneration," *The FASEB Journal*, vol. 10, no. 11, pp. 1249–1256, 1996.

[250] N. N. Than and P. N. Newsome, "Stem cells for liver regeneration," *QJM*, vol. 107, no. 6, pp. 417–421, 2014.

[251] Y. Cheng, B. Wang, H. Zhou et al., "Autophagy is required for the maintenance of liver progenitor cell functionality," *Cellular Physiology and Biochemistry*, vol. 36, no. 3, pp. 1163–1174, 2015.

[252] D. L. Schmucker and H. Sanchez, "Liver regeneration and aging: a current perspective," *Current Gerontology and Geriatrics Research*, vol. 2011, Article ID 526379, 8 pages, 2011.

[253] J. Zhao, H. Xu, Y. Li et al., "NAFLD induction delays postoperative liver regeneration of ALPPS in rats," *Digestive Diseases and Sciences*, vol. 64, no. 2, pp. 456–468, 2019.

[254] N. Horiguchi, E. J. N. Ishac, and B. Gao, "Liver regeneration is suppressed in alcoholic cirrhosis: correlation with decreased STAT3 activation," *Alcohol*, vol. 41, no. 4, pp. 271–280, 2007.

[255] I. Matot, N. Nachmansson, O. Duev et al., "Impaired liver regeneration after hepatectomy and bleeding is associated with a shift from hepatocyte proliferation to hypertrophy," *FASEB Journal*, vol. 31, no. 12, pp. 5283–5295, 2017.

[256] H. Alexandrino, A. Rolo, J. G. Tralhão, F. Castro e Sousa, and C. Palmeira, "Mitochondria in liver regeneration: energy metabolism and posthepatectomy liver dysfunction," *Mitochondrial Biology and Experimental Therapeutics*, pp. 127–152, 2018.

[257] T. Toshima, K. Shirabe, T. Fukuhara et al., "Suppression of autophagy during liver regeneration impairs energy charge and hepatocyte senescence in mice," *Hepatology*, vol. 60, no. 1, pp. 290–300, 2014.

[258] D. Palmes, A. Zibert, T. Budny et al., "Impact of rapamycin on liver regeneration," *Virchows Archiv*, vol. 452, no. 5, pp. 545–557, 2008.

[259] Y. P. Jiang, L. M. Ballou, and R. Z. Lin, "Rapamycin-insensitive Regulation of 4E-BP1 in Regenerating Rat Liver," *The Journal of Biological Chemistry*, vol. 276, no. 14, pp. 10943–10951, 2001.

[260] T. Kawaguchi, T. Kodama, H. Hikita et al., "Carbamazepine promotes liver regeneration and survival in mice," *Journal of Hepatology*, vol. 59, no. 6, pp. 1239–1245, 2013.

[261] M. Schiebler, K. Brown, K. Hegyi et al., "Functional drug screening reveals anticonvulsants as enhancers of mTOR-independent autophagic killing of Mycobacterium tuberculosis through inositol depletion," *EMBO Molecular Medicine*, vol. 7, no. 2, pp. 127–139, 2014.

[262] J.-J. Zhang, Q.-M. Zhou, S. Chen, and W. D. le, "Repurposing carbamazepine for the treatment of amyotrophic lateral sclerosis in SOD1-G93A mouse model," *CNS Neuroscience & Therapeutics*, vol. 24, no. 12, pp. 1163–1174, 2018.

[263] M. D. Bootman, T. Chehab, G. Bultynck, J. B. Parys, and K. Rietdorf, "The regulation of autophagy by calcium signals: do we have a consensus?," *Cell Calcium*, vol. 70, pp. 32–46, 2018.

[264] X. Chen, M. Li, D. Chen et al., "Autophagy induced by calcium phosphate precipitates involves endoplasmic reticulum membranes in autophagosome biogenesis," *PLoS One*, vol. 7, no. 12, article e52347, 2012.

[265] C. W. Lin, Y. S. Chen, C. C. Lin et al., "Amiodarone as an autophagy promoter reduces liver injury and enhances liver regeneration and survival in mice after partial hepatectomy," *Scientific Reports*, vol. 5, no. 1, article 15807, 2015.

[266] P. Guha, R. Tyagi, S. Chowdhury et al., "IPMK mediates activation of ULK signaling and transcriptional regulation of autophagy linked to liver inflammation and regeneration," *Cell Reports*, vol. 26, no. 10, pp. 2692–2703.e7, 2019.

[267] C. J. Jia, H. Sun, and C. L. Dai, "Autophagy contributes to liver regeneration after portal vein ligation in rats," *Medical Science Monitor*, vol. 25, pp. 5674–5682, 2019.

[268] S. Wang, C. Lee, J. Kim et al., "Tumor necrosis factor-inducible gene 6 protein ameliorates chronic liver damage by promoting autophagy formation in mice," *Experimental & Molecular Medicine*, vol. 49, no. 9, pp. e380–e380, 2017.

[269] H. Shi, Y. Zhang, J. Ji et al., "Deficiency of apoptosis-stimulating protein two of p53 promotes liver regeneration in mice by activating mammalian target of rapamycin," *Scientific Reports*, vol. 8, no. 1, article 17927, 2018.

[270] L. Ernster and G. Schatz, "Mitochondria: a historical review," *The Journal of Cell Biology*, vol. 91, no. 3, pp. 227s–255s, 1981.

[271] G. Lenaz, G. Tioli, A. I. Falasca, and M. L. Genova, "Complex I function in mitochondrial supercomplexes," *Biochimica et Biophysica Acta (BBA) - Bioenergetics*, vol. 1857, no. 7, pp. 991–1000, 2016.

[272] A. Signes and E. Fernandez-Vizarra, "Assembly of mammalian oxidative phosphorylation complexes I-V and supercomplexes," *Essays in Biochemistry*, vol. 62, no. 3, pp. 255–270, 2018.

[273] A. Bratic and N.-G. Larsson, "The role of mitochondria in aging," *The Journal of Clinical Investigation*, vol. 123, no. 3, pp. 951–957, 2013.

[274] M. Redza-Dutordoir and D. A. Averill-Bates, "Activation of apoptosis signalling pathways by reactive oxygen species," *Biochimica et Biophysica Acta (BBA) - Molecular Cell Research*, vol. 1863, no. 12, pp. 2977–2992, 2016.

[275] A. Navarro and A. Boveris, "Rat brain and liver mitochondria develop oxidative stress and lose enzymatic activities on aging," *American Journal of Physiology—Regulatory, Integrative and Comparative Physiology*, vol. 287, no. 5, pp. R1244–R1249, 2004.

[276] T.-C. Yen, Y.-S. Chen, K.-L. King, S. H. Yeh, and Y. H. Wei, "Liver mitochondrial respiratory functions decline with age," *Biochemical and Biophysical Research Communications*, vol. 165, no. 3, pp. 994–1003, 1989.

[277] J. Sastre, F. V. Pallardó, R. Plá et al., "Aging of the liver: age-associated mitochondrial damage in intact hepatocytes," *Hepatology*, vol. 24, no. 5, pp. 1199–1205, 1996.

[278] N. G. Larsson, J. Wang, H. Wilhelmsson et al., "Mitochondrial transcription factor A is necessary for mtDNA maintance and embryogenesis in mice," *Nature Genetics*, vol. 18, no. 3, pp. 231–236, 1998.

[279] G. Lenaz, "Role of mitochondria in oxidative stress and ageing," *Biochimica et Biophysica Acta (BBA) - Bioenergetics*, vol. 1366, no. 1-2, pp. 53–67, 1998.

[280] I. Shokolenko, N. Venediktova, A. Bochkareva, G. L. Wilson, and M. F. Alexeyev, "Oxidative stress induces degradation of mitochondrial DNA," *Nucleic Acids Research*, vol. 37, no. 8, pp. 2539–2548, 2009.

[281] M. Vermulst, J. H. Bielas, G. C. Kujoth et al., "Mitochondrial point mutations do not limit the natural lifespan of mice," *Nature Genetics*, vol. 39, no. 4, pp. 540–543, 2007.

[282] A. Hiona and C. Leeuwenburgh, "The role of mitochondrial DNA mutations in aging and sarcopenia: implications for the mitochondrial vicious cycle theory of aging," *Experimental Gerontology*, vol. 43, no. 1, pp. 24–33, 2008.

[283] S. Srivastava, "The mitochondrial basis of aging and age-related disorders," *Genes*, vol. 8, no. 12, p. 398, 2017.

[284] A. Trifunovic, A. Wredenberg, M. Falkenberg et al., "Premature ageing in mice expressing defective mitochondrial DNA polymerase," *Nature*, vol. 429, no. 6990, pp. 417–423, 2004.

[285] L. Tilokani, S. Nagashima, V. Paupe, and J. Prudent, "Mitochondrial dynamics: overview of molecular mechanisms," *Essays in Biochemistry*, vol. 62, no. 3, pp. 341–360, 2018.

[286] M. Liesa, M. Palacín, and A. Zorzano, "Mitochondrial dynamics in mammalian health and disease," *Physiological Reviews*, vol. 89, no. 3, pp. 799–845, 2009.

[287] V. Eisner, M. Picard, and G. Hajnóczky, "Mitochondrial dynamics in adaptive and maladaptive cellular stress responses," *Nature Cell Biology*, vol. 20, no. 7, pp. 755–765, 2018.

[288] L. L. Lackner, "Shaping the dynamic mitochondrial network," *BMC Biology*, vol. 12, no. 1, p. 35, 2014.

[289] H.-M. Ni, J. A. Williams, and W.-X. Ding, "Mitochondrial dynamics and mitochondrial quality control," *Redox Biology*, vol. 4, pp. 6–13, 2015.

[290] K. Palikaras, E. Lionaki, and N. Tavernarakis, "Coupling mitogenesis and mitophagy for longevity," *Autophagy*, vol. 11, no. 8, pp. 1428–1430, 2015.

[291] P. Fan, X.-H. Xie, C.-H. Chen et al., "Molecular regulation mechanisms and interactions between reactive oxygen species and mitophagy," *DNA and Cell Biology*, vol. 38, no. 1, pp. 10–22, 2019.

[292] G. Chen, G. Kroemer, and O. Kepp, "Mitophagy: an emerging role in aging and age-associated diseases," *Frontiers in Cell and Development Biology*, vol. 8, p. 200, 2020.

[293] A. Eiyama and K. Okamoto, "PINK1/Parkin-mediated mitophagy in mammalian cells," *Current Opinion in Cell Biology*, vol. 33, pp. 95–101, 2015.

[294] K. Okatsu, T. Oka, M. Iguchi et al., "PINK1 autophosphorylation upon membrane potential dissipation is essential for Parkin recruitment to damaged mitochondria," *Nature Communications*, vol. 3, no. 1, pp. 1016–1016, 2012.

[295] M. Lazarou, "Keeping the immune system in check: a role for mitophagy," *Immunology and Cell Biology*, vol. 93, no. 1, pp. 3–10, 2015.

[296] C. Kondapalli, A. Kazlauskaite, N. Zhang et al., "PINK1 is activated by mitochondrial membrane potential depolarization and stimulates Parkin E3 ligase activity by phosphorylating Serine 65," *Open Biology*, vol. 2, no. 5, pp. 120080–120080, 2012.

[297] S. Sekine and R. J. Youle, "PINK1 import regulation; a fine system to convey mitochondrial stress to the cytosol," *BMC Biology*, vol. 16, no. 1, p. 2, 2018.

[298] K. Okatsu, M. Uno, F. Koyano et al., "A Dimeric PINK1-containing Complex on Depolarized Mitochondria Stimulates Parkin Recruitment," *The Journal of Biological Chemistry*, vol. 288, no. 51, pp. 36372–36384, 2013.

[299] X. Yu, Y. Xu, S. Zhang et al., "Quercetin attenuates chronic ethanol-induced hepatic mitochondrial damage through enhanced mitophagy," *Nutrients*, vol. 8, no. 1, p. 27, 2016.

[300] H. Zhou, W. Du, Y. Li et al., "Effects of melatonin on fatty liver disease: the role of NR4A1/DNA-PKcs/p53 pathway, mitochondrial fission, and mitophagy," *Journal of Pineal Research*, vol. 64, no. 1, article e12450, 2018.

[301] M. Alauddin, T. Okumura, J. Rajaxavier et al., "Gut bacterial metabolite urolithin A decreases actin polymerization and migration in cancer cells," *Molecular Nutrition & Food Research*, vol. 64, no. 7, article 1900390, 2020.

[302] D. Ryu, L. Mouchiroud, P. A. Andreux et al., "Urolithin A induces mitophagy and prolongs lifespan in *C. elegans* and

increases muscle function in rodents," *Nature Medicine*, vol. 22, no. 8, pp. 879–888, 2016.

[303] P. A. Andreux, W. Blanco-Bose, D. Ryu et al., "The mitophagy activator urolithin A is safe and induces a molecular signature of improved mitochondrial and cellular health in humans," *Nature Metabolism*, vol. 1, no. 6, pp. 595–603, 2019.

[304] B. Troost, L. M. Mulder, M. Diosa-Toro, D. van de Pol, I. A. Rodenhuis-Zybert, and J. M. Smit, "Tomatidine, a natural steroidal alkaloid shows antiviral activity towards chikungunya virus *in vitro*," *Scientific Reports*, vol. 10, no. 1, article 6364, 2020.

[305] E. F. Fang, T. B. Waltz, H. Kassahun et al., "Tomatidine enhances lifespan and healthspan in *C. elegans* through mitophagy induction via the SKN-1/Nrf2 pathway," *Scientific Reports*, vol. 7, no. 1, article 46208, 2017.

[306] J. J. Wu, J. Liu, E. B. Chen et al., "Increased mammalian lifespan and a segmental and tissue-specific slowing of aging after genetic reduction of mTOR expression," *Cell Reports*, vol. 4, no. 5, pp. 913–920, 2013.

[307] X. Li, Z. Shi, Y. Zhu et al., "Cyanidin-3-O-glucoside improves non-alcoholic fatty liver disease by promoting PINK1-mediated mitophagy in mice," *British Journal of Pharmacology*, vol. 177, no. 15, pp. 3591–3607, 2020.

[308] S. Shan, Z. Shen, C. Zhang, R. Kou, K. Xie, and F. Song, "Mitophagy protects against acetaminophen-induced acute liver injury in mice through inhibiting NLRP3 inflammasome activation," *Biochemical Pharmacology*, vol. 169, article 113643, 2019.

[309] X. Yu, M. Hao, Y. Liu et al., "Liraglutide ameliorates non-alcoholic steatohepatitis by inhibiting NLRP3 inflammasome and pyroptosis activation via mitophagy," *European Journal of Pharmacology*, vol. 864, article 172715, 2019.

[310] T. Zhou, L. Chang, Y. Luo, Y. Zhou, and J. Zhang, "Mst1 inhibition attenuates non-alcoholic fatty liver disease via reversing Parkin-related mitophagy," *Redox Biology*, vol. 21, article 101120, 2019.

[311] P. Liu, H. Lin, Y. Xu et al., "Frataxin-mediated PINK1–Parkin-dependent mitophagy in hepatic steatosis: the protective effects of quercetin," *Molecular Nutrition & Food Research*, vol. 62, no. 16, article 1800164, 2018.

[312] J. A. Williams, H.-M. Ni, Y. Ding, and W. X. Ding, "Parkin regulates mitophagy and mitochondrial function to protect against alcohol-induced liver injury and steatosis in mice," *American Journal of Physiology - Gastrointestinal and Liver Physiology*, vol. 309, no. 5, pp. G324–G340, 2015.